TOXICOLOGY: MOLECULAR TOXICITY OF TUNGSTEN DISULPHIDE (WS_2) QUANTUM DOTS, ASSOCIATED TOXICOKINETICS AND ADME PROFILING

ANJU SURENDRANATH

PHD THESIS

2022

SREE CHITRA TIRUNAL INSTITUTE

FOR

MEDICAL SCIENCES AND TECHNOLOGY, TRIVANDRUM

Thiruvananthapuram

TOXICOLOGY: MOLECULAR TOXICITY OF TUNGSTEN DISULPHIDE (WS_2) QUANTUM DOTS, ASSOCIATED TOXICOKINETICS AND ADME PROFILING

A THESIS PRESENTED BY

ANJU SURENDRANATH

TO

SREE CHITRA TIRUNAL INSTITUTE FOR

MEDICAL SCIENCES AND TECHNOLOGY, TRIVANDRUM

Thiruvananthapuram

IN PARTIAL FULFILMENT OF THE REQUIREMENTS

FOR THE AWARD OF

DOCTOR OF PHILOSOPHY

2022

This thesis is dedicated to my beloved father
B.R Surendranath

CERTIFICATE

I, **Anju Surendranath**, hereby certify that I had personally carried out the work depicted in the thesis entitled, ***"Toxicology: Molecular toxicity of Tungsten disulphide (WS_2) quantum dots, associated toxicokinetics and ADME profiling"***. No part of the thesis contains any previously published datas and the matter embodied in the thesis has not been submitted for the award of any other degree or diploma prior to this date. Whether contributions of others are involved, every effort is made to clearly indicate this, with due reference to the literature and acknowledgement.

Place: Thiruvananthapuram

Date:

Signature

Name: Anju Surendranath

Reg.No: 2018/PHD/05

Dr. P V Mohanan

Toxicology Division

This is to certify that **Ms. Anju Surendranath** in the Toxicology Division of this institute has fulfilled the requirements prescribed for the Ph.D degree of the Sree Chitra Tirunal Institute for Medical Sciences and Technology, Trivandrum. The thesis entitled, **"*Toxicology: Molecular toxicity of Tungsten disulphide (WS_2) quantum dots, associated toxicokinetics and ADME profiling*"** was carried out under my direct supervision. No part of the thesis was submitted for the award of any degree or diploma prior to this date.

*Clearance was obtained from the Institute Animal Ethics Committee (IAEC) for carrying out the study. IAEC approval No: SCT/IAEC-377/NOVEMBER/2020/107.

Signature

Date: 22/09/2022

Approval of thesis

The thesis entitled "*Toxicology: Molecular toxicity of Tungsten disulphide (WS_2) quantum dots, associated toxicokinetics and ADME profiling*"

Submitted By

Anju Surendranath

For the degree of

Doctor of Philosophy

Of

SREE CHITRA TIRUNAL INSTITUTE

FOR

MEDICAL SCIENCES AND TECHNOLOGY, TRIVANDRUM

Thiruvananthapuram

Is evaluated and approved by

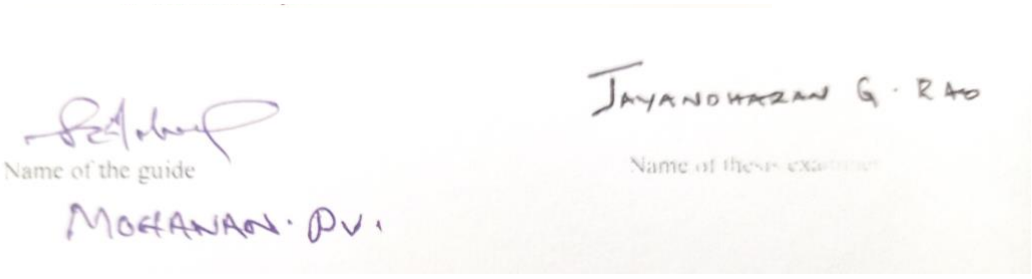

Acknowledgement

I express my sincere gratitude to The President, Dr Vijay kumar Saraswat, The Director In Charge Prof. Dr. K Jayakumar and The Head of Biomedical Technology Wing Dr. P R Harikrishna Varma, Sree Chitra Tirunal Institute for Medical Sciences and Technology for providing the necessary facilities and infrastructure for conducting my PhD work.

I sincerely thank the Director Prof. Sanjay Behari, former Director Prof. Dr Asha Kishore, Dean of Academic Affairs Dr Ajit Kumar V K, Associate Dean of Academic Affairs Dr PV Mohanan, Registrar Dr. Santhosh Kumar B, Deputy Registrar Ms. Radha M for their academic assistance throughout the tenure of my PhD.

I owe my deepest gratitude to the University Grants Commission (UGC, New Delhi) for the financial assistance as Junior Research Fellowship and Senior Research Fellowships (UGC Reference No:941/CSIR-UGC DEC 2016, Date: 17/09/2017).

I would like to sincerely thank my Doctoral Advisory Committee members, Dr. Ramesh P, Dr. Anilkumar P R and Dr. P P Lizymol for their sincere support throughout the tenure of my PhD.

I am grateful to Dr. Umasankar P R (SIC, DIMT), Dr. Harikrishnan V S (DLAS), Dr. Lizy K Krishnan and Dr. Rekha M.R (SIC, BST) for their immense support during my PhD work.

I am extremely delightful to Dr Rajeev Sukumaran and Ms Meena, CSIR-National Institute for Interdisciplinary Science and Technology (CSIR-NIIST), Trivandrum for their valuable help during my PhD tenure. I would like to thank Dr. Prathish K P, Mr. Joshi, Ms. Vaishnavi and staffs of Environmental Technology Division, CSIR NIIST, Trivandrum for their technical support. I also thank the staffs and technicians of STIC, CUSAT for their technical assistance.

I wholeheartedly thank the assistance provided by Ms. Jesna P V, Ms. Devika S L, Mr. Prem Mohan M (DIMT), Ms. Deepa K Raj (Division of Tissue Culture), Ms. Deepa (TRU), Ms. Jijo Wilson (DTERT), Ms. Prima S (PMD and Ms. Rajalekshmi (BST) during the course.

I express my sincere thanks to the staff and students of Toxicology Division for their support, which made my time here memorable. I would like to thank Dr. Remya N S, Dr. Syama S, Dr. Reshma V G, Dr. Sangeetha Vijayan, Dr. Megha K B, Dr. Prajitha N, Ms. Athira S S, Ms. Ashtami Jayakumar, Ms. Vandana Unnikrishnan, Ms. Varsha, Ms. Arathi Ashok, Mr. Joseph Xavier, Mr. Akhil Venugopal, Ms. Lekha, Mr. Shaji S, Mr. Harikumar G and Mr. Sudheesan for their never ending support.

I thank Dr. P V Mohanan, PhD Guide for the support.

I would like to acknowledge my family and friends who were always there for me during my good and bad times that always foster my endurance. I deeply admire my father Mr. B R Surendranath for his advices, care, love and sacrifice which always remind me about the path I should accompany. Your eternal blessing is the one which I believe sustained me so far.

I am sincerely thankful to my mother Mrs. Valsala Surendranath for her love, advice and sacrifices she made on my behalf. I thank my brother, Sanju Surendranath, who always stood for me during my ups and downs with his love and care. I thank my in-laws for their never ending support.

I am extremely adamant and thankful to my son Devanarayan N, who cherished my motherhood and always made my life worthful.

I am sincerely thankful and owed to my husband and my true motivator Mr. Nideesh G K, for his love, care and never ending support, which always prompt me to think judicious to devote towards my goal.

Anju Surendranath

Table of Contents

LIST OF FIGURES

LIST OF TABLES

ABBREVIATIONS

µg	microgram
µl	microlitre
AB/AM	Antibiotic/Antimicotic
ml	millilitre
nm	nanometer
NPs	Nanoparticles
QDs	Quantum Dots
ADME	Absorption, Distribution, Metabolism and Excretion
ALP	Alkaline phosphatase
ALT	Alanine Aminotransferase
AST	Aspartate Aminotransferase
NIR	Near Infrared Radiations
CNTs	Carbon Nanotubes
PEG	Poly Ethylene Glycol
PET	Positron Emission Tomography
SPECT	Single Photon Emission Computed Tomography
MRI	Magnetic Resonance Imaging
CT	Computed Tomography
UV	Ultraviolet
FRET	Fluorescence Resonance Energy Transfer
TMDC	Transition Metal Dichalcogenides
OECD	Organisation for Economic Co-operation and Development
FDA	Food and Drug Administration
EDTA	Ethylenediaminetetraacetic acid
EtBr	Ethidium Bromide

EU	Endotoxin Unit
FSC	Forward Scatter
SSC	Side scatter
ICP-MS	Inductively Coupled Plasma Mass Spectroscopy
H&E	Hematoxylin and Eosin
i.p	intraperitoneal
TCA	Trichloroacetic acid
SDS	Sodium dodecyl sulphate
CPM	Counts Per Million
PBS	Phosphate-buffered saline
MCV	Mean Corpuscular Volume
PLT	Platelet
RBC	Red Blood Corpuscles
WBC	White Blood Corpuscles
MCH	Mean Corpuscular Hemoglobin
MCHC	Mean Corpuscular Hemoglobin Concentration
GPx	Glutathione Peroxidase
GR	Glutathione Reductase
GSH	Reduced Glutathione
GSSG	Oxidised Glutathione
HGB	Hemoglobin
HCT	Hematocrit
NFKB	Nuclear Factor Kappa B
AO	Acridine Orange
PFA	Paraformaldehyde
CBB`	Coommassie Brilliant Blue
NaN_3	Sodium azide
DAPI	4′,6-diamidino-2-phenylindole
JC-1	tetraethylbenzimidazolylcarbocyanine iodide
RNS	Reactive Nitrogen Species
ROS	Reactive Oxygen Species
DCFH-DA	Dichloro-dihydro-fluorescein diacetate

FACS	Fluorescence activated cell sorting
PI	Propidium Iodide
LDH	Lactate Dehydrogenase
NRU	Neutral Red Uptake
MTT	3-(4,5-dimethylthiazol-2-yl)-2,5-diphenyl tetrazolium bromide
NCCS	National Centre for Cell Science
DMEM	Dulbecco's Modified Eagle Medium
FBS	Fetal Bovine Serum
DTG	Derivative tharmogravimetry
DTA	Differential Thermogravimetric Analysis
TGA	Thermogravimetric analysis
FTIR	Fourier Transform Infrared Spectroscopy
XRD	X-Ray Diffraction
XPS	X-ray Photoelectron Spectroscopy
HRTEM	Highe Resolution Transmission Electron Microscopy
DNA	Deoxy ribo Nucleic Acid
0D	Zero Dimensional
1D	One Dimensional
2D	Two Dimensional
3D	Three Dimensional
WS_2	Tungsten disulphide
MoS_2	Molybdenum disulphide
NMP	N Methyl Pyrolidone

SYNOPSIS

Title: Toxicology: ***Molecular toxicity of Tungsten disulphide (WS_2) quantum dots, associated toxicokinetics and ADME profiling***

Nanotechnology is an attractive field of science concerned with manipulating materials or devices in the scale of 1 to 100nm. It has profound scope in various interdisciplinary research fields. It is actively involved in the design, fabrication and application of the smallest functional organisation of the material. Rather than a single emerging scientific discipline, nanotechnology is rationale, which meets various traditional as well as modern scientific aspects like physics, chemistry, material science and engineering. The cumulative expertise of the above aspects of nanotechnology brings out novel outcomes. Nanoparticles (NPs) differ from their bulk counterpart in physico-chemical and mechanical characteristics. They possess unique and tunable electrical, optical and mechanical properties. Also related size dependant characteristics. Some NPs were renowned to exhibit optical, metallic and semi conducting properties. Various applications of nanotechnology therefore spans from electronics, opto electronics, sensing, energy storage to even biomedical applications, that brings about tremendous opportunities in these fields. Some among the profound application potential of NPs include targeted drug delivery, sensing, imaging, target analyte detection, tissue engineering scaffold designing, 3D printing, fluorescent biological labels, tumor detection, tumor therapy, pathogen detection *etc*.,. Quantum Dots (QDs) are extremely small sized (1-10nm), zero dimensional

semi conductor nanocrystals, which shows characteristic size dependant fluorescent properties. QDs possess tunable functionalities and high fluorescent quantum yield. They are extremely resistant to photobleaching when compared to conventional fluorescent dyes. QDs show size tunable narrow emission spectra, that can be excited at a single wavelength. Owing to these stringent characteristics along with high surface area, QDs are excellent candidates for various biomedical applications including targeted drug delivery, biosensor, bio imaging, imaging guided therapies, radiation therapy *etc*.,.*etc*

WS_2 QDs are inorganic semiconductor nanocrystals which belong to the family of transition metal dichalcogenides (TMDC). WS_2 is coming under the category of a new generation 2D material. TMDCs are sulphides, selenides and tellurides of group 5, 6 transition elements (Eg: WS_2, MoS_2, ReS_2, TaS_2, WSe_2 *etc.*). These are formulated as X-M-X, where 'M' is a transition metal atom, which is covalently sandwiched by two hexagonal planes of chalcogen atoms on either symmetry. WS_2 is a typical TMDC material, occurs in nature in the form of mineral tungstenite. It is composed of folded triple layer of S-W-S, in the same manner as carbon nanotubes composed of cyllindrical graphene sheets. Considering the chemical composition and characteristic bonding, atoms within each triple layer of WS_2 is covalently bonded. Weak van der Waals interactions exists between the layers. Therefore, exfoliation of various nano-dimensionalities such as mono/multi layers, nanotubes and quantum dots become possible by mechanical as well as chemical routes. They show excellent stability in aquous environments and possess large surface area that can be

manipulated and functionalised for various applications, specifically in the field of biomedicine.

Being an emerging class material, WS_2 QDs has got significant application possibilities such as target analyte detection, immunotherapy, drug/ gene delivery, photothermal therapy, photodynamic therapy, imaging guided therapies (PET, SPECT, CT, MRI) *etc.*,.

The toxicity of this emerging material was not deeply explored yet. Increased scientific attention, industrial and biomedical applications focussed towards these kind of materials always deepened the necessity of the indepth toxicological studies of the same. Safety and toxicity of NPs has become a major concern in the scientific community. To achieve this, the present study is aimed at the in-depth molecular toxicity studies of WS_2 QDs in both *in vitro* and *in vivo* systems.

In the present study, LN-229 human glioblastoma cell lines were used as an *in vitro* system for the nano-bio interactions and cytotoxicity studies of WS_2 QDs because the major application scope of QDs in biomedicine and theranostics are related to imaging guided therapies of brain.

LN-229 glial cells are non-neuronal cells of the central nervous system, which serves the function of nourishing the neurons. Due to high multiplication potential and comparable characteristics with primary astrocytes, LN-229 glioblastoma cells are been in the forefront of neurotoxicity researches from long back. Metal containing semi conductor QDs are of great interest in the diagnosis and treatment of most of

the neurodegenerative disorders. QDs got extraordinary attention to be used as imaging probes for therapies such as PET, SPECT *etc.,*. The traditionally employed core/shell type QDs consist of toxic heavy metals such as cadmium, lead *etc.,* and are found to be highly toxic to biological systems. Due to extremely small size, the QDs can even cross blood brain barrier and placental barrier evoking serious after effects. Therefore an indepth toxicological evaluation of QDs is necessary. Subsequently, the fabrication of highly biocompatible QDs has become a rising concern in the biomedical field. Among the notable TMDC materials, WS_2 QDs has got significant attention in disease diagnosis, imaging guided drug delivery, targeted tumor destruction and cancer immunology related fields in neuroscience. It is not surprising that the cellular uptake of any QDs and related nano-bio interaction can alter the normal biochemical processes in living cells. Therefore it is obligatory to analyse the potential toxicity of such materials, to avoid the adverse effects. Various factors such as size, morphology, crystallinity, solubility and aggregation tendency can inturn direct to various toxic effects in the biological system. Therefore such toxicity profiling datas represent strong foundations for laying the application possibilities of these emerging materials. It is highly expedited that most of the researches mask the relevance of toxicity profiling of nanomaterials while seeking the application scope. Therefore, it is highly imperative and mandatory to elucidate the indepth toxicity profiling of WS_2 QDs before validated to be safe for various biomedical applications. Hence in the present study, an effort was made to effectively elucidate the molecular toxicity profiling of WS_2 QDs in LN-229 human glioblastoma cell lines. Further acute toxicity studies were performed in Sprague Dawley rats.

The work hypothesised that the WS_2 QDs are highly fluorescent, non-toxic and non-immuno modulatory materials, which will be applicable in various biomedical applications. To validate the hypothesis, four objectives are formulated. The detailed objectives are given below;

Objective 1: Synthesis of Tungsten disulphide Quantum Dots (WS_2 QDs)

Objective 2: Optical and physico-chemical characterization

Objective 3: *In vitro* nano-bio interaction studies using LN-229 cells

Objective 4: Acute toxicity studies using Sprague Dawley rats

The entire thesis is composed of six chapters. **Chapter 1** is the introductory chapter, which detailed about the background of the study and its scientific relevance. The chapter has briefed about nanotechnology, nanoparticles in detail as well as the different classification of nanoparticles. Also briefed about QDs and its importance in the present era. It also gives an idea about the various photo-physical properties of QDs. A brief introduction about the significance of the branch of toxicology and nanotoxicology were also outlined in this introductory chapter. A brief discussion about the significance of LN-229 human glioblastoma cells in QD toxicity and related researches were also captured in this chapter.

The **second chapter** is basically the review of literature. It briefed about the various methods of synthesis employed for QDs as well as the structure and characterisation methods of QDs. This chapter outlined the importance of WS_2 QDs and the various

applications such as biomedical and non-biomedical applications of WS_2 QDs. This chapter also mentioned about the toxicity, safety, various parameters that contributes to QD toxicity as well as the mechanism of toxicity.

The **third chapter** described about the materials and methodologies adopted to fulfil the four objectives of the study.

Objective 1 is the synthesis of WS_2 QDs, which explained about the detailed synthesis strategy of solvothermal exfoliation using NMP solvent.

Objective 2 is about the optical and physico-chemical characterisation of the synthesised QDs using various sophisticated techniques. Size and morphology was confirmed using High-Resolution Transmission Electron Microscopy (HRTEM) analysis. Surface charge was analysed using Zeta potential, chemical composition and elemental oxidation states were analysed using Fourier Transform Infrared Spectroscopy (FTIR) and X-Ray Photoelectron Spectroscopy (XPS). Effective exfoliation from bulk WS_2 crystals was confirmed by X-Ray Diffraction (XRD). Thermal stability analysis was done using Thermogravimetric Analysis (TGA). Fluorescence emission spectra was analysed to elucidate the emission peak maxima of the QDs under 370nm excitation. Endotoxin content of the synthesised QDs was analysed as part of biological characterisation. Stability of the QDs was checked for 100 days period by observing both UV/Visible and fluorescence emission spectra of the particles at an interval of 20 days under room temperature.

The **third objective** includes nano-bio interactions and cytotoxicity analysis of WS_2 QDs using LN-229 glioblastoma cell lines. These are epithelial adherent type cells having a doubling time of approximately 24h. The cells were cultured in DMEM media supplemented with 10% Fetal Bovine Serum (FBS). Effective uptake of QDs was evidenced by fluorescent microscopy and flow cytometry analysis. Dose response and IC_{50} calculation were done using MTT assay. Varying range of concentrations of WS_2 QDs (10, 20, 40, 80, 160, 320 and 640µg/ml) were allowed to incubate with LN-229 cells for 24 and 48h and subsequent cellular metabolic activity was analysed. Lysosomal integrity after WS_2 QD exposure was analysed by Neutral Red Uptake (NRU) assay. Morphological anomalies after WS_2 QD exposure was analysed by phase contrast microscopy and Coomassie Brilliant Blue (CBB) staining. Reactive oxygen species (hydroxyl and peroxyl radical) release was quantified using DCFH-DA assay for 6h and 24h. Reactive Nitrogen Species generation after WS_2 QD exposure was analysed by Griess Reagent assay. The influence of inherent catalase activity of LN-229 cells in ROS scavenging was analysed by incubating with a known catalase inhibitor sodium azide. Lysosomal integrity after WS_2 QDs exposure in LN-229 cells was analysed using acridine orange immunostaining using fluorescent microscopy and subsequent quantitative expression analysis was also carried out to confirm the results. JC-1 probe staining was done to check the mitochondrial membrane potential and subsequent quantitative analysis was done using fluorescent spectroscopy. Cytoskeletal integrity and actin filament stabilisation was analysed using Rhodamine-phalloidin dye with the aid of fluorescent microscopy. The nucleus was counterstained using DAPI and visualised WS_2 QDs, localised around the nucleus.

Membrane integrity loss after WS_2 QDs treatment was analysed by ethidium bromide (EtBr) staining using FACS. Live/dead cell population followed by WS_2 QDs exposure was analysed by Calcein AM/PI staining using FACS. Cell cycle analysis was done by propidium iodide staining using flow cytometry to analyse the possibility of cell cycle arrest. NF kappa B expression analysis was done using FACS to evaluate the possible cytokine expression followed by WS_2 QDs treatment. Further, the cell death pathway mediated by WS_2 QDs exposure was evaluated using Annexin V/PI staining by flow cytometry and confirmed the same using Caspase 3 expression analysis.

Genotoxicity studies were done to evaluate the possible damage on genetic material on exposure to WS_2 QDs exposure. Hoechst staining was done to evaluate the nuclear damage and chromosomal condensation. Tritiated thymidine incorporation assay was done to evaluate the possible proliferation inhibition of the material. DNA ladder assay was carried out to evaluate the possible DNA fragmentation using agarose gel electrophoresis. The **fourth objective** of the study demonstrated the acute toxicity study in healthy Sprague Dawley rats (250-300g body weight) after intraperitoneal administration of WS_2 QDs at a dosage of 10mg/kg body weight. The rats were divided into four groups namely control (physiological saline), 3 days, 7 days and 14 days (WS_2 QDs treated). Body weight and clinical symptoms of all the experimental animals were monitored on a daily basis until the end of the experimental period. Blood, urine and feces were collected at the end of the experimental period.

Hematology and clinical chemistry parameters were analysed to evaluate normal functioning of the vital organs and normal physiological performance. Gross pathological examinations of the animals were done, to findout the possible gross lesions after WS_2 QD exposure. Histopathological observation of major organs such as liver, kidney, brain and spleen were observed to evaluate the possible tissue damages after WS_2 QDs administration. Various antioxidants such as reduced Glutathione (GSH), Glutathione Reductase (GR), Glutathione Peroxidase (GPx), Super Oxide Dismutase (SOD) and lipid peroxidation were analysed in the liver and brain of the experimental animals. Further blood kinetics and biodistribution of WS_2 QDs in liver, kidney, brain, spleen, blood, urine and fecal matter were analysed by Inductively Coupled Plasma-Mass Spectroscopy (ICP-MS). The kinetics study was done using ICP-MS analysis in fresh blood isolated from rats at different time intervals. Immunotoxicity in rats due to WS_2 QDs administration was analysed by spleenocyte proliferation analysis using tritiated thymidine incorporation assay.

The **fourth** chapter detailed the results obtained from the study and the **fifth** chapter is about the discussion. Both of these chapters were again divided into three sections. The first section detailed about the synthesis and characterisation of WS_2 QDs. Solvothermal exfoliation using NMP solvent is the synthesis method adopted for the synthesis of QDs. The physico-chemical characterisation of the material was done using various sophisticated techniques such as HRTEM, XRD, XPS, Zeta potential analysis, FTIR *etc.*,.

The synthesised QDs exhibited spherical morphology with an average particle size of 3-4nm. The HRTEM results confirmed that the synthesised WS_2 QDs are perfectly monodispersed, without showing any tendency of particle aggregation. WS_2 QDs dispersed in deionised water showed bright cyan green fluorescence under longer wavelength UV illumination (UV lamp). Absorbance spectra confirmed typical absorbance peak at 370nm and emission spectra showed emission wavelength at 500nm, that corresponds to cyan green fluorescence. The synthesized WS_2 QDs not only showed bright fluorescence but also were stable upto several days conserving its intrinsic fluorescence properties. FTIR spectra confirmed the chemical composition before and after exfoliation. XRD spectra confirmed the effective exfoliation of WS_2 QDs from crystalline bulk WS_2 powder. Significant reduction in XRD peak intensity and the broadening of peaks confirmed WS_2 QDs morphology. XPS spectra confirmed elemental composition and oxidation states of tungsten and sulphur in WS_2 QDs. TGA analysis revealed that a 1.5% weight loss was observed upto 450^0C temperature rise. Further increase in temperature upto 750^0C showed a characteristic 8% weight loss due to material degradation. This confirmed the excellent chemical stability of WS_2 QDs upto 450^0C temperature. DTA analysis confirmed that the net reaction favors an endothermic reaction with a characteristic melting point temperature of 466.65^0C. Zeta potential revealed the highly negative surface charge of the QDs, which also accounts for the high stability and least aggregation tendency of the WS_2 QDs. WS_2 QDs retained excellent stability upto 100 days, which was confirmed by both UV/Visible and fluorescence emission spectroscopy for about 100 days.

Endotoxin content was observed to be well below the United States Pharmacopia recommended levels of ≤ 0.5 EU/ml.

The second section detailed about the bio-nano interaction studies using LN-229 human glioblastoma cell lines. Fluorescent microscopy and flow cytometry confirmed the cellular uptake of WS_2 QDs. MTT, LDH and NRU assays for both 24 and 48h confirmed the non toxicity of WS_2 QDs upto 160µg/ml concentration. Further, a time and dose dependant cytotoxicity was observed, which was confirmed using phase contrast microscopy, Coomassie Brilliant Blue staining and Calcein AM/PI based live/ dead assay. IC_{50} value was observed to be 363.90µg/ml. ROS generation studies was done using DCFH-DA (hydroxyl/peroxyl radicals), Griess reagent assay (reactive nitrogen species) and confirmed that a dose and time dependant increase in ROS generation was observed at higher concentrations. JC-1 staining and AO staining confirmed an excellent mitochondrial activity and lysosomal integrity upto 320µg/ml concentration. Actin filament integrity after WS_2 QDs uptake was confirmed by Rhodamine phalloidin staining upto 320µg/ml concentration. Annexin V/PI and Caspase 3 expression analysis confirmed that the pathway of cell death followed by WS_2 QDs in LN-229 cells was apoptosis. Cell cycle analysis confirmed an extended S-phase at the highest concentration (320µg/ml) and DNA fragmentation was observed at this concentration. This further confirmed the apoptosis mediated cell death pathway followed by WS_2 QDs uptake in LN-229 cells.

The third section was about the acute toxicity studies in Sprague Dawley rats followed by intraperitoneal administration of 10mg/kg body weight WS_2 QDs in physiological saline. No observable level of clinical/ behavioural toxicity signs were observed in any of the treated animals when compared with the untreated control animals. Lack of significant reduction in body weight and organ weight (liver, kidney, brain and spleen) again confirmed the same. Hematology analysis in fresh blood samples collected from all the animals confirmed that a significant increase in WBC and platelet count was observed in 3^{rd} day treatment group but observed to be normal in 7 and 14 days treatment groups when compared with that of untreated control group animals. This could be because of the possible entry of extreme low dimension nanomaterials inside the lymphatic system and further evoke of an immediate onset reversible inflammatory response at higher concentrations. A significant increase in serum ALT and ALP level in the 3^{rd} day animals indicated an acute stress mediated loss of liver tissue integrity due to immediate onset particle exposure in rats. But these clinical parameters came back to normal level after 7 days of observation period. Urine analysis confirmed that all the major urine parameters were normal and highly comparable with that of the control animals.

Normal histology of liver, brain and spleen confirmed the absence of toxicity in the targeted organs after WS_2 QDs administration. Observable kidney tissue degeneration was evidenced in the 3^{rd} day group but significant tissue regeneration was observed in the 7^{th} and 14^{th} day treated animals. ICP-MS elemental detection analysis in urine and feces confirmed that a detectable amount of tungsten was evidenced in urine than feces, which confirmed that the excretion of the material from the system is via renal route (urine).

When compared to other organs, the presence of tungsten was evidenced more in kidney, which also confirmed the possibility of renal excretion pathway. The material was completely excreted out through renal excretion pathway. Comparable levels of serum creatinine in the treatment groups and control confirmed that the normal functioning of kidney was not altered as a result of WS_2 QDs exposure. Comparable levels of lipid peroxidation and antioxidant status (GR, GSH, GPx and SOD) in treatment and control groups suggested that no significant toxic responses were evidenced after WS_2 QDs i.p administration in Sprague Dawley rats.

The **sixth** chapter is the **summary and conclusion** of the study. Extreme nano dimension WS_2 QDs were successfully synthesised by solvothermal exfoliation strategy and effectively characterised using various sophisticated characterisation techniques. The synthesised WS_2 QDs were found to be extremely stable upto 100 days and retained excellent fluorescence during the period. Presence of strong cyan green fluorescence inside the cytoplasm of LN-229 cells confirmed the excellent imaging potential of the material. The bio-nano interaction studies confirmed its non-toxic nature upto 160µg/ml dose. Cytoskeletal integrity, mitochondrial membrane potential as well as lysosomal integrity was not adversely affected at the selected dose. Free radicals such as hydroxyl/ peroxyl and reactive nitrogen species were observed to be the contributing factors to the cytotoxicity of the material at higher concentrations. Intraperitoneal administration of 10mg/kg body weight of WS_2 QDs didnot evokes any organ toxicity in major organs however the degeneration in kidney may be due to the acute stress excerted by the material in kidney. Major excretion route of the administered WS_2 QDs was evidenced as renal route by kidney mediated

excretion. ICP-MS analysis showed that a significant amount of the administered WS_2 QDs was found in the urine samples when compared to feces. WS_2 QDs didnot evoke any evident toxic response upto 10mg/kg body weight i.p administration. Excellent fluorescence property shown by this material marked its prominence in *in vitro*/ *in vivo* imaging and other biomedical applications. The study proved that WS_2 QDs are excellent candidate materials validated to be safe material for biomedical applications.

CHAPTER 1: INTRODUCTION

1. INTRODUCTION

Nanotechnology is the field of science concerned with molecules whose size and thickness ranges in the scale of 1 to 100nm. According to British Standards Institution, nanoscale dimensions typically ranges from 1-1000nm, in which a nanomaterial possess any one of its external or internal dimension at this nanoscale range (Klaessig *et al*. 2011). The basic concept behind nanotechnology was coined by Richard Feynman in his lecture 'There is plenty of rooms at the bottom', at the American Physical Society meeting at California Institute of Technology in 1959, where Feynman described the concept of manipulating matter at the atomic scale. More than a decade after Feynman, a Japanese scientist Norio Taniguchi first coined the term 'Nanotechnology' to describe the semiconductor properties that occurred during the processes of separation, consolidation, and deformation of materials while thinning down to nanoscale architecture (Hulla *et al*. 2015). In a timeframe of within half a century, nanotechnology has reached far heights concerned with various scientific modalities such as electronics, optoelectronics, cosmetics, environmental remediation, energy storage to even biomedical technology offering tremendous outreach. With many diverse potential benefits, nanotechnology has been in the mainstream of science and technology offering a huge impact on human life every day. Some of the potential benefits of nanoscience and technology in biomedicine lies in biomaterial fabrication, tissue engineering, bioimaging, biosensors, antibacterial coatings of medical devices, drug delivery, tumor therapy, surgical tissue healing *etc*., (Anju *et al.* 2020). In addition to these, nanotechnology provides smart material fabrication for 3D printing and assists their application in tissue

engineering. In the area of food technology and cosmetics, a dramatic increase in the use of nanoparticles was evidenced over the past few decades especially in production, packaging, bioavailability and shelf life. While considering the integration of nanotechnology with biology, nanoarchitectonics that uses the fusion of artificial nano-systems with biological structures often attracts scientific attention in recent times, which finds applications in material science to biomedical technology (Ariga *et al.* 2019). Despite of the world's fastest-growing industry, however, due to lack of relevant toxicity profiling, much of the outputs of this emerging scientific discipline remains behind the curtain. Proper investigation of the toxicity profiling and further validation of various physico-chemical properties of nanoparticles are therefore mandatory to evaluate the hazardous effects of NPs in the living system. Yet then, nanotechnology is a rapidly growing industry with pretty voluminous applications and so is the future potential of the same.

1.1 Nanoparticles

Nanoparticles and nanostructured materials represent an actively investigating area of material science with potential expansions along various interdisciplinary arenas. Nanoparticles (NPs) are tiny microscopic materials with at least one dimension that lies within the nanometer scale of less than 100nm (Klaessig *et al*. 2011). It differs from its bulk counterpart in terms of physical, chemical, mechanical as well as optical characteristics (**Figure 1.1)**. The first scientific description about colloidal nanoparticle synthesis happened in 1857 when Michael Faraday reported the synthesis of colloidal gold NPs, which initiated the history of colloidal NP synthesis. Faraday often revealed that the physico chemical properties of these tiny structures

are extremely different from that of the bulk materials. This can be probably one of the earlier reports where quantum size effects were evidenced and described.

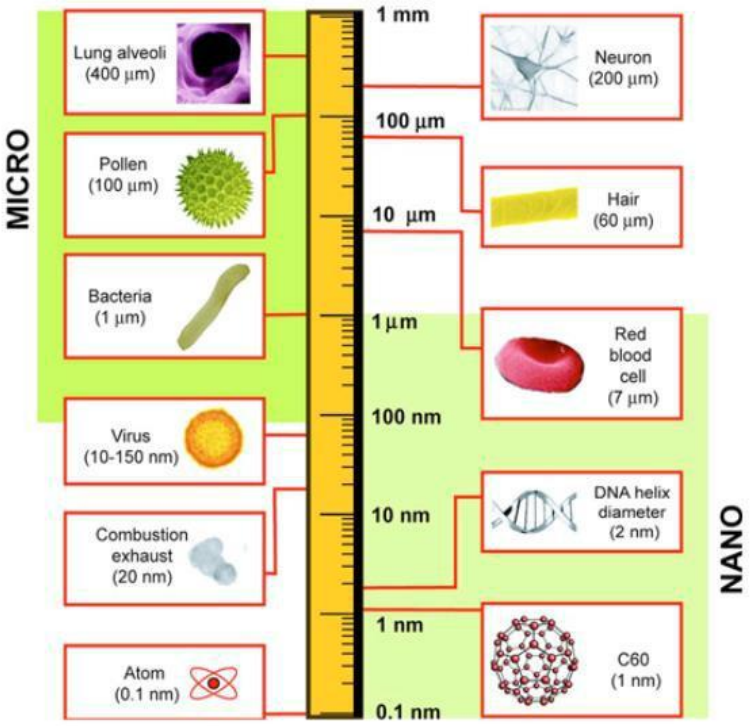

Figure 1.1: Logarithmic scale showing size of nanoparticles**.**
Adapted from (Buzea *et al.*2007)

A typical size-dependent property of quantum confinement is observed while thinning down the bulk materials to extremely small-sized particles such as semiconductor quantum dots (QDs). This strictly indicates that the various physico-chemical characteristics of NPs can get altered as a function of size (Chen *et al*. 2019). NPs possess a high surface area that accounts for their extreme surface reactivity. A large surface area to volume ratio is one suggestive for the reduction in the intrinsic melting temperature of NPs. NPs is often found to be ubiquitous in the environment. They may originate from natural as well as from synthetic sources. Naturally occurring NPs are often exposed into the atmosphere by various means

such as storm dust, volcanic eruption, forest fires, engine exhaust and biomolecules such as algae and fungi. Synthetic NPs or engineered NPs (ENPs) are man-made and results from incidental exposure. These are pure forms and the size typically ranges from 1-100nm exhibiting controlled surface morphology (Sadik. 2013). Some well-known examples include fullerene, graphene, carbon nanotubes, quantum dots and semiconductor NPs. Diverse range of ENPs currently exists in the market due to advancements in various synthetic strategies. Therefore the subsequent question of risk assessment becomes highly influential in recent times as there exist an exponentially increased fabrication and subsequent release of NPs into the environment.

1.2 Types of Nanoparticles

Nanoparticles can be classified into different types based on their size, morphology, dimensionality, physical and chemical characteristics.

1.2.1 Classification of NPs based of dimensionality

NPs are classified based on their dimensionality **(Figure 1.2).**

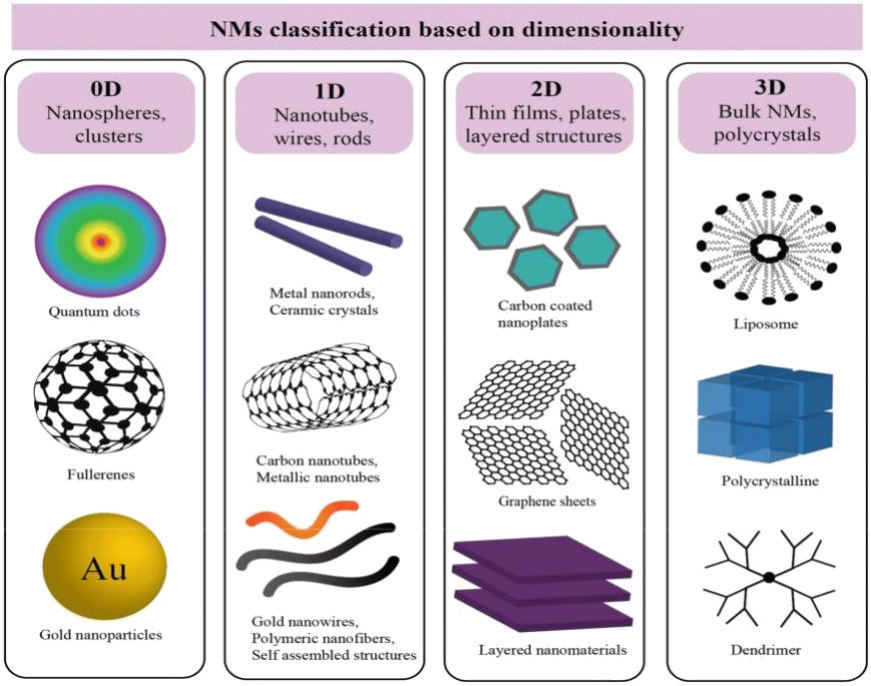

Figure 1.2: Classification of nanoparticles based on dimensionality. Adapted from (Poh *et al.* 2019)

1.2.1.1 Zero dimensional NPs

Zero dimensional NPs (0D NPs) are mostly spherical or quasi-spherical in morphology with dimensions less than 10nm, which exhibits ultra-small size (less than 10nm), quantum confinement effect and stable luminescence. Quantum dots (QDs) in general falls under this category. Active edge sites and quantum confinement effect endow them with novel properties such as high photoluminescence quantum efficiency (Jiang *et al.* 2018). QDs offer great potential in target analyte detection, biomolecular sensing, disease diagnosis and high contrast imaging-guided therapies (Yao *et al.* 2018). 0D NPs exhibits novel properties such as high chemical stability, chemical inertness, wavelength dependant optical emission and stable photoluminescence with reduced photobleaching effect (Chen *et al.* 2019).

1.2.1.2 One dimensional NPs

In one dimensional NPs (1D NPs), atleast one dimension falls outside the nanoscale limit whereas the rest of the two dimensions will be in the nanoscale. Classic examples include nanotubes, nanowires, nanorods, nanofibres and nanofilaments. They possess excellent electrical, mechanical and thermal properties when compared to other nano dimensionalities. These are widely explored for energy storage and energy harvesting purposes especially in solar cells, thermal conversion devices, piezoelectric devices and super-capacitors (Han *et al.* 2014). Nanowire like 1D nano-architecture has got significant attention owing to its space confined transport phenomena and stable electrical conductivity (Dresselhaus *et al.* 2003). In biomedical technology, 1D NPs like nanotubes are used for targeted sustainable drug release applications.

1.2.1.3 Two dimensional NPs

Two dimensional NPs (2D NPs) are composed of thin layers or sheets having individual layer thickness less than 10nm. 2D materials possess only one dimension (mostly layer thickness) in the nanoscale and the other two dimensions falls outside the nanoscale range. They possess high surface area to volume ratio which facilitates more atoms on its surface (Jayakumar *et al.* 2018). Therefore 2D materials can be used for targeted delivery of large amount of bioactive molecules. In biomedical technology, 2D materials can be used for various applications such as targeted sustainable drug release, NIR photothermal/photodynamic therapy, 3D printing scaffolds, tissue engineering scaffolds and enzyme immobilization (Anju *et al*. 2020).

1.2.1.4 Three dimensional NPs

Three dimensional NPs (3D NPs) are materials that are not confined to nanoscale at any of the dimensions. This class of NPs usually consists of bulk materials, multi nanolayers, and bundle of nanotubes or nanowires. Well-ordered 3D NP architectures have got significant attention in various applications but effective techniques to fabricate these structures in a cost-effective manner become the underlying default that hinders its advancements (Sun *et al.* 2019).

1.2.2 Classification based on physico-chemical properties

NPs are classified based on their physico-chemical properties **(Figure 1.3).**

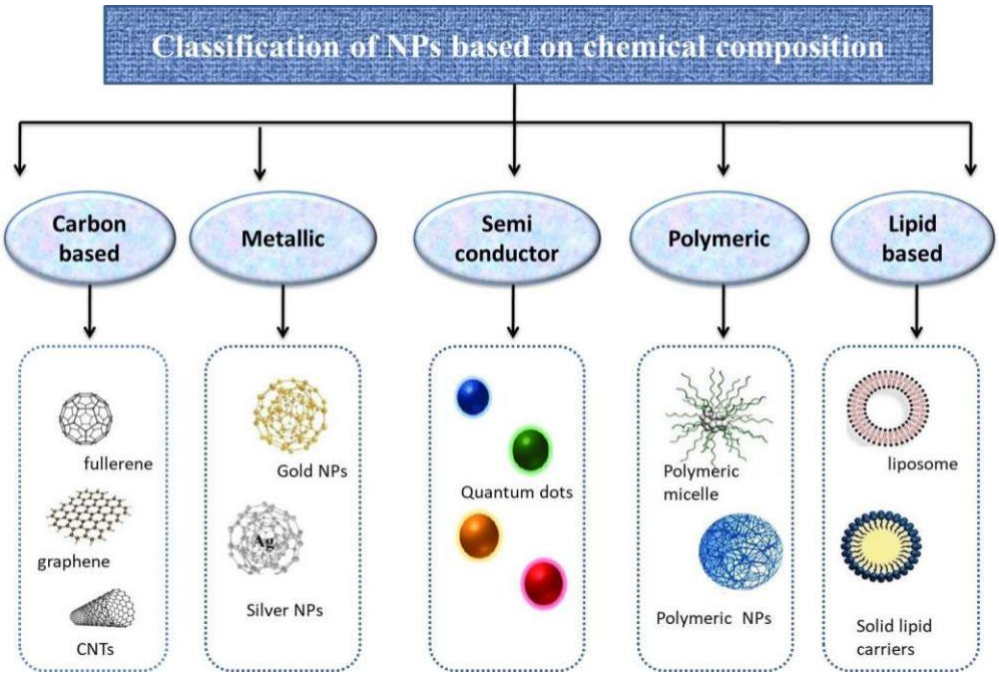

Figure 1.3: Classification of nanoparticles based on physico-chemical properties

1.2.2.1 Carbon NPs

Graphene, fullerene and carbon nanotubes (CNTs) represent classic examples of carbon-based NPs. Graphene with its honeycombed lattice structure attracted scientific attention owing to its intriguingly appealing characteristics well adapted for various applications, especially in biomedicine (Cherian *et al.* 2019). Buckyball structured fullerenes such as C60, C70 and fullerene soot created noteworthy interest for various commercial purposes like fillers and adsorbents for environmental remediation (Coro *et al.* 2016). Similarly, CNTs showed promising potential in fuel cells, environmental remediation and biomedical applications.

1.2.2.2 Metallic NPs

Metallic NPs exhibit the well-known phenomenon of localized surface plasmon resonance, which accounts for the unique electrical properties shown by these materials (*Garcia et al.* 2019). NP of alkali and noble metals usually falls under this category. They possess broad absorption characteristics in the entire visible region of the electromagnetic spectrum (El-Seedi *et al.* 2019).

1.2.2.3 Semiconductor NPs

Semiconductor NPs are fluorescent materials, which are of significant interest due to their unique physico-chemical characteristics such as large surface area, quantum confinement effects, stable luminescence and non-linear optical properties (Iwasawa *et al.* 2000). Typical semiconductor NPs possess size that ranges from a few to a few

tens of nanometers that accounts for the unique properties versatile from that of their bulk counterpart. They possess promising applications in solar cells, laser technology, nanoscale electronics, LEDs and biosensing.

1.2.2.4 Polymeric NPs

Polymeric NPs exist in a size range of 1 to 1000nm and can be used extensively to load active molecules either adsorbed on the surface or entrapped into the polymeric core (Zielinska *et al.* 2020). Polymeric NPs are widely used as drug carriers for controlled and sustainable drug release due to their ability to shield drugs or bioactive molecules from the external environment during circulation. Mostly exist in nanocapsule or nanosphere forms, which are recognized as reservoir systems. Nanocapsules are composed of an oily core; surrounded by polymeric shell in which the bioactive molecule is dissolved in the core for the sustainable release profile of the drug (Sadik. 2013). Nanospheres are composed of continuous polymeric networks in which the drug molecule can be either adsorbed on to the surface or retained inside the core for controlled drug release.

1.2.2.5 Lipid based NPs

Lipid based NPs represent a relatively recent colloidal drug delivery system that comprises lipid molecules in their solid state with an average size of 50-1000nm. These are the foremost among the promising colloidal carriers for organic bioactive molecules. Liposomes, solid-lipid NPs and nanostructured lipid carriers constitute the three major classes of lipid based NPs. They showed only a negligible level of

toxicity as per reports and can transport both hydrophobic as well as hydrophilic molecules (Knudsen *et al.* 2015). Add-on surface chemical modifications via polyethylene glycol (PEG) or gangliosides can significantly improve the circulation time of these nano formulations at the same time escaping from the immune system (R Rama *et al.* 2016).

1.2.2.6 Ceramic NPs

Ceramic NPs belong to inorganic, non-metallic NPs that are found in amorphous, dense, hollow, polycrystalline as well as porous morphology. Therefore these NPs found immense applications in the area of photocatalysis, photodegradation of toxins, and tissue engineering scaffold designing in biomedicine (Liu *et al.* 2017). These NPs are usually made up of carbides, oxides, phosphates and carbonates of metals or metalloids such as calcium, titanium or silicon based materials (Liu *et al.* 2017).

1.3 Importance of QDs in present era

Quantum dots (QDs) are semiconductor nanocrystals having a dimension less than 10nm, which possess excellent physico-chemical characteristics well adapted for various applications that span from electronics, optoelectronics to even biomedical technology. QDs were first discovered in 1980's by a Russian solid state Physicist Alexei Ekimov and the theoretical concept was elaborated by Alexander Efroz. Mostly QDs are composed of semiconductor materials from group II to V of periodic table (Jacak *et al.* 2013). QDs are regarded as particles with physical dimensions

smaller than the exciton Bohr radius. After more than two century of their introduction into the scientific world, the applicability of QDs has got far reaching heights due to their intriguingly appealing characteristics. QDs possess several advantages over bulk materials which include extremely small size (1-10nm), high surface area to volume ratio, tunable photoluminescence, high extinction coefficient, excellent quantum confinement effect, high stability against photo bleaching as well as excellent fluorescent intermittency (Bera *et al.* 2010). QDs possess narrow absorption spectra and size tunable broad excitation dependant emission spectral characteristics. They emit highly stable fluorescence with extremely reduced photobleaching effect when compared to conventional organic fluorescent dyes. Therefore QDs are excellent candidate choice in optoelectronics and imaging based biomedical applications.

Today, these materials are been extensively explored in laser technology, solar cells, light emitting diodes and liquid crystal display for energy storage and dissipation (Kargozar *et al.* 2020). High molar extinction coefficient of QDs is one reason for their stable bright fluorescence. This highly stable fluorescence emission enables extended dynamic imaging in biomedicine. Therefore QDs are excellent choice material for various imaging guided therapies such as Positron Emission Tomography (PET), Single Photon Emission Computed Tomography (SPECT), Magnetic Resonance Imaging (MRI) and Computed Tomography (CT). QDs are highly photostable, therefore these are ideal candidates for multimodal imaging to scrutinize various processes that happen inside the living system (Pawar *et al.* 2018). Concerning these aforementioned properties, QDs has got a significant reputation in the field of biomedicine.

QDs can be excited at any wavelength ranging from UV to far infrared. They are highly resistant to metabolic and chemical degradation. Therefore these are widely explored in photothermal and photodynamic therapies as photosensitizer molecules. This has become a revolutionary trend-set in cancer theranostics. QDs possess broad excitation and narrow size tunable emission spectra; therefore multiple QDs can be excited at a single wavelength. This typical feature can be explored to make QDs excellent candidates as donors or acceptors in Fluorescence Resonance Energy Transfer (FRET) based sensors. Also, QDs emits sharp and symmetric fluorescence emission spectra that account for the better sensitivity of QD based sensors. Alongside, larger stokes shift is a characteristic feature of QDs that significantly reduces auto fluorescence effect inside the biological system. This will further improve the sensitivity and selectivity while performing sensing and imaging applications in *in vivo* systems (Molaei. 2020). Due to extended fluorescence brightness and stability, live imaging of animals can be possible using QDs instead of organic fluorescent probes.

1.4 Photo-physical properties of QDs

Due to fine-tuned confinement of electron-hole pairs (excitons), QDs exhibits some unique photo physical properties strictly in contrast from their bulk counterpart. These include stable fluorescence emission characterized with broad absorption spectra and narrow size tunable emission spectra, reduced photobleaching effect, large stokes shift, photochemical robustness, reduced fluorescence intermittency as well as massive absorption extinction coefficients. QDs exhibit size dependant discrete energy levels and the energy gap increases with a decrease in size of QDs.

The typical wavelength of photon emission is therefore strictly dependant on the size of QDs rather than the chemical composition or morphology. The ability to control size will determine the emission wavelength and subsequently the color which the human eye can perceive. Smaller dots will therefore emit blue and the bigger ones will probably shift towards red. Thus a broad spectral wavelength from UV to infrared (400-4000nm) is possible with QDs (Pietryga *et al.* 2004). These unique and robust photo-physical properties make QDs highly versatile candidates for various biomedical applications with significant superiority over conventional fluorophores. Various photo-physical properties of QDs are detailed below;

1.4.1 Stable fluorescence emission

QDs emit fluorescence when their electrons get excited under an irradiation source and return to the ground state with the concomitant emission of photons. Fluorescence emitted by QDs were reported to be stable for several hours under continuous irradiation allowing high contrast imaging of potentially malignant tumor tissues (Mordorski *et al.* 2016). This emission can be tuned from UV to infrared spectral region by tuning the size of QDs. This emission is strictly resistant to photo bleaching effect when compared to conventional organic fluorescent dyes and probes.

1.4.2 Broad absorption spectra and narrow emission spectra

QDs; especially TMDC based QDs possess broad absorption spectra that make it excited along the entire range of UV/Visible spectrum of light. This typical feature

shown by QDs makes them an attractive choice for excitation dependent emission based applications. Therefore, QDs can be used for the fabrication of imaging probes to replace the conventional fluorescent dyes. Emission wavelength shown by QDs is mostly size dependent. Larger the QD size, red shift will predominates while smaller ones will emit blue to green fluorescence (Mordorski *et al.* 2014). Large bandgap between excitation and emission region shows that the QDs have excellent detection sensitivity as the entire emission spectra can be detected.

1.4.3 Fluorescent quantum yield

Fluorescent quantum yield (Φ_f) is an essential parameter to be analyzed during the assessment of the luminescent features of QDs. It is described as the ratio of the amount of emitted photons to that of the absorbed photons by a QD (de Araujo and Dominguez. 2020). This is a quantitative representation of the fluorescence emission efficiency of QDs.

1.4.4 Photochemical stability

QDs are more resistant to photochemical degradation than any other optical imaging probes or dyes. This will allow the tracking of cellular processes for an extended period time. This typical property is mainly attributed to the inorganic semiconductor nature and fluorescence intensity of QDs (Bailes. 2020). Several studies have reported that the chemical and thermal stability of QDs can be drastically improved by surface passivation techniques such as shell encapsulation using cross-linkable block copolymer ligands.

1.4.5 Reduced photobleaching

Photobleaching refers to the permanent photochemical alteration of a fluorescent dye or probe so that it no longer can able to fluoresce. Extended light irradiation followed by non-specific reactions damaging the chemical stability of the molecule is one suggestive reason for this phenomenon (Liu *et al.* 2017). QDs are far less susceptible to photobleaching. QDs can constantly emit fluorescence for about a thousand more cycles than any conventional fluorescent dyes due to this reduced photobleaching tendency and high fluorescence stability.

1.4.6 Stokes shift

Stokes shift is one common feature of QDs, which is the difference between the peak excitation and emission wavelengths under the same electronic transition of QDs (Xing and Rao. 2008). It is the pronounced quality of colloidal QDs typically ascribed to the splitting between dark and bright excitons. It is often referred to as the photoluminescence red shift relative to absorption. A large stokes shift is usually employed for QDs when compared to conventional organic fluorophores. A large stokes shift may usually indicate a comparatively fast relaxation from the initial excited state to the emissive state. It will drastically improve the detection specificity of QDs. Exceptionally large stokes shift of upto 400nm makes QDs excellent candidates for multicolor detection with a single wavelength excitation source.

1.4.7 Fluorescence intermittency

Fluorescence intermittency is a common phenomenon shown by all fluorescing materials such as dyes, probes or QDs. It is referred to as the random switching between the bright and dark states of a fluorescent material under continuous excitation (Bianco *et al.* 2005). This fluorescence intermittency or blinking is common in charged nanocrystals or when the QDs get ionized. In normal conditions, when a nanocrystal is neutral or non-ionised, the incoming photons excite the electron-hole pair with the emission of another photon; giving fluorescence. But once the QDs get ionized or when charges are exposed on their surface, non-radiative Augor recombination will occur leading to the transfer of this emitted energy to an extra electron (Frantsuzov *et al.* 2008). This will cause blinking and subsequent suppressing of the photoluminescence process in charged species. Surface defects also play key role in this phenomenon by acting as temporary traps whereby affecting the recombination of electrons and holes leading to blinking and reduction in quantum yield (Mishra *et al.* 2017). Blocking of crystal ionization and reducing surface defects are the only suggestive solutions for this phenomenon.

1.5 Toxicology

Toxicology is a scientific discipline that overlaps with biology, chemistry, medicine, epidemiology and pharmacology, which specifically deals with the intensive study of diverse adverse effects of chemicals or other substances in the living system alongside researching on its various diagnosis and treatment strategies (Klaassen. 2013). Toxicology aims to minimise the possible adverse outcomes of compounds such as drugs, chemicals and other materials in the human population and the environment. Paracelsus, the father of modern toxicology has historically stated that "Solely the dose determines that a thing is a poison or not", which means, the dose of any substance determines whether it is a poison or not and is a factor of prime importance in toxicology (Borzelleca. 2000). Therefore dose assessment is the most crucial factor while determining the toxicity of any compound and every substance in the universe is said to be toxic if administered above a specific dose (Eaton and Gilbert. 2008). A conventionally adopted strategy to analyze the relationship between dose and toxicity states that the increase in exposure to a chemical can increase its risk of eliciting a toxic response. Therefore toxicity can be increased with an increase in the administered dose, which is determined as dose response. However, various studies have reported the influence of endocrine disrupters which statistically encounters this straight-forward relationship between dose and toxic response in the living system (Klaassen *et al.* 2013). Toxicological studies include various key factors that critically involve the detection, identification and quantification of toxic effects or hazards that arise from the exposure of living beings with chemicals or toxicants.

It also deals with the issues concerned with public health aspects of toxicants/ chemicals as well as testing of novel pharmaceutical products beneficial to mankind. Since conventional toxicology deals with adverse effect identification at organ and organ system level, modern toxicology concerns with a deep investigation of adverse effects at the cellular, molecular and genome level. Infact, toxicology is a unique branch of science that is found to be able to achieve a perfect balance between scientific inventions and direct public sector application which most scientific disciplines still unable to achieve.

1.5.1 Nanotoxicology

Nanotoxicology represents a rapidly growing area of toxicology. Nanotoxicology is the study of the toxicity of nanoparticles with the intension of determining the possible adverse effects which any NP can impact in the living system. Stringent characteristics such as large surface area to volume ratio, extremely small size to penetrate deeper inside tissues and certain unique physico chemical properties will critically affects nanomaterial toxicity. Various other factors that lead to nanomaterial toxicity include different physico chemical properties of NPs such as their size, morphology, surface charge, crystalline nature, surface area, surface functionalization, ionic dissociation, colloidal stability and solubility. Apart from these inherent material characteristics, certain environmental factors such as ionic strength, pH, temperature and salinity can also influence nanomaterial behaviour, fate and the extend of nanomaterial toxicity (Walters *et al.* 2016). As nanotechnology evidenced a drastic steady-state growth

over the past few decades, nanoscale materials got significant hikes in various fields especially in electronics, optoelectronics, medicine and pharmacy. It was reported that a 10-30 fold increase was reported in the production of nano-based products over the past few years (Vance *et al.* 2015). Metallic NPs represent the fastest-growing category of nanotechnology, therefore a dramatically increased human and environmental exposure has been evidenced from the past few decades. This steady growth in nanotechnology and nanotechnological inventions always left behind unpredicted adverse effects which most of the researchers leave unnoticed. NPs can easily penetrate cell membranes without entering into any endocytosis pathways due to their extremely unique small size.

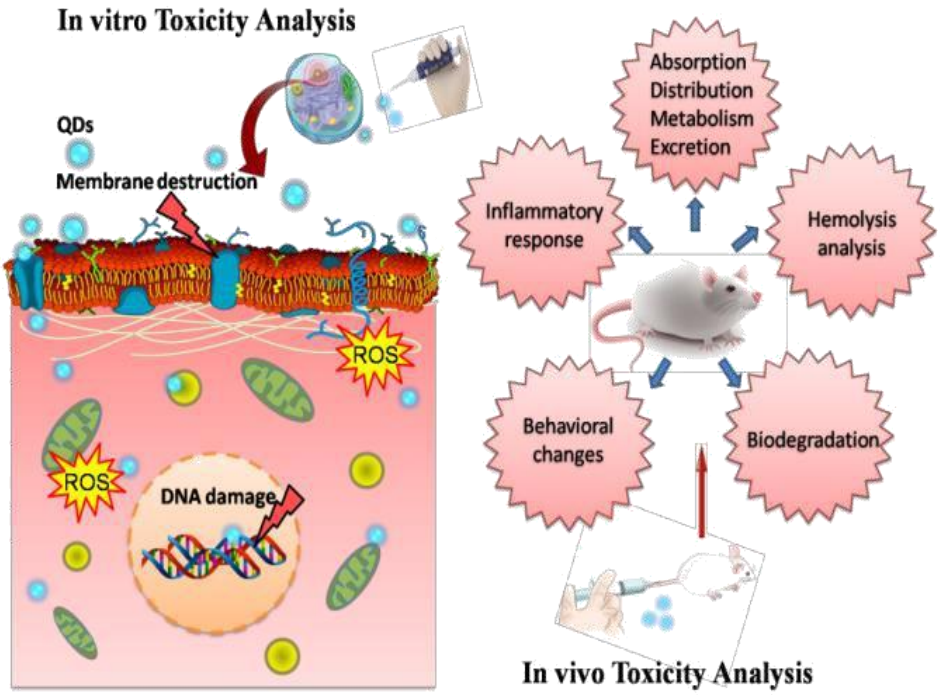

Figure 1.4: Various toxicity assessments after QDs exposure.
Adapted from (Anju *et al.* 2020).

Many NPs such as graphene NPs were reported to even cross placental as well as blood brain barriers causing serious adverse effects (Cherian *et al.* 2019). Even reproductive and further developmental toxic responses have been evidenced so far with many leading NPs which are currently under insight investigations. Apart from size and shape; morphology also represents a critical factor while considering nanomaterial toxicity and further complications. NPs while discarding without proper safety measures can enter into aquatic ecosystem as soluble ions and insoluble aggregates; can cause serious irreversible damages to aquatic flora and fauna. Thus the underlying consequences of nanomaterial toxicity spread along the entire strata of the ecosystem and environment. Proper evaluation and toxicity assessment of any nanomaterial is therefore a mandatory criterion to be executed before validating any nanomaterial safe intended for various applications, especially in the field of biomedical technology (**Figure 1.4)**.

1.6 LN-229 Glioblastoma cells in neurotoxicity

Glial cells are non-neuronal cells of the Central Nervous System (CNS), which particularly serves the function of providing nourishment to neurons. These cells are of prime importance in neurotoxicity and related researches due to their high potency in division and comparable characteristics with primary astrocytes. The major neuroglial cells include astrocytes, microglial cells and oligodendrocytes. These cells maintain a stable micro environment for the homeostasis of brain neurons. A typical reciprocal relationship exists in between neurons and glial cells that mark a vital compartment for the effective development and proper functioning of neurons.

Therefore any external or internal factors that affect normal glial cell functioning can directly or indirectly affect proper neuronal functioning. Any improper functioning or massive perturbations in glial cells can lead to major metabolic intermediate accumulation in the CNS leading to massive improper functioning of neurons, which inturn may lead to neuronal degeneration and related disorders (Aschner *et al.* 1999). Therefore glial cells marked its significance in neurotoxicological researches from long back itself.

Metal containing NPs and semiconductor NPs has got significant attention in the diagnosis and treatment strategies of most of the neurodegenerative disorders and glioblastoma like conditions. Especially Quantum dots have got significant attention to be used as imaging probes for imaging guided therapies of central nervous system disorders. Most of the metal containing NPs and QDs, due to extremely low size and surface charge can effectively cross the blood brain barrier (Lovisolo *et al.* 2018). Most of the traditionally employed QDs contain extremely toxic heavy metals such as cadmium and lead, which were already reported to be neurotoxic. Compared to such conventional QDs, TMDC based QDs shows the ability to emit strong excitation dependant fluorescence properties due to which MoS_2 and WS_2 QDs got significant attention in the disease diagnosis, imaging based drug delivery, targeted tumor destruction and cancer immunology related fields in neuroscience. Since majority of the applications of QDs spans in neurological fields, neurotoxicity assessments sounds an unavoidable factor. Even then, various factors such as size, morphology, crystallinity, aggregation tendency and solubility of such QDs can inturn direct to various toxicological effects in the biological system.

Cellular uptake of QDs and related nano-bio interactions can subsequently alter the normal biochemical processes in glial cells. Therefore it is obligatory to analyse the potential toxicity of such materials to probably avoid future adverse effects. Such toxicity profiling datas represents strong implications for analysing the possibility of further consequences while applying these materials for various biomedical applications.

Most of the researches till date masked the relevance of nanomaterial toxicity while seeking the huge application possibility of such emerging materials. A toxicological research potentially tries to alleviate this scenario by evaluating the indepth toxicity profiling of any nanomaterial having such fascinating application possibilities. To date, no systematic evaluation of QD interactions with brain cells was done that can put forward as a strong evidence before validating QDs safe for various applications (Zhang *et al.* 2019). Since quantum dots and related researches represent a potential candidate in neuroscience and related biomedical fields, QD toxicity in glial cells sounds a necessity. Apart from its potential applications, the proper indepth assessment of toxicity represents an unavoidable factor. The exposure dose and subsequent cellular responses are key factors in toxicology. Therefore, proper elucidation of a perfect dose that suits a non-toxic response is mandatory before subjecting these materials for direct application purposes. With the widespread use of such semiconductor QDs, potential neurotoxicity elucidation is inevitable. Based on these reasons, LN-229 glioblastoma cells seems a suitable candidate material for the *in vitro* toxicity and nano-bio interaction studies of the synthesised WS_2 QDs.

1.7 Motivation of the study

QDs gained prominent status in imaging based and biosensor designing applications due to its prolonged fluorescence emission properties alongside reduced photobleaching effect. Most of the conventionally employed QDs consist of toxic heavy metals such as cadmium and lead, which evokes serious side effects once it enters a living system. Therefore, development of biocompatible and non-toxic QDs seems essential to sustain biomedical researches especially in imaging guided theranostics.

TMDC based nanomaterials and quantum dots has got scientific attention and fundamental research progress very recently owing to their intriguingly appealing characteristics well suited for various biomedical applications. WS_2 is a relatively new material that belongs to the family of TMDC compounds, which marked significant focus in various interdisciplinary arenas due to its potential characteristics that surpass the major defects associated with graphene family of compounds. Such compounds like WS_2 and MoS_2 show easiness of exfoliation into various nanodimensionalities (0D, 1D and 2D). High sensitivity, high spatial resolution, deeper tissue penetration ability and high contrast-non invasive fluorescence emission characterised with these materials hold them as promising candidates in biomedical researches. But while exfoliating down to QD dimensionalities, unprecedented adverse effects due to extreme small size, morphology and chemical composition always limit its further advancement.

It is assumed that these materials are safe over a wide range of concentrations but none of the studies proved its long term exposure adverse effects and further mechanism of action. No reliable studies proposed a safe dose for this material still.

Metallic NPs and semiconductor QDs represents a promising category of NPs which focussed scientific attention from very long back itself, therefore a dramatically increased human and environmental exposure has been evidenced from the past few decades. This steady growth in nanotechnology and nanotechnological inventions always left behind unpredicted adverse effects, which most of the researchers leave unnoticed. Most of the researches related to TMDC based semiconductor materials focus on developing new innovative applications but none of them has contributed in elucidating its inherent toxic nature and thereby proposing a safe dose for its general biomedical applications. Also, the maximum safe doses that avoid environmental adverse effects need thorough investigation. Therefore, apart from researches on the potent application possibilities of these materials, an in depth toxicological evaluation of the same in *in vitro* and *in vivo* systems seems a mandatory criterion. Before validating any new material safe intended for biological applications, a comprehensive toxicity profiling of the compound is obligatory. Based on the above said observations, an effective strategy was adopted to synthesise highly fluorescent WS_2 QDs and to further elucidate the toxicological profiling of the material for futuristic applications.

1.8 Objectives

Transition metal dichalcogenide family compound WS_2 and its highly fluorescent nanodimension; the quantum dots; marked renaissance in the field of optoelectronics, energy storage, biosensor designing and imaging guided biomedical applications. Proper toxicity profiling is considered as a mandatory criterion before validating this material safe intended for such applications. Hence an effort was made to elucidate the toxicity profiling of WS_2 QDs in detail. Based on the available literature, it was hypothesised that WS_2 QDs are highly fluorescent and non-toxic transition metal based QDs applicable for imaging based therapies in biomedical scenario. To achieve the hypothesis, four major objectives were formulated, which are detailed below;

Objective 1: Synthesis of Tungsten Disulphide Quantum Dots (WS_2 QDs)

Objective 2: Optical and physico-chemical characterization

Objective 3: *In vitro* cytotoxicity studies in LN-229 human glioblastoma cells

Objective 4: *In vivo* studies using Sprague Dawley rats: biodistribution, organ toxicity, immunotoxicity by spleenocyte proliferation, histopathology (brain, liver, kidney, spleen), toxico-kinetics and elemental analysis by ICP-MS (brain, liver, kidney, spleen, blood, urine and feces).

Interaction of nanoparticles with living system depends primarily on its physico-chemical characteristics such as size, shape, morphology, chemical composition, surface charge, elemental state and surface functionalization.

Therefore proper elucidation of the fundamental properties of any nanoparticle is essential before validating them to be safe intended for various applications; especially biomedical applications. In the present study, WS_2 QDs of bright cyan green fluorescence was synthesised using solvothermal exfoliation method. The synthesised QDs exhibits spherical morphology and monodispersive nature without agglomeration tendency. The bio-nano interactions and cytotoxicity elucidation was conducted using LN-229 glioblastoma cell lines. Varying concentration from extreme low to high concentrations under varying exposure time was used for *in vitro* studies to determine the safe dose and IC_{50} value. Acute toxicity evaluation was done in Sprague Dawley rats after intraperitoneal administration of 10mg/kg body weight dosage of WS_2 QDs. Also, the *in vivo* biodistribution status, blood kinetics and immunotoxicity were elucidated after intraperitoneal administration of QDs. The experimental design of the study is summarised in **Figure 1.5**.

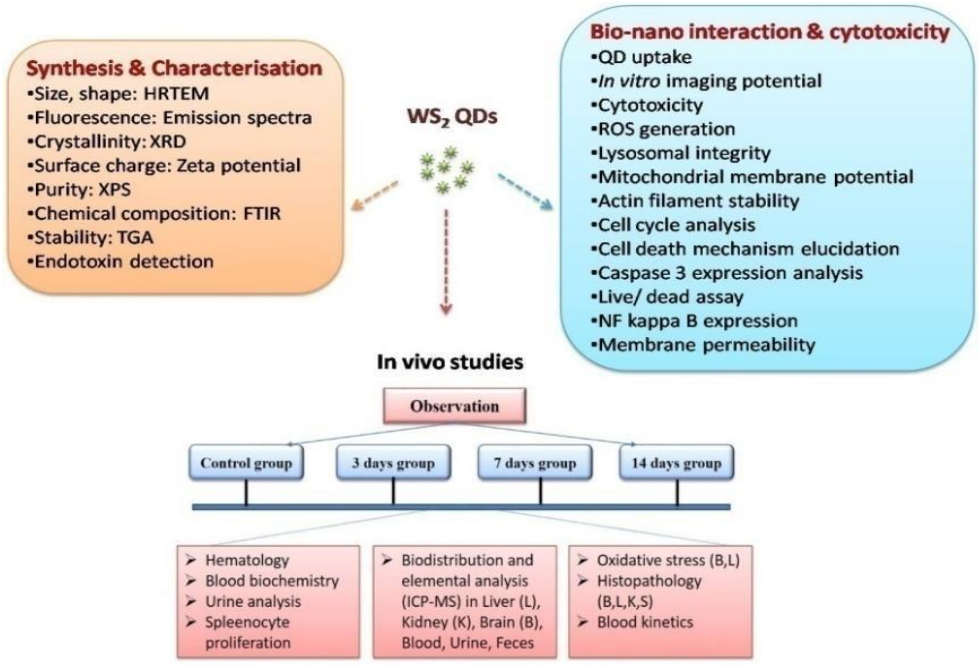

Figure 1.5: Experimental design of the thesis

1.9 Thesis Outline

The entire thesis is divided into six parts. The **first chapter** is the **introduction**, which describes the background of the study and the connotation of the study. This chapter briefed about the classification of nanoparticles, significance of quantum dots in the present era, photophysical properties of quantum dots and the toxicity. A precise description about the motivation of the study and the significance of glial cells in neurotoxic behaviour of QDs are also included in this chapter.

The **second chapter** briefed about the **review of literature** available regarding the thesis topic. This chapter detailed about the available literature regarding the various synthesis routes, structure and characterisation of QDs and various applications of QDs. This chapter also discussed about the toxicity of QDs, various routes of exposure and mechanism of toxicity associated with nanoparticles and QDs.

The **third chapter** detailed about the **materials and methods** adopted for the study. This chapter is further divided into different sections. The first section detailed about the synthesis and physico-chemical characterisation of WS_2 QDs. The synthesis strategy adopted involves solvothermal exfoliation. The second section of this chapter described about the cellular uptake, nano-bio interactions and cytotoxicity elucidation of the material in LN-229 human glioblastoma cell lines. The third section of this chapter detailed about the acute toxicity studies in Sprague Dawley rats after intraperitoneal administration of WS_2 QDs *in vivo*. This section discussed about the organ toxicity, biodistribution, blood kinetics, immunotoxicity and related pathological changes associated with the QDs under *in vivo* conditions.

The **fourth chapter** detailed about the results of the study. This chapter is also divided into three subsequent sections. The first section detailed about the results of the synthesis and characterisation part. The second section is about the results of bio-nano interaction studies and cytotoxicity elucidation in LN-229 glioblastoma cells. The third section detailed about the acute toxicity studies after intraperitoneal administration of WS_2 QDs, which explains about the fate of this nanosystem in *in vivo* conditions. The biochemical and hematological parameters, target organ toxicity, biodistribution status, toxicokinetics, immuno toxicity evaluation and related pathological anomalies were detailed in this section.

The **fifth chapter** is about the **discussion** of the results. This chapter is also divided into three sections. Section one discussed about the synthesis and physico-chemical characterisation part. The second section discussed on the bio-nano interaction studies and cytotoxicity of the material. The major outcomes of the *in vitro* studies are discussed in this section in detail and compared with the status of the available literatures about similar materials. The last section of this chapter discussed about the acute toxicity studies in rats.

The **sixth** and the final chapter detailed about the **summary** and **conclusion** of the whole thesis work.

CHAPTER 2: REVIEW OF LITERATURE

2. REVIEW OF LITERATURE

2.1 Nanoparticles Vs Quantum Dots

Nanoparticles (NPs) and quantum dots (QDs) have been widely studied for the past few decades for optoelectronic, catalytic and sensing applications. NPs are ultrafine particles having structural dimensions less than 100nm at least in one direction. Because of their ultrafine size, NPs possess certain unique material characteristics that are suitable for practical applications in various fields. Size dependant properties such as quantum confinement in semiconductor NPs, superparamagnetism in magnetic NPs and surface plasmon resonance in some metallic NPs are among a few (Khan *et al.* 2019). They possess high surface area when compared to their bulk counterpart. Based on size, morphology, physical and chemical characteristics, multidimensional NPs are being manufactured day by day. This includes nanofibers, nanowires, nanosheets, nanostars, nanospheres, nanoflowers, nanoreefs, nanowhiskers, monolayers as well as QDs (Yan *et al.* 2016).

QDs are colloidal semiconductor nanocrystals having dimension less than 10nm, which endow them with certain unique physico-chemical characteristics well adapted for various applications especially in electronics, opto-electronics and biomedical technology. QDs were first discovered from glass crystals in 1980's by Alexei Ekimov, a Russian physicist (Ekimov *et al.* 1981). Later, an American chemist Louis E Brus has observed similar phenomenon in colloidal systems also. He proposed that the confinement of electrons is the characteristic that bestows any particle with quantum properties (Brus. 1983). QDs are a group of atoms made of semiconductor

materials that have a promising adaptability to revolutionize the whole scientific disciplines ranging from photovoltaics to biomedical technology. Each nanocrystal comprises hundreds to thousands of atoms located at the crystal surface that facilitates the increased surface area of QDs. A perfect quantum crystal makes bright luminescence and the band gap is determined by its size. They exhibit strong light dependant electrical and optical properties. Upon absorption of light and resultant electron hole recombination, excitons are generated on the outer orbital of these nanocrystals that contributes to its strong fluorescence emission. QDs exhibit broad absorption spectra and size tunable narrow emission spectra. QDs are photochemically robust in nature and are resistant to photobleaching effect shown by most of the organic fluorescent dyes. By adjusting the dot size and composition, energy states can be fine-tuned based on its applications. QDs are very much resistant to photo-chemical degradation and photobleaching. Due to the presence of dangling bonds or unpaired outer shell electrons, QDs shows a typical property of fluorescence intermittency. Although depicted as spheres; according to certain previous literatures, it can exist in certain other morphological forms such as monolayers also, analogous to their bulk counterpart (Shin *et al.* 2006). Mostly monolayer forms are found in transition metal dichalcogenide (TMDC) family of compounds since their bulk material is mostly in the 2D form. Apart from carbon dots (C- dots), most of the QDs that have been synthesised so far involves toxic metals (CdSe, CdTe, PbS, CdSe/ZnS, CdTe/ZnS *etc*.,). Although they have stable excellent fine-tuned characteristics, the inherent toxicity of some reported QDs makes them unsuitable candidates for most of the biomedical applications.

2.2 Synthesis methods of QDs

Various methods have been reported for the synthesis of QDs of varying size and shape such as liquid exfoliation, mechanical exfoliation, chemical vapour deposition, lithium intercalation *etc*.,

2.2.1 Liquid exfoliation

Solvothermal and hydrothermal liquid exfoliation methods are among the most reliable reported synthesis strategies of QDs derived from 2D materials (Cheng *et al.* 2020). Basically sonication and temperature assisted liquid exfoliation synthesis involves the use of either water or various solvents (**Figure 2.1**). Several studies have reported the efficient exfoliation of QDs using this method. Apart from the universal solvent; water, generally employed good solvents include N,N-Dimethyl formamide (DMF), Ethylene glycol (EG), N-methyl pyrollidone (NMP), Ethanol-water mixture *etc*.,. It has been reported that a much consistent and efficient exfoliation is possible with the use of these 'good solvents' when compared to direct exfoliation in water. Sometimes this involves the use of surfactants/ detergents such as CTAB and one recent study have reported the exfoliation possibility using surfactant assisted exfoliation (Yan *et al.* 2016). NMP is regarded as the best solvent for WS_2 QDs synthesis as it minimises the energy needed for the exfoliation; yielding monodispersed QDs.

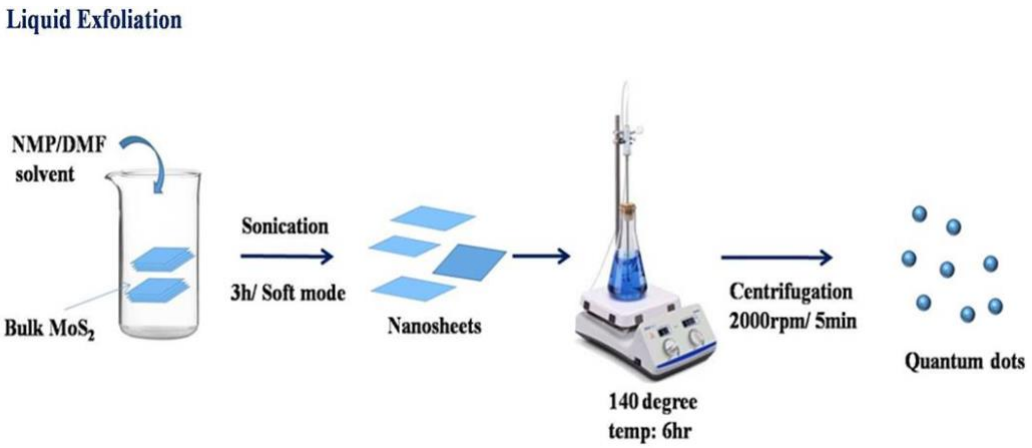

Figure 2.1: Schematic representation of liquid exfoliation synthesis of TMDC based QDs. Adapted from (Anju *et al.* 2020)

2.2.2 Mechanical exfoliation

Mechanical exfoliation involves techniques such as grinding, sonication, cutting as well as scotch-tape assisted methods to weaken the interlayer van der Waals interactions of bulk particle. This method usually employs for high quality yield of metallic nanoparticles such as TMDC nanosheets. But while employing this technique; especially scotch-tape assisted exfoliation for QD synthesis, a very low yield is usually expected, which makes it an inappropriate synthesis strategy. Scotch-tape assisted mechanical exfoliation is the generally practising method for nanosheet synthesis. Some studies have reported the effectiveness of this technique in QD synthesis. Sonication is the simplest mechanical force to exfoliate bulk material into QD crystals; even then, the choice of effective solvent is a mandatory criterion. Solvent assisted sonication processes yield good results when compared to scotch-tape assisted methods. A non-ionic pluronic 107 surfactant assisted mechanical

exfoliation of WS_2 nanodots was reported by (Zhao *et al.* 2016), in which the synthesised QDs represent excellent candidate for Hydrogen Evolution Reaction (HER) performance. Turbulent shear mixing (TSM) strategy is also an effective strategy for the synthesis of QDs, which involves the process of breaking down of the respective bulk material (Zhu *et al.* 2017).

2.2.3 Laser pulse ablation

Compared to other synthesis strategies, laser ablation method is a convenient method for the synthesis of QDs with minimal usage of chemical ligands and reducing agents. It is a simple, cheap and environmental friendly sustainable strategy for the synthesis of QDs. Nanoparticles can be tailored down to QDs in a very short time. Femtosecond laser ablation method for QD synthesis is therefore a very effective and time saving method compared to other top down and bottom up strategies. A recent study by (Xu *et al.* 2019) reported a facile and novel synthesis strategy for bright blue luminescent WS_2 QDs with an average size of 2.1nm using femtosecond laser pulse ablation. There are several laser ablation techniques such as metal-organic chemical vapour deposition, laser-chemical vapour deposition, low pressure chemical vapour deposition, chemical beam epitaxy, plasma-assisted chemical vapour deposition, and plasma-enhanced chemical vapour deposition. Femtosecond Laser Ablation in Microfluidics (FLAM) is considered as the latest novel strategy in QD synthesis for obtaining perfectly monodispersed QDs that possess deeply intense fluorescence emission (Yang *et al.* 2017). This technique can also be used for improving the

optical and chemical characteristics of QDs via P-type doping using surfactants such as diethylenetriamine (DETA) (Caigas *et al.* 2018).

2.2.4 Intercalation assisted exfoliation

Intercalation is the method of inserting small molecules or alkali metals in the interspaces of layered bulk material with the aid of electrochemistry or ultrasound waves. The combination of intercalation chemistry along with solvothermal exfoliation is a very effective strategy for the synthesis of QDs from layered compounds and 2D materials. Li, Al, Na and K ion intercalations are generally been employed for the effective synthesis of metallic QDs (Zhang *et al.* 2016). Noble metals like Cu, Ag as well as divalent metals like Ca, Sr, Ba and transition metals like V, Fe, Co, Ni, Cr, Mn *etc*., can also be used as intercalating agents depending upon the nature of the bulk compound (Dresselhaus. 2013). Insertion of these molecules will reduce the van der Waal's forces between the adjacent layers of bulk compound. However, there are certain drawbacks for this synthesis strategy. Alkali metal ion intercalation can sometimes lead to loss of semiconducting properties of certain QDs by phase transition as well as considerable morphological changes can be expected (Dresselhaus. 2013).

2.2.5 Chemical Vapour Deposition (CVD)

Chemical vapour deposition (CVD) involves processes by which a solid material is deposited from its vapour phase via a chemical reaction that occur on a substrate at

high temperature. The resulting material will be powder, thin film or solid crystal. Monodispersed QDs can be synthesised using this method by controlled tuning of CVD parameters such as temperature, flow rate, choice of precursor molecules *etc*., on a typical synthesis substrate. The mostly employed substrates are SiO_2 and copper substrates. Substrate temperature is the most critical factor that influences the chemical reaction. One such effective synthesis strategy was adapted by Xu *et al*. (2019), in which the controlled growth of large scale WS_2 monolayers was accomplished using CVD. They have reported the growth behaviour of hexagonal monolayers of WS_2 using the chemical precursors such as WS_2 powder and sodium thiosulphate ($Na_2S_2O_3$). It was identified that a discrete segmentation of photoluminescence property was found in hexagonal domains of WS_2 QDs synthesised via CVD showing symmetric patterns of dark and bright spots (Sheng *et al.* 2017).

2.2.6 Free radical etching

Free radicals are formed as a result of breakage of covalent bonds via chemical reactions by certain molecules. Due to more number of unpaired electrons present in the outer orbital, free radicals show high chemical reactivity. They possess high oxidising potential. Therefore these free radicals can be used for the cleavage of weak interactions that exist between the adjacent layers of bulk layered materials to form QDs. Hydroxyl (OH^-) radicals are excellent free radical moieties that can be used for this purpose (Li *et al.* 2014). A controlled size distribution can be achieved by maintaining adequate electrolyte composition.

2.2.7 Bottom-up synthesis

Bottom up synthesis approach refers to the miniaturisation of individual material components as individual atom by atom or molecule by molecule self-assembly; whereby leads to the formation of ultrafine QD crystals. Typical examples of bottom up strategy include epitaxial growth, hydrothermal synthesis, inert gas condensation and colloidal dispersion synthesis methods. Among these, hydrothermal method has become the most promising one-pot method for the large scale synthesis of semiconductor nanocrystals. In hydrothermal synthesis method, the chemical precursors are mixed in water and allowed to proceed with temperature treatment under controlled laboratory conditions **(Figure 2.2).** Using this method the dimensions can be easily facilitated via controlling the amount of precursors and fine tuning the reaction parameters (Hang *et al.* 2019). Colloidal methods are comparatively simple and traditional that uses a well-established wet chemical approach. Under controlled laboratory conditions of temperature, pressure and humidity, the solutions of individual precursor ions are mixed together to form insoluble precipitates. Mostly; this method is followed for the synthesis of inorganic, metallic and semiconductor QD crystals. All these bottom up synthesis methods are very much cost effective and mostly devoid of harsh toxic organic solvents. In the formation of self-assembly, various physical forces will allow the individual atoms or molecules to form clusters of QD crystals. The molecular interactions usually involve non covalent interactions such as weak van der Waals interactions, hydrogen bonding, hydrostatic attractions as well as ionic bonds.

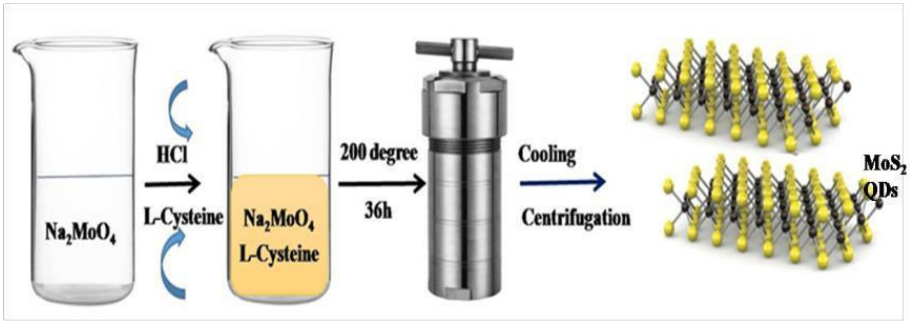

Figure 2.2: Schematic representation of bottom up synthesis method for the synthesis of TMDC based QDs. Adapted from (Anju *et al.*2020)

2.3 Structure and characterisation of QDs

2.3.1 Structure of QDs

QDs are ultrafine semiconductor particles showing enhanced optical and electronic properties that differ entirely from their bulk counterpart due to the phenomenon of quantum confinement. These are otherwise referred to as 'artificial atoms' due to its discrete electronic states and wave functions that resembles the ones in real individual atoms (Reimann and Manninen. 2002). Generally; QDs are fabricated out of semiconducting materials and consists of a few hundreds to a few million atoms. Size of each QD ranges from 2-20nm but recent reports suggests that the size is strictly restricted upto 10nm to retain the intrinsic properties of QDs. QDs are not only confined to 0D but also 1D architectures such as quantum wires and 2D structures such as quantum wells and quantum films exist.

The process of light emission in QDs is termed as photoluminescence (PL). Upon

exposure to an irradiation source like UV light, QDs will get excited to occupy a higher energy state. This is followed by a non radiative fall back of the high energy photons to a lower energy state with the subsequent release of energy in the form of fluorescence (Hou *et al.* 2008). The highest electronic energy level occupied by the electrons at room temperature is termed as valence band (VB) whereas the lowest energy band is termed as the conduction band (CB). The energy difference that exists between the VB and CB is termed as band gap, which is a typical feature of semiconductor QD crystals. This bandgap can be perfectly tuned to make these materials suitable for various electronic and optoelectronic applications. According to literatures, as the size of the QD crystal decreases, the bandgap will increases. Therefore more energy is needed to excite the QDs and subsequently more energy fluorescence emission will become possible. Because of this property, from the same material composition, by tuning the dot size and bandgap, multi-fluorescence can be emitted. Thus QDs can be perfectly tuned during the fabrication process itself according to which fluorescence it should emit.

A perfect quantum confinement effect is observed when the size of the QDs is too small to be comparable with that of the wavelength of electron. As the size becomes narrower, the confinements of its dimension makes energy levels discrete, which will inturn widen the energy gap or bandgap. These band gap and emission wavelengths are inversely proportional. Smaller the QDs, more squeezing of electron hole pairs will happen that will inturn leads to higher energy level and shorter wavelength emission resulting in blue fluorescence. At the same time larger QDs will emit red

fluorescence. There are various types of QDs such as core type QDs, core/shell type QDs and alloyed QDs, dependant on which the structure also changes considerably.

2.3.1.1 Core type QDs:

Core type QDs consist of a single component material with uniform internal composition (sulphides, selenides or tellurides of transition metals). By changing the nanocrystal size, electrochemical and luminescence properties of these QDs can be tuned accordingly. TMDC QDs shows excellent structural stability owing to the presence of ripple structure similar to graphene but at the same time; in contrast; they possess various polymorphism such as 3R, 2H and 1T, which corresponds to the rhombohedral, hexagonal and tetragonal atomic stacking sequence respectively (Toh *et al.* 2017). In MoS_2 and WS_2 like materials, the presence of weaker van der Waals forces between the adjacent layers makes the crystal cleave along the monolayer surface easily, providing a perfect crystalline morphology for the respective QDs (Khan *et al.* 2019).

2.3.1.2 Core/ shell type QDs:

Core/ shell type QDs consist of a semiconductor core metallic component with shell consisting another distinct semiconductor material such as CdSe/ZnS, InAs/CdSe QDs. Usually both core and shell in these type QDs consist of type II–VI, IV–VI, and III–V semiconductors in the periodic table (Vasudevan *et al.* 2015). They show an improved quantum yield when compared to other types.

2.3.1.3 Alloyed QDs:

Alloyed QDs are formed by alloying two different semiconducting materials having different band gap energies. Their chemical composition and internal structure are the major parameters that can be used to fine-tune the properties of such alloyed type QDs. It is often observed that, once the shell has obtained a particular thickness, the quantum efficiency begins to decrease to a considerable extend in these type of QDs.

2.3.2 Characterisation of QDs

Various sophisticated techniques are generally employed for the characterisation of QDs, which are detailed below.

2.3.2.1 UV/Visible Spectroscopy

UV/Visible spectroscopy is one of the most versatile techniques used to detect nearly every molecule. When the UV/Visible light is passed through the sample, the transmitted light is recorded to detect the material characteristics. Possible aggregation tendency of the synthesised QDs can be analysed using this technique. Also dimerisation of nanospheres can be analysed by observing a shift towards longer wavelength within the UV/Vis spectra. Aggregation of particle causes a decrease in the intensity of peak absorbance without causing any shift in wavelength (λmax) at which the peak was observed (Worsfold *et al.* 2019). The peak width of the absorbance spectra will give an idea about the monodispersive nature of QDs. Different sized QDs absorb at different wavelength, therefore absorbance spectra

analysis is an easy way for analysing the polydispersity of the QDs. Depending upon the shape and morphology of the material, the absorbance spectra can vary.

2.3.2.2 Fluorescence emission spectroscopy

Fluorescence emission spectroscopy is used to analyse the fluorescence emitted from the sample. QDs emit fluorescence of different wavelength. Inorder to determine the emission spectrum of a typical QD, the wavelength corresponds to maximum absorption is provided so as to excite the particle inorder to emit light of specific wavelength. A monochromator is then used to detect the typical fluorescence emission spectra of the given sample. The relative fluorescence intensity is depicted by graphical data. It is possible to determine the exact band position so as to determine the size distribution pattern more precisely using this technique (Mutavdžić *et al*. 2011). As the homogenicity in size of the QDs is directly related to the fluorescent maximum position (FMP), this is considered to be a reliable methodology for the size determination of QDs.

2.3.2.3 Transmission Electron Microscopy (TEM)

In Transmission Electron Microscopy, a high energy beam of electrons are focussed on to a very thin particle and subsequently the transmitted electrons are focussed to image the particle. It is useful to get information about the inner surface morphology, growth characteristics, size, composition, crystallinity and stress state of the sample using TEM. The interaction between atoms and electrons is used to analyse the crystal structure and morphology of the particle. Instead of a light microscope, it uses

high energy electron beam to focus the object and therefore the maximum optimal resolution attained through TEM is very high. It can be used to analyse the internal structural characteristics of the sample. Sample preparation is an important criterion in TEM. The specimen should be thin enough so as to minimise the energy loss while acquiring the image. An improved version of TEM is High Resolution Transmission Electron Microscope (HR-TEM), which gives a more precised crystallographic image of the specimen at nuclear level (Buseck *et al.* 1989). HR-TEM differs from conventional TEM in which the images are formed alongside the atomic lattice level. Cross sectional HR-TEM provides information about the diffraction data. These diffraction pattern characteristics will give information about nano, micro, single and poly crystalline phases of the sample. It is also possible to get the chemical compositional information using the digitally recorded HR-TEM images.

2.3.2.4 Scanning Electron Microscopy (SEM)

SEM is a surface analysis method which offers a three dimensional visual perspective of the material. SEM is an electron microscopic technique that produces images of a sample under vacuum by scanning its surface using a focussed beam of high energy electrons (5-100 keV) (Van *et al.* 2012). Narrow electron beam is focussed on to the particle and the backscattered secondary electrons are focussed to obtain high resolution and high magnification images. The intensity of these secondary backscattered electrons is directly related to the atomic composition of the sample.

2.3.2.5 Zeta potential

Zeta potential is a method to analyse the surface charge of a particle in colloidal state. NPs usually have a typical charge on its outer surface which attracts the counter ions in its immediate vicinity to form a thin layer. The electric potential at the boundary of this double layer is the zeta potential value of that particle. The normal zeta value ranges from +100 to -100mV. The magnitude of this zeta value is used to predict the colloidal stability of the sample (Nimesh *et al.* 2017). Zeta potential value which exceeds the limit of +25 to -25mV is considered to have better repulsive force to attain good colloidal stability. Small zeta value predicts for the possible aggregation tendency of the particle due to van der Waals forces that acts upon them.

2.3.2.6 Fourier Transform Infrared Spectroscopy (FTIR)

FTIR is a method for measuring the infrared absorption and emission spectra which gives information about the bonding and chemical composition of a material. A change in the characteristic absorption band indicates a change in the chemical composition of the material or sample contamination. FTIR gives information about the oxidation, reduction, and decomposition like chemical reactions (Radu *et al*. 2012). It is also useful in the identification and characterisation of unknown material. Infrared radiations of about 10,000 to 100cm^{-1} is been propagated to the sample and the amount of the absorbed radiation is converted to vibrational or rotational energy of the sample molecules (Horlick. 1968). Each molecule will give a typical fingerprint vibrational spectral band, which makes FTIR efficient for chemical group identification.

2.3.2.7 X-ray Photoelectron Spectroscopy (XPS)

XPS also known as Electron Spectroscopy for Chemical Analysis (ESCA) is a surface sensitive quantitative spectroscopic technique used to determine the chemical state, chemical shift, elemental composition and electronic state of elements in a compound. It also provides information about the possible category of elements to which a typical metal is bonded to and its corresponding oxidation states (Paparazzo. 1988). XPS has an average analysis limit of upto 2-5nm depth of a compound. It is typically accomplished with the excitation of sample using high energy Al kα x-rays followed by emission of photoelectrons from the sample. From the binding energy and photoelectron peak intensity, the subsequent elemental identity can be revealed.

2.3.2.8 X-ray Diffraction (XRD)

XRD provides information about the crystallinity, molecular connectivity and chemical composition of a sample. The most widely used one is single crystal XRD. XRD pattern is the fingerprint of the periodic atomic arrangements in a compound, which can be used to analyse the crystal orientation, crystal defects, strain as well as the average grain size of the material (Kohli. 2012). The working principle of XRD is based on Bragg's law ($n\lambda = 2d\sin\theta$), in which a beam of X-rays is allowed to pass through the sample and the diffracted radiations are subsequently analysed by the detector (Patel and Parsania. 2017). Diffraction patterns observed in a perfect crystalline sample is very narrow. Line broadening can be occurred in particles having size below 100nm due to incomplete destructive interference in the scattering directions.

2.3.2.9 Inductively Coupled Plasma Mass Spectrometry (ICP-MS)

ICP-MS is one among the characterisation techniques for the detection of the typical elements in a compound in solution state, which uses a high temperature ionisation source like plasma coupled to a mass spectrometer. It can be used to analyse the particle concentration, its chemical composition and size distribution.

It is possible to directly detect and quantify the signals generated as a result of the atomisation and ionisation of the sample when introduced into plasma. ICP-MS is comparatively a simple and easy technique when it comes to sample preparation (Beauchemin. 2017). Mainly two types of ICP-MS techniques exist, Single particle ICP-MS and Hyphenated ICP-MS. It is an ideal characterisation technique for the detection of metal based NPs because of its excellent elemental sensitivity and specificity.

2.4 WS_2 QDs and its importance

WS_2 QDs belongs to the family of compounds known as transition metal dichalcogenides, having immense applications especially in the field of biomedicine and technology. A detailed account on WS_2 QDs is been included below.

2.4.1 Transition Metal Dichalcogenides (TMDCs)

Extensive research on graphene and its analogues has reignited an extra ordinary interest in search for other two dimensional materials exhibiting spectacular characteristics such as optical, electronic, sensing *etc.*,.The family of 2D materials generally include many chemical groups like 2D transition metal dichalcogenides (TMDCs), transition metal dioxides (TMDOs), 2D clay materials including layered double hydroxides (LDHs) and Laponite, hexagonal boron nitride (hBN), graphitic C_3N_4 (g-C_3N_4), silicene, stanene, antimonene, borophene, bismuthene, graphyne, graphdiyne, indium selenide, rhenium disulphide, germanene *etc.*, (Anju *et al*. 2020). The very recent member is ultrathin black phosphorus monolayers and the list still continues (Kurapati *et al*.2016).

TMDCs are inorganic chemical moieties with the generalized formula MX_2, where M represents a transition metal atom covalently sandwiched by two hexagonal planes of chalcogen atom (X) **(Figure 2.3).** This unique family of compounds exhibits some profound combinations of fundamental characteristics such as tunable bandgap, atomic thickness, semiconductive nature, excellent charge carrier mobility, spin-orbit coupling as well as electronic, opto-electronic and mechanical properties suitable for various applications. They possess interesting electro catalytic and optical properties also. Zero dimensional (0D), one dimensional (1D) as well as 2D nanomaterials can be easily exfoliated from bulk TMDC materials using mechanical and solvent assisted chemical methods. These peculiar characteristics make them exceptional among other 2D materials for applications in various fields such as energy storage,

electronics, opto-electronics, spinctronics to even biomedical technology. All TMDC compounds are semiconductors which exhibit tunable bandgap ranging from 1-2 eV suitable for electronic and opto-electronic applications (Meckbach *et al*. 2018). High stability in aqueous environments and large surface area facilitates these materials useful for biomedical applications. Quantum confinement effect introduced while thinning down to ultrafine structures is another major breakthrough that enables direct bandgap and bandgap depending properties well suited for various opto-electronic applications as well as imaging guided therapy like biomedical applications. This stringent contrast between photoluminescence emissions of thin layers to bulk counterpart is due to quantum confinement of layered d-electrons in the conduction and valence bands.

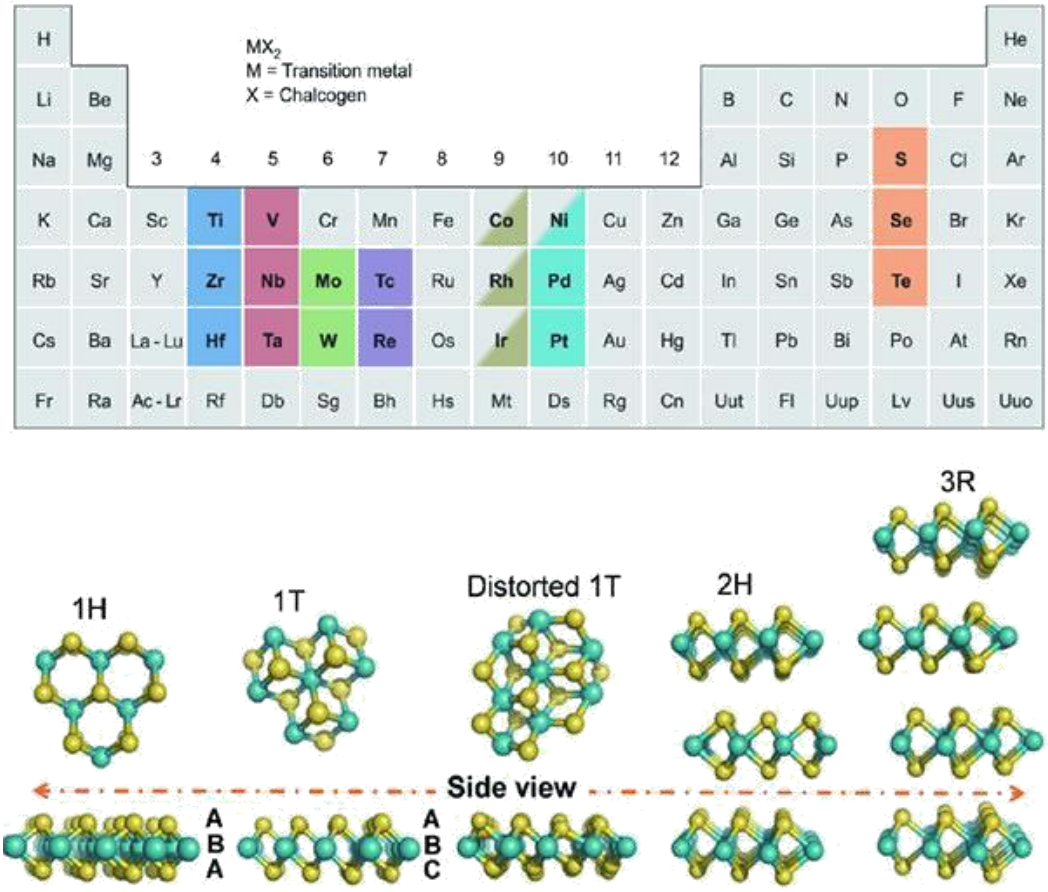

Figure 2.3: Chemical composition and structural backbone of TMDC compounds. Adapted from (Habib *et al*. 2019)

Almost all TMDC members exhibit excitation dependant emission properties. It is proposed that the emission wavelength of TMDC QDs increases with red shift of excitation wavelength. Usually this red shift occurs from the formation of even deeper trap states which accounts for the unoccupied sulphide and metal ions on the surface of these QDs. Even though the exact mechanism behind this excitation dependant emission behaviour of TMDC based QDs are not unravelled, yet then it is highly anticipated that polydispersity of QDs, presence of trap state vacant ions, transistors, photovoltaic devices and detectors have been effectively came out of TMDC compounds that decipher its high application potential. Multiple extrema in

multiple discrete electronic states as well as heterogenicity of ground states could be the possible factors that contributes to the same (Caigas *et al.* 2018). The valence/conduction bands of TMDC monolayers makes them extremely well adapted candidates for spinctronics and valleytronics. Molybdenum disulphide (MoS_2), tungsten disulphide (WS_2), and tungsten diselenide (WSe_2) are the most extensively studied ones among the major TMDCs. Untill a few decades before; there have been very limited information available regarding the use of TMDCs in the area of biomedicine and biomedical technology. Recent studies have concentrated on nanostructured TMDCs, which resembles a hot topic in the field of science and technology with a lot of innovative research potentials still unexplored. A strong resurgence of enthusiasm towards TMDCs happened after the discovery of the first MoS_2 based transistor (Radisavljevic *et al.* 2011) and with the knowledge regarding the property of strong photoluminescence of MoS_2 monolayers (Splendiani *et al.* 2010). These are promising candidates for quantum technologies because of the direct bandgap dependant semiconducting properties. Applications of TMDCs ranges from nanoelectronics, nanophotonics to biomedical applications as a substitute for carbon based materials which spans throughout a wide spectra of interdisciplinary arenas.

2.4.2 Tungsten Disulphide Quantum Dots (WS_2 QDs)

Tungsten disulphide (WS_2) is a TMDC compound having a layered structure similar to graphite, which occurs in nature in the form of a rare mineral known as 'tungstenite'. It has a trigonal prismatic structure and possesses anisotropic nature. Analogous to graphene crystal structure, it consists of 'W' atom sandwiched between two hexagonal planes of 'S' atoms by van der Waals interactions **(Figure 2.4).** Thus it can be easily exfoliated along the inter layer plane.

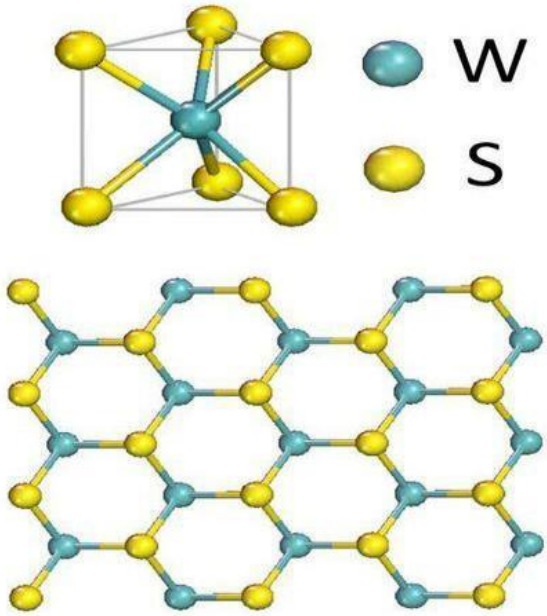

Figure 2.4: Molecular structure of Tungsten Disulphide. Adapted from Forget graphene, 2D laser uses tungsten disulphide (electronicsweekly.com)

It is a component of certain catalysts involved in hydrodesulphurisation and hydrodenitrification reactions. Among the notable 2D materials, WS_2 has gained considerable attention owing to its ability to form monolayers. Photoluminescent zero dimensional QDs based on this material is in the spotlight of researches in recent times owing to its attractive characteristics. Most of the QDs developed so far involve some toxic heavy metals such as cadmium and lead. As toxic heavy metal free quantum dots, TMDC based QDs is gaining attention due to excellent chemical stability, good thermal conductivity and stable optical properties of this emerging material. Compared to its nanosheet dimensionality, WS_2 QDs exhibit strong fluorescence and outstanding optical properties when tailored down to quantum confinement dimensionality. Excitation dependant emission has been reported in several studies for WS_2 QDs, which is a very interesting property that can be attributed for multicolour imaging (Bai *et al.* 2017). When compared to conventional toxic metal containing QDs, WS_2 QDs are proved to be excellent candidates due to its inherent low toxicity profile and stable dispersive nature. Therefore these can be utilised for various applications such as target analyte detection, detection of heavy metal intoxication in physiological medium *etc*.,. Recent studies have reported the possibilities of peptide conjugation to WS_2 QDs and its further applications (Mohid *et al.* 2019). WS_2 QDs is a typical TMDC member showing certain key properties such as extreme small size, strong fluorescence emission and size tunable narrow emission spectra.

The typical broad absorption spectra and tunable narrow emission spectra allow these QDs with large stokes shift, which is advantageous in high penetration tissue imaging and sensing platforms. Due to direct tunable bandgap in contrast to graphene family of compounds, its optical properties are much more precise and efficient. Many investigations are still in frontier with various top down and bottom up approaches to get good quality QDs out of TMDC compounds.

2.5 Applications of WS_2 QDs

WS_2 QDs possess voluminous applications in the fields of both biomedical and non-biomedical arenas. The various applications of WS_2 QDs are detailed below

2.5.1 Non- biomedical applications

The major non biomedical applications of WS_2 QDs spans in the fields of electronics, optoelectronics, photovoltaics, energy storage and catalysis.

2.5.1.1 Electronics and optoelectronics

Due to the quantum mechanical behaviour arises from specific energy gaps, QDs find its applications in a wide variety of electronics like solar cells, light emitting diodes, transistors to quantum computing. The optical, magnetic and electronic

properties of QDs can be tuned for various electronic applications. Ultrabright and stable fluorescence makes QDs efficient alternatives for white-light emitting diodes (Sadeghi *et al.* 2018). Quantum Dots Light Emitting Diode (QD-LEDs) displays and Quantum Dots-White Light Emitting Diode (QD-WLEDs) displays are currently gaining attention because QDs possess the capability to inherently produce monochromatic light, which are more efficient than colour filtered light sources. QDs are excellent substitutes for phosphors used in conventional LEDs. These can emit light in highly specific Gaussian distribution pattern by consuming very less power, which is a distinguishing property of QD based LEDs. The ability of QDs to precisely tune an optical spectrum makes it attractive candidate for Liquid Crystal Displays (LCDs) in electronics. QDs can be used to enhance the backlighting of LCD, which is reported to subsequently render colour richness, high contrast as well as a steady 30-40% increase in the visible spectrum imaging.

2.5.1.2 Photovoltaics and energy storage

Photovoltaics are the technology by which the conversion of light energy into electrical energy occurs with the aid of semiconducting materials, which exhibits the phenomenon of photovoltaic effect. Quantum dots have got attention as photovoltaic materials that make them attractive candidates for multi-junction solar cells (Shin *et al.* 2006). Wide band gap containing semiconductor QDs sensitized solar cells have become a sensation in solar cell fabrication technology in recent times. These extremely small molecules were reported to excite two or multiple excitons or electron hole pairs instantly while absorbing a single photon.

This principle is known as multiple exciton generation (Halim. 2013). It was proposed that the solar power conversion efficiency could be drastically increased by combining QDs with existing dyes or by using QDs alone as sensitizer source. By tuning the size and bandgap of these QDs, studies have suggested that the entire spectrum of visible and infrared wavelength radiations can be utilized for energy storage purpose (Sargent. 2012). One major advantage of using QDs in solar cell fabrication is that; QDs can be easily processed and incorporated into solar cells to bring about high power conversion efficiency.

2.5.1.3 Catalysis

High density of atomic defect sites has long been reported to be key active principle for the design of catalysts because they can lower the energy barrier of the stipulated chemical reaction (Swaminathan *et al.* 2016). This can be achieved using QDs as they possess rich atomic edge defects. Development of TMDC based hydrogen evolving catalysts has got significant attention for practical application of fuel cells and water splitting device fabrication due to their intrinsic electrocatalytic properties. One study reported the effectiveness of WS_2 QDs/cobalt diselenide hybrid material as a catalyst for hydrogen evolution reaction (Hussain *et al*. 2018). This heterostructured electrode demonstrated excellent catalytic activity and long term stability owing to its abundant active edge defects and strong chemical electronic coupling between the chemical moieties.

2.5.2 Biomedical applications of WS_2 QDs

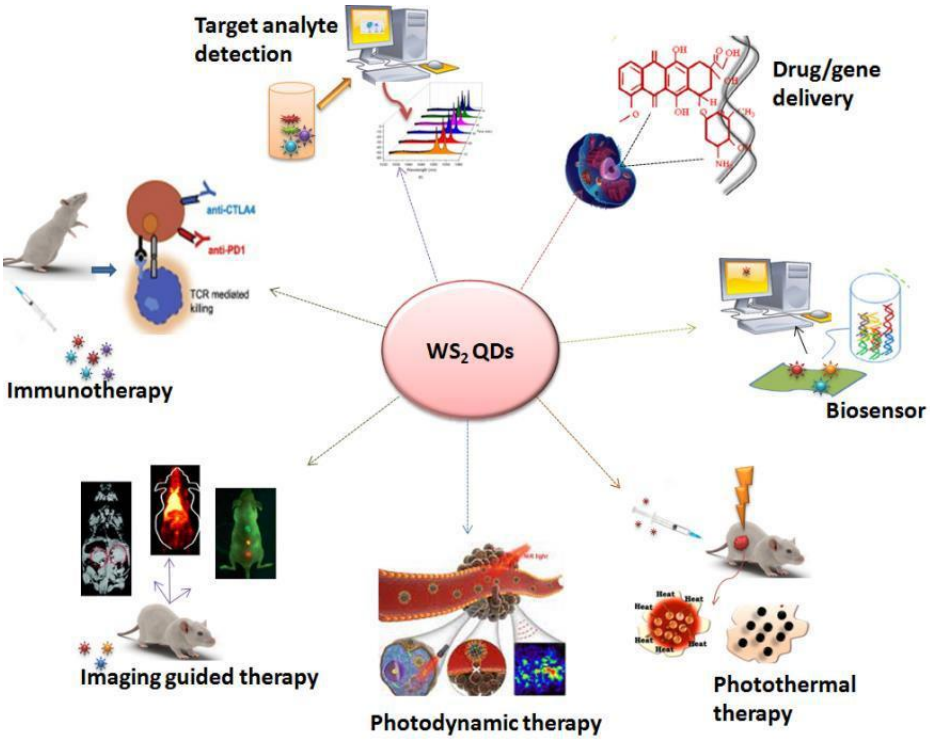

Figure 2.5: Biomedical applications of WS_2 QDs

Several organic dyes are currently been employed for the purpose of bio imaging, bio sensing as well as target analyte detection based applications but the pronounced photo bleaching tendency upon laser or other light source irradiation makes them unable to fulfil the expectations of research community. In such situation, QDs got significant hike to substitute conventional organic dyes by overcoming all the drawbacks of organic fluorophores. Exceptional photo physical properties of WS_2 QDs such as high quality fluorescence, size-tunable emission, strong light absorbance, brightness and photostability impart significant application possibilities for these materials in biomedical and healthcare modalities (**Figure 2.5)**. Unique and

stable fluorescence makes them suitable candidates for *in vitro* and *in vivo* bio-labelling by substituting organic fluorescent dyes. Various possible biomedical applications of WS_2 QDs are depicted and explained in detail below.

2.5.2.1 Drug delivery

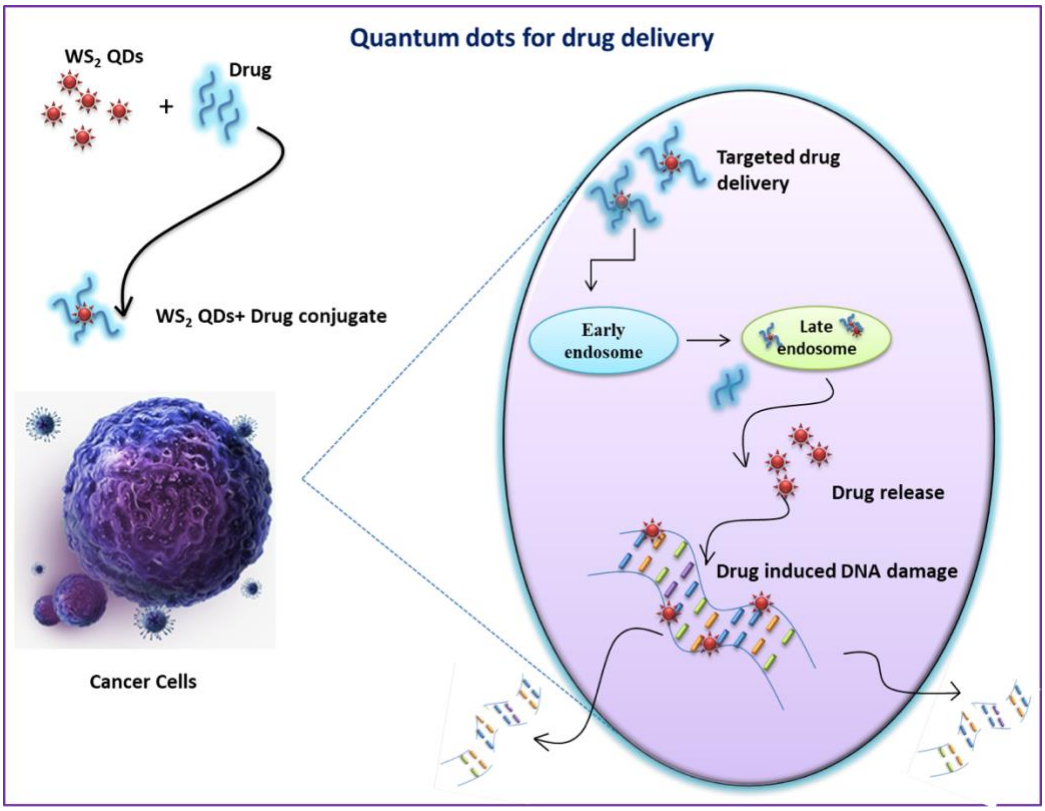

Figure 2.6: Schematic representation of TMDC based QDs for drug delivery

TMDC based NPs are reported to be potent candidates for drug delivery and sustainable drug release applications **(Figure 2.6).** Compact size and compatibility of various surface modification makes QDs better candidates than any other NP dimensionality for targeted drug delivery. Superior brightness due to narrow emission fluorescence of QDs facilitates easy identification of target drug population

also. WS_2 QDs were reported to be excellent targeted drug delivery agents due to their intrinsic fluorescence emission properties and high surface area to volume ratio in its quantum dot dimensionality. Drug loading efficiency and drug retention capacity is also reported to be higher for these QDs (Yan *et al.* 2016). Extremely stable fluorescence emission with reduced photo bleaching effect shown by this material can be facilitated for targeted drug delivery as there is the possibility for tracking the route of drug distribution using such QDs. Ultra small WS_2 QDs having lateral size less than 5nm can get effectively escaped out from the absorption by reticulo-endothelial system, thereby effectively excreted out through kidney facilitating least tendency of accumulation of this material in the physiological system (Liao *et al.* 2018). This also accounts for the wide spread acceptability of WS_2 QDs for drug delivery like biomedical applications.

2.5.2.2 Gene delivery

Gene delivery is a successful clinical therapy used for the treatment of life threatening conditions such as cancer and neurodegenerative disorders. This therapy always demands for an efficient gene delivery vector for targeted and systematic delivery of gene. Different dimensionalities of NPs were investigated as vectors for gene delivery (Blanco *et al.* 2017). Recently, TMDC based QDs and 2D NPs were greatly investigated for gene therapy owing to their intriguingly appealing characteristics such as high surface area, chemical inertness and gene loading efficiency. It was reported that a multifunctional nanoplatform employing

polyethyleneimine functionalised WS_2 QDs was developed for imaging guided gene therapy of highly malignant tumor (Zhang *et al.* 2016). High surface area and chemically inert nature of this material makes it a suitable gene delivery vector when compared to other conventional gene delivery vectors.

2.5.2.3 Photothermal therapy

Photothermal therapy (PTT) is a treatment modality employed for tumor cell destruction, which uses infrared (IR) or near infrared (NIR) radiations to heat the contrast agents that are localised inside the tumor tissues. This will increase temperature inside the tumor micro environment and subsequently lead to hyperthermia mediated cell death (Li *et al.* 2020). TMDC NPs and QDs such as WS_2 QDs with a characteristic NIR absorption efficiency has been evidenced as potential candidates for PTT mediated cancer treatment **(Figure 2.7).** Yong and collegues in 2015 has reported the efficiency of novel WS_2 QDs for imaging guided photothermal therapy mediated tumor cell ablation (Yong *et al*. 2015). Due to extreme smaller size, these are reported to have effective renal clearance also.

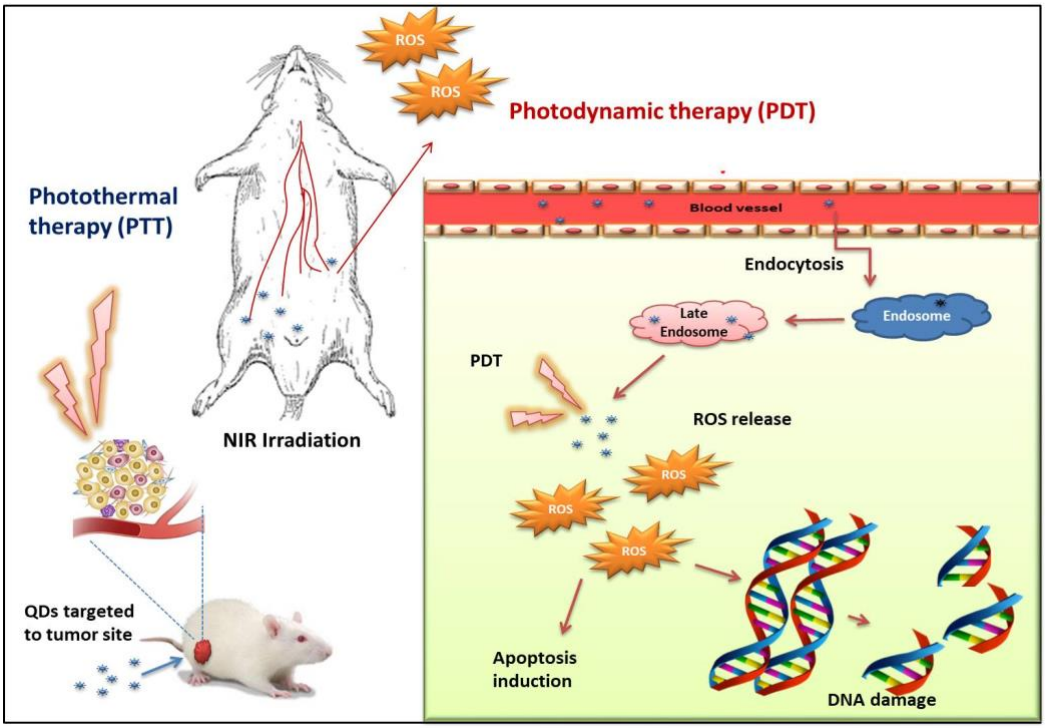

Figure 2.7: Quantum dots mediated Photothermal therapy and Photodynamic therapy

2.5.2.4 Photodynamic therapy

Photodynamic therapy (PDT) is a minimally invasive clinical treatment modality that uses light absorbing photosensitizers to induce the production of cytotoxic singlet oxygen species inside tumor tissues upon longer wavelength light irradiation, whereby mediate tumor cell destruction (Luby *et al.* 2019). Besides exerting photothermal effect, WS_2 QDs are excellent photosensitizers also, which can be used for tumor ablation via PDT. PDT shows high tissue selectivity as it generate singlet oxygen species only in areas where photosensitizers are accumulated leaving behind the normal tissues.

Lack of deeper tissue penetration limit accounts for the drawback of most of the currently employed photosensitizers. But TMDC based QDs such as WS_2 QDs and MoS_2 QDs accounts for its excellent deeper tissue penetration effect that makes them attractive candidates for PDT (Yin *et al.* 2020) **(Figure 2.7).** Usually, combination therapy of PTT and PDT is suggested to improve tumor cell ablation; as an initial hyperthermia will induce softening of tumor tissues that facilitates intra-tumoral blood flow. This blood flow will further enhance the transport of more singlet oxygen species towards the tumor site for PDT.

2.5.2.5 Immunotherapy

Immunotherapy has now become the fourth most appealing therapy for cancer theranostics globally. Immunotherapy uses the technique of stimulating the body's own immune system to destroy the cancer cells by ensuring reduced metastasis and improved antitumor effect. Use of various NPs, QDs and liposomes in cancer immunotherapy has become a trend set from the past few decades (Anju *et al.* 2020). It was reported that WS_2 nanotubes and inorganic fullerene like MoS_2 NPs were able to induce detectable levels of inflammatory cytokines such as interleukins to evoke sufficient inflammatory responses in tumor cells at the same time ensuring protective antioxidant and detoxification mechanisms (Pardo *et al.* 2014). Some TMDC materials were reported to activate TNF-α secretion, dendritic cell maturation and killer T cell activation and thereby induce an inflammatory response to check the tumor cell progression (Rajendrakumar *et al.* 2018).

2.5.2.6 Imaging guided therapies

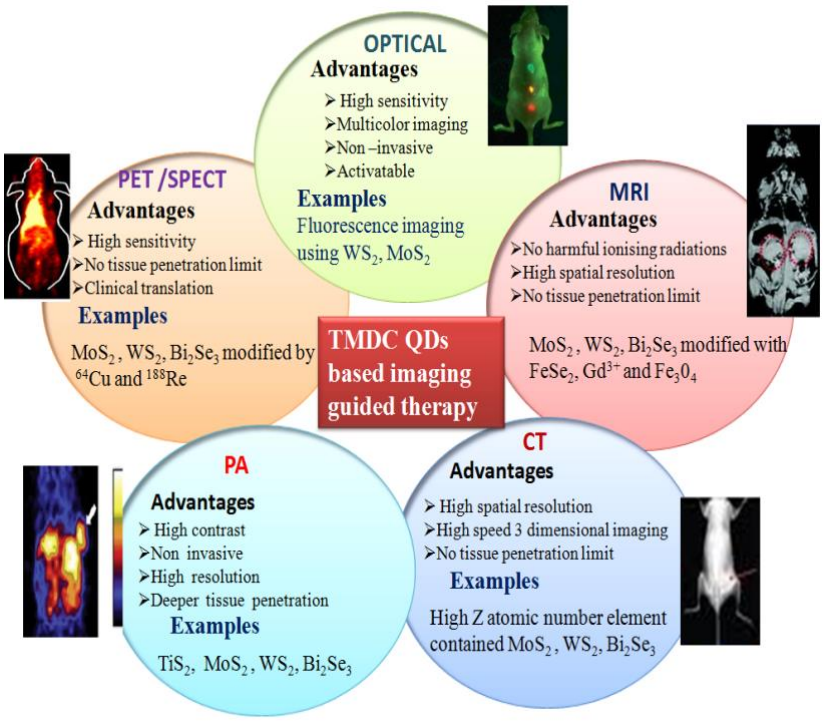

Figure 2.8: QD based imaging guided therapies

Integration of multimodal imaging based therapeutic strategies into one single nanoplatform has been put forward as a promising strategy in cancer diagnosis and treatment. TMDC based QDs such as WS_2 QDs are been recently investigated as suitable materials for imaging guided therapies (Yang *et al.* 2018). Deeper tissue penetration, non invasive nature and strong NIR absorbance makes them suitable contrast agents for Computed Tomography (CT), Magnetic Resonance Imaging (MRI), Photo-Acoustic imaging (PA), Positron Emission Tomography (PET) and Single Photon Emission Computed Tomography (SPECT) (Chen *et al.* 2018) **(Figure 2.8).** Imaging of deeper tissues can be achieved using QDs by adjusting the

size and chemical composition to ensure high contrast imaging with deeper tissue penetration.

2.5.2.7 Target analyte detection and biosensors

NPs have been recently investigated as efficient candidate materials for target analyte detection and biosensing applications. TMDC QDs such as WS_2 and MoS_2 are in high demand due to their efficacy for the same. One recent study has reported the potency of WS_2 QDs based electrochemical platform for the detection of ferritin in biological samples (Garg *et al.* 2020). The peroxidase like activity of WS_2 makes it a suitable substitute as enzyme mimics for the detection of H_2O_2 like molecules. Another recent study has reported the effective fabrication of lysine functionalised WS_2 QDs to be used as artificial enzyme mimics for oxidative biomarker sensing (Garg *et al.* 2020). In another recent study, WS_2 QDs embedded genochip based sensing platform was investigated for the detection of DNA sequence; specific for meningitis, a life threatening disease (Gupta *et al.* 2020).

2.6 Toxicity and safety of QDs

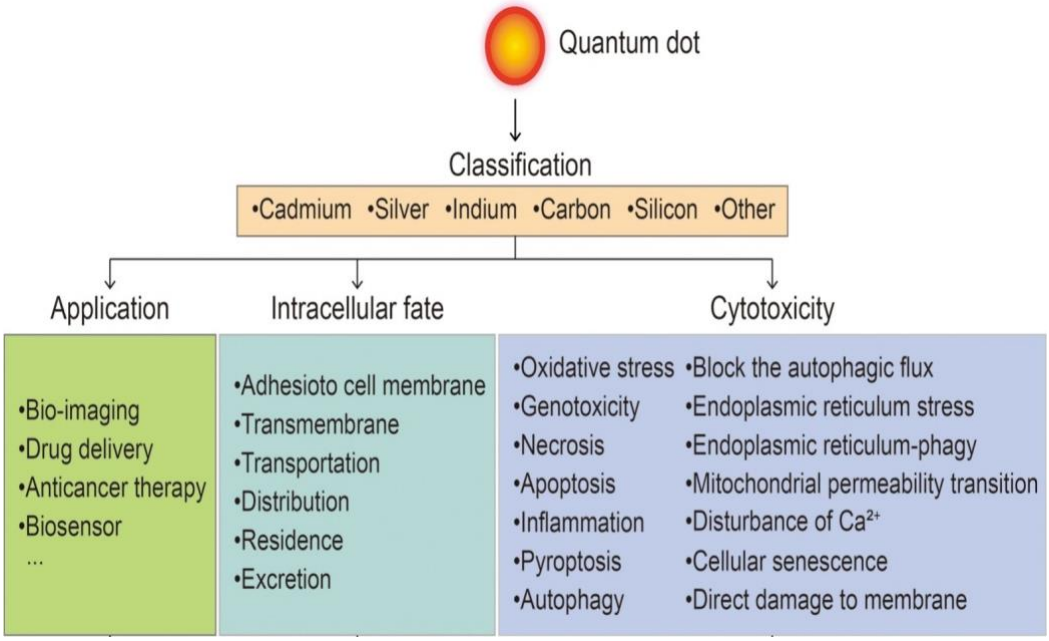

Figure 2.9: Toxicity of QDs and associated consequences. Adapted from (Liu *et al.* 2020)

QDs are excellent candidates in nanotechnology researches due to its potent applications in wide arenas especially in biomedical technology. Even though significant attention has been given in developing QDs for biomedical applications, scientific community still has a concept that all QDs are toxic; therefore, they cannot be used for practical applications in biomedical science. QDs, especially toxic metal containing QDs were reported to elicit some serious side effects in the biological system and physiological environment especially once it is exposed in severe doses **(Figure 2.9).** Generally, traditionally employed Cadmium containing QDs are toxic and keeping this as a general criterion; researchers are extrapolating the same as universal for all types of QDs. These assumptions generally reverberate QD

researches. Diverse types of QDs are being synthesised day by day and each individual QD design is having its own unique combination of fundamental physico-chemical properties. This inturn determines its toxicological impacts or lack thereof. QD toxicity depends on various factors like its inherent characteristics as well as the environmental factors with which these are exposed to. Major factors that contribute to the toxicity of QDs include its physico-chemical characteristics like chemical composition, size, shape, morphology, surface charge as well as dose, route of exposure, frequency of exposure, mechanism of action *etc*.,. Some toxic heavy metals such as Cadmium (Cd^{2+}) containing QDs like CdSe/ZnS, CdTe, CdS QDs were reported to be extremely toxic to a majority of cells such as primary human hepatocytes, primary nephrocytes, HeLa cells, Vero cells, oocytes, ovarian cells and WTK-1cells mainly due to leaching of its heavy metal core. This is infact the most dangerous fact about core/shell type QDs (Sharma *et al.* 2013). This cannot be the reason for other types of QDs such as those derived from 2D layered materials like TMDC based QDs and carbon dots. QDs are still therefore a long way from realising its potential for biomedical applications. This makes the importance of developing non toxic QDs that can be safely used for various biomedical applications.

2.7 Different parameters influencing QD toxicity

Toxicity of QDs is not stringently dependant on the chemical composition of the material but a lot of other factors altogether activate the potential toxic impact which the QDs can elicit in the biological system **(Figure 2.10).**

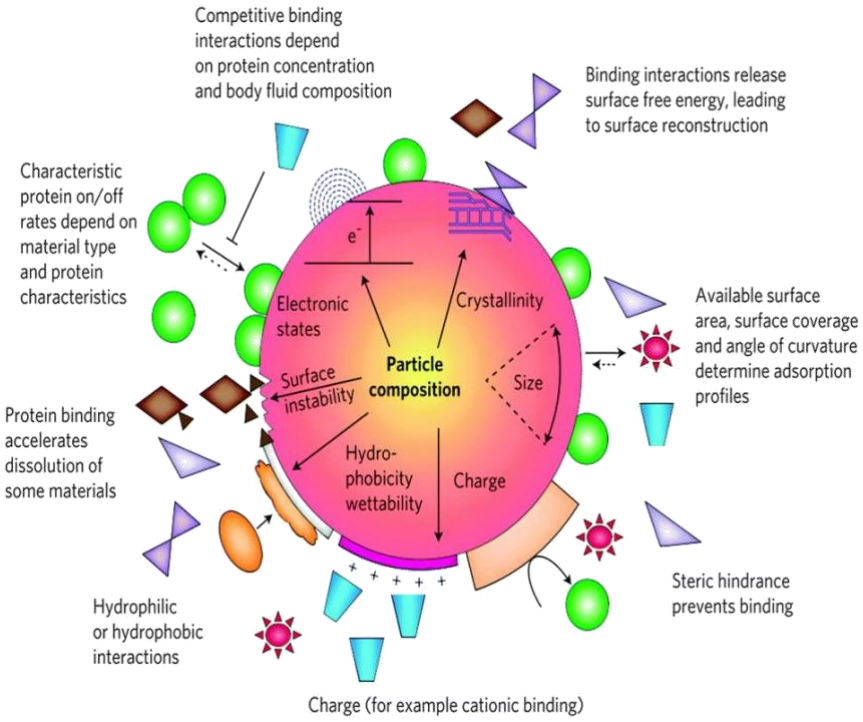

Figure 2.10: Various parameters that contributes to QDs toxicity. Adapted from (Lazarovits *et al.*2015)

2.7.1 Chemical composition

Toxicity of QDs is greatly influenced by its chemical composition and ionic dissociation. Due to varying pH inside the various compartments of biological system, chances are very high for these particles to dissociate into their respective ions; especially for metal ions. Most of the QDs consist of toxic heavy metals such as Pb and Cd as the core component. Among these core metals, Cd belongs to class A element, whose usage is strictly regulated under current environmental policy (Chen *et al.* 2012). Upon cellular uptake, these elements can impart severe toxic responses. Some QDs have found to be more toxic only after the hydrolytic/photolytic/oxidative degradation of its core component (Lu *et al.* 2019). This leaching process can be reduced to a considerable extend by surface modification strategies using polymers.

2.7.2 Size

A unique aspect of NP toxicity is its size-dependant intracellular uptake and routing. When compared to the bulk counterpart; QDs can be directed to various cell organelles easily due to their extremely small size, which leads to unique motifs of cytotoxicity. Relatively small size allows QDs to easily penetrate into various endothelial barriers whereby it can enter into the blood stream. Smaller NPs having lateral dimension less than 10nm can get easily escaped through the cell barriers via mechanisms like translocation. From the blood stream these QDs can be carried easily to other vital organs such as heart, liver, kidney, spleen, brain, bone marrow *etc*., (Dukhin and Labib. 2013). As the size get reduces; the more will be the toxic potential of QDs so that they can get entered into even sub cellular organelles and cause reactive oxygen species production. This will indirectly harm the entire cellular metabolism. Moreover smaller sized particles undergo more dissociation when compared to its bulk counterpart.

2.7.3 Morphology

Morphology of NPs can strongly affect the extend of toxic effect it can elicit upon interaction with the biological system. Various studies have confirmed that spherical shape favours more endocytic uptake pathway (Champion and Mitragotri. 2006). Spherical NPs are more prone to access endocytosis pathways than nanotubes and nanofibres. QDs being spherical in shape can therefore get endocytosised easily. Shape of NP can strictly determine the extend of physical damage it can cause to the cell membrane and subsequent cell damage. However, protein corona formation

around these NPs will greatly reduces this toxic effect due to accumulation of protein coat around the NP surface (Lee *et al.* 2015).

2.7.4 Surface charge

Surface charge of NP will directly influence the toxic effect it elicits in the physiological system. Surface charge can be extensively modified using charged polymers such as polyethyleneglycol (PEG), pluronics, dextran, polyethyleneimine (PEI), folic acid *etc*.,. Positively charged particles are found to be more toxic because it can easily enter cell and sub cellular organelles due to the possible electrostatic attraction that exist between negatively charged membrane glycoproteins and positively charged particles. These NPs can also form adduct with negatively charged DNA eliciting possible genotoxic effect. This can cause prolongation of G_0/G_1 cell cycle event (Liu *et al.* 2011). Enhanced capacity of opsonisation is also found with positively charged NPs facilitating phagocytosis and complement system activation (Alexis *et al.* 2008). In contrary; negatively charged NPs and QDs have no effect on cell cycle that ensures the usage of negatively charged QDs for various biomedical applications.

2.7.5 Ionic dissociation

Under the influence of various factors such as pH variation, QDs can be disintegrated into their respective ions inside the physiological system (Hu *et al.* 2016). Hydrolytic and oxidative degradation are the most frequently occurred ones. Loss of this chemical stability will greatly influence the effect of QDs inside the living system.

UV illumination used to analyse QD localisation promotes QD dissociation to a greater extend by the process of photolysis (Samadi and Farzinia. 2018). Most of the QDs contain toxic heavy metals and the dissociation of these metal ions will become more toxic to vital organs. Accumulation of these toxic metal ions over long term leads to severe organ failure. Surface modification is the strategy that can be adopted to avoid ionic dissociation to a considerable extend.

2.7.6 Dose

Dose is the quantity of uptake and dosage is the rate of application of dose for any substance in the field of medicine, nutrition and toxicology. Various researches showed that the toxicity of QDs is inevitably dependant on the dose of exposure rather than the chemical composition. Dose dependant responses are collectively contributed by the synthetic, chemical and biological identity of any NPs. Dose and related properties of NPs will greatly contribute to the processes such as uptake, transport and biotransformation of any NP (Graham *et al.* 2017). For careful risk assessment and regulatory processes of NPs, strict dose evaluations are therefore mandatory.

2.7.7 Route of exposure

QDs usually enter into host system physiology via various routes such as oral, olfactory, respiratory as well as dermal either during production, transport, usage and research activities (Srikanth. 2020). NPs dispersed in air can enter the body through inhalation process and get deposited along the respiratory tract from nose to lungs.

Entry via olfactory and respiratory routes will lead to alveolar deposition, inflammation and fibrosis. Inorder to translocate from alveolar surface to the circulatory system and to other organs, QDs must avoid capture by alveolar macrophages (Ellenbecker and Tsai. 2015). QDs being extremely small in size can easily penetrate through skin pores. Underneath the dermal layer, is rich with blood vessels, lymph and macrophages and therefore the absorbed NPs can be easily entered into blood and translocated to different organs.

2.7.8 QD- protein corona

QDs can get rapidly surrounded by protein layers inside the biological fluid. This colloidal behaviour is known as protein corona formation, which have a great influence in the behaviour of NPs inside the physiological system. Protein corona will be formed as a result of the reciprocity of competition of various proteins present in the biological fluid. It was reported that, this protein corona formed QDs will avoid nonspecific binding to the cell membrane and therefore reduces the unwanted internalisation of QDs (Zyuzin *et al.* 2017). Therefore, inorder to target QDs to specific cellular compartments, protein surface functionalisation can be taken into account as an effective strategy, which will avoid unwanted cellular localisation of QDs. Protein corona formation will lead to increase in residence time of NPs in early endosome stages also.

2.7.9 Stability

Chemical stability is a major factor that determines the possible toxic response NPs can elicit in the physiological system. Various studies have proved that chemically

stable metallic NPs possess no significant toxicity where as those NPs and QDs which are able to get oxidised, reduced or leached have strong tendency to induce cytotoxic and genotoxic responses with the release of metal ions. In solution, NPs have showed a great tendency to adsorb a large amount of ions and other chemical moieties. These adsorbed moieties can be protein like biological macromolecules also, which further leads to protein denaturation and loss of protein function (Auffan *et al.* 2009). Dissociation into ions can make the compound even more toxic, for example; dissociation of ZnO NPs will release Zn^{2+} ions and $Zn(OH)^{-1}$ ions, which will become predominantly more toxic by changing the pH of the physiological system. Similar way, Cd containing QDs when leached or disintegrated leads to serious heavy metal intoxication. Some NPs like CeO_2 will get reduced when come into contact with biological media which further elicit strong cytotoxic effects (Fukui *et al.* 2002). Loss of colloidal stability and subsequent aggregation of QDs will tend to granuloma formation followed by acute inflammation.

2.8 Mechanism of toxicity

QDs evoke toxic adverse effect by various mechanisms such as generation of ROS, oxidative stress, apoptosis/ necrosis pathway activation, mitochondrial/ lysosomal damage, ER stress and calcium elevation, up-regulation of certain inflammatory mechanisms as well as by eliciting genotoxic effects **(Figure 2.11).**

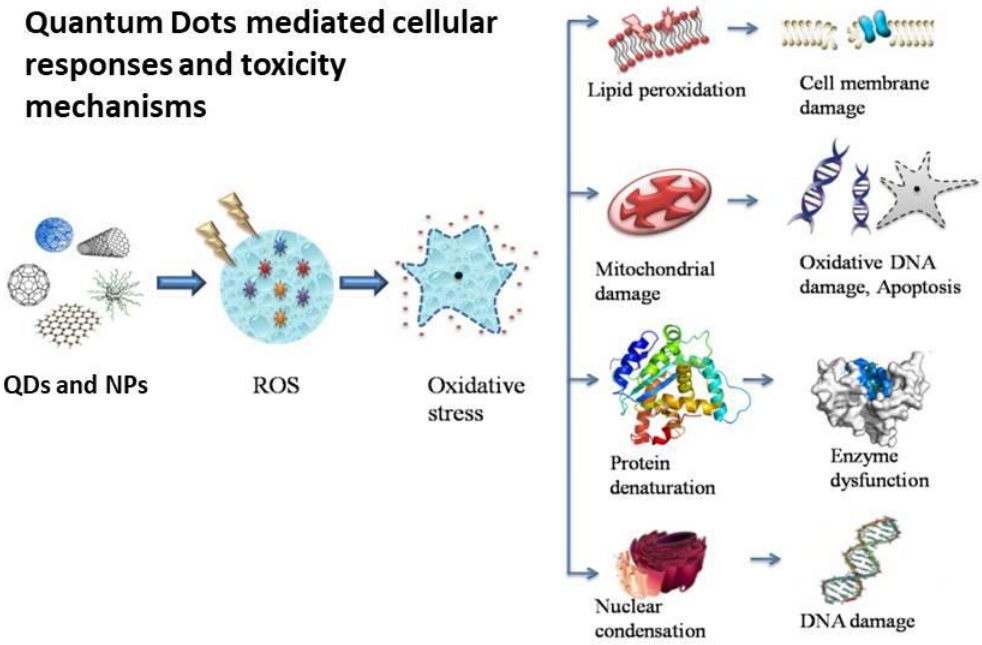

Figure 2.11: QDs mediated cellular responses and toxicity mechanisms

2.8.1 ROS production and oxidative stress

ROS constitutes highly reactive species of molecular oxygen that consist of a pool of reactive species such as hydrogen peroxide, hydroxyl radical, super oxide radicals, singlet oxygen, hypochlorous acid *etc*.,. These are generated either as intrinsic factors as a result of cellular metabolism, immune responses and mitochondrial respiration as well as extrinsically due to environmental contamination, cigarette smoke, engineered NPs expulsion and drug metabolism. NPs upon dissolution can mediate ROS release and these ROS can potentially damage various biological responses. This disconcertion of the normal cellular homeostasis will subsequently accounts for DNA damage, chromosomal aberration, lipid peroxidation, protein denaturation, metabolic inhibition to even carcinogenesis. Also, exposure of NPs can lead to potential loss of mitochondrial membrane potential and unpredictable activation of MAP Kinase pathway and AKT/ ERK/ AMPK signalling pathways, which will

further enhance apoptosis and cell death (Fu *et al.* 2020). High levels of ROS in mitochondria can induce membrane phospholipid damage which subsequently facilitates membrane depolarisation (Akhtar *et al.* 2020). Metallic NPs were reported to evoke cytokine signalling pathways mediating severe immune responses involving IL-1β, TNF-α, and TGF- β, which are involved in the pathogenesis of fibrosis (Liu *et al.* 2020). Moreover, ROS will potentially harm cellular oxidant and antioxidant balance.

2.8.2 Cell membrane and membrane protein damage

Mostly, cell membrane and protein damage mediated by NPs can be due to ROS mediated oxidative stress and further lipid peroxidation mechanisms. Lipid peroxidation mediated membrane protein denaturation and membrane damage constitutes one of the key pathophysiological responses of NP mediated cell damage (Hou *et al.* 2019). ROS such as superoxide radicals and hydroxyl free radicals can activate various signalling pathways such as MAPK pathway and AKT/ ERK signalling pathways which will subsequently lead to membrane disruption. Apart from this, some NPs can facilitate direct mechanical destruction of cell membranes. Asymmetric and anisotropic shapes of NPs can cause larger deformation of membrane compartments followed by higher magnitude of membrane rupture. When compared with that of spherical NPs, nanorods and nanosheets were reported to be more potent for easy disruption of cell membrane to facilitate entry of NPs without entering endocytosis pathways (Matula *et al.* 2016).

2.8.3 Mitochondrial damage

Mitochondrion is one of the most sensitive organelles that plays crucial role in various processes such as cellular energy metabolism, oxidative phosphorylation, cell differentiation and apoptosis. It is well known that mitochondria have a close link towards ROS generation. At the same time, excess ROS production can subsequently damage mitochondrial functions. NP uptake and localisation inside mitochondria can induce excess ROS production which will lead to oxidative stress, lipid peroxidation and mitochondrial membrane disruption (Alsaedi *et al.* 2019). Various proteins such as Bcl-2, Bax, Caspase *etc*., are involved in the normal regulated apoptosis mechanism. NPs that enter inside mitochondria will critically alter the regulation of these proteins whereby either activate or inactivate Caspase cascade of apoptosis. Cytochrome C, which is present in the intermembrane space of mitochondria, is a crucial enzyme regulating intrinsic apoptotic pathway. This will help in the formation of apoptosome complex and further activation of Caspase-9 and Caspase-3 enzymes. These are some possible targets of NPs induced mitochondrial damage (Zhang *et al.* 2020).

2.8.4 Lysosomal damage and autophagy

Lysosomes are known as ‘suicidal bags’, which consists of an acidic lumen containing around 60 acid hydrolases class of enzymes and a single outer phospholipid membrane. The acidic vesicles present inside the lysosomal compartment contains hydrolases that catalyse the secretion and degradation of

macromolecules and are subsequently linked to other intracellular structures such as endoplasmic reticulum, golgi bodies and endosomes for further trafficking. Lysosomes also sense the cellular metabolic status of a cell by sensing the nutritional level inside the cell and promote autophagy in necessary conditions (Blott and Griffiths. 2002). Therefore any damage to lysosomes can potentially alter the cellular metabolism and fate of the cell. Normal lysosomal functions depend on the intra-lysosomal pH and vesicular type H^+-ATPase activation. It is anticipated that intracellular uptake of NPs of any dimensionality can critically alter these conditions whereby alters the pH inside the lysosome. This altered pH will affect the function of acid hydrolases enzymes that are involved in lysosomal mechanisms. Mainly via clathrin mediated and caveolae mediated endocytosis; NPs reaches the lysosomes. Several studies have reported that the massive uptake of NPs can induce cytosolic acidification making acid hydrolases inactive and promote necrosis. On the other hand, partial permeabilization results in ROS generation leading to apoptosis (Vandebriel De Jong. 2012). In contrast, QDs can cause lysosomal swelling (Peynshaert *et al.* 2017). Increased presence of autophagososmes due to NP uptake is probably due to impaired lysosomal trafficking due to actin filament degradation (Stern *et al.* 2012).

2.8.5 Apoptosis and necrosis

NPs have the ability to produce ROS which is the main causative factor for all the cellular damages. These highly reactive molecules can regulate various cellular fates inside the cell such as apoptosis, necrosis, necroptosis and autophagy. Necrosis is the

nonspecific cell damage often resulting from trauma, toxic exposure, NP exposure or viral/bacterial infections. Necroptosis is regulated necrosis involving various signalling cascades. Morphology, concentration, dosage and exposure are the critical factors that affect NP mediated necrosis. One such example is; C60 nanofullerene at high doses induces ROS mediated necrosis in glioblastoma cells (Harhaji *et al.* 2007). Size, morphology, concentration, dosage and exposure time are the various factors affecting NP mediated apoptosis. ROS generation mediated by NPs is attributed to apoptosis induction in healthy cells by regulating apoptotic genes and proteins such as Bcl-2, Bax, Caspases and Cytochrome C. An increase in Bax/ Bcl-2 ratio is an indicator for selective apoptosis undergoing cells (Shafagh *et al.* 2015). Indirect generation of ROS by stimulating immune cells is another possible mechanism of NP mediated apoptosis (Kermanizadeh *et al.* 2015). Analysis of mitochondrial functions by monitoring calcium homeostasis and NADPH oxidase levels also marks suggestive alternates to assess apoptosis. Therefore analysing the immune status of cells and possible mitochondrial function analysis marks crucial factors for determining the apoptosis and necrosis mediated cell death in a cell prior to NP entry.

2.8.6 Inflammatory responses

NPs show better adhesive and penetration properties towards immune cells and epithelial cells. NF-κB and COX-2 pathways are the major inflammatory pathways that get altered as a result of NP uptake by cells. NPs like metallic NPs once reaches the blood stream will interact with plasma proteins, which lead to the formation of protein corona surrounding the NPs. The major protein components of this protein

corona include IgM, IgG and fibrinogen, which are commonly detected in almost all NP-protein corona complexes (Vinluan and Zheng. 2015). These immunoglobulins are directly involved in inflammatory responses. Protein corona formation is highly dependent on the chemical composition, morphology, surface charge, exposed chemical groups on NP surface and hydrophobicity. When these protein corona formed NPs interacts with the immune cells like macrophages and neutrophils, the protein part will tend to act as ligands for the receptors of such cells to further bind and evoke inflammatory responses. This will eventually leads to the expression of various pro-inflammatory cytokines such as IL-1, IL-1β, and TNF-α, which are directly involved in the up-regulation of inflammatory response pathways (Lawrence. 2009). It was reported that certain NPs induces the production of IL-13, which is a pro inflammatory cytokine and growth factor that promotes mast cell proliferation. These activated mast cells will further secrete histamines, arachidonic acid and cytokine like inflammatory mediators (Song *et al*. 2019).

2.8.7 Intracellular Ca^{2+} elevation and ER stress

NPs can mediate endoplasmic reticulum (ER) stress by triggering elevated Ca^{2+} levels. ER plays pivotal role in controlling Ca^{2+} homeostasis and protein folding. NP uptake by ER can lead to unchecked release of Ca^{2+} into cytosol that cause ER stress. This high level of Ca^{2+} will subsequently activate the phosphorylation of CREB transcription factor which will further induce the activation of PPP2 (protein phosphatase-2). This protein will regulate certain critical pathways in cellular metabolism (Christen *et al.* 2014). Therefore ER stress induced PPP2 protein expression is an indicator of NP induced cytotoxicity. This ER stress can trigger

apoptosis also. ER stress can further lead to accumulation of misfolded proteins that forces the cell to undergo apoptosis to avoid further critical implications. High doses of NPs can lead to high ROS production, which can evoke membrane damage to various sub cellular organelles and disruption of Ca^{2+} homeostasis. In neuronal cells, this imbalance can lead to cerebral edema like conditions.

2.8.8 Genotoxicity and DNA damage

Large surface area, high cellular penetration efficacy and comparatively smaller size make NPs; especially QDs get rapidly uptaken by cells and even at the nuclear level. Decrease in size will eventually evoke an extraordinary increase in its reactivity that will further lead to subsequent unwanted interaction with cellular bio-entities (Barabadi *et al.* 2019). This will greatly accounts for the unacceptable level of toxic impacts it can impose at the genetic and genomic level. ROS generation and further oxidative stress mediated DNA damage accounts for the major mechanism by which NPs induce genotoxicity**.** This will ranges from chromosomal aberration, chromosome condensation to DNA breakage depending upon the extend of toxicity induced by such materials. Massive generation of ROS usually overwhelms the antioxidant system inside the body which will lead to the oxidation of biological macromolecules like nucleic acids and proteins. Many carcinogenic NPs and chemicals induce this irreversible genotoxic effect by causing DNA double strand breaks and consequent genetic mutation (Wypij *et al.* 2020).

CHAPTER 3: MATERIALS AND METHODS

3. MATERIALS AND METHODS

3.1 Chemicals

Tungsten disulphide, N-methyl pyrollidone, sodium azide, Griess reagent, Histopaque, thiobarbituric acid, trypan blue and DNA isolation kit were purchased from Sigma Aldrich (USA). MTT and neutral red reagents were from SRL laboratories Pvt Ltd, India. Endosafe PTS kit was acquired from Charles River (USA). DMEM and fetal bovine serum (FBS) were obtained from Gibco Life technologies (USA), calcein AM, JC-1 Dye (Mitochondrial Membrane Potential Probe) and CyQUANT^{TM} LDH cytotoxicity assay kit were purchased from ThermoFisher Scientific (USA). Cytopainter Rhodamine-phalloidin dye was from Cytoskeleton, Inc (USA). Coomassie brilliant blue and Folin's reagent were bought from Merck, India. Haematoxylin, eosin, ethidium bromide, Hoechst 33342, antibiotic/antimycotic solution and 0.25% trypsin were purchased from Himedia, India. NF kappa B primary antibody and Alexa fluor/ Rhodamine tagged fluorescent secondary antibodies were purchased from Abcam (UK). Annexin/PI apoptosis assay kit from Invitrogen (USA). Caspase 3 primary antibody was procured from Cell Signalling Technology (USA). 3H-tritiated thymidine was obtained from American Radiolabelled Chemicals Inc. Apoptotic DNA ladder kit was procured from Roche Diagnostics (Germany). Diethylene triamine penta acetic acid (DTPA) and pyrogallol were procured from CDH analytical reagents, India. Reagents for hematological analysis were purchased from Horiba (Japan). Reagents for urine and blood biochemistry analysis were procured from Erba Mannheim (Germany).

3.2 Equipments

UV/Vis spectrophotometer (UV 1601, Shimadzu, Japan,Cary 100 Bio, Varian Inc, USA, Lambda 25, UV/Vis spectrophotometer, Perkin Elmer, USA). Fluorescence emission spectroscopy (FP-8200 (JASCO Inc. Japan). Zeta potential: Malvern Zetasizer Nano ZS (USA) supplied with DTS Nano V4.2 software. Fourier Transform Infrared Spectroscopy (FTIR) spectroscopy (Shimadzu, IR Prestige 21, Diamond ATR mode), with a spectral range 4000 cm^{-1} - 400 cm^{-1}. X-Ray Diffraction (XRD) using D8 Advance Twin- Twin Diffractometer (Bruker, USA), equipped with Kα1 and Kα2 copper radiations; data analysis was done using Topaz 6.0 software. High Resolution Transmission Electron Microscopy (HRTEM); JOEL/JEM 2100 equipped with LaB 6 electron gun with a point resolution of 0.23nm and lattice resolution of 0.14nm;operating at 200 kV. X-ray Photoelectron Spectroscopy (XPS), PHI 5000 Versaprobe Scanning ESCA Microprobe (Physical Electronics, USA) with a scanning monochromatic Al κα1 X-ray source. Thermogravimetric analysis (TGA): Perkin Elmer STA 600. Inductively Coupled Plasma-Mass Spectroscopy (ICP-MS), Endotoxin content: Endosafe PTS. Laminar air flow (Mark Air particulars, India). Sonicator (Maxsell, India), CO_2 incubator (Sanyo, Japan and Panasonic, Japan). Flow cytometry (FACS Aria III (BD Biosciences) and Imaging Flow Cytometry FACS (Flowsight, Amnis). Phase contrast microscope (Leica/Leica DMC 2900, Olympus CX31, Japan), Fluorescent microscope (Axio Scope A1 Carl Zeiss, Germany).

Tissues homogenizer: (Polytron P 3100 homogenizer, Switzerland). Hematology analyser: Nihon Kohden (Japan). Biochemistry analyser: Erba Mannheim XL300 (Germany). Urine analysis: Uro-dipchek 300 (Erba Mannheim, Germany). Microtome: Leica RM 2125 RT, Germany. Monochromator based multimode microplate reader (BioTeck Instruments, USA), Incubator shaker (New Brunswick Scientific, USA), Fluorescent microplate reader (Tecan Infinite 200 Pro, Switzerland), Refrigerated centrifuge (Eppendorf, USA), Transilluminator, Bio Imaging system (Syngene, UK). Scintillation counter (Hidex, Finland).

3.3 Animal husbandry and welfare

Healthy Sprague Dawley rats were procured from the Division of Laboratory Animal Science Biomedical Technology Wing, Sree Chitra Tirunal Institute for Medical Sciences and Technology (Institution of National Importance, under Govt. of India), Trivandrum. Healthy Sprague Dawley rats weighing 300-350g were chosen for the *in vivo* acute toxicity and biodistribution studies.

All the animals were provided with proper care and maintained at 12h light and dark cycle maintaining constant temperature of 22 ± 2°C and relative humidity of 30-70%. Animals were provided with standard pellet diet and water *ad libitum.* In addition, each animal cage was carefully labelled for name, experiment number, number of animals, date of commencement and end of experimental period. Individual animals were marked using picric acid for identification. A period of 5 days was provided for acclimatisation before the beginning of experiments. All the animals were routinely monitored for health

by cage side observation. The animals were handled humanely without causing any pain or stress and with due care for their welfare. All the necessary care and management of the animals were carried out in compliance with the regulations of Committee for the Purpose of Control and Supervision of Experiments on Animals (CPCSEA).

3.4 Animal ethics

All the experiments were carried out after getting the approval of Institute Animal Ethics Committee (IAEC). Animal experiments were strictly confined to the guidelines of IAEC guidelines which are approved by the CPCSEA, Govt of India. IAEC approval No: SCT/IAEC-377/NOVEMBER/2020/107.

3.5 Synthesis and characterisation of tungsten disulphide quantum dots (WS_2 QDs)

WS_2 QDs of spherical morphology was synthesised by solvothermal exfoliation method using N-methyl pyrolidone (NMP) solvent by following the experimental conditions depicted in **Figure 3.1**

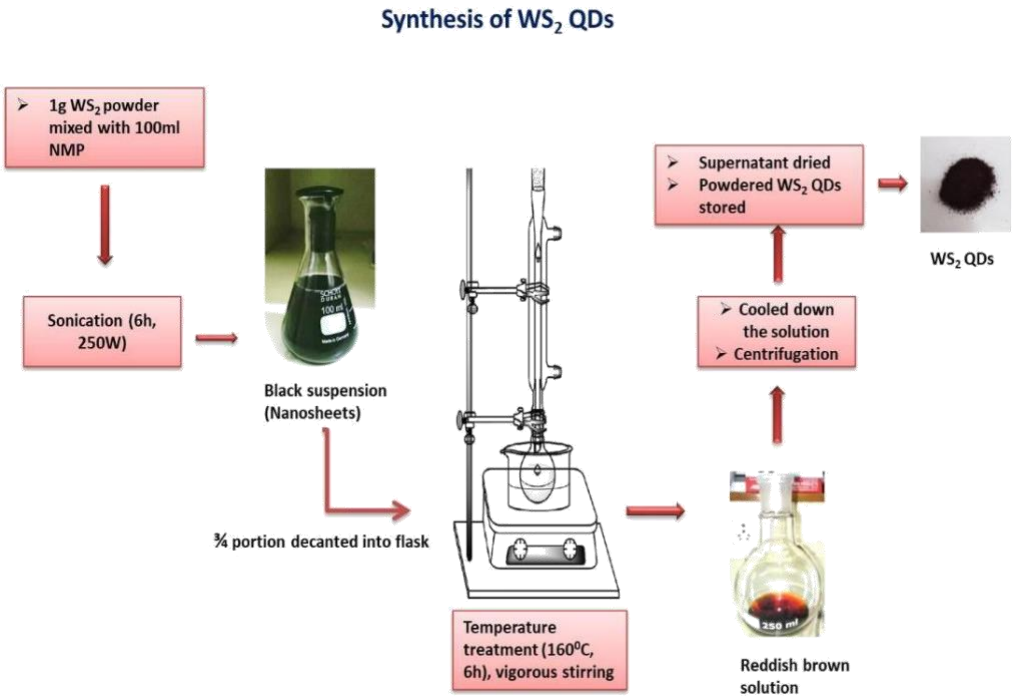

Figure 3.1: Schematic representation of detailed synthesis procedure for WS_2 QDs synthesis

3.5.1 Synthesis of tungsten disulphide quantum dots (WS_2 QDs)

WS_2 QDs were synthesized by solvothermal exfoliation method using N-methyl pyrrolidone (NMP) solvent by modifying the protocol suggested by Shengjie Xu *et al.*, (2015). In a typical experiment, 1g bulk tungsten disulphide (WS_2) powder (size 1µm, 99% purity) was added to 100ml N-methyl pyrrolidone (NMP) solvent and mixed well using a magnetic stirrer for 5 minutes. The black suspension was then allowed to sonicate continuously for 6h at 250W power under soft mode. Top 2/3 portion was decanted into a round bottom flask and underwent temperature treatment for 6h under vigorous stirring (1500rpm). The resultant reddish brown suspension was then centrifuged at 2000rpm for 10minutes to remove the unexfoliated bulk powder. The supernatant was further collected and dried. The brown powder was collected and stored for further use.

3.5.2 Physico-chemical characterisation of WS_2 QDs

3.5.2.1 Absorbance Spectra

Absorbance spectra was analysed to detect the presence of WS_2 QDs in solution and to detect the excitation wavelength of the QDs. WS_2 QDs dispersed in water was placed in a quartz cuvette and placed inside the slot of a UV/Vis spectrophotometer (Cary 100 Bio, Varian Inc, USA) and scanned over a range of wavelength from 250nm to 700nm. The typical absorbance peak of WS_2 QDs was determined from the absorbance spectra graph.

3.5.2.2 Fluorescence Emission Spectra

Fluorescence emission spectroscopy was used to analyse the emission wavelength and fluorescence intensity of WS_2 QDs. WS_2 QDs was carefully transferred into a glass cuvette and placed inside the slot of the spectrofluorometer. The excitation wavelength was set as 370nm and scanned the possible emissions over a range of wavelengths from 300-800nm (FP-8200, JASCO Inc. Japan).

3.5.2.3 Fourier Transform Infrared Spectroscopy (FTIR)

FTIR spectroscopy was used to analyse the chemical nature and functional groups present in the material. The intact material identification is possible by analysing the fingerprint regions of the FTIR spectrum which is distinct for individual compound. FTIR spectra of both bulk WS_2 and WS_2 QDs were analysed to evaluate the possible

material changes and chemical deformations occurred while thinning down to QD confinement under vigorous sonication and temperature treatments (Shimadzu, IR Prestige 21, Diamond ATR mode, with a spectral range 4000 cm^{-1} - 400 cm^{-1}).

3.5.2.4 X-Ray Diffraction (XRD)

X ray diffraction pattern of WS_2 QDs was analysed to confirm the effective exfoliation of QDs from bulk WS_2 particles. XRD data will give the detailed information about the preferred crystal orientation, structure and phase identification of the material. XRD pattern of the material was obtained using D8 Advance Twin- Twin Diffractometer (Bruker, USA), equipped with Kα1 and Kα2 copper radiations. Data analysis was done using Topaz 6.0 software.

3.5.2.5 High Resolution Transmission Electron Microscopy (HRTEM)

Size and morphology of the QDs were analysed using HRTEM; JOEL/JEM 2100 equipped with LaB6 electron gun with a point resolution of 0.23nm and lattice resolution of 0.14nm operating at 200 kV. The synthesised WS_2 QDs dispersion was directly deposited on a 300 mesh carbon coated copper grid. The solvent was allowed to dry by evaporation. The samples were then observed under image mode and diffraction mode.

3.5.2.6 X-Ray Photoelectron Spectroscopy (XPS)

The surface physico-chemical characteristics such as binding energy of individual tungsten (W) and sulphur (S) atoms, their chemical state and conformations were

analysed using XPS. XPS analysis of WS_2 QDs was done by X-ray Photoelectron Spectroscopy, PHI 5000 Versaprobe Scanning ESCA Microprobe (Physical Electronics, USA) with a scanning monochromatic Al κα1X-ray source.

3.5.2.7 Thermogravimetric Analysis

Phase transitions, desorption and thermal decomposition of the material was analysed using thermogravimetric analysis (Perkin Elmer STA 600). Mass, time and temperature were considered as basal measurement parameters in TGA analysis. TGA analyser measures the change in mass of the material over time with a constant increase in temperature. Phase transformation and melting temperature of QDs can be determined by DTA (Differential Thermal Analysis). The rate of change in material weight (% material decomposition) was analysed by DTG (Derivative Thermo Gravimetric) curve. 10mg WS_2 QDs was placed on a platinum base and loaded on to the instrument and proceeded for thermal analysis. Temperature range was set between 35-720^{0}C under inert atmosphere and at a rate of 7^{0}C/min temperature rise.

3.5.2.8 Zeta Potential

Zeta potential was used to analyse the surface charge of WS_2 QDs. Using a Zetasizer Nano ZS (Malvern, 52 USA) instrument equipped with DTS Nano V4.2 software, the Zeta potential (ζ) of the sample was analysed.

3.5.2.9 Stability analysis of WS_2 QDs

Stability of the synthesized WS_2 QDs (0.5mg/ml) was analysed using UV/Vis spectroscopy continuously for a period of 100 days at an interval of 20 days. Typical absorbance peak value for the individual experiment was recorded at 370nm and represented in graphical representation. Also the fluorescence emission reading at 500nm was recorded using fluorescent reader to analyse the fluorescence stability of the synthesized QDs (Tecan Infinite 200 Pro, Switzerland).

3.5.3 Fluorescent microscopic observation of dried WS_2 QD pellets

Dried WS_2 QDs was deposited on a microscopic glass slide and observed under fluorescent microscope using green filter to analyse the fluorescence emission of the QDs.

3.5.4 Endotoxin detection

Endotoxin content of WS_2 QDs was assessed using Charles River Endosafe PTS Kit. The principle behind is, the endotoxin present in the sample will form gel clot when reacts with Limulus amebocyte lysate in the kit. The gel clot formed will be directly proportional to the amount of endotoxin present in the sample. Briefly, 100µg/ml of WS_2 QDs was dispersed in endotoxin free water and centrifuged at 14000rpm for 15min. The supernatant was collected and subjected to endotoxin contamination detection. 25µl of the supernatant was added to the cartridge well and loaded on to

the Endosafe PTS. Readings were procured and the endotoxin content in the sample was expressed in EU/ml.

3.6 In vitro cytotoxicity and bio-nano interaction studies using LN-229 glioblastoma cells

Cellular interactions and *in vitro* cytotoxicity studies were done using LN-229 human glioblastoma cell lines. These are epithelial adherent type cells having a doubling time of approximately 24h. Various cell viability assays, free radical generation assessment, mitochondrial activity, cytoskeletal integrity, genotoxicity, intracellular organelle integrity studies and apoptosis in presence of WS_2 QDs were analysed using LN-229 glioblastoma cells (**Figure 3.2**).

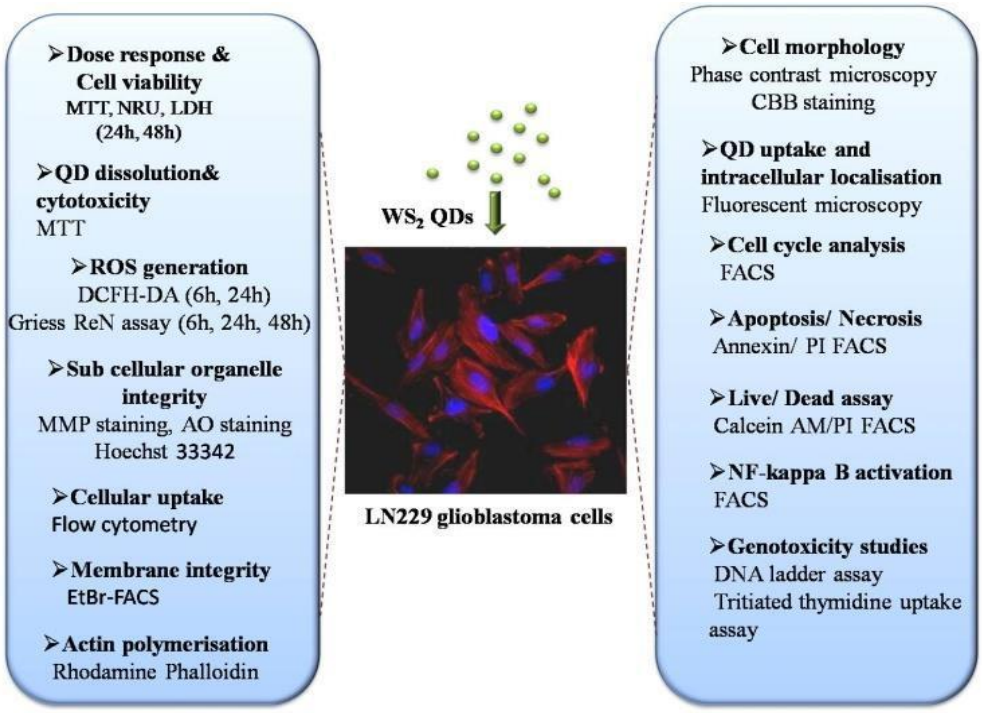

Figure 3.2: Flow chart of cellular interactions of WS_2 QDs with LN-229 glioblastoma cells

3.6.1 Collection and culturing of LN-229 cells

LN-229 human glioblastoma cells were collected from National Centre for Cell Science (NCCS), Pune, India. Cells were grown in Dulbecco's Modified Eagle Medium (DMEM) supplemented with 10% FBS and 1% Antibiotic/Antimicotic (AB/AM) solution. The cells were maintained at 37^0 C in a 5% CO_2 supply incubator under sterile conditions.

3.6.2 Cell culture and particle treatment

LN-229 cells were cultured in DMEM medium supplemented with 10% FBS and 1% AB/AM solution. Cells were seeded in appropriate seeding density depending on the assays performed and kept in a CO_2 incubator with 5% CO_2 at 37^0 C temperature. 2mg/ml stock solution of WS_2 QDs were prepared freshly prior to each experiment and sonicated in a bath sonicator for 10 minutes to ensure proper dispersion of QDs. The cells were then exposed to varying concentrations of WS_2 QDs (10, 20, 40, 80, 160, 320 and 640µg/ml) made out of 2mg/ml concentrated stock, for different time durations (6, 24 and 48h). To nullify the effect of QD fluorescence and related interferences, separate QD blanks were kept for all the individual concentrations during each experiment. For FACS assays, separate compensation matrix files were created with particle alone blank to avoid QD interference with the assays. All the FACS data analysis was performed by incorporating this compensation matrix file to minimize particle effect on assay. All the experiments were done in triplicates to minimize error.

3.6.2.1 Particle uptake analysis by Flow Cytometry

Particle uptake by LN-229 cells was analysed using flow cytometry as per the protocol suggested by Kumar *et al.,* (2015). In flow cytometry, forward scatter (FSC) represents the size of the cell and side scatter (SSC) represents the cell granularity. Increase in cell granularity is a suggestive of QD uptake and subsequently the side scatter also increases, which is a criterion for evidencing cellular uptake of NPs. While the FSC of the cell remains the same. In a typical experiment, LN-229 cells were seeded at an initial seeding density of $3x10^5$ cells/well and kept undisturbed overnight in a 5% CO_2 incubator. Cells were then exposed to 40µg/ml and 80µg/ml of WS_2 QDs and again incubated for another 24h. The cells were then harvested by trypsinisation and centrifuged at 1200 rpm. The pellet was resuspended in 500µl PBS. The cells were analysed by flow cytometry (Amnis FlowSight, Luminex Corporation). 10000 single cells were acquired based on area/ aspect ratio and the count of SSC intensity was plotted on histogram. The increase in SSC will be directly proportional to the granularity ie, particle uptake.

3.6.2.2 Cellular uptake and intracellular localisation of WS_2 QDs

QDs are excellent bioimaging materials due to its inherent fluorescent properties which makes them suitable candidates for bioimaging without further addition of any fluorescing tags. Therefore inorder to further confirm the cellular uptake and *in vitro* imaging potential of WS_2 QDs, LN-229 glioblastoma cells served as the major subject cell lines. Briefly, $1x10^5$ cells were seeded on a cell culture plate and incubated overnight at 37^0 C in a CO_2 incubator supplemented with 5% CO_2 for the

cells to attain morphology and confluence. Cells were fixed using 1.2% paraformaldehyde and permeabilised using 0.1% triton-X-100. WS_2 QDs were added at selected concentrations of 100µg/mL and incubated for 4h. Inorder to understand the possible localisation of QDs inside cytoplasm, the cells were counterstained with Rhodamine-phalloidin (cytoskeleton) and DAPI stains (nucleus). Washed twice with cold PBS and viewed under fluorescent microscope (Axio Scope A1, Carl Zeiss, Germany).

3.6.2.3 Dose response by MTT Assay

Cells were assessed as a function of mitochondrial metabolic activity using MTT (3-(4, 5-Dimethylthiazol-2-yl)-2, 5-Diphenyltetrazolium Bromide) colorimetric assay followed by the method described by Morgan (1998). The viable cells will reduce MTT dye to insoluble purple colored formazan crystals, which are further solubilised by adding DMSO and read spectrophotometrically. Cells were seeded in a 96 well plate at an initial seeding density of $1x10^4$ cells/well and incubated overnight. The cells were then exposed to 10, 20, 40, 80, 160, 320 and 640µg/ml concentrations of WS_2 QDs for 24h and 48h respectively. Untreated cells were used as negative control and the cells exposed to 0.02% phenol served as the positive control. The medium was then replaced with 100µl MTT reagent (50µg/ml in DMEM medium) and again incubated for 3h in dark. Media was discarded and purple colored formazan crystals were solubilised using 100µl DMSO and again incubated for 15min in dark. Readings were procured at 540nm using a multiplate reader (ELx808 ultra-microplate reader, Biotech instruments, USA).

3.6.2.4 Analysis of WS_2 QDs interference with MTT result

Many NPs and QDs may directly interact with MTT reagent and interfere with the assay. Particle interference with MTT result can be analysed by incubating QDs with MTT reagent. Varying concentrations of WS_2 QDs (10, 20, 40, 80, 160, 320 and 640µg/ml) were incubated for 24h in a 96 well plate followed by incubation with 100µl MTT (50µg/ml) for 3h. 100µl DMSO was added and incubated for another 15min. Absorbance was measured at 540nm using multiplate reader (ELx808 ultra-microplate reader Biotech instruments, USA).

3.6.2.5 QD dissolution and related cytotoxicity

Effect of particle dissolution in medium and related cytotoxicity was analysed using MTT assay. 10, 20, 40, 80, 160, 320 and 640µg/ml of WS_2 QDs were incubated with DMEM supplemented with 10% FBS for 72h and the solution was centrifuged at 10000 rpm for 10min. The supernatant was collected. Cells were seeded at an initial density of $1x10^4$ cells/well in a 96 well plate and incubated overnight to attain confluence. The cells were then exposed to the respective QD supernatants and again incubated for another 24h. MTT assay was carried out as per section **3.6.2.3**.

3.6.2.6 Neutral Red uptake Assay

Neutral Red Uptake assay (NRU assay) provides a quantitative estimation about cell viability and lysosomal activity. It is based on the ability of viable and active cells to

incorporate the supravital neutral red dye inside the acidic lysosomes (Borenfreund and Puerner. 1985). Briefly, LN-229 cells cultured at an initial density of $1x10^4$ cells/ well were incubated with varying concentrations of WS_2 QDs (10, 20, 40, 80, 160, 320 and 640 µg/ml) for 24 and 48h at 37^0 C in a 5% CO_2 incubator. Untreated cells were kept as negative control and the cells exposed to 0.02% phenol served as the positive control. Media was replaced with 1% neutral red dye and again incubated for 3h in dark. Cells were washed with PBS and the neutral red dye inside the lysosomes was solubilised using acid/ alcohol reagent (1%, v/v, acetic acid and 50% ethanol). Incubated on a shaker incubator at 60rpm for 30min. Absorbance was measured at 540nm using microplate reader (ELx808, Biotech instruments, USA). Subsequent images were procured using a phase contrast microscope (Leica, fitted with Leica DMC 2900 Camera).

3.6.2.7 Lactate Dehydrogenase Assay for cytotoxicity

Lactate dehydrogenase is an oxido-reductase enzyme present in all living systems which catalyses the interchange of lactate to pyruvate with the concomitant conversion of NAD^+ to NADH. In response to a toxin exposure or injury, this LDH will get released into the blood stream or physiological medium. Therefore quantitation of LDH release has a significant clinical importance. In a typical experiment, LN-229 cells were seeded on a 96 well plate at a seeding density of $1x10^4$ cells/well followed by WS_2 QDs treatment at 10, 20, 40, 80, 160, 320 and

640µg/ml concentrations for 24h and 48h. By the time, if any cell damage occurs, LDH get released into the media. Therefore 50µl of the cell culture supernatant was taken out into a separate 96 well plate and 48µl LDH buffer and 2µl LDH substrate (NADH) were added according to the protocol specified in kit (Sigma Aldrich, Cat. No: MAK066-IKT). Initial reading was taken using a microplate reader at 450nm (Tecan Infinite 200 Pro, Switzerland) and kept the same for 30 min incubation. Final readings were also recorded after the incubation time. The difference between these readings was the amount of NADH released, which was directly proportional to the LDH release from the cytosolic compartment. 0.02% phenol was used as positive control.

3.6.2.8 Cellular morphology analysis by phase contrast microscopy

Cellular morphology of LN-229 cells followed by WS_2 QDs exposure for 24 and 48h was analysed using phase contrast microscopy. Cells were seeded in a 6 well plate at a seeding density of $1x10^5$cells/well and incubated overnight in a 5% CO_2 incubator at 37^0C for the cells to attain confluence. WS_2 QDs were added at selected concentrations of 10, 20, 40, 80, 160, 320 and 640µg/ml. Cells without QD exposure was kept as negative control. Cellular morphological changes after 24 and 48h was observed and images were procured using phase contrast microscope (Leica) fitted with camera (Leica DMC 2900).

3.6.2.9 Live/ Dead assay by Calcein AM/ PI FACS

Membrane damage followed by cell death was analysed by double staining with Calcein AM and PI. This assay works on the principle based on the conversion of the cell permeant non-fluorescent Calcein AM dye to fluorescent Calcein dye by intracellular esterase activity in live cells. In contrast; PI is a cell impermeant dye to live cells, but is permeable to dead cells with compromised cell membrane integrity. When PI gain access to nucleic acids, its fluorescence increases dramatically and is therefore efficient in identifying dead cell population. Briefly, LN-229 cells were seeded in a 6 well plate at an initial density of $1x10^6$cells and incubated for 24h for the cells to attain confluence. Media was replaced with fresh media containing 40, 80, 160, 320 and 640µg/ml concentrations of WS_2 QDs and again incubated for 24h. Cells without WS_2 QDs treatment was kept as negative control. 6µM Calcein was added to all the wells and incubated for 30 min followed by 2µM PI. Cells were washed twice with ice cold PBS and centrifuged at 1300rpm for 10 minutes. FACS analysis was done using Flowsight Amnis at a fluorescence emission of 520nm and 630nm for Calcein AM and PI respectively. A total event of 10000 cells per sample was acquired, and the data were analyzed using Ideas 6.2 software.

3.6.2.10 ROS generation studies

Reactive oxygen species such as hydroxyl, peroxyl and NO radicals were analysed using DCFH-DA assay and modified Griess reagent assays after incubation of LN-229 cells with WS_2 QDs for varying time periods.

3.6.2.10.1 Detection of reactive oxygen species by DCFH-DA Assay

Hydroxyl and peroxyl free radical generation as a result of WS_2 QDs exposure was analysed using 2′, 7′-Dichlorodihydrofluoresceindiacetate (DCFH-DA) assay. Upon exposure to DCFH-DA, the ROS generated inside the cells will oxidise this compound into dichloro fluorescein (DCF), which emits green fluorescence, which is further quantified using fluorescent plate reader (Halliwell and Whiteman. 2004). Briefly, LN 229 cells were seeded in a 96 well plate at an initial seeding density of $1x10^4$ cells/well and incubated overnight. After the cells reached 80% confluence, the media was removed and 100µl (2 µM/well) DCFH-DA was added to each well. The cells were incubated in dark for 45min at 37^0C supplemented with 5% CO_2. Varying concentrations of WS_2 QDs (10, 20, 40, 80, 160, 320 and 640 µg/ml) was allowed to expose to cells for 6h and 24h. Cell alone was kept as negative control and 0.1mM H_2O_2 treated cells were used as positive control. After incubation, media was replaced with 100µl PBS and quantitatively estimated the fluorescence at excitation/emission wavelengths of 495 and 530nm using a fluorescent microplate reader (Tecan infinite Pro).

3.6.2.10.2 Detection of reactive nitrogen species by Griess reagent assay

Griess reagent assay was performed to evaluate the reactive nitrogen species generation followed by WS_2 QD treatment in LN-229 cells. LN-229 cells at an initial density of $1x10^4$ cells/well were seeded in a 96 well plate and incubated overnight. The cells were then exposed to 10, 20, 40, 80, 160, 320 and 640µg/ml of WS_2 QDs

and again incubated for 6h, 24h and 48h respectively in a 5% CO_2 incubator at 37^0 C. Cell alone was kept as negative control. 0.02µg/ml phenol was used as positive control. 50µl of supernatant was collected and treated with equal volume of Griess reagent. Cells were then incubated for 10min at room temperature. Absorbance was subsequently measured using a multiwell plate reader (Tecan Infinite Pro). The concentration was calculated from the sodium nitrate (0.5, 1, 2, 4, 6, 8 and 10 µg/ml) standard graph.

3.6.2.10.3 Influence of catalase activity on ROS generation

Catalase activity is expressed by all cells. When compared to normal cells, catalase activity is about 50% less in tumour cells, which could significantly affect the removal of H_2O_2 from tumor micro-environment making tumor cells more susceptible to ROS mediated cell death. Influence of catalase activity on the ROS induced by WS_2 QDs exposure in LN-229 cells was analysed using catalase inhibitor sodium azide (NaN_3). Cells were seeded at a seeding density of $1x10^4$ cells/well in a 96 well plate and allowed to incubate overnight. Cells were pre-incubated with 0.1mM NaN_3 for 1h. Medium was replaced with fresh medium containing 10, 20, 40, 80, 160, 320 and 640µg/ml of WS_2 QDs. ROS generation was estimated using DCFHDA**.** After 45min incubation with DCFHDA dye, fluorescence emission was analysed as described in **3.6.2.10.1.** Results were compared with cells directly exposed to varying concentrations of WS_2 QDs in the absence of catalase inhibitor.

3.6.2.11 Coommassie Brilliant Blue staining for morphology analysis

Morphological abnormalities in cells after WS_2 QDs exposure was analysed using Coommassie Brilliant Blue (CBB) staining. Briefly, $1x10^4$ cells were seeded on a cover slip in a 4 well plate and allowed to incubate overnight for the cells to attain morphology. Varying concentrations (20, 40, 80, 160 and 320µg/ml) of WS_2 QDs were then exposed to cells and incubated for 24h. Untreated cells were kept as negative control. After the incubation period, the cells were fixed using 1.4% PFA and permeabilised using 0.1% triton-X-100. CBB stain was added and incubated for another 15 minutes. Washed with ice cold PBS thrice and imaged under phase contrast microscope (Olympus CX31, Japan, fitted with Q-Imaging Go-3 camera).

3.6.2.12 Lysosomal Integrity by Acridine Orange

Lysosomal membrane integrity in cells after WS_2 QDs exposure was analysed using Acridine Orange (AO) staining. AO is a metachromatic dye that gets entrapped inside acidic lysosomal vacuoles, which will shift its intact fluorescence emission from green (inside less acidic cytosol) to red (highly acidic lysosomes) (Sohaebuddin *et al.* 2010a). Briefly, LN-229 cells were seeded at an initial density of $1x10^4$ cells/well in a 96 well plate and incubated overnight in a 5% CO_2 incubator at 37^0 C. The cells were then exposed to 10, 20, 40, 80, 160, 320 and 640µg/ml of WS_2 QDs
and incubated for 24h. Untreated cells were kept as negative control. To nullify the effect of QD fluorescence, separate QD blanks were kept for individual concentrations. After incubation period, media was replaced with AO (6µg/ml) and

kept for 20min incubation in dark. The cells were washed with ice cold 1xPBS thrice and images were procured using fluorescent microscope (Axio Scope A1 Carl Zeiss, Germany). Fluorescence was quantitatively estimated using fluorescent microplate reader (Tecan infinite Pro). Separate emissions were noted for red fluorescence (excitation/emission at 485/620) and green fluorescence (excitation/emission at 485/530). Ratio of red/ green fluorescence was analysed to represent quantitative AO uptake.

3.6.2.13 Mitochondrial Membrane Potential by JC-1 probe

Mitochondrial membrane potential followed WS_2 QDs exposure was analysed using JC-1 probe (5, 5′, 6, 6′ tetrachloro-1,1′,3,3′-tetraethylbenz-imidazolylcarbocyanine iodide). JC-1 is a cationic lipophilic dye that exist in monomeric form inside the cytoplasm emitting green fluorescence whereas inside healthy mitochondria it will get aggregate forming polymeric structure with a shift in fluorescence towards red region showing intact mitochondrial membrane potential (Shukla *et al.* 2015). Briefly, LN-229 cells were seeded at an initial density of $1x10^4$ cells/well in a 96 well plate and incubated overnight in a 5% CO_2 incubator at 37^0C. The cells were then exposed to 10, 20, 40, 80, 160, 320 and 640µg/ml of WS_2 QDs and incubated for 24h. Cells without QD exposure was kept as negative control. Separate QD blanks were kept for individual concentrations to nullify the effect of inherent QD fluorescence interference with the assay. 5µl of 200µM stock JC-1 probe was added to all the wells and incubated for 20 min in dark. Removed media and washed with

PBS twice. Images were procured using fluorescent microscope (Axio Scope A1 Carl Zeiss, Germany).

Fluorescence was quantitatively estimated using fluorescent microplate reader (Tecan infinite Pro). Separate emissions were noted for green fluorescence (excitation/emission at 485/530nm) and red fluorescence (excitation/emission at 550/600nm). Ratio of red/ green fluorescence was analysed to represent quantitative JC-1 uptake.

3.6.2.14 Cytoskeletal integrity by Rhodamine-phalloidin staining

Cytoskeletal integrity of cells followed by WS_2 QDs exposure was analysed by Rhodamine-phalloidin staining. Phalloidin is a bicyclic peptide isolated from *Amanita phalloides*, which is conjugated with red fluorescent Rhodamine dye to properly visualise F-actin filaments. It will selectively bind to F-actin filaments in fixed cells. Briefly, LN-229 cells were seeded at an initial seeding density of $1x10^4$ cells/well and incubated overnight. WS_2 QDs were treated at selected concentrations of 40, 80, 160 and 320µg/ml and again incubated for 24h at 37^0C in a 5% CO_2 incubator. Untreated cells were kept as negative control. The cells were washed with PBS and fixed using 1.4% paraformaldehyde for 15min. Excess aldehyde was then quenched using 0.1M glycine and permeabilised using 0.1% triton-X-100 for 1min. Actin filaments were subsequently stained using Rhodamine-phalloidin dye (3µl in 500µl PBS) for 30min. Nucleus was counterstained using DAPI (1µl) for 2min. The

cells were then observed under a fluorescence microscope using red, green and blue filters for Rhodamine, WS_2 QDs and DAPI respectively (Axio Scope A1, Carl Zeiss, Germany).

3.6.2.15 Membrane integrity by Ethidium bromide staining: FACS

Cell membrane integrity in LN-229 cells after WS_2 QDs exposure was analysed using Ethidium bromide (EtBr) staining. EtBr will enter only damaged cells with highly challenged membrane permeability and selectively excludes viable cells having intact cell membrane (Aeschbacher *et al.* 1986). Briefly, LN-229 cells were seeded at a seeding density of $1x10^6$ cells/well. WS_2 QDs were added at varying concentrations of 20, 40, 160 and 320µg/ml and again incubated for another 24h. Untreated cells were kept as negative control. Cells were harvested and washed with PBS. 1µl of 100µg/ml EtBr was added and again incubated for 15min at 37^0C. Cells were centrifuged (1500rpm, 5min) and resuspended in ice cold PBS. FACS analysis was done using Imaging Flow Cytometry using 630nm long pass filter (Amnis FlowSight, Luminex Corporation). A total event of 10000 cells per sample was acquired, and the datas were analyzed using Ideas 6.2 software.

3.6.2.16 Cell Cycle Analysis using PI by Flow Cytometry

Cell cycle analysis and different cell cycle events in LN-229 cells exposed to WS_2 QDs was analysed using Propidium Iodide (PI) by Flow cytometry. PI directly intercalates into the major and minor grooves of DNA double stranded helix subsequently generating a red fluorescent signal at 600nm with an excitation of

488nm. Briefly, LN-229 cells were seeded at a seeding density of $3x10^5$ cells/ well and incubated overnight for the cells to attain confluence. WS_2 QDs were treated at varying concentrations of 20, 40, 80, 160 and 320µg/ml and again incubated for 24h. Untreated cells were kept as negative control. Cells were trypsinised and washed with ice cold 1xPBS. Cells were then fixed using ice cold 70% ethanol added drop wise to the cells with gentle vortexing to avoid cell aggregation and kept in ice for 2h (cells can be kept in this condition for a few days without damage). The cells were then washed with ice cold PBS (1500rpm, 5min) and resuspended in 300µl staining solution containing 100 µg/ml RNase A, 50µg/ml Propidium Iodide and 0.1% Triton X-100. Incubated overnight at 4^0C and resuspended in ice cold 1xPBS. Flow cytometry analysis was done with 630 long pass filter (Bechman Coulter, CytoFlex).

3.6.2.17 Apoptosis by Annexin/PI FACS

Apoptosis mediated cell death following WS_2 QDs exposure was analysed using Annexin/PI apoptosis kit (Alexa Fluor® 488 Annexin V/Dead Cell Apoptosis Kit, Thermo Fisher scientific, USA). The assay is based on the principle that; during apoptosis, phosphatidyl serine (PS) molecules located in the inner plasma membrane compartment will flip outside to get exposed to cell impermeable Annexin V dye. This dye is having high affinity towards PS molecules. Briefly, LN-229 cells were seeded at an initial seeding density of $3x10^6$ cells/ well in a six well plate and allowed to incubate overnight for the cells to attain morphology and confluence. WS_2 QDs were added at varying concentrations of 20, 40, 80, 160 and 320µg/ml and incubated for 24h to allow the cells to interact with the particles. Cells without WS_2 QDs treatment was kept as negative control. 500µl Trypsin/EDTA was added to all the

wells for the cells to get detatched from the plate surface. Excess media was added to the trypsinised samples and centrifuged at 1500rpm for 5min to harvest the cells. Media was removed and replaced with 100µl 1xAnnexin Binding Buffer. 5µl of Annexin V was added and incubated for 15 min, followed by 1µl of 100µg/ml PI and again incubated for another 5min. Centrifuged at 1500rpm for 8min and washed twice to remove the excess dye. Finally the cells were resuspended in 500µl 1xAnnexin Binding Buffer and kept on ice prior to FACS analysis. FACS analysis was done using Amnis Flowsight Flow cytometry at a fluorescence emission of 530nm and 575nm for Annexin V and PI respectively. Four separate controls were set for gating such as cells alone, cells with Annexin V alone, cells with PI alone and cells treated with both Annexin V and PI. Separate compensation matrices were created prior to FACS analysis for nullifying the bleaching effect of individual dyes. A total event of 10000 cells per sample was acquired, and the data were analyzed using Ideas 6.2 analysis software.

3.6.2.18 Caspase 3 expression: FACS

Caspase 3 is a prominent member in the cysteine-aspartic acid protease (caspase) family, which plays a crucial role in regulating both intrinsic (mitochondrial) and extrinsic (death ligand mediated) apoptosis pathways. It is a downstream effector caspase in the apoptosis pathways. Caspase 3 exists as zymogens (inactive form) under normal conditions but with the initiation of apoptosis signalling cascade only, Caspase 3 undergo proteolitic processing at the conserved amino acid sequences (aspartic acid residues) and get dimerized to form active enzyme. In a typical experiment, $3x10^5$cells were seeded on a 6 well plate and incubated overnight for the

cells to attain confluence. The cells were then treated with varying concentrations of WS_2 QDs (40, 80, 160 and 320µg/ml) and incubated for 24h for the cells to interact with the QDs. Untreated cells were kept as negative control. Cells were harvested by trypsinisation and fixed using 1.4% paraformaldehyde for 15 min and permeabilised using 0.1% triton-x-100 for another 5 min. The cells were then incubated with BSA/Glycine in PBST (PBS in 0.1% Tween 20) blocking solution for 30 min to prevent unwanted protein binding. The cells were then washed with ice cold PBS. Primary Caspase 3 antibody was added (1:100 dilution) and incubated overnight at 4^0C. Rhodamine conjugated secondary antibody was added and again incubated for 2h. Washed with ice cold PBS twice and resuspended in 500µl PBS. FACS analysis was performed using Amnis Flowsight Flow cytometry FACS. A total event of 10000 cells per sample was acquired, and the data were analyzed using Ideas 6.2 analysis software.

3.6.2.19 NF-kb Activation Assay: FACS

Nuclear Factor Kappa B (NF-κB) is a transcription factor that regulates and co-ordinates the transcription of genes responsible for cytokine production, cell proliferation and cell survival. It also regulates a plethora of signalling cascades responsible for cellular resistance to invading pathogens and cell cycle regulation. To evaluate the possibility of NF-κB activation associated with the interaction of LN-229 cells with WS_2 QDs, NF-Kb activation study was carried out. The cells were seeded at an initial seeding density of $3x10^5$ cells/well and incubated overnight. The cells were then treated with varying concentrations of WS_2 QDs (20, 40, 80, 160 and 320µg/ml) and incubated for 24h for cells to interact with the QDs.

Untreated cells were kept as negative control. The cells were trypsinised and fixed using 1.4% paraformaldehyde for 15 min and permeabilised using 0.1% triton-x-100 for another 5 min. The cells were then incubated with BSA/Glycine in PBST (PBS in 0.1% Tween 20) blocking solution for 30 min to prevent unwanted protein binding. The cells were washed with PBS twice. Anti NF-Kb primary antibody was added at 1:1000 dilution in PBS and incubated overnight at 4^0C. After PBS rinse, Alexafluor tagged secondary antibody was added and again incubated for another 2h in dark at room temperature. Cells were washed using ice cold 1xPBS and resuspended in 1ml 1xPBS. FACS analysis was done using Amnis Flowsight Flow cytometry FACS. Separate compensation matrix file was created for QD alone treated sample to prevent QD interference with analysis. A total event of 10000 cells per sample was acquired, and the data were analyzed using Ideas 6.2 analysis software.

3.6.2.20 Genotoxicity Studies

Genotoxic potential of WS_2 QDs in LN-229 human glioblastoma cells was analysed by tritiated thymidine incorporation assisted cell proliferation analysis, DNA ladder assay and nuclear/chromosomal condensation using Hoechst 33342 staining.

3.6.2.20.1 Tritiated Thymidine Incorporation Assay

Cell proliferation status after QD treatment was analysed by tritiated thymidine incorporation assay using radiolabelled thymidine (^{3}H- thymidine).This assay measures the incorporated radioactive tritium labelled thymidine into the replication strands of DNA during cell division (Goodell *et al.* 2017). Briefly, LN-229 cells

were seeded on a 6 well plate at a seeding density of $1x10^4$ cells/well and incubated overnight. Varying concentrations of WS_2 QDs were added and again incubated for 48h by adding 0.5µCi of tritiated thymidine. Cells without any particle treatment were kept as negative control and 0.02% phenol treated cells were used as positive control for data comparison and analysis. After the incubation period, the cells were fixed using 5% TCA and subsequently lysed using SDS/NaOH lysis buffer. Radioactivity was measured using scintillation counter (Hidex, Finland) and expressed in CPM.

3.6.2.20.2 DNA Ladder Assay

Apoptosis is a distinct pathway of programmed cell death characterised with DNA double strand breaks, typically inter-nucleosomal DNA fragmentation (Saadat *et al.* 2015). Therefore, DNA ladder assay is a reliable method for the detection of apoptosis mediated DNA fragmentation and subsequent genotoxicity. Briefly, $1x10^6$ cells were cultured in a 6 well plate and incubated overnight for the cells to attain morphology and confluence. Varying concentrations (40, 80, 160, 320 and 640µg/ml) of WS_2 QDs were allowed to incubate with the cells for 24h in a CO_2 incubator supplied with 5% CO_2 at 37^0C. Cells without QD treatment was kept as negative control. After the incubation period, the cells were harvested. Apoptotic cells usually float over the media, therefore to avoid loss of apoptotic cells, cell supernatant was first centrifuged and collected the cells and rest of the attached cells were trypsinised and harvested (1500rpm, 8min). DNA isolation was done using Gen Elute DNA isolation kit (Roche) as per the manufacturer's instructions. The DNA was then quantified using a spectrophotometer at 260nm and 280nm respectively

(NanoDrop 1000, Eppendorf Biophotometer). Typical absorbance of 1.0 at 260nm corresponds to 50µg/ml of dsDNA. Accordingly, the exact concentration of DNA samples was calculated and a final concentration of 25µg/ml DNA was loaded into individual wells. The purity of the extracted DNA was analysed by taking the ratio of absorbance at 260nm and 280nm and a typical value that ranges from 1.6 to 1.9 corresponds to pure dsDNA. The extracted DNA samples were electrophoresed on a 1.8% agarose gel containing 0.5µg/ml ethidium bromide in 1X TAE (Tris/Acetate/EDTA) running buffer and run at 5 V/cm for 1-2h. Ikb DNA ladder (HiGenoMB, Himedia) and a positive control (supplied in kit) having apoptotic bands were loaded in separate wells for comparison. DNA bands were then visualized using GelDoc trans-illuminator system (Bio Imaging system, Syngene, UK).

3.6.2.20.3 Hoechst staining for DNA nuclear condensation

Chromosomal condensation is an indication of apoptosis. DNA of healthy cells follows an even distribution inside the spherical nucleus. During processes like apoptosis, the DNA becomes highly condensed. Dyes that bind to DNA such as Hoechst 33342 can be used to analyse chromosomal condensation. Briefly, LN-229 cells were seeded at an initial seeding density of $1x10^5$ cells/well and allowed to incubate overnight. Media was replaced with fresh media containing varying concentrations of WS_2 QDs (20, 40, 80, 160 and 320µg/ml) and allowed to incubate for another 24h. The cells were washed with PBS and fixed using 1.2% paraformaldehyde. The cells were then stained with Hoechst 33342 (1µg/ml) for

5min, washed with PBS and observed under fluorescent microscope, Axio Scope.A1 (Carl Zeiss, Germany) using blue filter.

3.7 Acute toxicity studies using Sprague-Dawley rats

In vivo acute toxicity studies were done using Sprague-Dawley rats at a dosage of 10mg/kg body weight of WS_2 QDs intraperitoneally. Detailed experimental design is given in **Figure 3.3.**

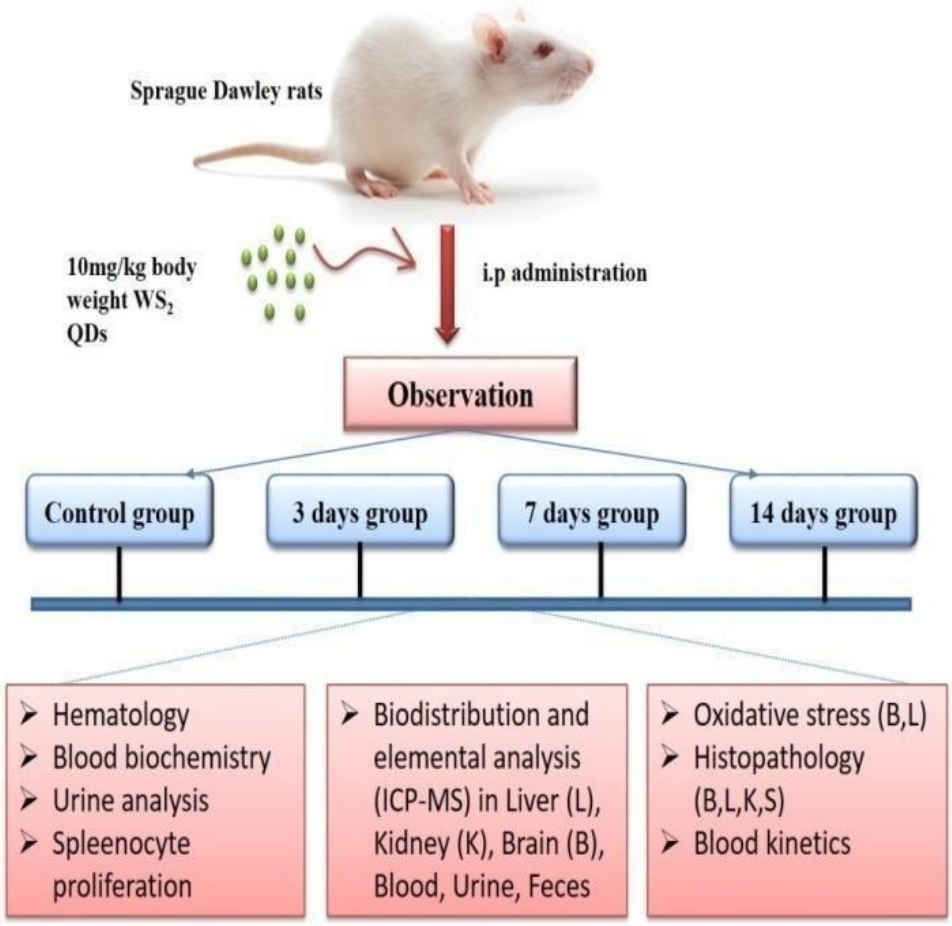

Figure 3.3: Schematic representation of *in vivo* experiments in Sprague Dawley rats

3.7.1 Experimental design and dosage

Healthy Sprague-Dawley rats weighing 300-350g were used for the study. Animals were randomly divided into 4 groups of 3 animals each; representing control (untreated groups), 3 days, 7 days and 14 days based on the period of observation. The detailed experimental design is depicted in **Table 3.1**. The first group received no treatment, hence named as control groups. All the other three groups were administered with 10mg/kg body weight WS_2 QDs in physiological saline and subsequently kept under observation for 3 days, 7 days and 14 days period. The animals were euthanized by cervical dislocation on 3^{rd}, 7^{th} and 14^{th} days respectively.

Groups	**Route of exposure**	**Number of animals**		
		3 days	**7 days**	**14 days**
Control	Intraperitoneal (i.p)		3	
10mg/kg body weight WS_2 QDs	Intraperitoneal (i.p)	3	3	3

Table 3.1: Experimental design and dosage of *in vivo* acute toxicity studies

3.7.2 Clinical/ behavioural signs of toxicity

Home, cage side observations were carried out regularly (twice a day till the completion of experiments) to check for any clinical or behavioural signs of toxicity. All the animals were carefully monitored for any unusual behavioural patterns like staggering, spinning, hunched body posture, lethargy, lack of grooming, skin coat texture, reduced food/water intake *etc*.,.

3.7.3 Body weight of animals

Body weight loss/ gain were carefully monitored on a regular basis throughout the experimental period and prior to sacrifice.

3.7.4 Euthanisation and sample collection

All the animals were euthanized after respective observation periods. Urine and fecal matter were collected on the day end of each experiment. Body weight was noted. Blood samples for hematology, serum biochemistry, blood kinetics and elemental analysis were collected from the optical sinus of each animal into non-vacuum blood collection tubes. Blood samples for serum biochemistry were collected in plain tubes containing clot accelerator to accelerate blood clotting. Blood samples for hematology were collected in K3 EDTA coated tubes to prevent blood clotting. The animals were subsequently euthanized by cervical dislocation.

3.7.5 Organ weight

Major organs such as liver, kidney, brain and spleen were collected from the euthanized animals and wet weight of organs was noted.

3.7.6 Gross pathology

Euthanised animals were subjected for gross pathology analysis. The animals were carefully observed for any visible lesions, lumps, color changes or body/ organ/ tissue damages.

3.7.7 Target organ toxicity

Organs such as liver, kidney, brain, spleen and blood collected from the experimental animals were subjected for detailed organ toxicity analysis. Hematology analysis was done to analyse various blood parameters after QD exposure. Serum biochemistry analysis was done to analyse liver and kidney functions. Urine analysis was done to evaluate kidney function after WS_2 QDs exposure during the experimental period. Spleenocyte proliferation status was analysed using tritiated thymidine incorporation assay to evaluate immunotoxicity associated with WS_2 QDs exposure in experimental animals. Liver, kidney, brain and spleen were subjected to histopathology analysis. Liver and brain samples were analysed for antioxidant status. A portion of liver, kidney and brain along with blood, urine and fecal matter were subjected to elemental detection using Inductively Coupled Plasma Mass Spectrometry (ICP-MS) to study, biodistribution status. Blood taken at 1h, 3h, 6h, 24h, 72h, 7 days and 14 days were subjected to ICP-MS analysis for blood toxicokinetics of the QDs *in vivo*.

3.7.7.1 Hematology

Blood samples for hematology analysis were transferred to K3 EDTA coated tubes soon after blood collection and immediately subjected for hematology analysis. WBC (White Blood Corpuscles), RBC (Red Blood Corpuscles), haemoglobin (HGB) level, haematocrit (HCT), MCH (Mean Corpuscular Haemoglobin), MCHC (Mean Corpuscular Haemoglobin concentration), MCV (Mean Corpuscular Volume) and Platelet (PLT) count were measured using automated hematology analyser (Nihon Kohden).

3.7.7.2 Serum biochemistry

Kidney and liver function analysis was done using serum biochemistry analysis. Blood samples were collected in plain blood collection tubes supplemented with clot accelerator and allowed to clot for serum biochemistry analysis. Serum was separated by centrifugation at 3500rpm for 10min. All the serum samples were subjected to serum biochemistry analysis to detect Alanine Aminotransferase (ALT), Aspartate Transaminase (AST), Alkaline Phosphatase (ALP), Glucose (GLU), Cholesterol (CHO), Triglycerides, Albumin, Protein and Creatinine using the biochemical analyser, Erba Mannheim XL300 (Germany).

3.7.7.3 Urine analysis

Urine collected in sterile air tight tubes were subjected for urine analysis to detect proper kidney functioning after WS_2 QDs administration. Various parameters such as pH, specific gravity, leukocytes, ketone bodies, bilirubin, urobilinogen, protein, glucose, nitrates and presence of blood cells were analysed using Uro-dipchek 300 (Erba Mannheim, Germany).

3.7.7.4 Biodistribution: Inductively Coupled Plasma Mass Spectroscopy (ICP-MS)

Biodistribution analysis by detection of elements in tissue samples was done using Inductively Coupled Plasma Mass Spectroscopy (ICP-MS). This technique allows the precise and sensitive detection of elements having atomic mass that ranges from

7- 250 or even higher. It uses the technique of atomisation of samples and further detection of the elements even at trace amounts. Samples are initially processed by acid digestion to remove the organic contents. Then the atomic elements present in the digested samples were allowed to pass through high temperature argon plasma, which leads to the subsequent ionisation of the sample. These ions were further sorted out on the basis of their mass. Hence it is a reliable technique to detect the elements present in the sample both quantitatively and qualitatively.

3.7.7.4.1 Sample processing

Liver, kidney, brain, blood, urine and fecal matter collected from all the experimental animals were subjected to lyophilisation. Approximately 0.1g of the lyophilised tissue (100µl in case of urine samples) was carefully transferred to clean Teflon tubes. Tissue samples were carefully treated with 3ml of 65% HNO_3 and 2ml of H_2O_2. Acid digestion of samples was done until the samples were completely digested in a microwave digester (MARS5, Version 194A07). This process ensures the complete removal of organic matter content in the samples leaving only heavy metals behind. The resultant residue was transferred into tubes by rinsing with ultrapure water making a final volume of 20ml.

3.7.7.4.2 Element detection

The elemental detection in acid digested samples was carried out using Inductively Coupled Plasma Mass Spectroscopy (ICP-MS).

3.7.7.5 Histopathology

Histopathology analysis was carried out in liver, kidney, brain and spleen tissues of the experimental animals to analyse changes in tissue pathology as a result of material exposure. All the tissue samples were washed in physiological saline containing antibiotic/ antimicotic solution and transferred into 10% neutral buffered formaldehyde immediately after euthanization to prevent tissue degradation.

3.7.7.5.1 Tissue processing

Tissue samples were cut into individual small sessions so as to fit in the tissue processing cassette. Tissues were washed under running tap water for 1h to remove the formalin traces and gradually infiltrated in paraffin wax inorder to make thin sectioning for further staining procedures. The detailed procedure is given in **Table 3.2.**

Solutions	Duration
Acetone I	20 min
Acetone II	20 min
Acetone III	20 min
Acetone IV	20 min
Xylene I	15 min
Xylene II	15 min
Xylene III	15 min
Xylene IV	15 min
Paraffin I	1h
Paraffin II	1h

Table 3.2: Sample processing procedure for histopathology

3.7.7.5.2 Embedding

Paraffin infiltrated tissues were removed out of the cassettes and carefully placed inside the moulds. Molten paraffin wax was carefully poured over the cassettes to fill the cassettes and made sure that the tissues were aligned carefully inside the paraffin blocks. The blocks were allowed to cool down before sectioning.

3.7.7.5.3 Sectioning and slide preparation

The sectioning of the tissues embedded in cassettes was done using microtome fitted with sharp disposable metal blades. Prior to sectioning, the paraffin blocks containing tissues were cooled to avoid cracking. The block was carefully placed in the slot of microtome for sectioning. The sliced tissue sections were carefully placed over warm waterbath to remove wrinkles. The sections were placed over albumin coated clean glass slides and incubated at 55^0C for 2h. Hematoxylin and Eosin staining was done to analyse tissue morphological features.

3.7.7.5.4 Haematoxylin and Eosin (H&E) staining

Haematoxylin and Eosin staining was used to identify different tissue sections and to analyse the morphological changes (Fischer *et al.* 2008). Tissues were sectioned and stained as per the protocol described in **Table 3.3**. Regressive haematoxylin staining was used in which; the excess haematoxylin was removed from the processed tissues using acid-alcohol solution and counterstained with Eosin. Haematoxylin stains nuclei whereas Eosin stains cytoplasm and extracellular matrix regions of tissues. The sections were mounted using DPX to provide better optical clarity.

Process	Duration
Xylene I	10min
Xylene II	10min
Absolute alcohol	5min
70% alcohol	5min
Distilled water	5min
Harris Hematoxylin	20min
Distilled water	Rinse
Acid alcohol	1-2 dips
Distilled water	Rinse
Scott's tap water	10min
Distilled water	Rinse
Eosin	15min
Distilled water	1-2 dips
70% alcohol	2min
Absolute alcohol	5min
Xylene I	10min
Xylene II	10min
Completely dried Xylene and mounted in DPX	

Table 3.3: Haematoxylin and Eosin staining procedure

3.7.7.6 Antioxidant assays

Antioxidant status in major organs such as brain and liver was estimated after 3, 7 and 14 days of intraperitoneal administration of WS_2 QDs.

3.7.7.6.1 Sample preparation

Liver and brain samples were collected from all the experimental animals and were subjected to various antioxidant assays. The organs were washed in physiological

saline and transferred to ice container. 10% tissue homogenate was prepared in 0.1M phosphate buffer (pH 7.4). Tissue homogenates were further centrifuged at 3500rpm for 10 min at 4^0C and the respective supernatants were used to perform all the antioxidant assays.

3.7.7.6.2 Total protein estimation

Lowry's method was used to estimate the total protein content in the tissue homogenate. This method is highly sensitive in determining protein concentrations. It is based on the principle of reactivity of peptide nitrogen with Cu^{2+} followed by the subsequent reduction of Folin's Ciocalteu phosphomolybdic phosphotungstic acid to heteropolymolybdenum blue, which is quantitatively estimated (Geiger and Bessman. 1972). The experimental design is depicted in **Table 3.4**. Solution C was prepared by mixing 50ml of sodium carbonate (1g in 50ml distilled water), 1ml of sodium potassium tartarate (10mg/ml) and 5mg copper sulphate. Readings were recorded at 660nm using spectrophotometer (Lambda 25, UV/Vis spectrophotometer, Perkin Elmer, USA). Bovine Serum Albumin (BSA) standard was used to calculate final protein concentration of test samples.

REAGENTS	**BLANK (ml)**	**TEST (ml)**
Distilled water	1	0.9
Sample (tissue homogenate)	0	0.1
Solution C	5	5
Incubate at room temperature for 10 minutes		
Folin's reagent	0.5	0.5
Incubate in dark for 30 minutes. Read OD at 660nm		

Table 3.4: Procedure for total protein estimation in tissue samples

3.7.7.6.3 Lipid peroxidation (LPO)

Lipid peroxidation was analysed following the protocol of Okado-Matsumoto and Fridovich (2001). Oxidative damage to lipids was assessed by estimating the amount of malondyaldehyde (MDA), the metabolic by-product of lipid peroxidation process. The detailed experimental design is described in **Table 3.5.** The pink colored end product formed as a result of the metabolic reaction between MDA and thiobarbituric acid (TBA) in the reaction system was quantitatively estimated at 532nm (Lambda 25, UV/Vis spectrophotometer, Perkin Elmer, USA).

REAGENT	**BLANK (ml)**	**TEST (ml)**
0.8% Thiobarbituric acid	1.5	1.5
8.1% SDS	0.2	0.2
20% acetic acid	1.5	1.5
Sample (tissue homogenate)	0	0.2
Distilled water	0.8	0.6
Kept in a boiling water bath for 1h at 90^0C		
Cooled in running tap water, added 1ml distilled water		
Centrifuged at 3500rpm for 10min, supernatant collected. Read at 532nm		

Table 3.5: Procedure for lipid peroxidation analysis in tissue samples

3.7.7.6.4 Reduced Glutathione (GSH)

GSH level in tissue homogenate was detected by the method reported by Moron *et al*., (1979). Samples were prepared by mixing 0.2ml tissue homogenate and 0.8ml 5% TCA in 1:5 dilutions. Centrifuged at 3500rpm for 10min (4^0C), the supernatant was collected and used as sample for the remaining procedures. The experimental design is shown in **Table 3.6**. GSH on reaction with DTNB [5, 5'-dithiobis-(2-

nitrobenzoic acid)] formed a yellow colored product which was quantitatively estimated at 412nm (Lambda 25, UV/Vis spectrophotometer, Perkin Elmer, USA).

REAGENT	**BLANK (ml)**	**TEST (ml)**
0.2M phosphate buffer	4	4
Sample	0	0.5
Distilled water	0.5	0
2mM DTNB	0.5	0.5
DTNB was added just before reading absorbance at 412nm		

Table 3.6: Procedure for GSH estimation in tissue samples

3.7.7.6.5 Glutathione peroxidase (GPx)

GPx is a cytosolic enzyme that catalyses the oxidation of GSH to its oxidised form GSSG. GPx activity in the tissue homogenate was quantitatively assessed following the protocol reported by Rotruck *et al.*, (1973). The experimental design is depicted in **Table 3.7** and the readings were taken at 412nm (Lambda 25, UV/Vis spectrophotometer, Perkin Elmer, USA).

REAGENT	**BLANK (ml)**	**TEST (ml)**
0.1M Phosphate buffer (pH:7)	0	0.4
Sodium azide	0	0.1
EDTA	0	0.1
Sample (tissue homogenate)	0	0.1
H_2O_2	0	0.1
Distilled water	1	1
4mM GSH	0	0.2
Incubated for 0min, 1.3min and 3min at 37^0 C for each test groups		
10% TCA	0	0.5

Centrifuged at 3500rpm for 5min at 4^0C. Collected supernatant.

Supernatant	0	1
0.3M phosphate solution	4	4
0.6mM DTNB	0.5	0.5

Read OD at 412nm

Table 3.7: Procedure for GPx estimation in tissue samples

3.7.7.6.6 Glutathione reductase (GR)

Glutathione reductase (GR) is a critical molecule in resisting cellular oxidative stress, which catalyses the conversion of GSSG back to GSH in the presence of NADPH whereby maintaining a reduced cellular environment for normal cellular metabolism. The experiment was done following the method described by Mize and Langdon (1962) and is depicted in **Table 3.8.** The readings were noted at varying time periods of 0, 1, 2 and 3min at 340nm using spectrophotometer (Lambda 25, UV/Vis spectrophotometer, Perkin Elmer, USA).

REAGENT	**BLANK (ml)**	**TEST (ml)**
0.1M phosphate buffer (pH:7.6)	2.1	2.0
0.5mM EDTA	0.5	0.5
20mM GSSG	0.15	0.15
Incubate at 37^0 C for 10 min		
2mM NADPH	0.15	0.15
Sample (tissue homogenate)	0	0.1
Read OD at 340nm for 0min, 1min, 2min, 3min		

Table 3.8: Procedure for GR estimation in tissue samples

3.7.7.6.7 Superoxide dismutase (SOD)

Superoxide dismutase specifically dismutates the potentially harmful singlet oxygen species and superoxide free radicals present inside the cellular microenvironment. The detailed experimental procedure is given in **Table 3.9,** which followed the method described by Marklund and Marklund (1974). Pyrogallol was added and the absorbance was measured for varying time periods of 0, 1, 2 and 3min at 420nm (Lambda 25, UV/Vis spectrophotometer, Perkin Elmer, USA).

REAGENT	**BLANK (ml)**	**TEST (ml)**	**STANDARD (ml)**
0.1M Tris buffer	3.1	2.5	2.6
1mM EDTA	0.1	0.1	0.1
1mM DTPA	0.5	0.5	0.5
Sample (tissue homogenate)	0	0.1	0
Pyrogallol	0	0.5	0.5
Read OD at 420nm for 0min, 1min, 2min and 3min			

Table 3.9: Procedure for SOD estimation in tissue samples

3.7.7.7 Spleenocytes proliferation assay

Spleenocytes proliferation assay was used to analyse the immunotoxicity. Spleenocytes were isolated from the spleen of animals of each experimental group (3, 7 and 14 days) to access the proliferating capacity. The spleen was immediately washed with ice cold PBS containing AB/AM and was gently teased over a metallic mesh kept on a 10mm petridish. 3ml of single cell suspension was carefully layered over 1ml histopaque and centrifuged at 1500rpm for 40min. The resulting buffy coat containing spleenic lymphocytes were collected and washed with PBS thrice. Cells were then seeded at a density of $2x10^5$ cells/well in a six well plate with RPMI

medium supplemented with 10% FBS and incubated for 48h. 0.5µCi of tritiated thymidine was added to each well and incubated for another 24h. After the incubation time, the cells were fixed using 5% trichloroacetic acid (TCA) and subsequently lysed using SDS/NaOH lysis buffer. The cells were centrifuged at 1500rpm for 10min. After centrifugation, 100µl of the supernatant was taken and directly added to 1ml scintillation fluid. The radioactivity was immediately measured using Scintillation Counter (Hidex, Finland). The experiment was done in triplicates (n=3). The values were expressed as mean ± SD of counts per minute (CPM).

3.7.7.8 Blood kinetics

Estimation of blood kinetics followed by WS_2 QDs administration was done by ICP-MS in blood collected at regular intervals of 1h, 3h, 6h, 24h, 72h, 7 days and 14 days to detect the presence of the compound in the blood after administration. This was used to analyse the maximum extend of retention of the material in the physiological medium soon after material administration. 100µl of blood was directly processed by acid digestion as described in section **3.7.7.4.1.** ICP-MS analysis was done to estimate the presence of elements.

3.8 Statistical Analysis

All the experiments were done in triplicates and the values were expressed as mean ± SD. Statistical comparison between the control and experimental values were done using students' t-test. In the results, analysis $p<0.05$ was considered significant and the degree of significance is represented in Asterisk (*$p< 0.05$, **$p< 0.01$ and ***$p<0.001$).

CHAPTER 4: RESULTS

4. RESULTS

4.1 Synthesis of tungsten disulphide quantum dots (WS_2 QDs)

Tungsten disulphide quantum dots (WS_2 QDs) was synthesized (**Figure 4.1**) by solvothermal exfoliation method from bulk WS_2 crystals. Excess solvent was removed by temperature treatment at 180^0C, which is near to the boiling point of NMP solvent. The total yield after complete exfoliation process was approximately 30% (when 1g of bulk WS_2 powder was used). The synthesized WS_2 QD pellets were brown in color. An yellowish-brown solution was obtained (0.5mg/ml dispersion) after dispersion in water, with a characteristic absorbance peak at 370nm and emission at 500nm. Under longer wavelength UV light exposure (370nm), bright cyan green fluorescence was observed. The QDs in water dispersion was stable upto 100 days without losing its characteristic features.

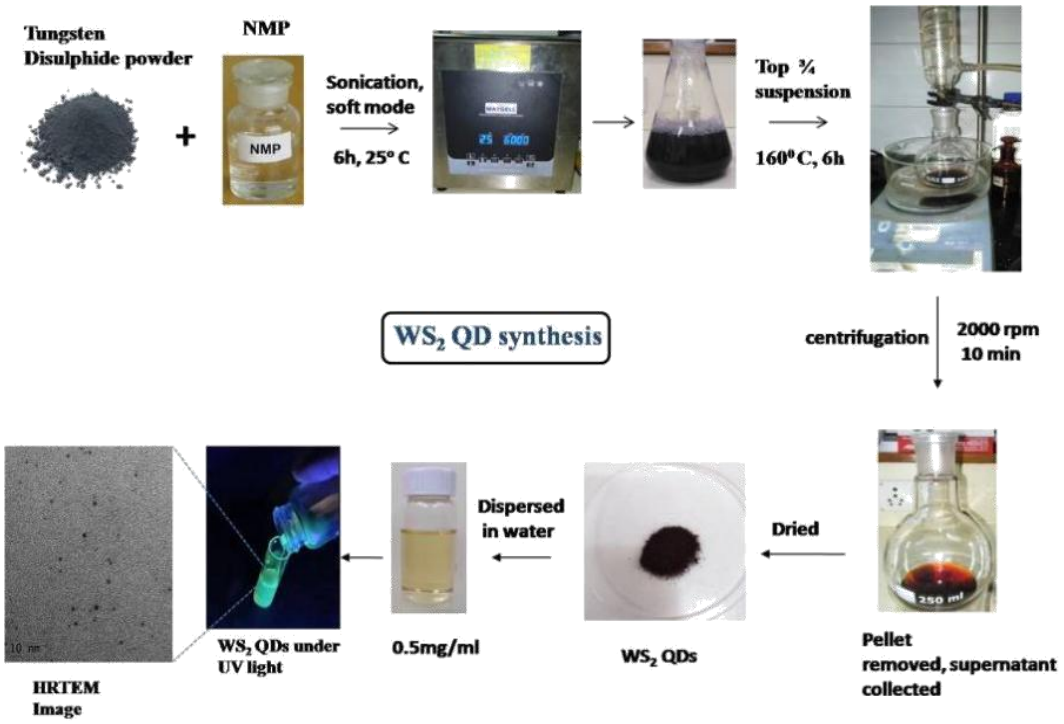

Figure 4.1: Schematic representation of WS_2 QDs synthesis using solvothermal exfoliation method

4.2 Physico-chemical characterisation of WS_2 QDs

The physico-chemical characterizations of WS_2 QDs were carried out using various techniques and are detailed below.

4.2.1 Absorbance spectra

The synthesized WS_2 QDs was subjected to absorbance spectra analysis and showed a characteristic absorbance peak at 370nm (**Figure 4.2)**. The shorter wavelength absorbance was observed because the pristine crystalline structure has changed to quantum dot morphology. Therefore the absorbance spectra got shifted towards the region of shorter wavelength.

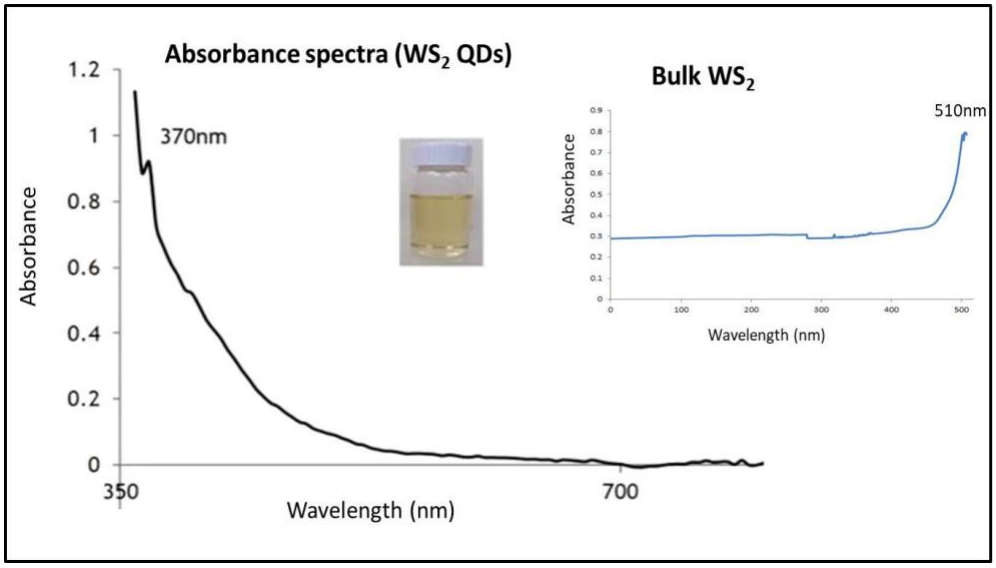

Figure 4.2: Absorbance spectra of WS_2 QDs showing characteristic absorbance at 370nm.

4.2.2 Fluorescence emission spectra

The synthesized WS_2 QDs was analyzed for its emission spectra when excited at 370nm and observed a characteristic emission ranges from 450-500nm that corresponds to the region of cyan green spectrum (**Figure 4.3)**. The fluorescence peak position was observed in agreement with the size distribution of 3-4nm. The sharpness in peak was probably due to the extreme small size of the particles as well as due to excited state mixing usually found in transition metal based nanomaterials (Chia *et al.* 2014, Swart *et al.* 2019). The synthesized WS_2 QDs not only showed bright fluorescence but also were stable upto 100 days conserving its intrinsic fluorescence properties. Inset image in **Figure 4.3** showed UV illumination after 370nm wavelength UV exposure.

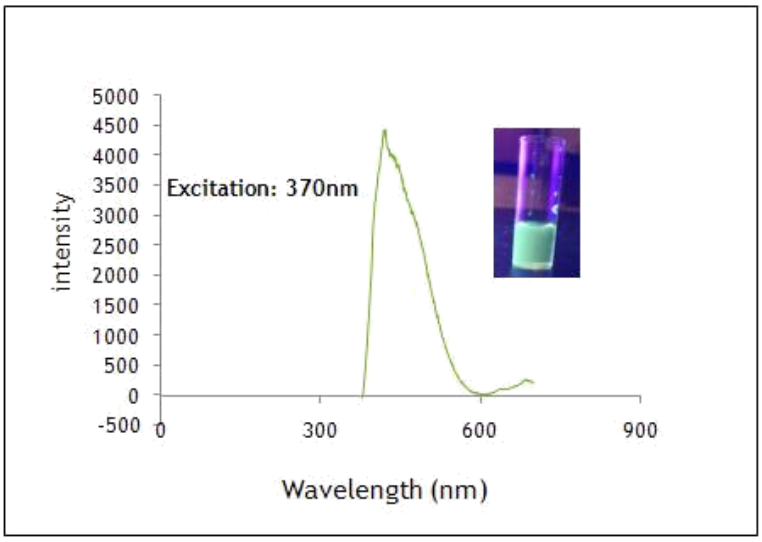

Figure 4.3: Fluorescence emission spectrum of WS_2 QDs, showing characteristic emission corresponds to cyan green fluorescence

4.2.3 Fourier Transform Infrared Spectroscopy (FTIR)

FTIR spectra (ATR-FTIR) of both bulk WS_2 crystals and WS_2 QDs were subjected to analyse the chemical composition while thinning down to QD structures under vigorous temperature and sonication processes. In was evident from the FTIR spectra that all the intrinsic peaks of bulk WS_2 crystals were found intact in WS_2 QDs even after exfoliation and confirmed that the chemical composition of the material is intact. **Figure 4.4** shows that the characteristic peaks at ~887cm^{-1} in bulk material and ~923cm^{-1} in WS_2 QDs corresponds to S-S vibrations. The bands positioned at ~542cm^{-1} in WS_2 QDs and ~597cm^{-1} in bulk material were related to W-S vibrations. Characteristic peaks at 1261cm^{-1} (C-N stretching) and 2914cm^{-1} (CH_2 asymmetric stretching) were probably due to the attachment of NMP residues over the WS_2 QDs surface. Peaks at 1403cm^{-1} and 1618cm^{-1} showed stretching deformations of hydroxyl groups. The typical peak observed at 2960cm^{-1} confirmed the presence of hydroxyl groups over the WS_2 QDs surface. Moreover, the presence of hydroxyl and carboxyl groups over the WS_2 QDs surface is responsible for the high water dispersibility and stability of the synthesized WS_2 QDs.

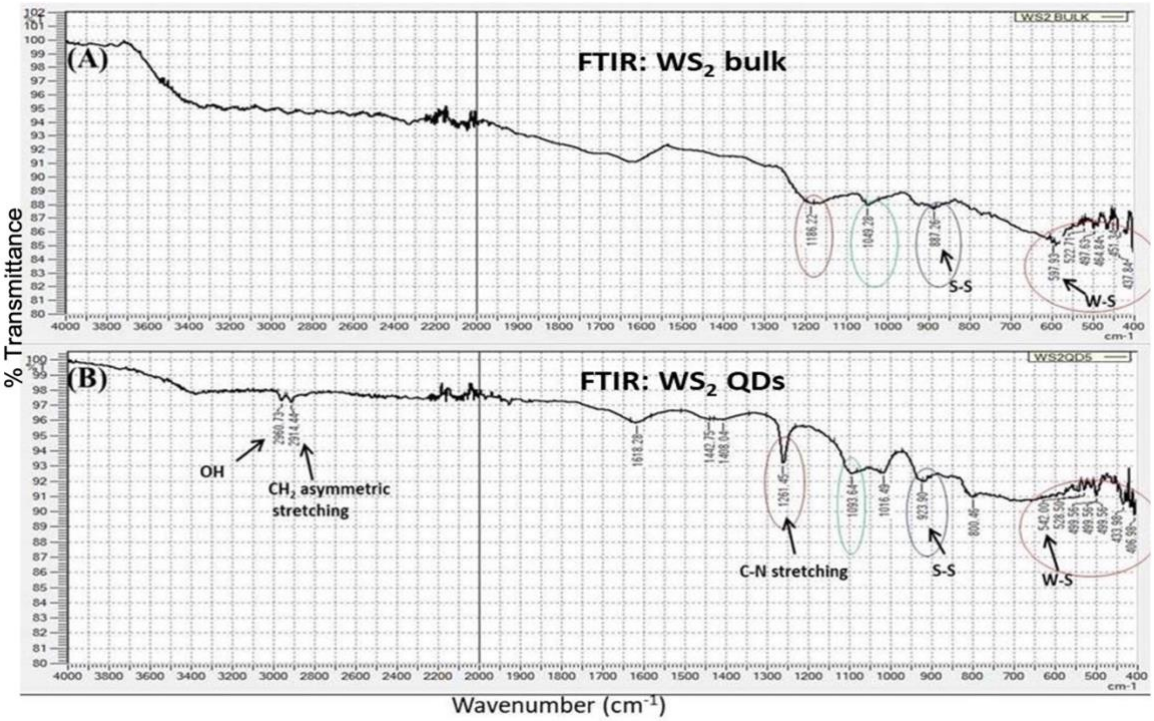

Figure 4.4: FTIR spectra of bulk WS_2 and WS_2 QDs showing characteristic peaks before and after material exfoliation

4.2.4 X-Ray Diffraction (XRD)

Effective exfoliation of bulk material into quantum dot morphology was confirmed by XRD. Significant reduction in peak intensity was observed in WS_2 QDs when compared to bulk material. Broadening of peaks attributed to the extreme low nano-dimension of the material. Two broadened peaks at 2θ =19.8 and 28.9 corresponds to the diffraction peaks at (002) and (101) lattice planes of WS_2 (**Figure 4.5**). Broad hump without sharp diffraction patterns showed that the synthesized WS_2 QDs are amorphous in nature. This confirmed the effective exfoliation from highly crystalline bulk powder to amorphous WS_2 QDs.

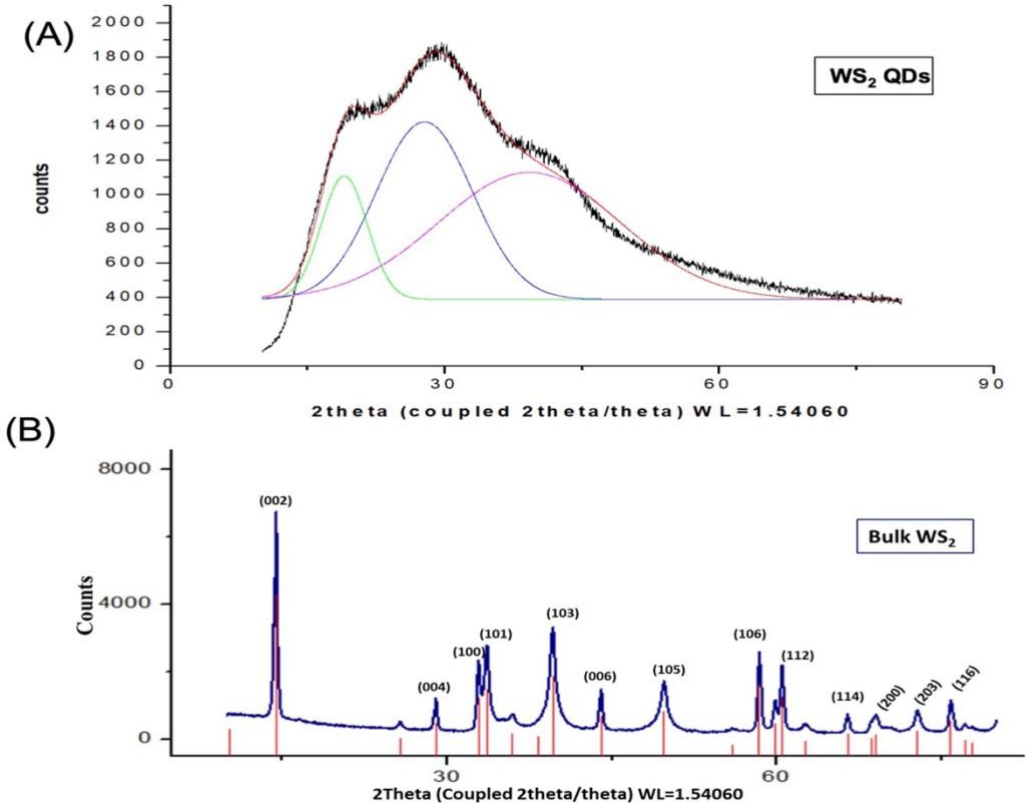

Figure 4.5: XRD of WS_2 QDs (A) and bulk WS_2 (B), showing the reduction in intensity and further broadening of characteristic peaks observed in bulk material while thinning down to QD confined morphology.

4.2.5 HR-TEM

HR-TEM images of WS_2 QDs showed in **Figure 4.6** confirmed the ultra small size and characteristic spherical morphology of WS_2 QDs. Size distribution pattern was observed in the range of 3-4nm. The synthesized WS_2 QDs showed a monodispersive nature without aggregation. Lattice fringes showed d-spacing of 0.24nm corresponds to the (101) crystalline phase. The diffused ring SAED pattern showed that the synthesized WS_2 QDs are in amorphous nature.

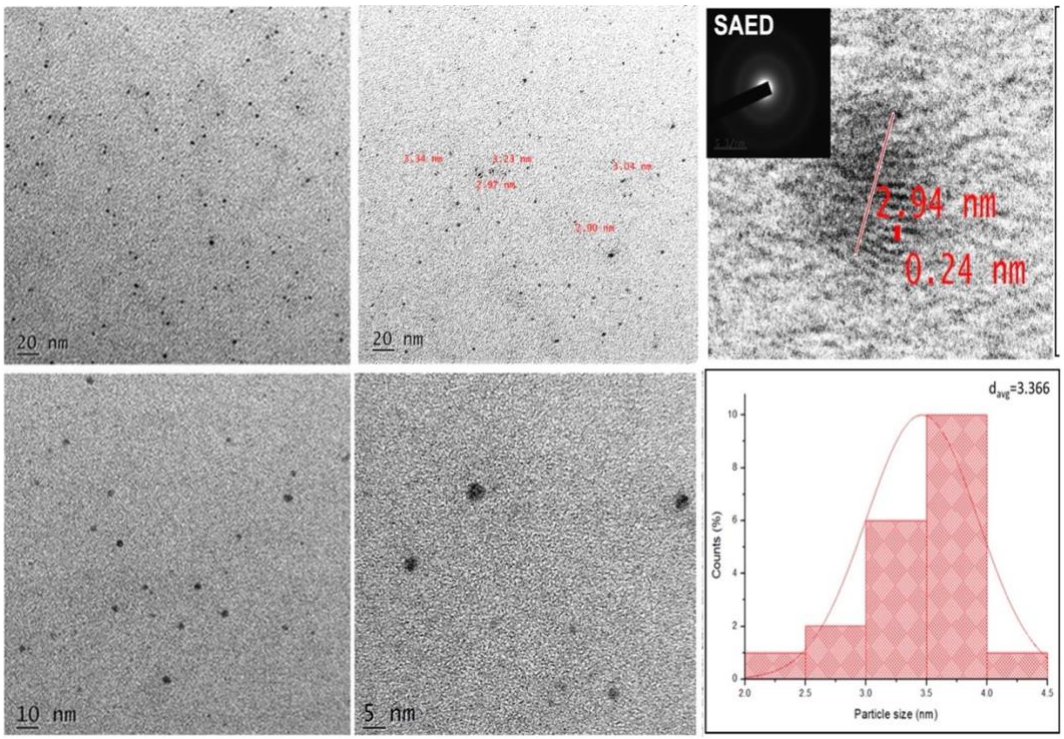

Figure 4.6: HR-TEM images of WS_2 QDs from higher to lower magnifications, showing ultrafine structural morphology. SAED pattern showed diffused ring pattern that corresponds to amorphous nature with extreme low nanodimension of the material

4.2.6 X-Ray Photoelectron Spectroscopy (XPS)

XPS spectra were analyzed to confirm the surface elemental characteristics such as chemical composition and elemental state of WS_2 QDs. XPS spectra confirmed the chemical composition of WS_2 QDs **(Figure 4.7**). The XPS spectrum confirmed the S/W ratio as 1.75 that closely resembled the intact chemical composition of WS_2. Bands at 31.2eV and 33.2eV represented the characteristic elemental state of $4f_{7/2}$ and $4f_{5/2}$ respectively. These two distinct peaks of 4f level 'W' atoms represented the $^{+}4$ valence state of tungsten. A small peak at 36.2eV lies outside the main W4f envelope corresponds to the metal oxide phase. XPS spectra of Sulphur showed distinctive peaks at 160.2eV and 161.8eV that corresponds to $S2p_{3/2}$ and $S2P_{1/2}$ respectively This indicate the $^{-}2$ valence state of Sulphur atoms. A small peak at 166eV suggested the presence of SO_4^{2-}.

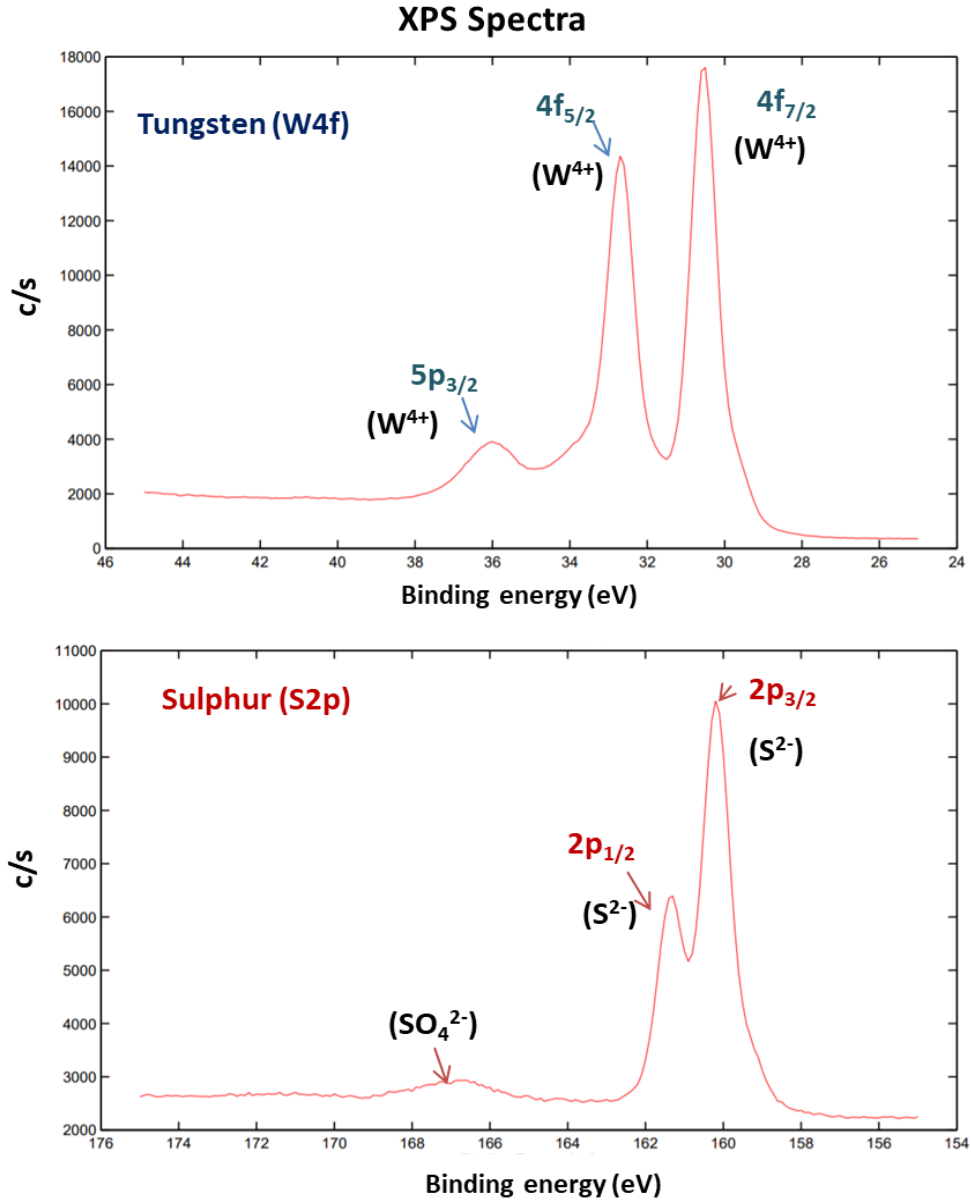

Figure 4.7: XPS spectra of individual elements such as tungsten (W) and sulphur (S) showing binding energy and valence state of individual elements

4.2.7 Thermogravimetric Analysis

Thermogravimetric analysis was done to analyze the degradation tendency of the synthesized WS_2 QDs and to check the thermal stability of the material, degradation temperature and the rate of degradation of WS_2 QDs.

4.2.7.1 TGA

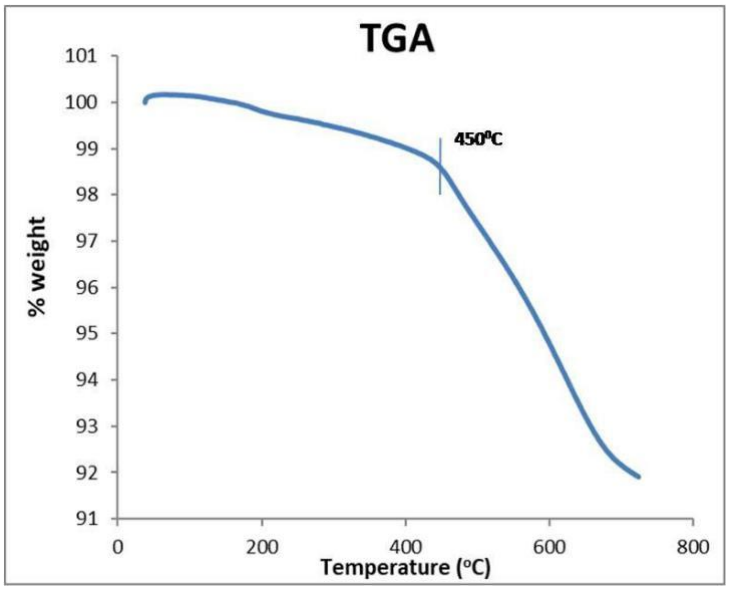

Figure 4.8: TGA analysis of WS_2 QDs

It was evident from the TGA report (**Figure 4.8**) that 1.5% weight loss was observed at a temperature of 450^0C that corresponds to surface NMP solvent degradation. Further heating upto 700^0C showed a net weight loss of approximately 8% possibly because of the negligible exothermic effect due to prime disulfide decomposition into tungsten and sulphur with subsequent oxidation of sulphur and sulphur oxide loss. The surface residual NMP solvent completely decomposed when heated at 700^0C temperature or above.

4.2.7.2 DTA

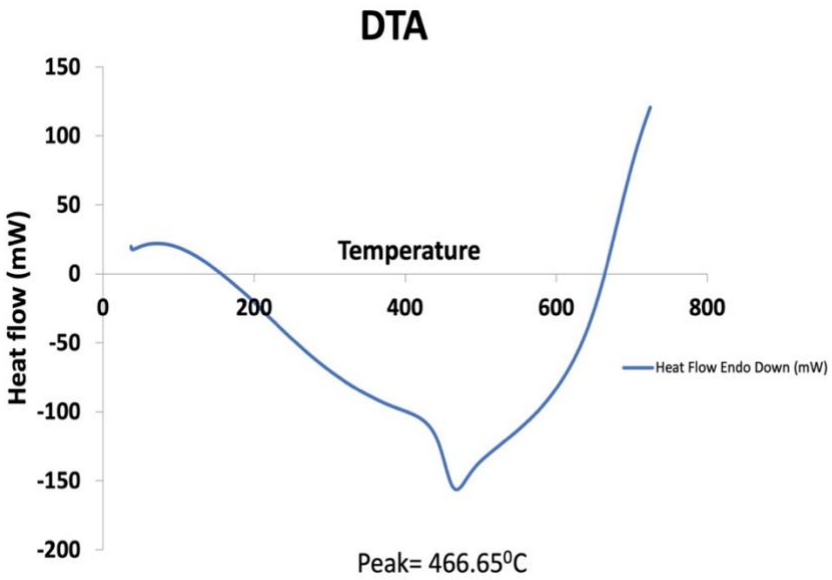

Figure 4.9: DTA (Differential thermogravimetric analysis) of WS_2 QDs

Differential Thermal Analysis (DTA) showed that the net reaction favored an endothermic reaction with subsequent absorption of heat energy (enthalpy/delta H= ⁻ 382.1994J/g). Area under the DTA peak corresponds to the enthalpy change. Melting peak temperature of WS_2 QDs was observed as 466.65^0C from the DTA curve shown in **Figure 4.9**.

4.2.7.3 DTG

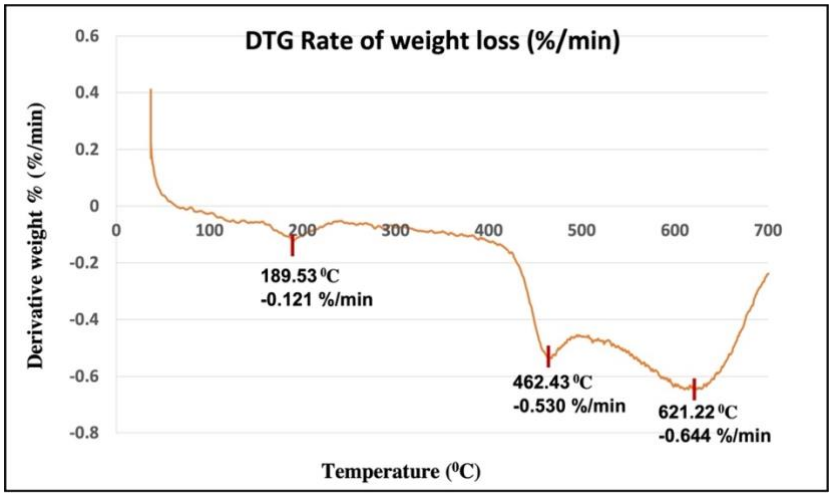

Figure 4.10: DTG (Derivative thermogravimetry) analysis of WS_2 QDs

The rate of weight loss was determined by Derivative Thermogravimetry (DTG). **Figure 4.10** showed that three distinct peaks corresponds to material degradation was evident. It was observed that, 0.121%/min degradation occurred at 189.53^{0}C, 0.530%/min degradation was observed at 462.43^{0}C. Further 0.644%/min degradation was observed at 621.22^{0}C. Negative value in graph represents that the net degradation favors an endothermic reaction with the subsequent absorption of heat energy.

4.2.8 Zeta Potential

Surface charge of the synthesized WS_2 QDs was analyzed by zeta potential analysis. **Figure 4.11** showed that the synthesized WS_2 QDs possess a net negative surface charge of -25mV at pH 7. The pH was fixed as 7 because the material needs to be exposed directly to live cells for further biological studies.

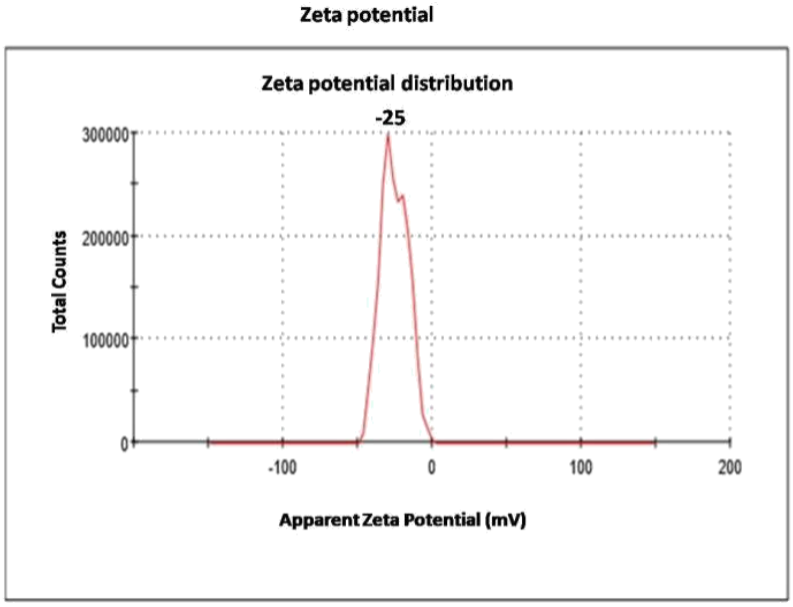

Figure 4.11: Zeta potential analysis for surface charge of WS_2 QDs

The negative surface potential value is an evidence of the electrostatic repulsive forces. The significance of zeta potential is that its value predicts the long term or short term stability of the synthesised material. A highly negative zeta value showed that the synthesised QDs are highly stable without any coagulation or flocculation tendency. On the other hand, emulsions with low zeta potentials tend to coagulate or flocculate possibly leading to poor physical stability. In general, when the zeta potential of an emulsion is high, the repulsive forces exceed the attractive forces resulting in a relatively stable system.

4.2.9 Stability analysis of WS_2 QDs

The stability of the synthesized QDs is an inevitable factor while considering the application possibilities of the material. WS_2 QDs were analyzed for its stability for a period upto 100 days kept at room temperature. WS_2 QDs dispersed in deionised

water was kept at room temperature and spectrophotometric readings were procured at every 20 days interval. Both UV/Visible **(Figure 4.12)** and Fluorescence emission **(Figure 4.13)** readings clearly showed that the synthesized QDs exhibit excellent stability for upto 100 days without material decomposition thereby by retaining its intrinsic fluorescent properties. This high stability is an important feature especially in terms of biomedical applications.

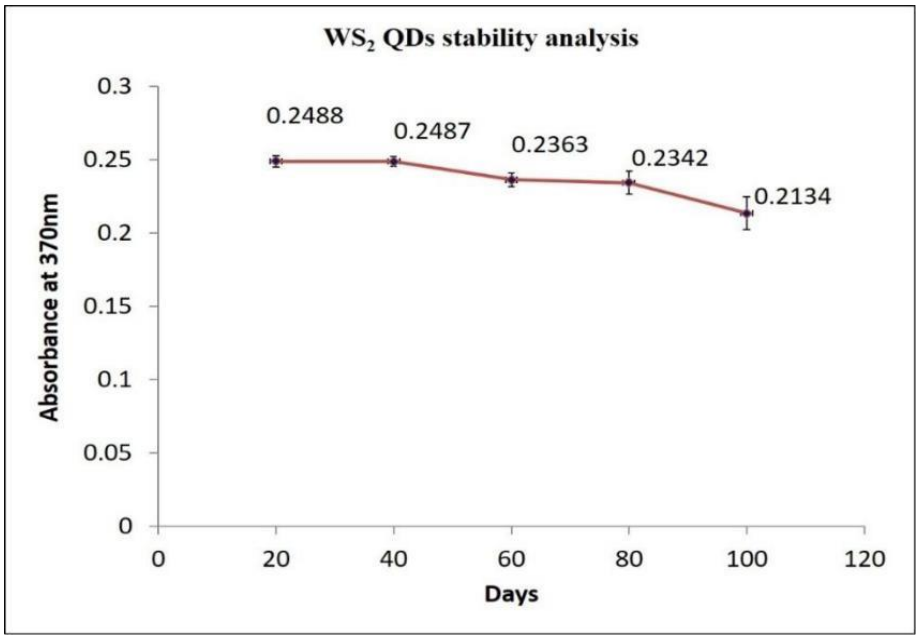

Figure 4.12: Stability analysis of WS_2 QDs by UV/Vis spectroscopy

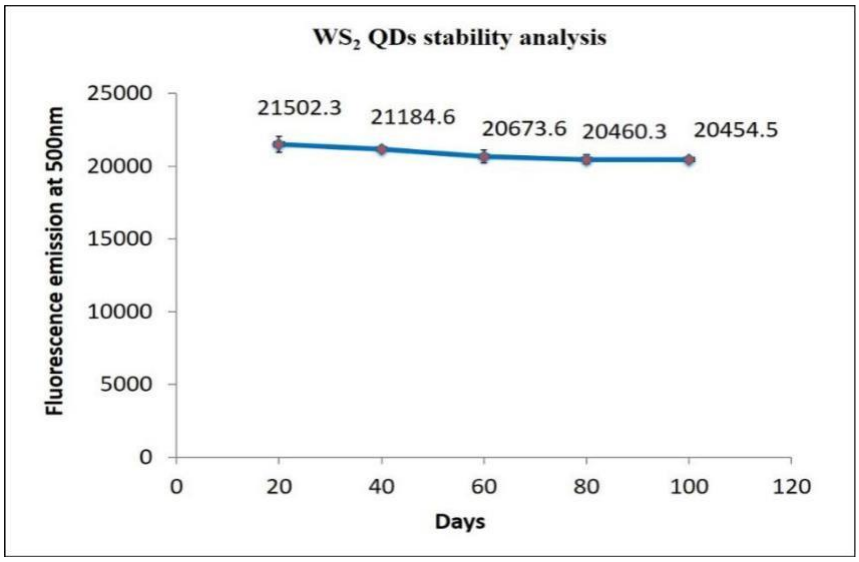

Figure 4.13: Stability analysis of WS_2 QDs by Fluorescence emission spectroscopy

4.3 Fluorescent microscopic observation of dried WS_2 QDs pellets

Fluorescent microscopic observation of dried WS_2 QDs showed bright cyan green fluorescent particles in the microscopic slide **(Figure 4.14).**

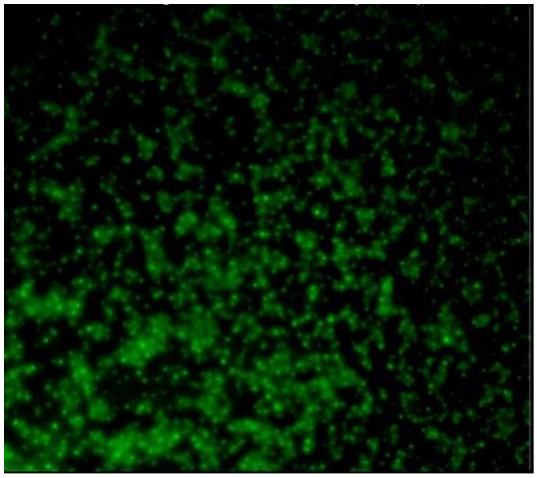

Figure 4.14: Fluorescent microscopic observation of dried WS_2 QDs,

4.4 Endotoxin detection

The synthesized WS_2 QDs were subjected to endotoxin detection as it is a critical factor that accounts for the adverse effects of NPs inside the living system. Endotoxin content was assessed using Charles River Endosafe PTS Kit. The results showed that the endotoxin level was 0.05 EU/ml and was well below the United States Pharmacopia recommended levels of ≤ 0.5 EU/ml.

4.5 In vitro cytotoxicity and bio-nano interaction studies using LN-229 glioblastoma cells

4.5.1 Collection and culturing of LN-229 cells

LN-229 human glioblastoma cells were selected for cellular uptake, *in vitro* cytotoxicity, genotoxicity studies and imaging analysis followed by WS_2 QDs exposure. These are epithelial adherent type cells having a doubling time of approximately 24h. The cells were collected from National Centre for Cell Science (NCCS), Pune, India. The cells were grown in Dulbecco's Modified Essential Medium (DMEM) supplemented with 10% FBS and 1% Antibiotic/Antimicotic (AB/AM) solution. Incubation conditions of the cells include continuous 5% CO_2 supply at 37^0 C in a CO_2 incubator under sterile conditions.

4.5.2 Particle uptake by flow cytometry

WS_2 QDs uptake by LN-229 glioblastoma cells was confirmed by flow cytometry. More particle uptake will increase the cellular granularity, which account for the principle behind the flow cytometry mediated cellular uptake of NPs. WS_2 QDs uptake was studied by considering FSC/SSC alterations when compared with the untreated control cells. **Figure 4.15** showed that a concentration dependant shift in SSC was observed for 40µg/ml and 80µg/ml WS_2 QDs treated cells when compared with that of untreated cells. No alterations in FSC showed that no morphological alterations were occurred following QD uptake.

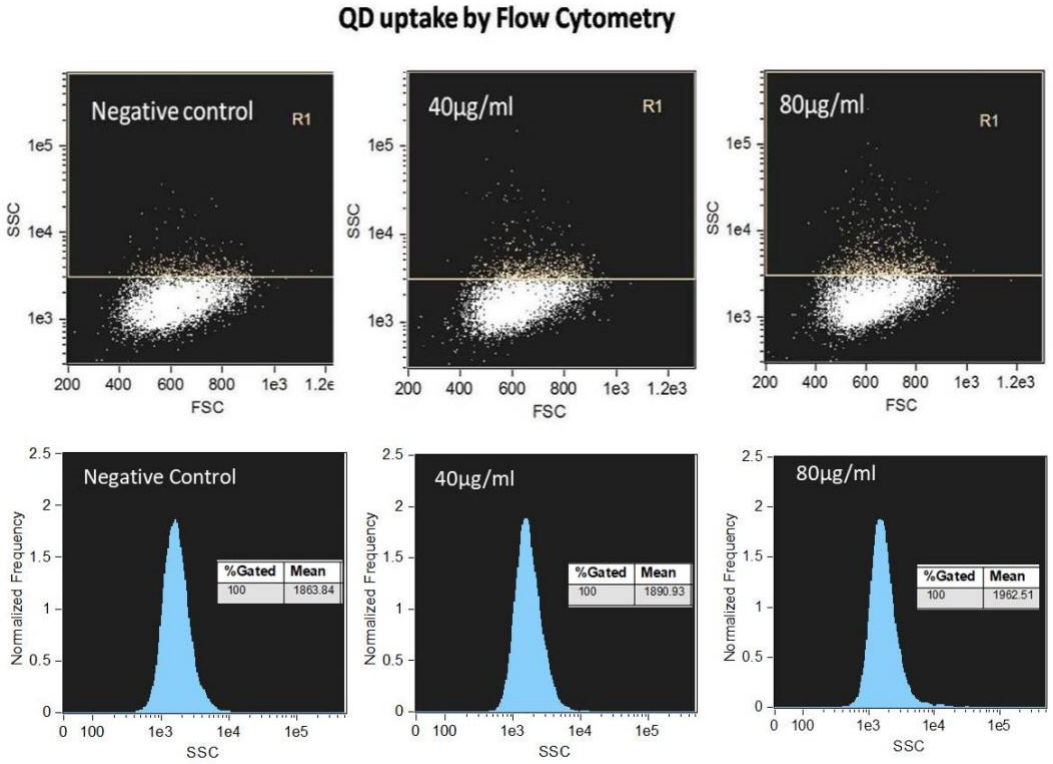

Figure 4.15: Flow cytometry analysis of cellular uptake of WS_2 QDs. Negative control represents untreated control cells

4.5.3 QD uptake and intracellular localisation

Since WS_2 QDs possess excellent fluorescent properties, intracellular uptake was confirmed by fluorescent microscopy. To visualize cellular morphology and to analyze the intracellular localization of QDs, the actin filaments were stained using Rhodamine-phalloidin and the nucleus was counter stained using DAPI. **Figure 4.16** showed that WS_2 QDs were localized inside the cytoplasm and around the nucleus with the emission of bright cyan green fluorescence.

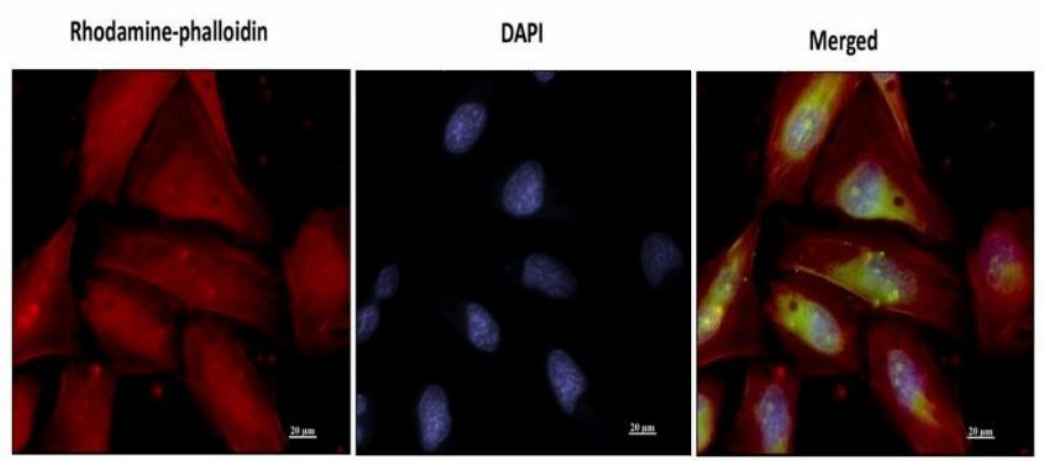

Figure 4.16: Cellular uptake and intracellular localization of WS_2 QDs. Actin filaments were stained using Rhodamine-phalloidin and nucleus counterstained using DAPI

4.5.4 Dose response by MTT assay

MTT assay was used to evaluate the mitochondrial metabolic activity after WS_2 QDs exposure on LN-229 cells. **Figure 4.17** indicated a dose dependent reduction in cell viability; particularly after 160µg/ml concentration. A statistically significant reduction in mitochondrial activity was observed at 160µg/ml (84.33%), 320µg/ml (67.55%) and 640µg/ml (39.68%) concentration at 24h incubation.

A statistically significant reduction in mitochondrial activity was observed in 160µg/ml (74.16%), 320µg/ml (65.12%) and 640µg/ml (33.87%) at 48h incubation of WS_2 QDs. It was noted that at both 24 and 48h incubation, the highest selected concentration (640µg/ml) showed a response similar to that of the positive control (0.02% phenol).

IC_{50} calculation: Concentration v/s cell viability graph was plotted using MS-Excel, with concentration of WS_2 QDs on the x-axis and cell viability on the y-axis. To estimate the IC_{50} value, plot the x-y graph and fit the data with a straight line (linear regression). In the equation y=mx (y=0.1374x) **(Figure 4.17 B),** "x" represents the IC_{50}. Substitute the "y" value as 50 (represents 50% cell viability) to obtain the IC_{50}.

The half maximal inhibitory concentration (IC_{50}) is the measure of the potency of a material in inhibiting a specific biological function. IC_{50} value was calculated as 363.90µg/ml. This IC_{50} is the concentration of WS_2 QDs, which exhibited 50% cell viability for LN-229 human glioblastoma cells.

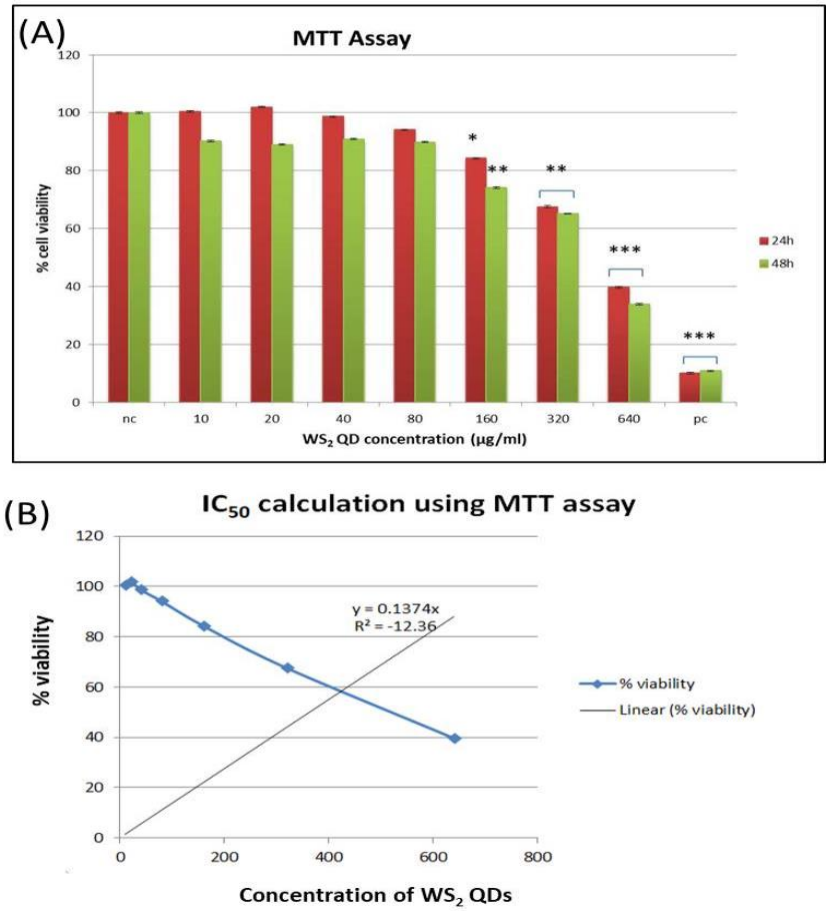

Figure 4.17: MTT assay on LN-229 cells exposed to WS_2 QDs of varying concentrations (10, 20, 40, 80, 160, 320 and 640µg/ml) for 24h and 48h incubation. Values were expressed in percentage viability with respect to negative control (untreated cells). 0.02% phenol was used as positive control. The datas were represented as mean ± SD of three independent experiments. Statistical significance with negative control was represented with asterisk above each graph (*$p<0.05$, **$p< 0.01$ and ***$p<0.001$). (B) Represents the graph used to calculate IC_{50} value from the MTT assay.

4.5.5 Analysis of WS_2 QDs interference with MTT result

Some NPs show the tendency to interfere with MTT reagent giving false results. Absorbance at 540nm for varying concentrations of WS_2 QDs incubated with MTT reagent showed that the particles did not show any significant interference with MTT reagent. **Figure 4.18** showed similar absorbance peaks comparable to that of media alone (control).

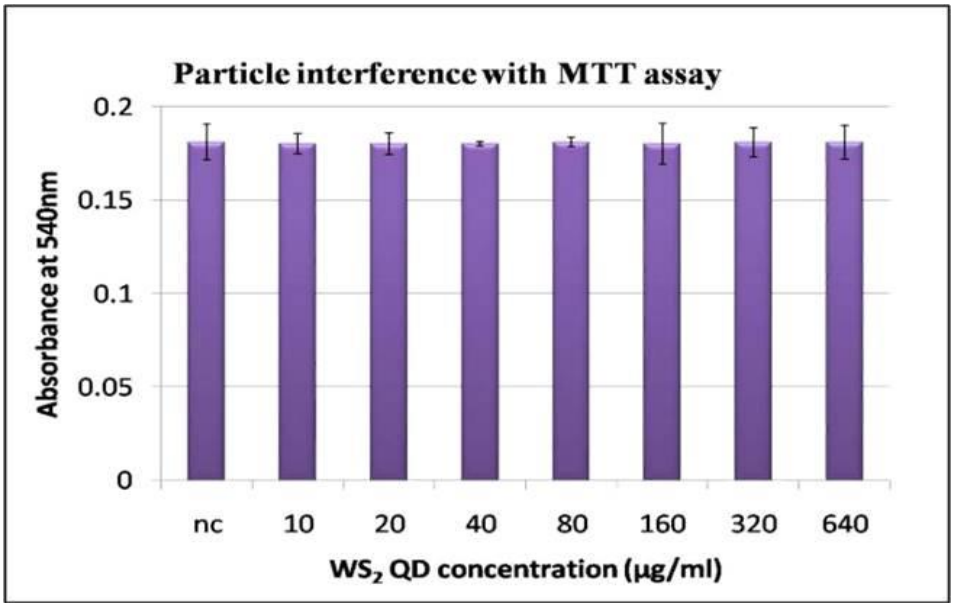

Figure 4.18: MTT assay on cell culture medium incubated with varying concentrations (10, 20, 40, 80, 160, 320 and 640µg/ml) of WS_2 QDs. The datas were expressed as mean ± SD of three independent experiments

4.5.6 QD dissolution and related cytotoxicity

Cytotoxicity of nanomaterials can also be due to material dissociation and subsequent release of ions. **Figure 4.19** showed that no evidence of material dissolution related cytotoxic response was observed for any of the selected concentrations of WS_2 QDs exposed cells. For all the selected concentrations, the cell viability was found to be comparable with that of untreated control cells. A statistically significant reduction in mitochondrial activity was observed in direct QD exposed cells. On the other hand, no significant changes were observed in supernatant treated cell groups. The percentage cell viability of cells exposed to supernatant of 640µg/ml WS_2 QDs was 90.89% whereas the same for direct particle exposed cells was 39.68%.

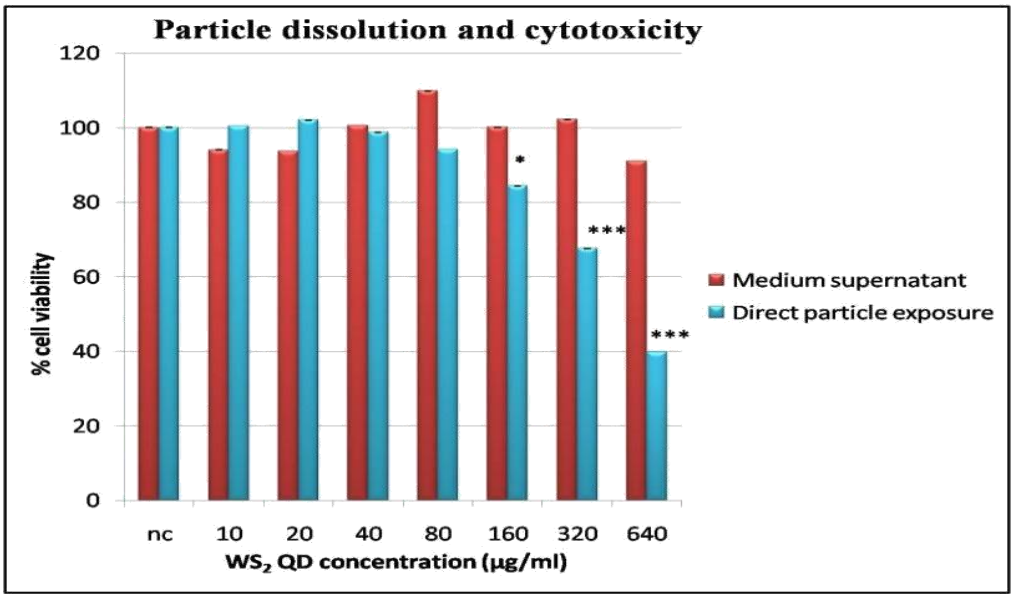

Figure 4.19: MTT assay on culture media supernatant of WS_2 QDs and direct WS_2 QDs exposed LN-229 cells. The values were expressed in percentage cell viability with respect to untreated negative control. The datas were represented as mean ± SD of three independent experiments. Statistical significance with negative control was represented with asterisk above each graph (*p<0.05 and ***p<0.001)

4.5.7 Neutral red uptake assay (NRU Assay)

Lysosomal integrity and resultant cell viability was analyzed using neutral red uptake assay. Results showed that a dose dependant reduction in lysosomal integrity was found in both 24h and 48h WS_2 QDs exposure (**Figure 4.20)**. The cells treated with 80µg/ml (81.01%), 160 µg/ml (78.12%), 320 µg/ml (60.86%) and 640µg/ml (28.3%) of QDs showed a statistically significant reduction in lysosomal activity at the end of 24h. No significant reduction in lysosomal activity was observed for lower concentrations upto 40µg/ml. Similarly, for 48h incubation, 80µg/ml (87.41%), 160µg/ml (81.19%), 320µg/ml (64.83%) and 640µg/ml (53.35%) showed a statistically significant reduction in lysosomal integrity. It was found that more than 80% of cells were active and viable upto 160µg/ml concentration. The highest selected concentration (640µg/ml) showed a response similar to that of positive

control (0.02% phenol) in 24h incubation. **Figure 4.21** showed microscopic images of neutral red dye uptaken lysosomes of LN-229 cells, for 24h (A-H) and 48h (I-P). This further confirmed the results. At 640µg/ml, most of the cells were found to loss the lysosomal integrity at 48h incubation and exhibited highly challenged cell morphology with more than 50% cells having morphology similar to dead cells.

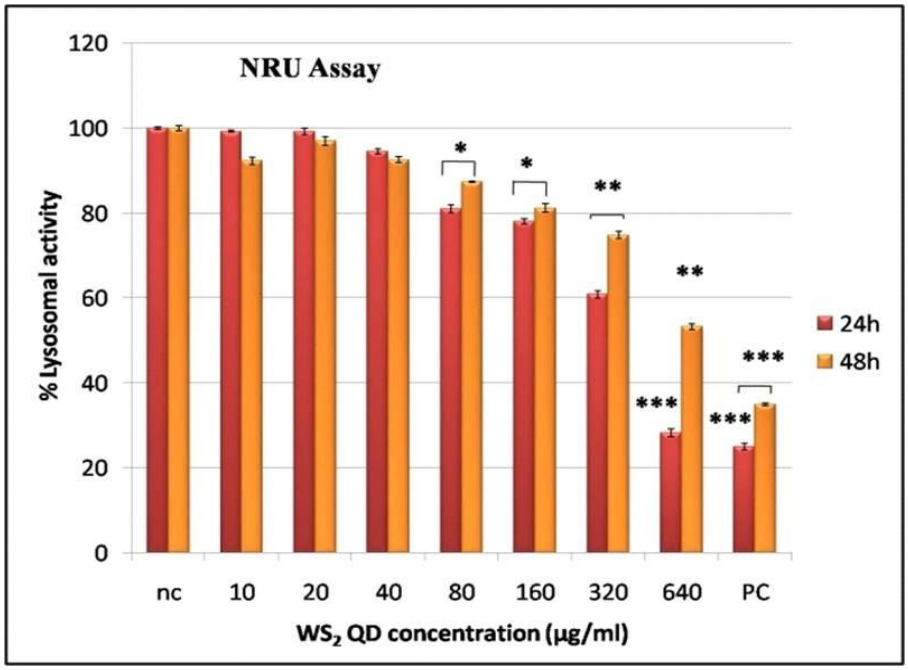

Figure 4.20: Neutral red uptake assay in LN-229 cells exposed to varying concentrations (10, 20, 40, 80, 160, 320 and 640µg/ml) of WS_2 QDs for 24h and 48h. Values were expressed in percentage lysosomal activity with respect to untreated control cells. The datas were represented as mean ± SD of three independent experiments. Asterisk denotes statistically significant difference (*p<0.05, **p< 0.01 and ***p<0.001)

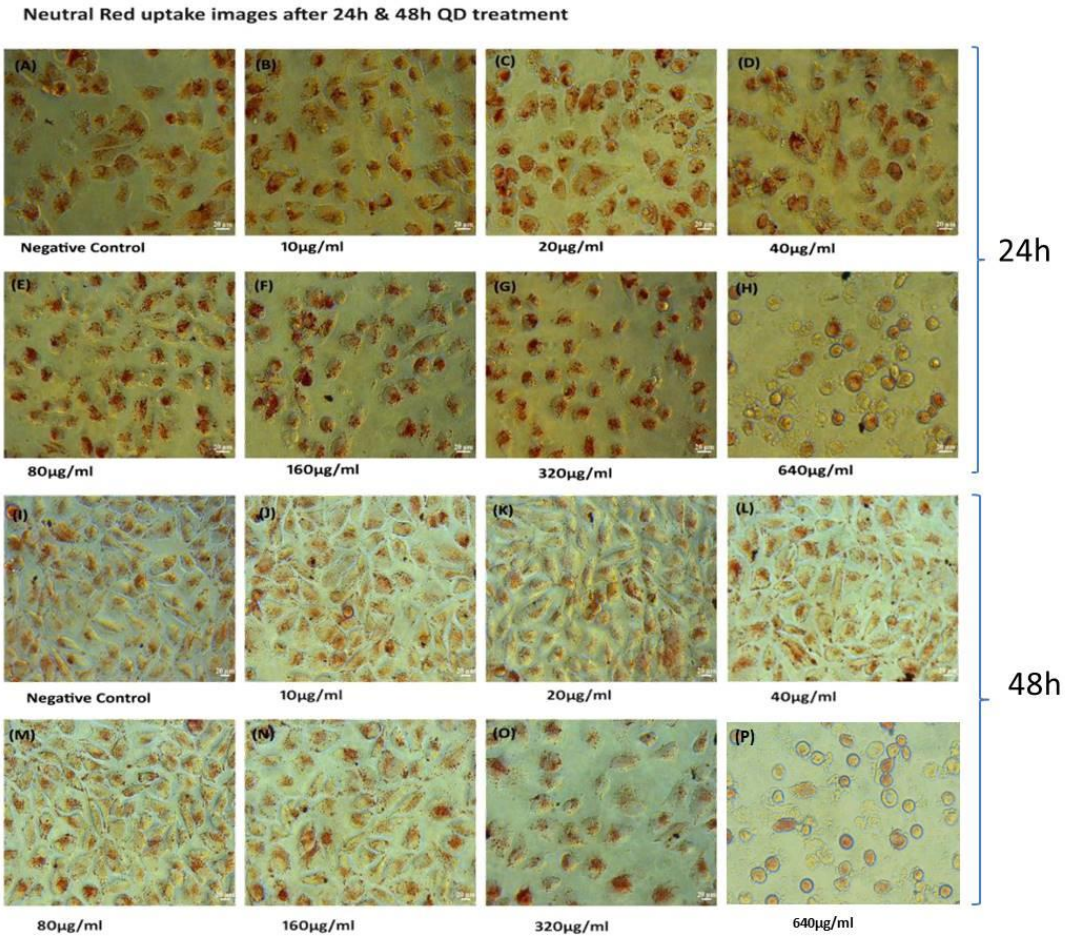

Figure 4.21: Neutral red dye uptake images of LN-229 cells exposed to WS_2 QDs for 24h (A-H) and 48h (I-P). Images show lysosomes with red granules. Magnification; 20x and scale bar represents 20µm.

4.5.8 Lactate dehydrogenase assay for cytotoxicity

Cytotoxic response associated with cell membrane damage will lead to the release of cytosolic lactate dehydrogenase (LDH) enzyme. **Figure 4.22** showed the quantitative estimation of LDH and is directly proportional to the cytotoxicity of the material. For All the selected concentrations were almost comparable with that of untreated negative control cells at 24h exposure. With 24h exposure of WS_2 QDs, a statistically significant dose dependant cytotoxic response with respect to LDH release was

evidenced from 160µg/ml onwards. Similarly, statistically significant dose dependant increase in LDH release was found at the end of 48h QD exposure.

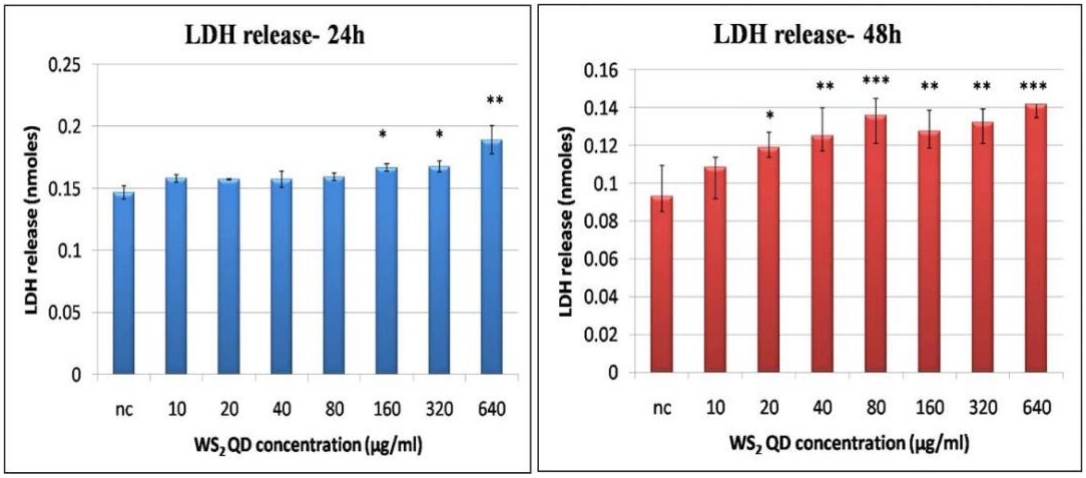

Figure 4.22: LDH release after 24h and 48h exposure of varying concentrations of WS_2 QDs with LN-229 cells. Values were expressed in terms of LDH release in nmoles. Negative control represents untreated control cells. The datas were represented as mean ± SD of three independent experiments. Asterisk denotes statistically significant difference (*p<0.05, **p< 0.01 and ***p<0.001)

4.5.9 Cellular morphology analysis by phase-contrast microscopy

LN-229 cells, after 24h and 48h WS_2 QDs exposure was visualized using phase contrast microscope to analyze the morphological changes in response to WS_2 QDs exposure. **Figure 4.23** showed that no distinct morphological anomalies were observed upto 320µg/ml concentration. But at 640µg/ml concentration, typical cellular phenotypic changes visible. More than 50% of the cells were found to be shrunken and dead following 640µg/ml WS_2 QDs exposure for 24h. Similarly, after 48h WS_2 QDs exposure (upto 160µg/ml concentration) the morphology of the cells

was comparable with that of untreated control cells. But onset of morphological alterations such as blebbing was visible at 320µg/ml. At 640µg/ml concentration, more than 80% of the cells lost their morphological integrity, got shrunken and found to be non viable.

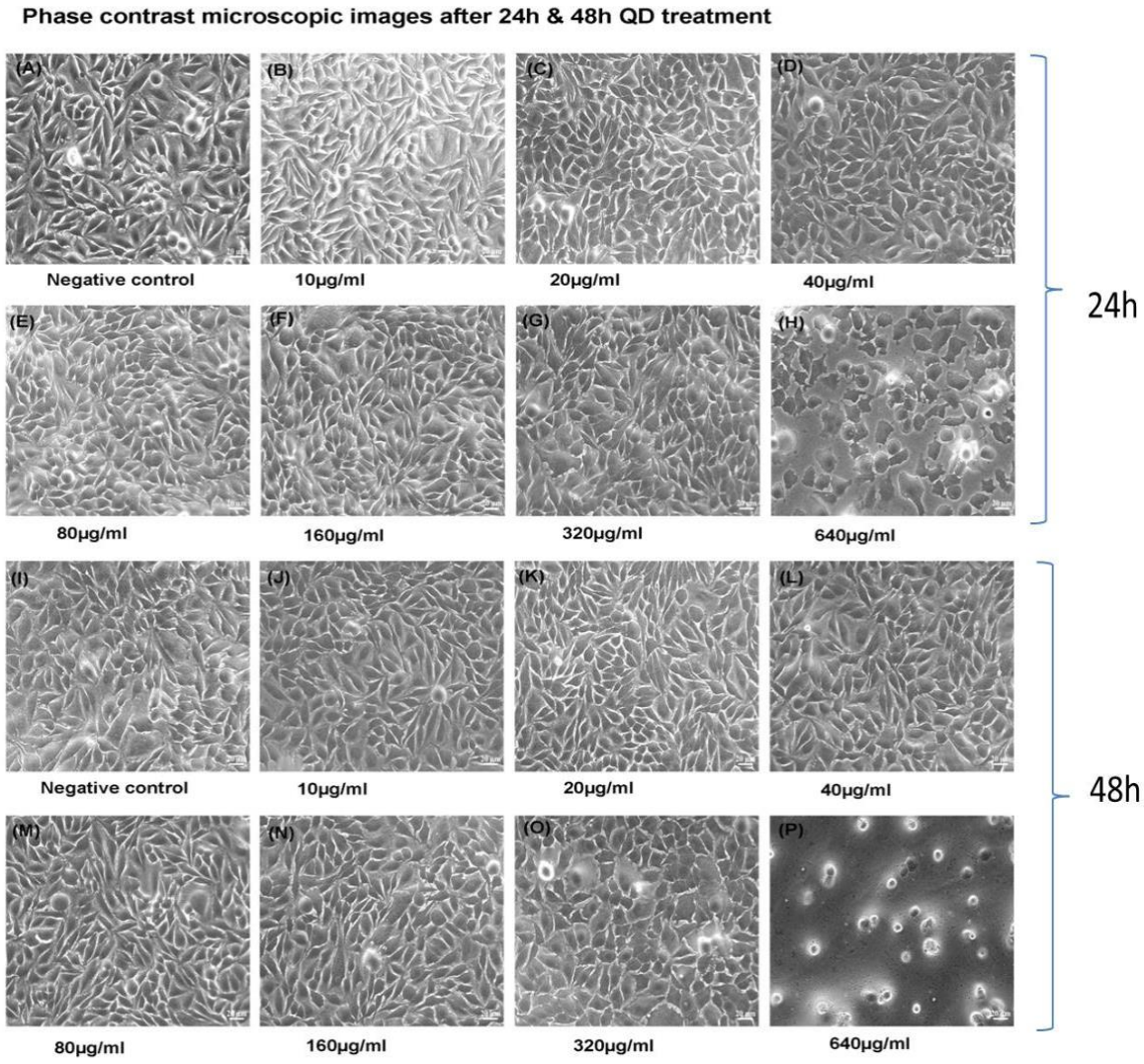

Figure 4.23: Phase contrast microscopic images of LN-229 cells exposed to WS_2 QDs for 24h (A,B,C,D,E,F,G,H) and 48h (I,J,K,L,M,N,O,P) respectively. Magnification; 20x and scalebar represent 20µm

4.5.10 Live/Dead assay by Calcein AM/ PI FACS

Live/dead cell population after 24h WS_2 QDs exposure in LN-229 cells was analyzed using Calcein AM/PI FACS. The live cells will stain Calcein whereas PI will penetrate those cells with challenged membrane permeability. **Figure 4.24** indicates that a slight dose dependent increase in dead cell population was evident in all the treated cell populations. After 24h QD exposure, up to 80µg/ml concentration, more than 90% of cells were found to be viable which correlates with the MTT results. More than 80% of the cells were found to be viable upto 320µg/ml concentration, whereas for the highest selected concentration of 640µg/ml, a significantly increased dead cell population was found. It was evident that the membrane permeabilization was elicited in 640µg/ml WS_2 QDs treated cells, which eventually tend to an increased uptake of PI.

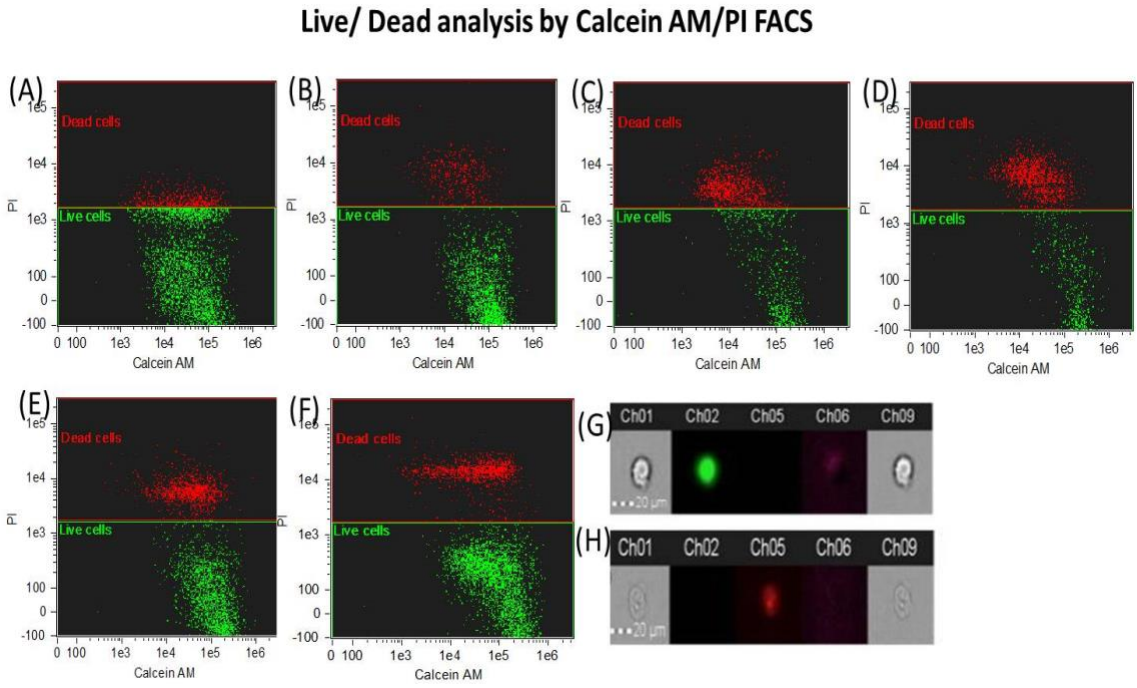

Figure 4.24: Calcein AM/PI FACS for live/dead analysis associated with membrane permeability. (A) Negative control (untreated cells), (B) 40µg/ml, (C) 80µg/ml, (D) 160µg/ml, (E) 320µg/ml and (F) 640µg/ml concentrations of WS_2 QDs treated cells. (G) Representative image for Calcein positive cells and (H) representative image for PI positive cells used to analyze FACS data. In representative cell images, Ch01 and Ch09 represents phase contrast image of cells, Ch02 Calcein positive cells, Ch05 PI positive cell

4.5.11 ROS generation studies

4.5.11.1 Detection of reactive oxygen species by DCFH-DA Assay

ROS generation in LN-229 exposed to varying concentrations of WS_2 QDs was analyzed using DCFH-DA assay. The results indicate that; for both 6h and 24h QD exposure, a statistically significant increase in hydroxyl free radicals was evidenced at both 320µg/ml and 640µg/ml treatment groups (**Figure 4.25**). The highest selected concentration (640µg/ml) showed a response similar to the H_2O_2 treated positive control group. For concentrations upto 160µg/ml, free radical release response was found to be similar to that of untreated control cells.

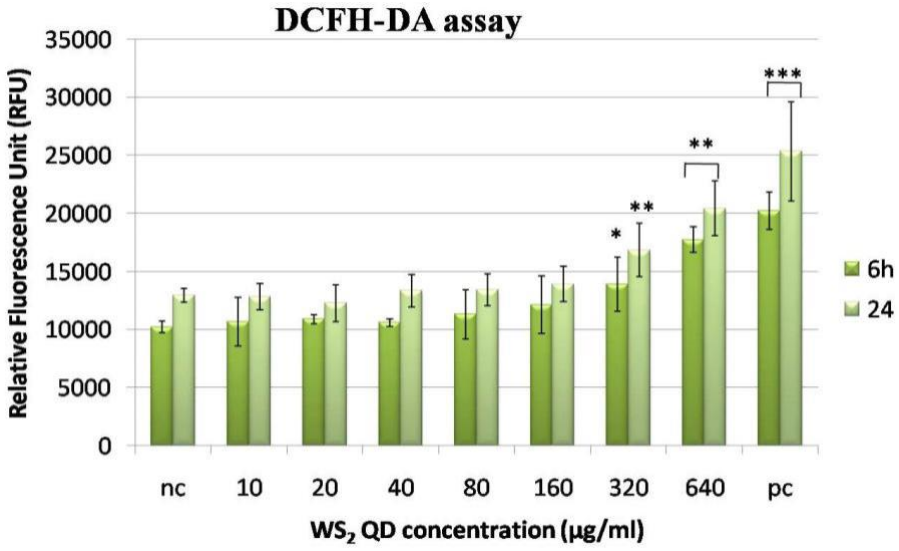

Figure 4.25: Hydroxyl free radical release in LN-229 cells exposed to WS_2 QDs for 6h and 24h. Values were expressed in terms of Relative Fluorescence Unit (RFU) due to fluorescence quantification. H_2O_2 treated cells were used as positive control and untreated cells were kept as negative control. The datas were represented as mean ± SD of three independent experiments. Asterisk denotes statistically significant difference (*$p<0.05$, **$p< 0.01$ and ***$p<0.001$)

4.5.11.2 Detection of reactive nitrogen species by Griess reagent Assay

Reactive nitrogen species (RNS) release in response to WS_2 QDs treatment was analyzed using Griess reagent assay after 6h, 24h and 48h. **Figure 4.26** showed that no statistically significant increase in RNS production was evidenced upto 80µg/ml concentration. A statistically significant gradation in RNS release was found at 640µg/ml. Results were analyzed using nitrite release standards using varying concentrations of sodium nitrate standard.

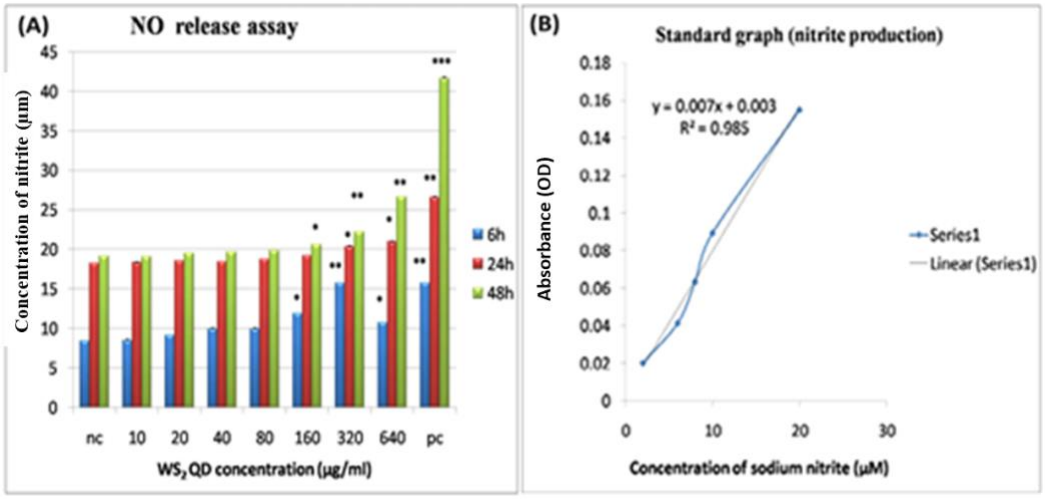

Figure 4.26: (A) RNS free radical release in LN-229 cells exposed to WS_2 QDs for 6h, 24h and 48h. (B) Standard graph of nitrite release used for data analysis. Values were expressed in terms of concentration of nitrite released (µM). 0.02% phenol treated cells were used as positive control and untreated cells were kept as negative control. The data represent mean ± SD of three independent experiments. Asterisk denotes statistically significant difference (*$p<0.05$, **$p< 0.01$ and ***$p<0.001$)

4.5.11.3 Influence of catalase activity on ROS generation

To analyze whether the similarity of hydroxyl radical release in treatment groups with untreated control cells is due to the inherent catalase activity of glioblastoma cells, influence of catalase activity on ROS generation was analyzed. NaN_3 was used as catalase inhibitor to selectively inhibit catalase activity in LN-229 cells and further DCFHDA assay was done. **Figure 4.27** showed that in presence of catalase inhibitor, a similar trend of hydroxyl radical release was found which was almost comparable with that of control. This made it confirmed that the lack of significant difference of hydroxyl radical release in treatment groups and control was not because of the catalase activity of the cell but because of the poor radical generation efficiency of the WS_2 QDs in LN-229 cells.

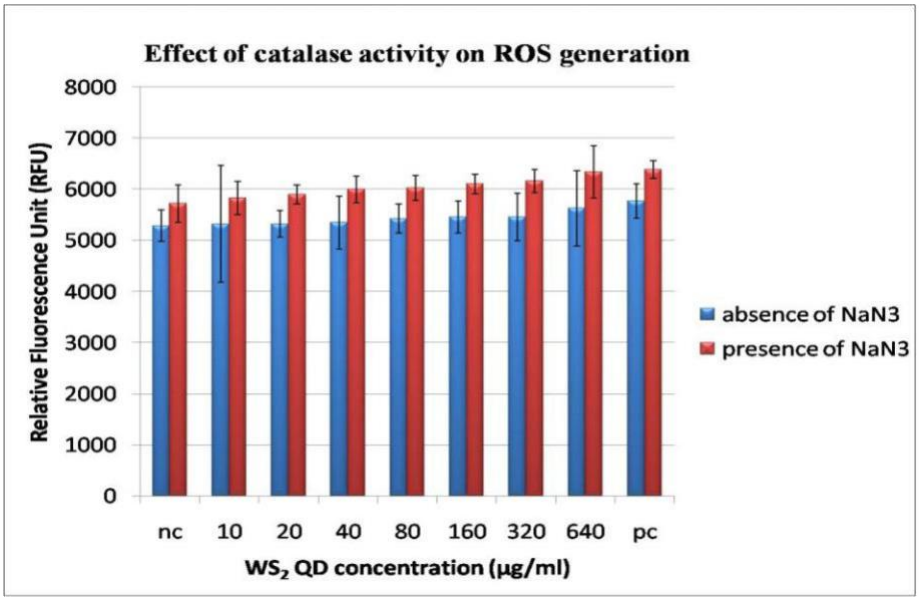

Figure 4.27: Effect of catalase activity on LN-229 cells exposed to catalase inhibitor NaN_3. 0.1µM NaN_3 pretreatment was given to inhibit catalase activity. The values were expressed in relative fluorescence unit (RFU). The data represent mean ± SD of three independent experiments

4.5.12 CBB staining for morphology analysis

Coomassie Brilliant Blue (CBB) staining was used to analyze the cellular morphology of LN-229 cells after 24h and 48h of WS_2 QDs exposure. **Figure 4.28** showed that, with 24h WS_2 QDs treatment, for all the selected concentrations upto 320µg/ml, cells retained intact cellular phenotype and were comparable with that of the negative control cells. Inset showed higher magnification (40x) images of the cells for clarity. **Figure 4.29** depicted LN-229 cells after 48h WS_2 QDs exposure. It was evident from the microscopic stained images that; upto 160µg/ml concentration, the cells retained intact cellular phenotype whereas at 320µg/ml morphological abnormalities were visible with a visibly significant reduction in cell number.

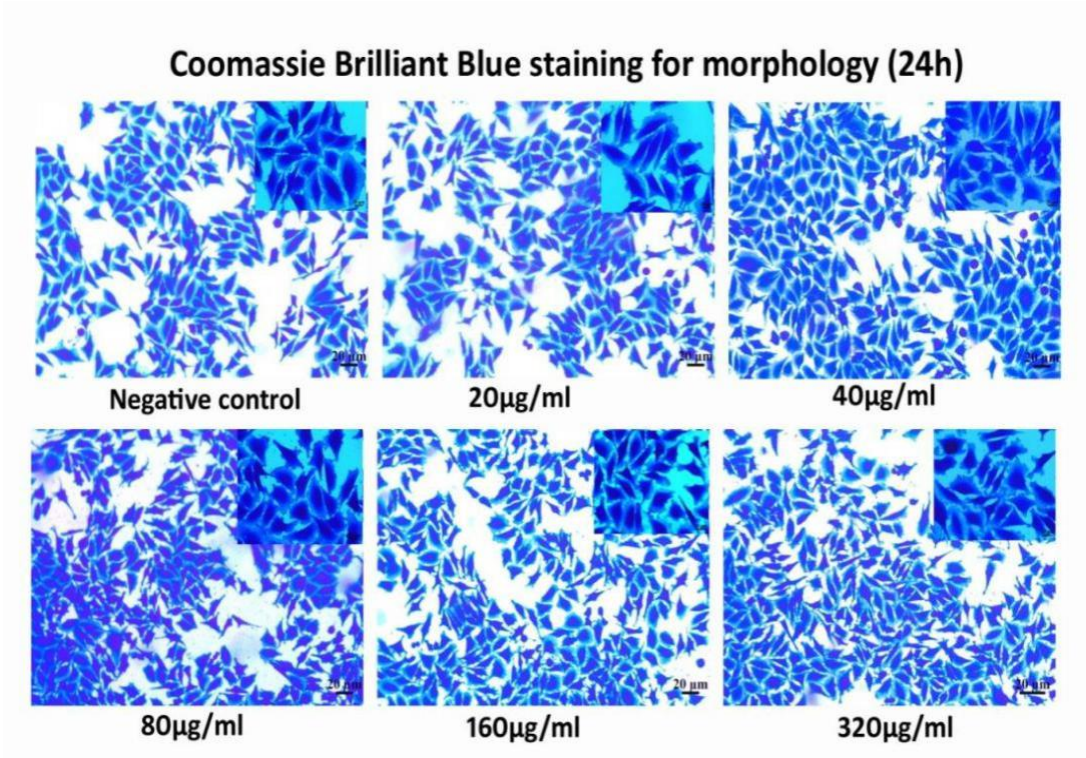

Figure 4.28: Coomassie brilliant blue stained images of LN-229 cells after 24h QD exposure. Magnification; 20x. Inset shows higher magnification images (40x). Scale bar represents 20µm

Coomassie Brilliant Blue staining (48h)

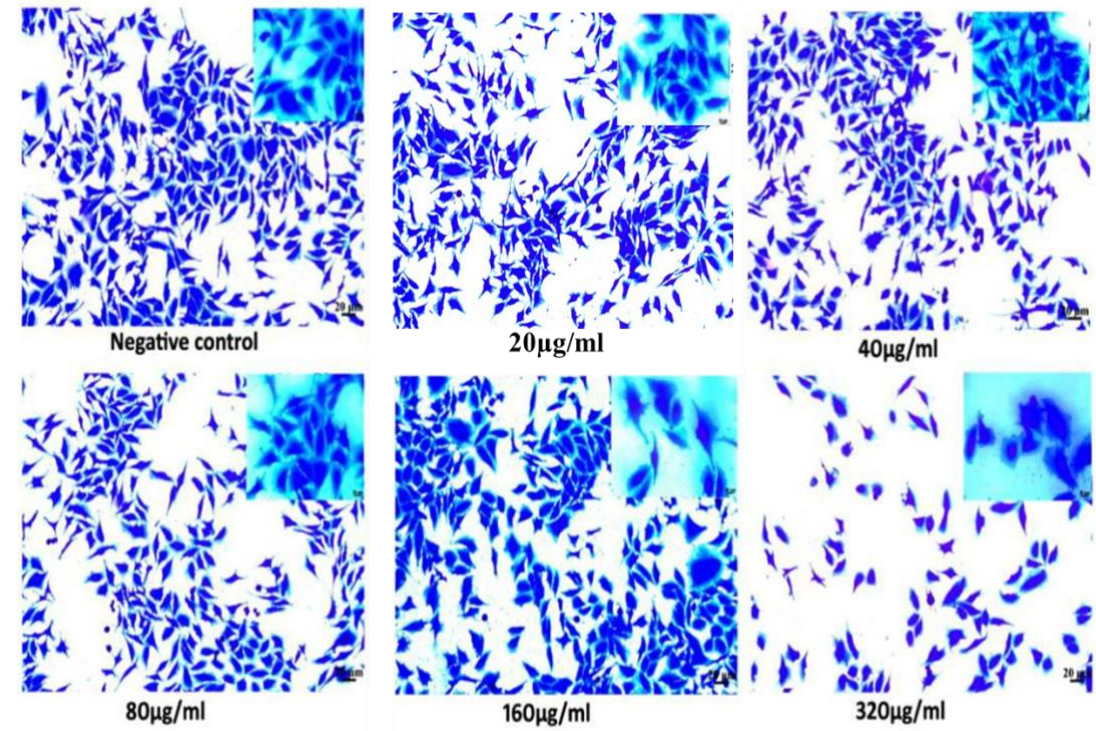

Figure 4.29: Coomassie brilliant blue stained images of LN-229 cells after 48h QD exposure. Magnification; 20x. Inset shows higher magnification images (40x). Scale bar represents 20µm

4.5.13 Lysosomal integrity by acridine orange staining

Lysosomal integrity assessment after 24h WS_2 QDs exposure on LN-229 cells was analyzed using acridine orange immuno staining. Acidic lysosomal compartment makes acridine orange emits red fluorescence. Reduction in red fluorescence is an indicative of loss of lysosomal integrity. **Figure 4.30 (A-F)** showed that WS_2 QDs exposure for 24h duration caused no significant lysosomal integrity loss in LN-229 glioblastoma cells at any of the selected concentrations. A slight difference was observed in 320µg/ml exposed cells when compared to untreated negative control cells. **Figure 4.30 (G)** represents quantitative estimation of acridine orange uptake, which strictly coincides with the qualitative analysis results.

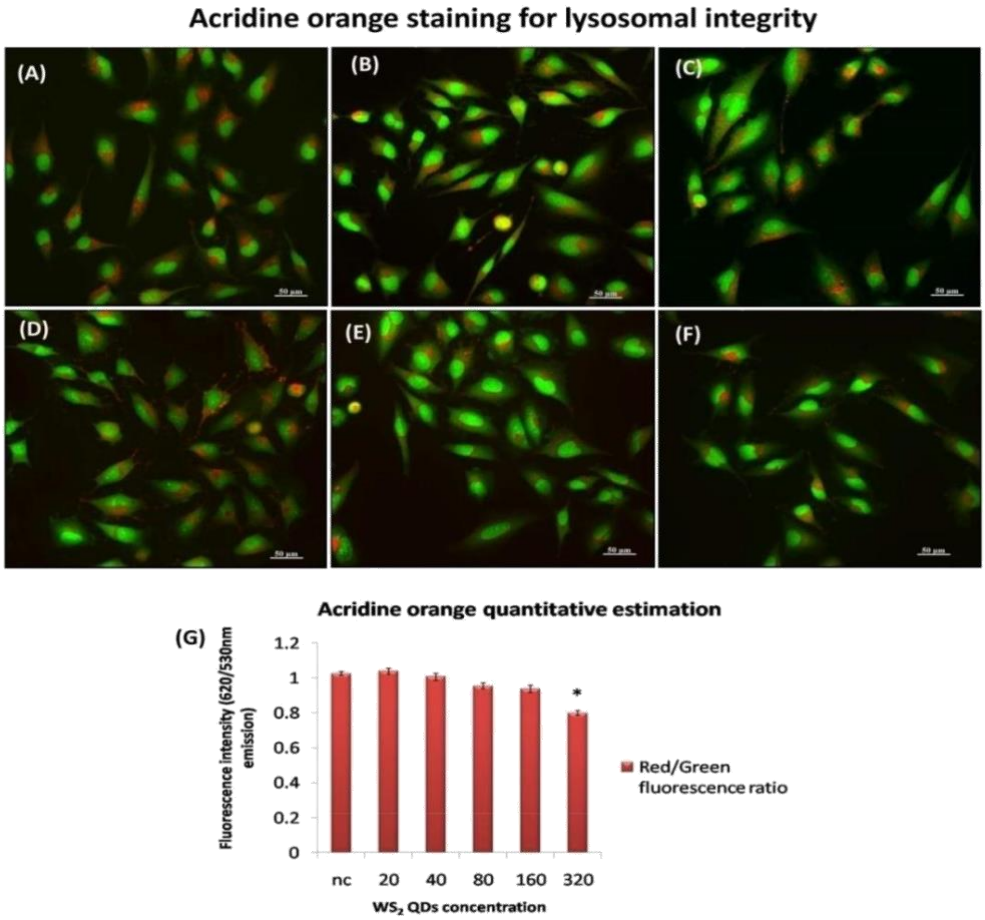

Figure 4.30: Acridine orange staining for lysosomal integrity in LN-229 cells exposed to varying concentrations of WS_2 QDs. Figure (A) represent untreated negative control, (B) 20µg/ml, (C) 40µg/ml, (D) 80µg/ml, (E) 160µg/ml and (F) 320µg/ml. Red fluorescent granules represent intact lysosomes and green fluorescence indicates the cytoplasm. Magnification (20x) and scalebar represent 50µm. Figure (G) represents quantitative estimation of acridine orange uptake

4.5.14 Mitochondrial membrane potential by JC-1 probe

JC-1 staining was used to analyze the mitochondrial membrane integrity after 24h WS_2 QDs exposure in LN-229 glioblastoma cells. Rod shaped red fluorescent granules indicate intact mitochondria and green fluorescence represent cytoplasm. Reduction in red fluorescence is an indicative of loss of mitochondrial membrane

potential. **Figure 4.31 (A-F)** showed that WS_2 QDs exposure for 24h duration caused no significant reduction in mitochondrial membrane potential on LN-229 glioblastoma cells at any of the selected concentrations. All the concentrations showed a similar response with that of negative control except for 320µg/ml exposed cells, in which a noticeable reduction in red fluorescence was found. This indicates a dose dependent cytotoxic response. Quantitative analysis of JC-1 uptake in LN-229 cells represented in **Figure 4.31(G).**

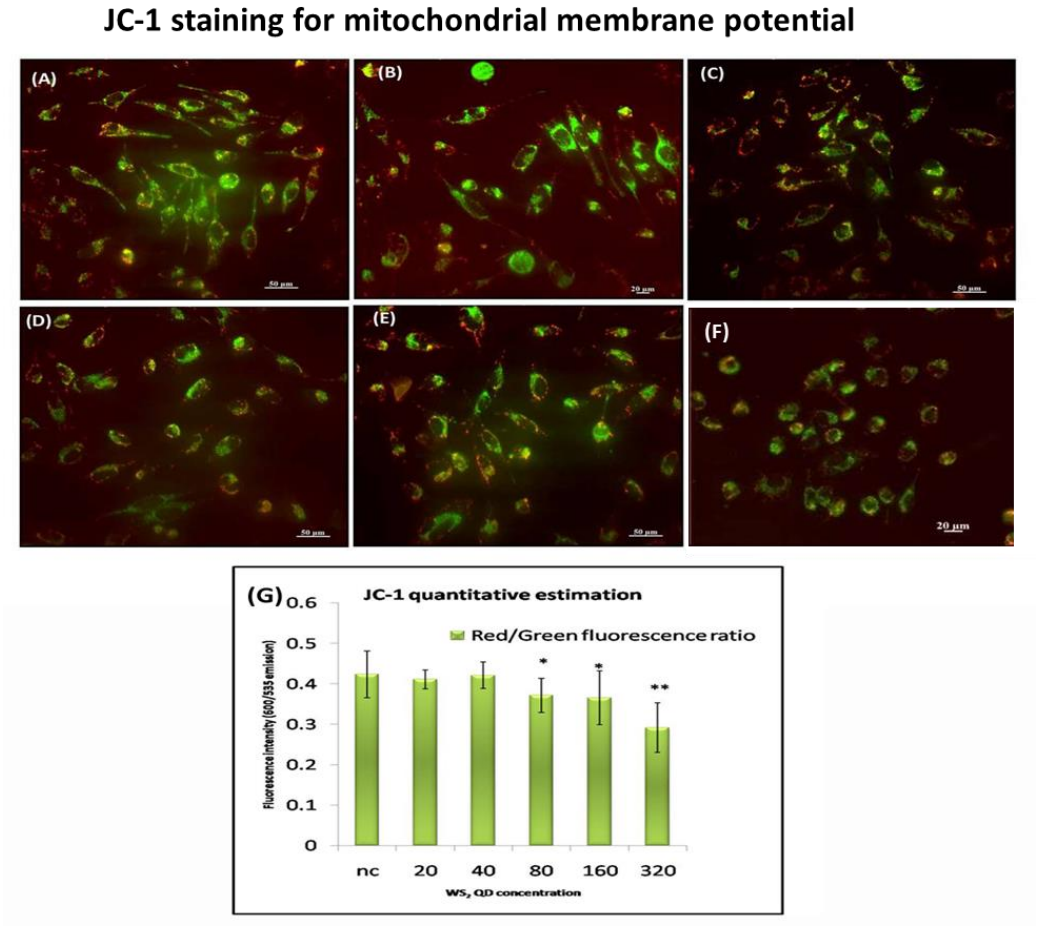

Figure 4.31: JC-1 staining for mitochondrial membrane potential. Figure (A) negative control, (B) 20µg/ml, (C) 40µg/ml, (D) 80µg/ml, (E) 160µg/ml and (F) 320µg/ml. Red fluorescent rod shaped structures inside represent active mitochondria. Magnification (20x) and scalebar represent 50µm. Figure (G) represent quantitative estimation of acridine orange uptake

4.5.15 Cytoskeletal integrity by Rhodamine-Phalloidin staining

Rhodamine-phalloidin staining was used to analyze the actin filament stability and associated cytoskeletal integrity. It was evident from **Figure 4.32** that, no significant cytoskeletal abnormalities were observed at any of the selected concentrations. Even at the highest concentration (320µg/ml), the cells maintained cytoskeletal integrity and intact actin filaments. Nucleus was counterstained with DAPI to observe any nuclear condensation followed by WS_2 QDs treatment. Cyan green fluorescent WS_2 QDs were visible inside the cytoplasm. No visible cytoskeletal retractions were observed in any of the selected concentrations.

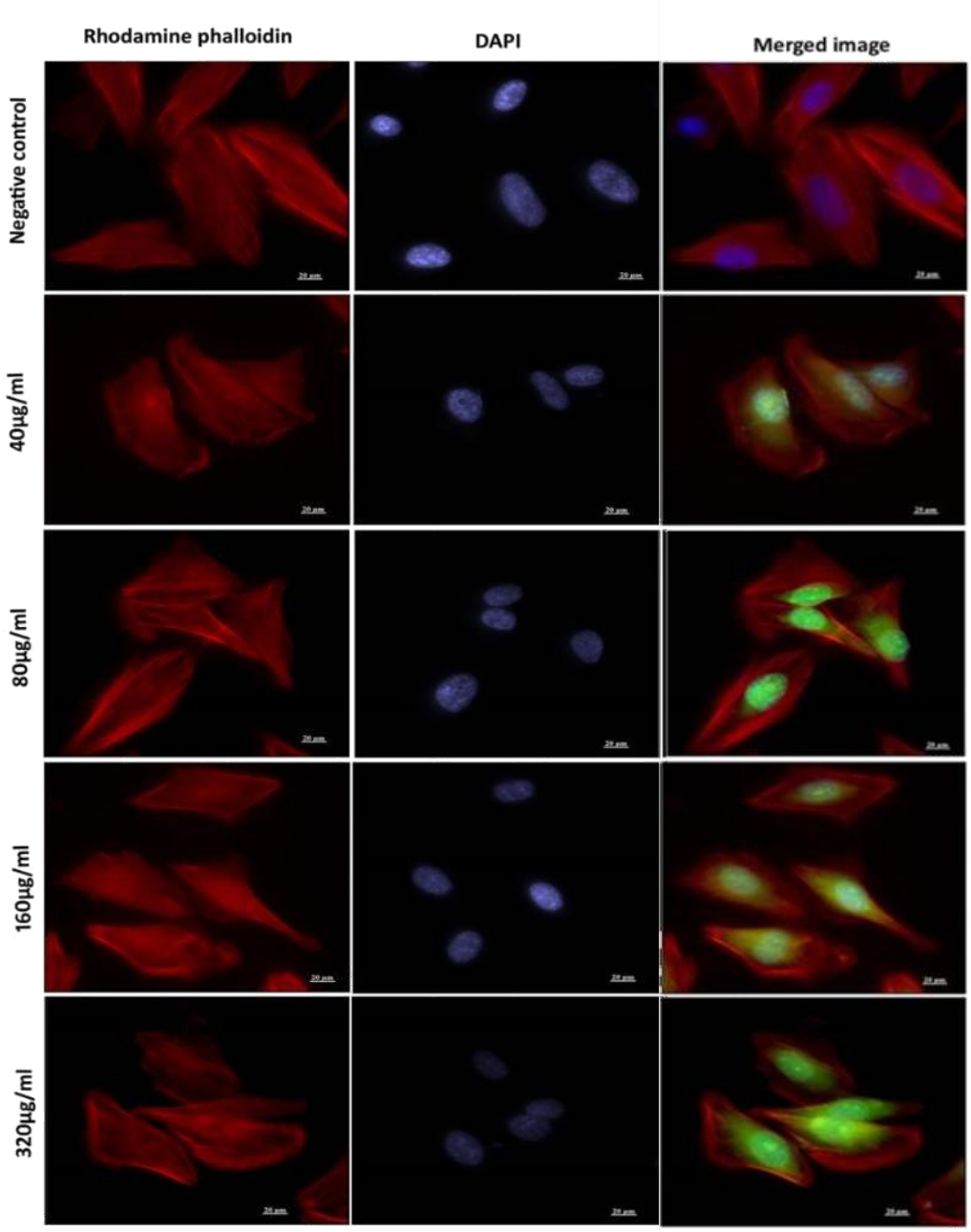

Figure 4.32: Rhodamine-phalloidin staining for cytoskeletal integrity analysis after 24h WS_2 QDs exposure (40, 80, 160 and 320µg/ml) on LN-229 glioblastoma cells. Cells were counterstained with DAPI stain for nuclear condensation. Fluorescent WS_2 QDs were localized inside the cytoplasm. Magnification; 40x and scalebar represent 20µm

4.5.16 Membrane integrity by ethidium bromide: FACS

Ethidium bromide FACS was used to analyze membrane integrity in LN-229 cells after WS_2 QDs exposure. **Figure 4.33** indicate the histogram representation that

showed a concentration dependant reduction in cell membrane integrity was observed in the cells treated with higher concentrations of WS_2 QDs. A very slight reduction in membrane integrity was observed at the highest selected concentrations (160µg/ml and 320µg/ml) when compared to the untreated control cell population.

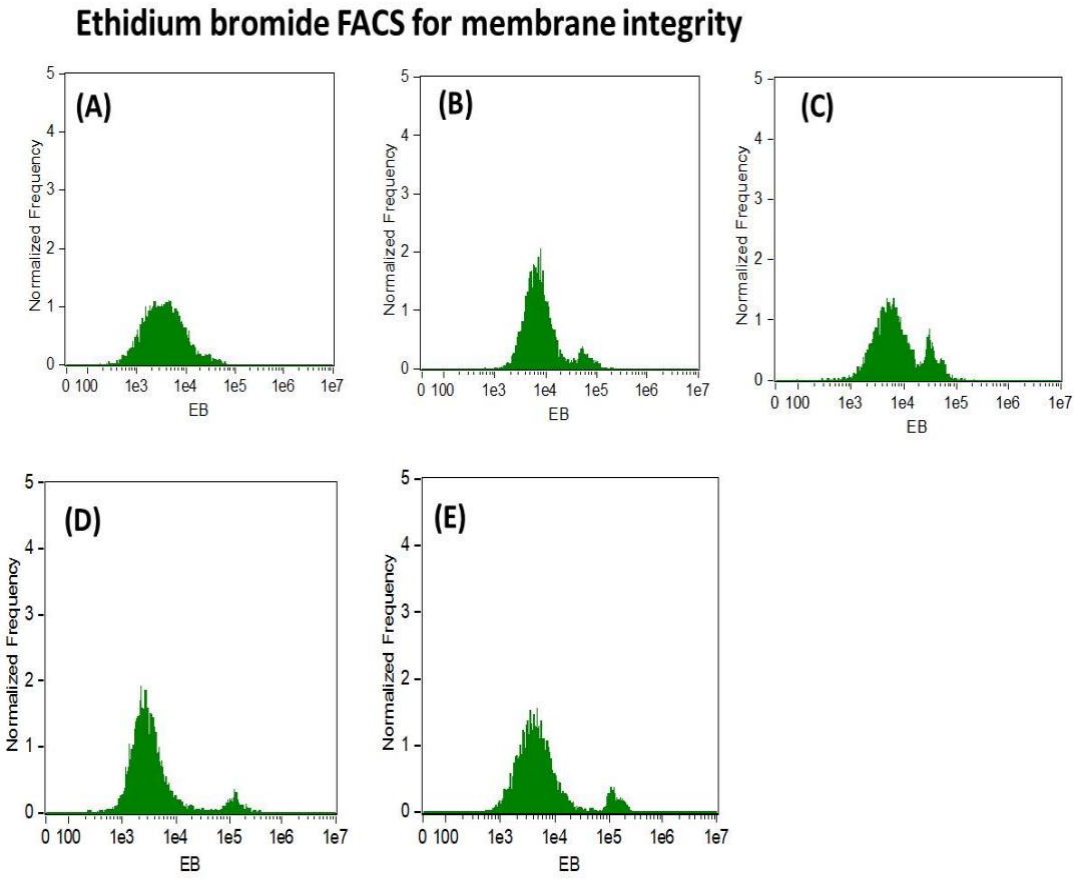

Figure 4.33: Ethidium bromide (EtBr) FACS for cell membrane integrity. Membrane damaged cells will take up EtBr, form adduct with DNA and fluoresce as red inside the nucleus. (A) Represent untreated negative control cells, (B) 20µg/ml, (C) 40µg/ml, (D) 160µg/ml and (E) 320µg/ml.

4.5.17 Cell cycle analysis: PI flow cytometry

Cell cycle analysis was done in LN-229 cells exposed to varying concentrations of WS_2 QDs. Results indicate that, except for the 320µg/ml concentration, all the other treatment groups showed a similar trend of G0/G1, S and G2 phase when compared with that of the negative control (**Figure 4.34**). No sub G1 population was evidenced in any of the treatment groups. At 320µg/ml concentration, an extended S phase was found (28.83%).

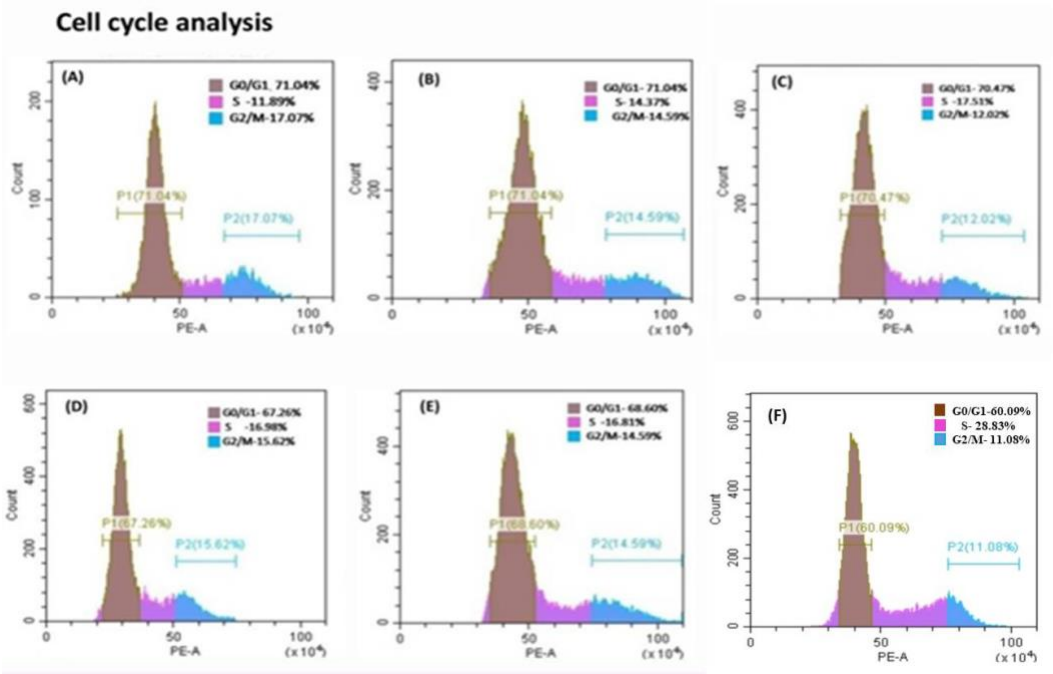

Figure 4.34: Cell cycle analysis in LN-229 cells after WS_2 QDs exposure. (A) negative control, (B) 20µg/ml, (C) 40µg/ml, (D) 80µg/ml, (E) 160µg/ml and (F) 320µg/ml concentration WS_2 QDs treated cells.

4.5.18 Apoptosis by Annexin V/PI: FACS

Annexin V/ PI FACS analysis was carried out to analyze the apoptosis mediated cell death in WS_2 QDs exposed LN-229 cells. In the FACS data, P1 population represent normal healthy cells, P2 indicate early apoptotic cells, P3 corresponds to late apoptotic cells and P4 represent dead/ necrotic cells (**Figure 4.35)**. The results showed that a significantly increased early apoptotic and late apoptotic cell population were observed in 160µg/ml and 320µg/ml concentrations. Also an increased dead cell population was evidenced in 320µg/ml concentration. 20, 40 and 80µg/ml WS_2 QDs treated groups were found to be similar to that of untreated control cells. Even then, more than 70% of the cells were observed to be healthy at the highest concentration also, which evidenced the nontoxic nature of the synthesized WS_2 QDs.

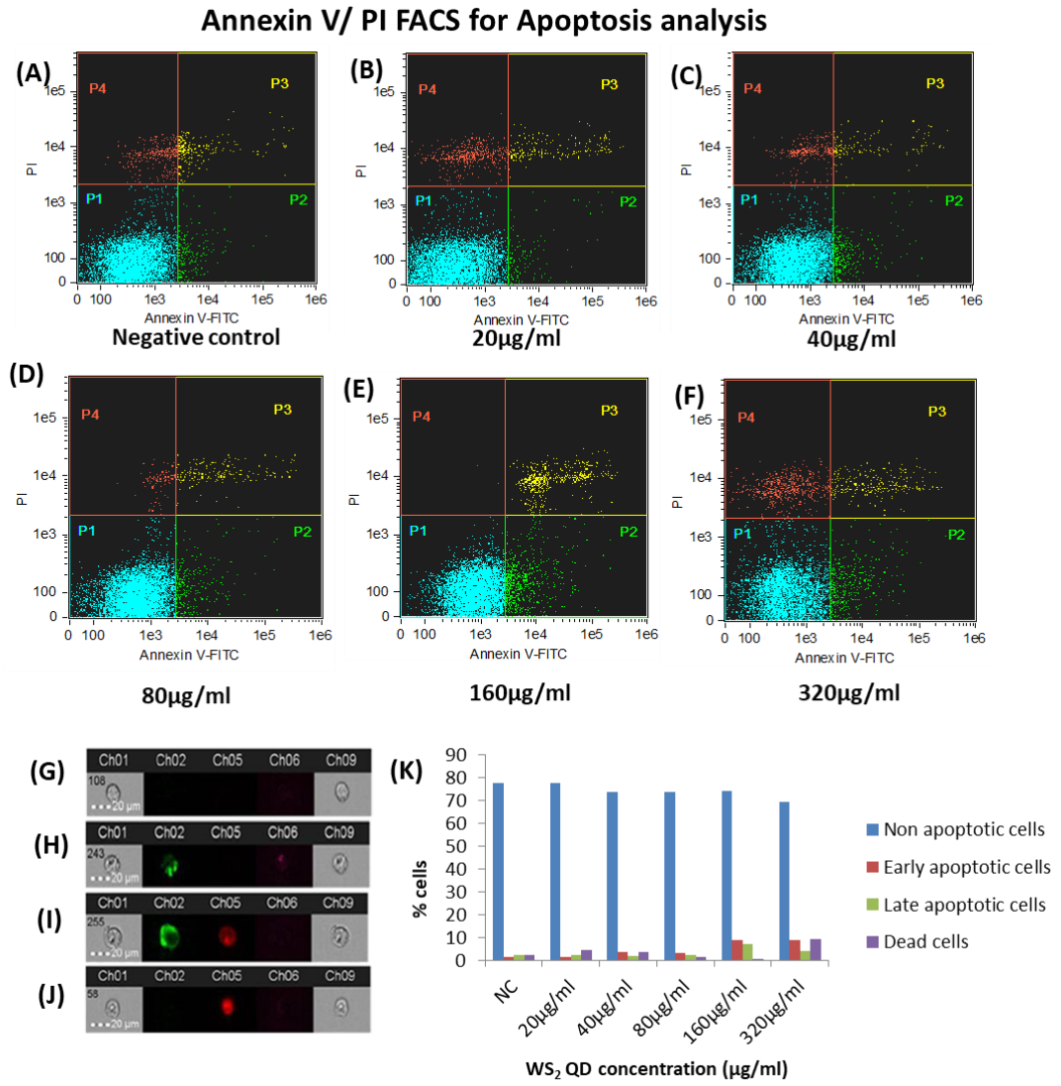

Figure 4.35: Annexin V/PI FACS of LN-229 cells exposed to varying concentrations of WS_2 QDs (A-F). P1, P2, P3 and P4 quadrants represent live cells, early apoptotic, late apoptotic and necrotic stages of LN-229 cells. Figure (G) indicate the representative image of P1 quadrant live cells, (H) represent P2 quadrant Annexin positive early apoptotic cells, (I) represent P3 quadrant with both Annexin and PI double positive late apoptotic cells and (J) represent PI positive dead cells. (K) Quantitative representation of cell population in each quadrant

4.5.19 Caspase 3 expression analysis: FACS

Caspase 3 expression was analyzed to confirm apoptosis pathway of cell death after WS_2 QDs exposure. Caspase 3 expression is usually observed in apoptosis mediated cell death only. A significantly increased Caspase 3 expression was observed at the highest concentration of 320µg/ml, which confirmed that the cell death pathway mediated by WS_2 QDs exposure was apoptosis mediated (**Figure 4.36**).

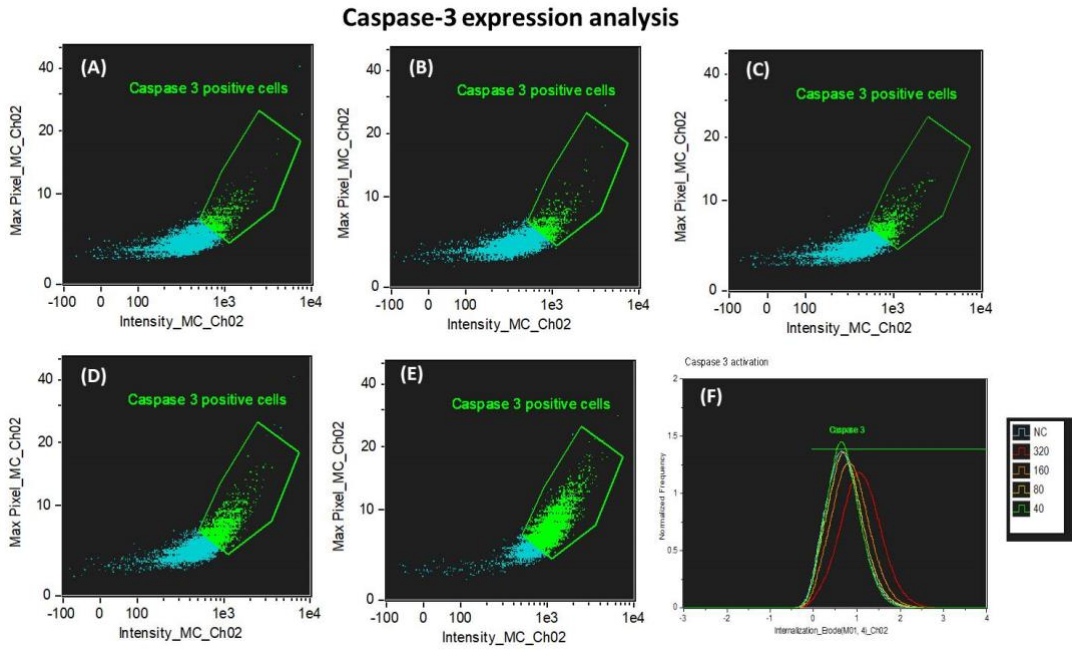

Figure 4.36: Caspase 3 expression analysis by FACS. (A) Untreated negative control cells, (B) 40µg/ml, (C) 80µg/ml, (D) 160µg/ml and (E) 320µg/ml concentration exposed LN-229 cells. (F) Represents the frequency distribution histogram of Caspase 3.

4.5.20 NF-KB activation assay: FACS

NF-κB expression was analyzed by FACS assay after 24h exposure of WS_2 QDs on LN-229 glioblastoma cells**. Figure 4.37** shows that a slight concentration dependent NF-κB expression was found in cells exposed to 320µg/ml WS_2 QDs. Rest of the concentrations were similar to that of the untreated control cells showing very minute level of NF-κB expression, which is an intrinsic characteristic for glioblastoma cells.

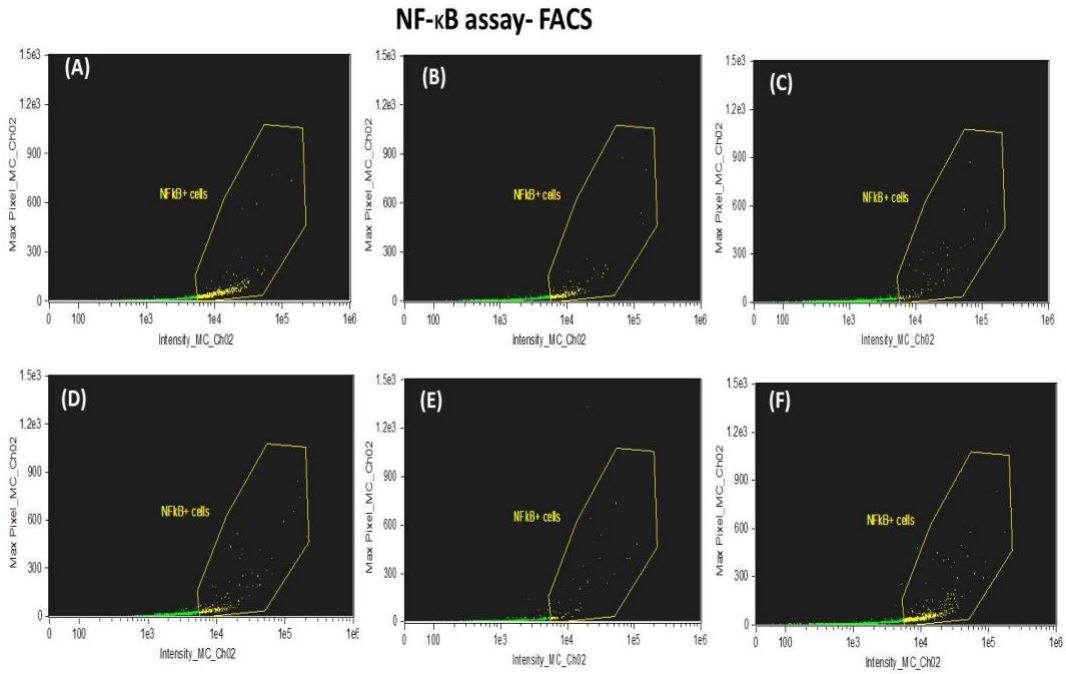

Figure 4.37: NF-KB expression analysis by FACS assay after WS_2 QDs exposure on LN-229 cells for 24h. Untreated cells were kept as negative control. (A) Untreated negative control cells, (B) 20µg/ml, (C) 40µg/ml, (D) 80µg/ml, (E) 160µg/ml and (F) 320µg/ml concentration exposed LN-229 cells.

4.5.21 Genotoxicity studies

4.5.21.1 Tritiated Thymidine incorporation assay

Cell proliferation status after 48h WS_2 QDs exposure on LN-229 cells was analyzed by tritiated thymidine incorporation assay. **Figure 4.38** indicates that a significant reduction in cell proliferation was observed in 320µg/ml (461±64.71) and 640µg/ml (138.3±26.5) concentrations. The highest selected concentration 640µg/ml showed a significant reduction in cell proliferation.

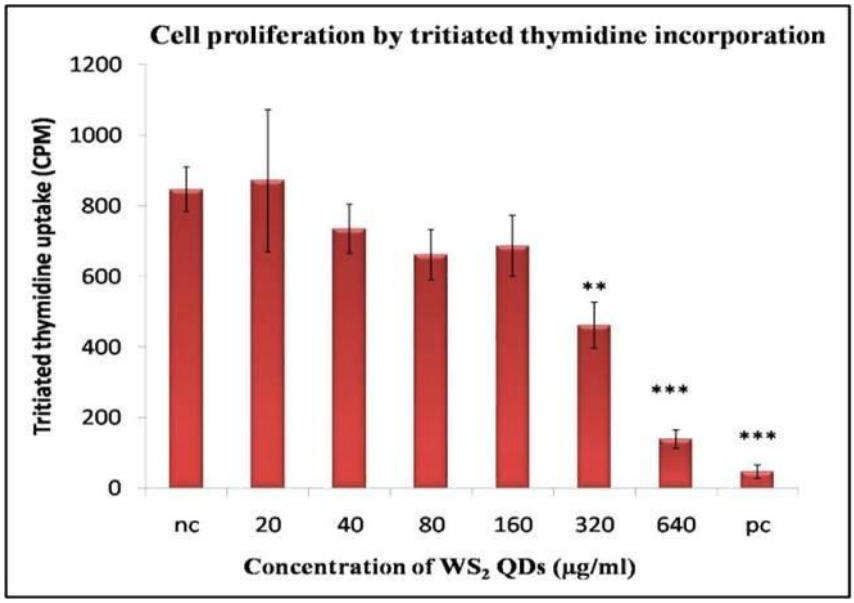

Figure 4.38: Cell proliferation status after 48h WS_2 QDs exposure on LN-229 cells by tritiated thymidine incorporation assay. Untreated cells were used as negative control and 0.02% phenol treated cells were kept as positive control for data comparison and analysis. The data represents mean ± SD of three independent experiments. Asterisk denotes statistically significant difference with control (**p< 0.01 and ***p<0.001)

4.5.21.2 DNA ladder assay

DNA ladder assay was done to evaluate the possible DNA fragmentation. **Table 4.1** showed purity report of DNA samples used for DNA ladder experiment. The purity of DNA samples was determined by taking the ratio of absorbance at 260:280nm. Values in between 1.6 to 1.9 represent pure DNA. DNA ladder assay was done to evaluate the possible DNA fragmentation and further DNA damage following WS_2 QDs treatment. The results showed that for 40, 80 and 160µg/ml concentrations, no visible DNA fragmentation was observed (**Figure 4.39)**. But for the highest concentrations of 320 and 640µg/ml, two distinct DNA bands similar to positive control was evident, which corresponds to DNA ladder formation at higher concentrations.

The results depicted 2 clear DNA fragments similar to the positive apoptotic cells shown in 'Lane 8'. Therefore, it can be inferred that WS_2 QD exposure resulted in chromosomal DNA degradation into small internucleosomal fragments, a biochemical hallmark of cells undergoing apoptosis. But for the lower concentrations, DNA was similar to that of untreated negative control.

DNA samples	Purity ($A_{260/280nm}$)
Negative control	1.807
40µg/ml	1.595
80µg/ml	1.674
160µg/ml	1.757
320µg/ml	1.813
640µg/ml	1.674

Table 4.1: Purity of DNA samples isolated from LN-229 cells treated with varying concentrations of WS_2 QDs. Untreated cells were kept as negative control for comparison

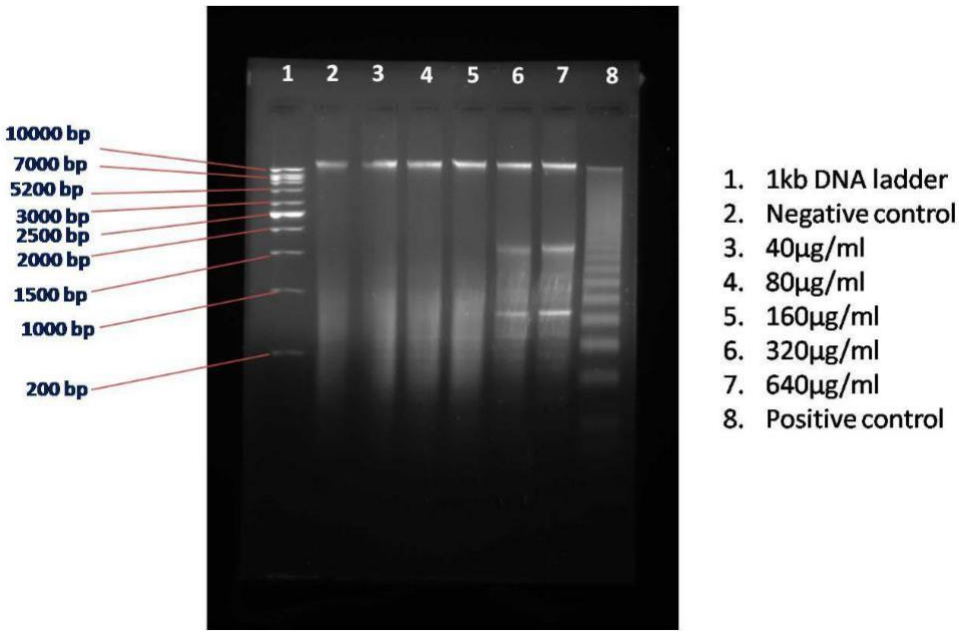

Figure 4.39: DNA ladder assay for DNA fragmentation analysis after WS_2 QDs exposure

4.5.21.3 Hoechst staining for DNA nuclear condensation

Hoechst 33342 staining was used to analyze the nuclear and chromosomal condensation after WS_2 QDs exposure on LN-229 cells. No nuclear/ chromosomal condensation was visible at any of the selected concentrations upto 160µg/ml. At 320µg/ml, a dose dependant chromosomal condensation and subsequent nuclear shrinkage was visible after 24h WS_2 QDs exposure (**Figure 4.40**).

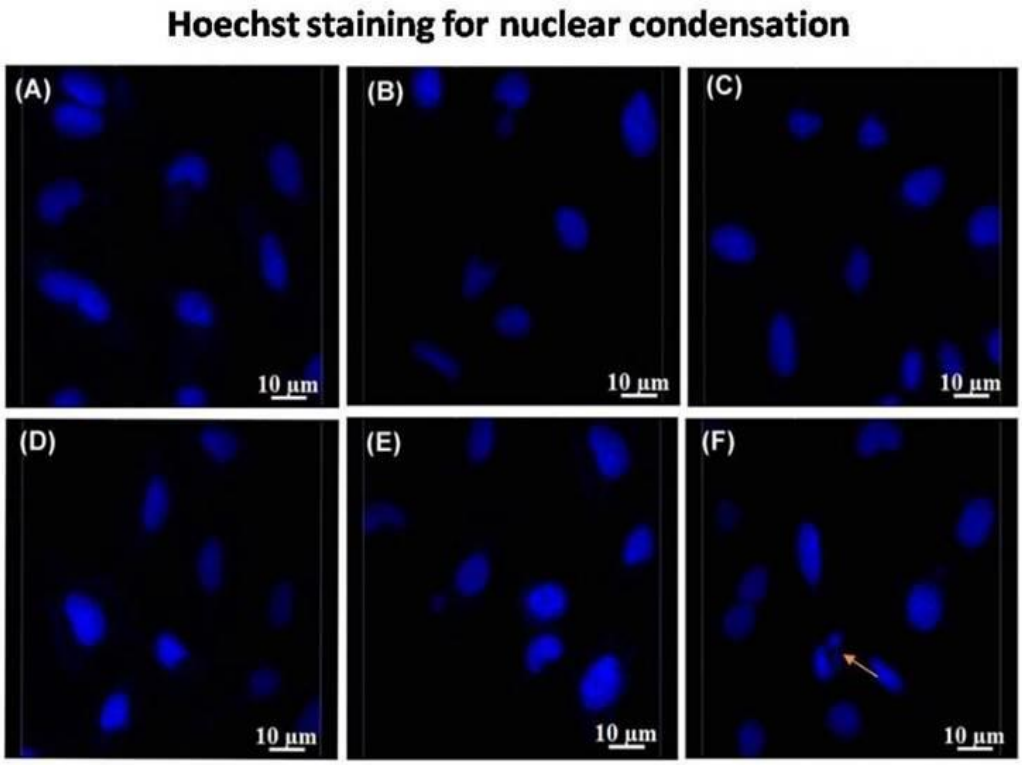

Figure 4.40: Nuclear/chromosomal condensation analysis by Hoechst staining in LN-229 glioblastoma cells exposed to WS_2 QDs for 24h. Untreated cells were kept as negative control. (A) Represent negative control, (B) 20µg/ml, (C) 40µg/ml, (D) 80µg/ml, (E) 160µg/ml and (F) 320µg/ml concentration exposed LN-229 cells. Magnification; 40x and scalebar represent 10µm

4.6 Acute toxicity studies using Sprague-Dawley rats

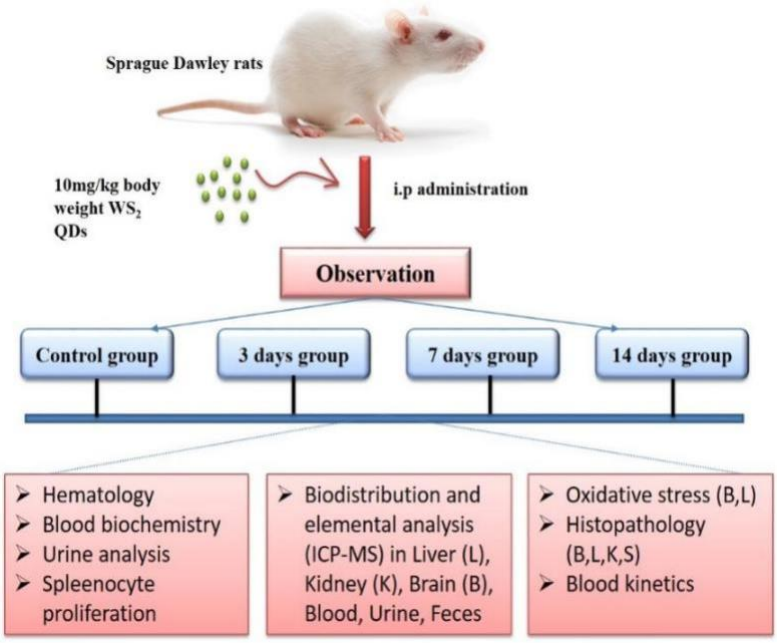

Figure 4.41: Schematic representation of *in vivo* experimental design.

4.6.1 Clinical/ behavioural signs of toxicity

10mg/kg body weight WS_2 QDs were administered to Sprague Dawley rats via i.p route (single exposure). Animals were observed for 3, 7 and 14 days for any clinical and behavioral changes after WS_2 QDs exposure. A set of clinical and behavioral signs associated with toxicity was evaluated. All the animals were found healthy and none of the animals showed any signs of clinical or behavioral toxicity during the observation period and prior to euthanization (**Table 4.2**).

Dose	Clinical/ behavioural symptoms	Period of observation		
		3 days	7 days	14 days
10mg/kg body weight	Changes in skin and fur colour	Normal	Normal	Normal
	Eyes	Normal	Normal	Normal
	Mucous membrane	Normal	Normal	Normal
	Respiratory rhythm	Normal	Normal	Normal
	Gastrointestinal problems	Normal	Normal	Normal
	Motor coordination	Normal	Normal	Normal
	Reflexes	Normal	Normal	Normal
	Convulsions	Normal	Normal	Normal
	Ocular signs	Normal	Normal	Normal
	Cardiovascular signs	Normal	Normal	Normal
	Salivation	Normal	Normal	Normal
	Pilo-erection	Normal	Normal	Normal
	Responsiveness to surroundings	Normal	Normal	Normal
	Grooming	Normal	Normal	Normal
	Analgesia	Normal	Normal	Normal

Table 4.2: Clinical and behavioral signs of Sprague Dawley rats exposed to WS_2 QDs, n=3

4.6.2 Body weight of animals

Body weights of animals were observed throughout the experimental period and expressed in terms of absolute body weight gain. Initial body weight of the animals was given in **table 4.3**. **Table 4.4** showed that the body weight gain of the treated animals was comparable with that of control group animals.

Test groups	Initial body weight (g)
Control	340.05 ± 36.37
3rd day	310.4 ± 34.17
7th day	356.9 ± 17.97
14th day	333.9 ± 25.75

Table 4.3: Initial body weight of the experimental animals.
Data represent mean ± SD

Dose	Route exposure	Observation period			
		Control (g)	**3rd day(g)**	**7th day(g)**	**14th day(g)**
10mg/kg	i.p	13.3 ± 1.21	10.64± 3.1	13.88 ± 2.5	16.86 ± 4.9

Table 4.4: Body weight gain (in grams) after WS_2 QDs administration in Sprague Dawley rats. Rats without any treatment were used as control group. The data represent mean ± SD, n=3

4.6.3 Organ weight

Organ weight of the animals treated with WS_2 QDs were analyzed and expressed in terms of absolute wet weight. No significant change in organ weight was observed in any of the treated animals and was comparable with that of the control group (**Table 4.5**).

Group	Liver (g)	Kidney (g)	Brain (g)	Spleen (g)
Control	10.84 ± 1.56	1.92 ± 0.35	1.74 ± 0.15	0.7 ± 0.18
3rd day	9.58 ± 1.86	2.6 ±0.26	1.67 ± 0.04	0.76 ± 0.09
7th day	11.49 ± 2.71	2.07 ± 0.46	1.82 ± 0.12	0.71 ± 0.11
14th day	10.06 ± 1.25	1.89 ± 0.19	1.67 ± 0.07	0.56 ± 0.03

Table 4.5: Organ weights of animals exposed to WS_2 QDs. Values are represented as absolute organ weight in grams, n=3. The data represent mean ± SD of three independent experiments

4.6.4 Gross pathology

Gross pathological observation did not show any noticeable level of pathological anomalies or lesions in the organs of rats administered with WS_2 QDs (**Figure 4.42**).

Figure 4.42: Gross pathology of Sprague Dawley rats exposed to WS_2 QDs

4.6.5 Hematology

Blood from the treated animals and control animals were collected in K3 EDTA coated tubes and immediately subjected to hematology analysis. Results indicate that a significant increase in platelet count was observed for 3rd day (848 ± 50.92***) group animals when compared with that of untreated control group but falls in the normal range. The platelet count came back to normal level by 7th days. A significant increase in WBC count was observed in the 3rd day treatment group (20.86 ± 4.47*) but came back to normal by 7th and 14th days. All the other hematological parameters were comparable and similar to that of control animals (**Table 4.6**).

Parameters	Control	3rd day	7th day	14th day	**Normal Range** (Ostergaard *et al.* 2010, Delwatta *et al*. 2018)
WBC ($10^3/mm^3$)	12 ± 3.72	20.86 ± 4.47*	16.09 ± 1.91	13.03 ± 1.93	6-17
RBC ($10^6/mm^3$)	8.02 ± 0.18	6.98 ± 1 .19	8.91 ± 2	8.04 ± 0.73	7-10
Platelets (10^9/L	682.33 ± 35.1	848 ± 50.92**	787.33 ± 35.38	763.3 ± 21.93	450-885
HGB (g/dl)	14.33 ± 0.28	12.86 ± 1.19	16.16 ± 0.45	14.73 ± 0.49	11-18
HCT (%)	37.13 ± 1.4	32.53 ± 3.01	41.46 ± 11.26	37.23 ± 1.3	36-48
MCV(μm^3)	46.26 ± 0.70	47.03 ± 3.81	46.23 ± 2.07	46.46 ± 2.48	41-51
MCH (pg)	17.86 ± 0.2	18.56 ± 1.35	18.03 ± 0.92	18.36 ± 1.04	13-41
MCHC(g/dl)	38.63 ± 0.81	39.56 ± 0.77	38.96 ± 0.2	39.56 ± 0.5	21-95

Table 4.6: Hematology analysis in blood of rats exposed to WS_2 QDs. Various parameters such as WBC, RBC, Platelets, HGB, HCT, MCV, MCH and MCHC were analyzed. The data represent mean±SD of three independent experiments. Asterisk above values denote statistically significant difference compared with the control group (*$p<0.05$, **$p<0.01$)

4.6.6 Serum biochemistry

Serum biochemistry analysis was used to assess liver and kidney functions after WS_2 QDs administration in rats after the respective observation periods. Various serum biochemical parameters were analyzed.

4.6.6.1 Liver function tests

Liver function in rats exposed to WS_2 QDs was assessed by serum biochemistry analysis. Blood was collected on 3rd, 14th and 21st day post exposure of WS_2 QDs from all the experimental animals before euthanization. A statistically significant increase in ALT and ALP level was found in the 3rd day treatment group. Similarly, significant increase in ALT and AST level was found in 7th day treatment group. After 14 days all the biochemical parameters came down to normal level similar to that of control group (**Table 4.7**).

Group	**Protein (g/dl)**	**Albumin (g/dl)**	**ALT (IU/L)**	**AST (IU/L)**	**ALP (IU/L)**
Control	9.03 ± 1.76	3.46 ± 0.45	65.6 ± 6.5	142.8 ± 21.4	151.6 ± 72.6
3rd day	9.1 ± 2.76	3.6 ± 0.35	96.06±8.6 *	143± 12.9	407± 101.8**
7th day	10.3 ± 0.65	4.6 ± 0.2	100.4±13	296± 124.8*	190 ± 93.3
14th day	10.35± 0.07	4.25 ± 0.07	78.2 ± 18.5	137.6 ± 26.2	215 ± 73.14

Table 4.7: Liver function test in rat exposed to WS_2 QDs, n=3. The data represent mean±SD. Asterisk above values denotes statistically significant difference, compared with the control group (*$p<0.05$, **$p<0.01$)

4.6.6.2 Kidney function tests

Kidney function tests of rats exposed to WS_2 QDs intraperitoneally was assessed by serum creatinine estimation and direct urine analysis.

4.6.6.3 Serum creatinine estimation

Serum creatinine level estimation after WS_2 QDs administration in Sprague Dawley rats was analyzed. Results suggested that no significant changes in serum creatinine level was observed in any of the treatment groups and were comparable with that of the control group (**Table 4.8**).

Group	**Serum creatinine level (mg/dl)**
Control	0.91 ± 0.10
3^{rd} day	0.97 ± 0.09
7^{th} day	1.07 ± 0.05
14^{th} day	0.93 ± 0.04

Table 4.8: Serum creatinine level analysis after intraperitoneal administration of WS_2 QDs in rats, n=3. The data represent mean ± SD

4.6.7 Other biochemical parameters

Other general biochemical parameters such as glucose, cholesterol and triglyceride level in blood of WS_2 QDs administered rats were analyzed. Results were summarized in **Table 4.9**. A significant increase was observed in glucose level of 3^{rd} day treatment group, which was found to be normal in 7^{th} and 14^{th} day groups. A significant increase in triglycerides level was noticed in the 7^{th} and 14^{th} day treatment groups. Cholesterol level was found to be normal in all the treatment groups and was comparable with that of control group.

Group	Glucose (mg/dl)	Cholesterol (mg/dl)	Triglycerides (mg/dl)
Control	64.06 ± 8.53	46 ± 11.9	76 ± 6.08
3rd day	179.7 ± 14.5**	49 ± 17.57	66.6 ± 11.3
7th day	115.8 ± 55.5	58.3 ± 4.6	149 ± 45.08*
14th day	80.7 ± 6.9	61 ± 22.6	144.5 ± 81.3*

Table 4.9: General biochemical parameters such as glucose, cholesterol and triglyceride level post intraperitoneal administration of WS_2 QDs, n=3. The data represent mean ± SD. Asterisk above values denotes statistically significant difference, compared with the control group (*p<0.05 and **p<0.01)

4.6.8 Urine analysis

Urine was collected on 3rd day, 7th day and 14th day post intraperitoneal administration of WS_2 QDs. The results were summarized in **Table 4.10.** Urine analysis report suggests that leukocyte, nitrite, urobilinogen, ketone bodies and glucose content were normal and comparable with that of control groups. pH and specific gravity of urine was found to be comparable with that of control groups. No further treatment related anomalies were observed in the kidney.

Parameters	**Control**	**3rd day**	**7th day**	**14th day**
Leukocyte	Negative	Negative	Negative	Negative
Nitrite	Positive	Positive	Positive	Positive
Urobilinogen (mg/dl)	0.1 (N)	0.1 (N)	0.1 (N)	0.1 (N)
pH	6.0	6.0	6.0	7
Blood	Negative	Negative	Negative	Negative
Specific gravity	1.025	1.020	1.025	1.025
Ketones (mg/dl)	160	160	160	160
Bilirubin (mg/dl)	Moderate	Small	Moderate	Small
Glucose (mg/dl)	100	100	100	100

Table 4.10: Urine analysis of rats administered with WS_2 QDs.

4.6.9 Biodistribution: Inductively Coupled Plasma Mass Spectroscopy (ICP-MS)

Major organs collected from the treated animals and control were subjected to ICP-MS analysis to detect the biodistribution status of the material after i.p administration of the compound. **Figure 4.43** suggested that a comparatively high amount of the material was retained in kidney (239±31.5 ppb) after 7 days observation period. All the other organs such as liver (70.6±20 ppb), brain (95.6±13.5 ppb) and blood (32±3.5 ppb) evidenced the presence of the material more on the 7th day. From the results, it was evident that 7th day showed the maximum biodistribution of the material and afterwards by 14 days came back to comparable level to that of control.

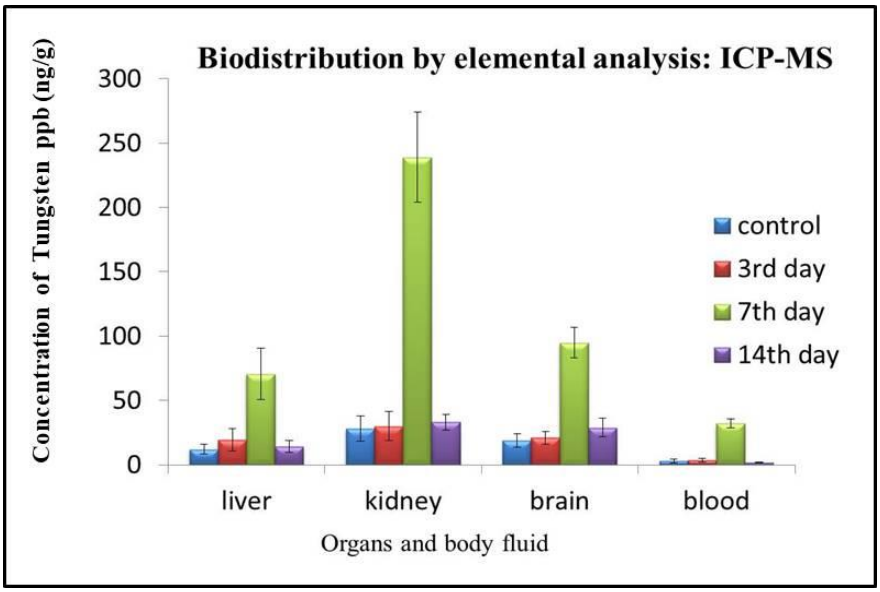

Figure 4.43: Biodistribution analysis by ICP-MS showing concentration of tungsten in major organs such as liver, kidney, brain and blood of control, 3rd day, 7th day and 14th day treatment groups. N=3, Data represents mean ± SD

Urine and feces collected from both the control and treatment group animals were subjected to ICP-MS analysis to elucidate the excretion route. **Figure 4.44** suggested that the major excretion route of the compound is via renal excretion as a major amount of the element tungsten was detected in urine than feces. Both 3rd day (14.5±2.6 ppb) and 7th day (45±4.5 ppb) urine observed a higher content when compared to 14th day (8.6±2.3 ppb). This suggested that trace amout of tungsten noticed within the animals after 14 days period. The amount of the administered material detected in feces of the treatment groups (3rd day: 4±0.4 ppb, 7th day: 4.1±1.3 ppb, 14th day: 5±2.1 ppb). These findings along with high material detection in kidney strengthened the possibility of renal excretion of the compound.

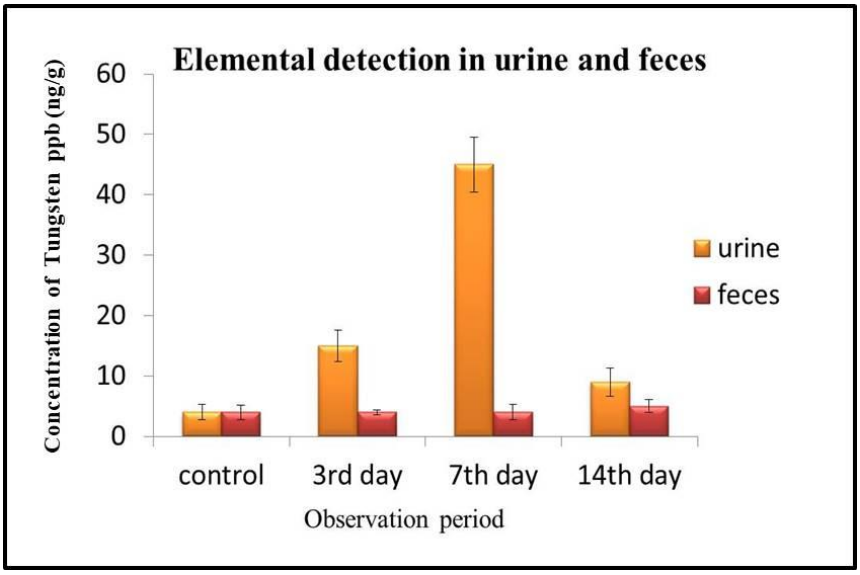

Figure 4.44: ICP-MS analysis for the detection of the compound in urine and feces. N=3. Data represents mean±SD.

4.6.10 Histopathology

Histopathology of vital organs such as liver, kidney, brain and spleen of 3rd day, 7th day and 14th day treated animal samples were compared with that of the control animal organs (**Figure 4.45**). No noticeable tissue lesions were observed. 3rd day liver tissues showed slight inflammation and was observed to be normal in the 7th and 14th days liver tissues. Vacuolated hepatocytes were visible in the 14th day liver tissue. Kidney histology showed prominent damages in the 3rd day group. Degenerated renal tubules were observed in the 3rd day kidney but prominent tissue regeneration was evidenced in the 7th and 14th day treated groups. Slight haemorrhage fractions were visible in the 7th and 14th day kidney tissue. Healthy Bowman's capsule was noticed in the tissue sections and the epithelial lining covering the Bowman's capsule seemed intact.

Brain histology showed normal brain morphology in all the treatment groups and were comparable with that of the control. No neuronal swelling, vacuolation or tissue degeneration was observed. Active glial cells and neurons were visible. No lesions or macrophage infiltrations were observed in the spleen of the treated group rats. Tissue sections showed normal white pulp (active matured RBCs) and white pulp (lymphoid tissues).

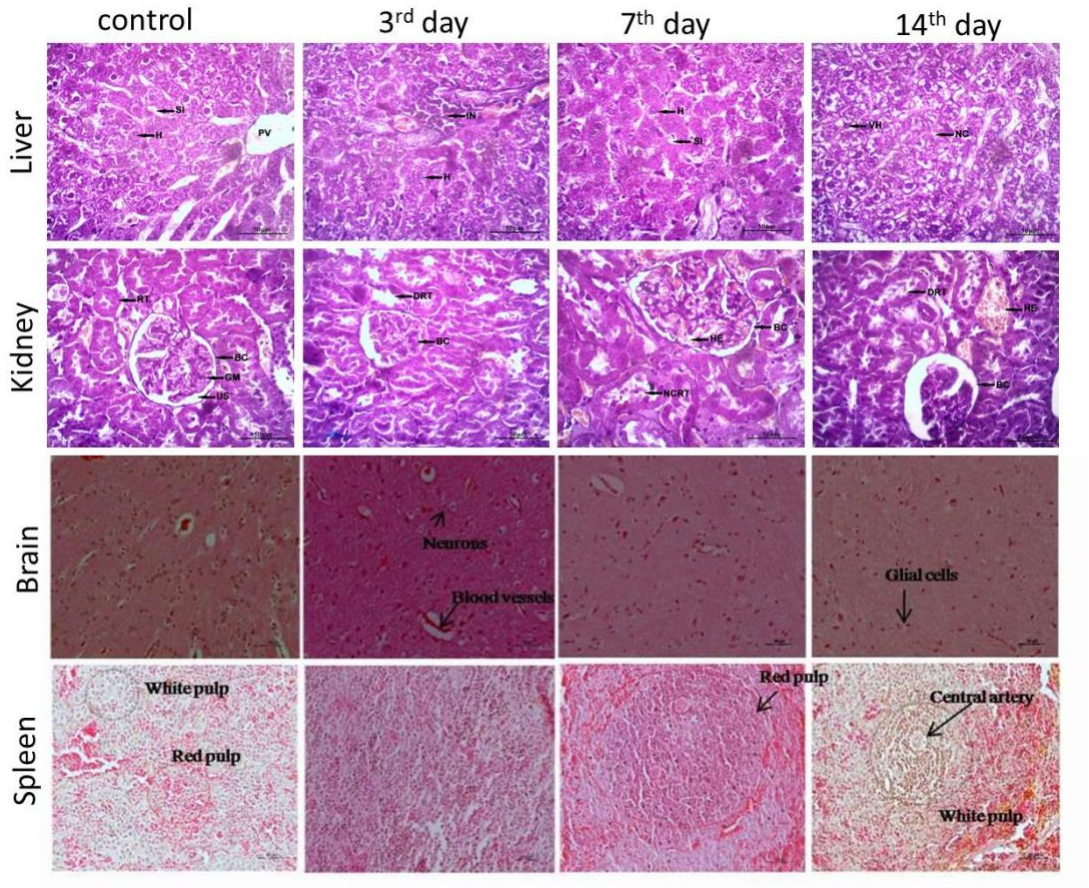

Figure 4.45: Histological observations of liver, kidney, brain and spleen tissues of control, 3rd day, 7th day and 14th day treatment groups. Magnification; 40x and scalebar represent 50µm. Representations in the images (H- Hepatocytes, HE- Haemorrhage, NC- Necrotic Cell, SI- Sinusoids, US- Urinary Space, G- Glomerulus, BC-Bowman's Capsule, RT- Renal Tubules, DRT- Degenerated Renal Tubule, PV-Portal Vein, NCRT- Necrotic RT, IN- Inflammation, VH- Vacuolated Hepatocytes).

4.6.11 Antioxidant Assays

Brain and liver tissues were collected from all the experimental animals and analyzed for antioxidant status in 10% tissue homogenate. Various antioxidant assays such as lipid peroxidation, reduced glutathione (GSH), glutathione reductase (GR), glutathione peroxidase (GPx) and superoxide dismutase (SOD) activities were analyzed in the 10% tissue homogenate. Total protein estimation was done using Folin's reagent assay.

4.6.11.1 Total protein estimation

Total protein content in brain and liver tissue homogenate was analyzed using Lowry's method. BSA standard was used to calculate protein concentration of the test samples. From **Figure 4.46**, it was evident that no significant changes were observed in the total protein content of the test animals with respect to control. Total protein content in all the test group liver homogenates was comparable with that of the control group liver homogenates. Similarly, the total protein content in brain tissue homogenates of the entire test animals was comparable with that of the control group brain tissue homogenates. No significant changes were observed in any of the treated groups with respect to control.

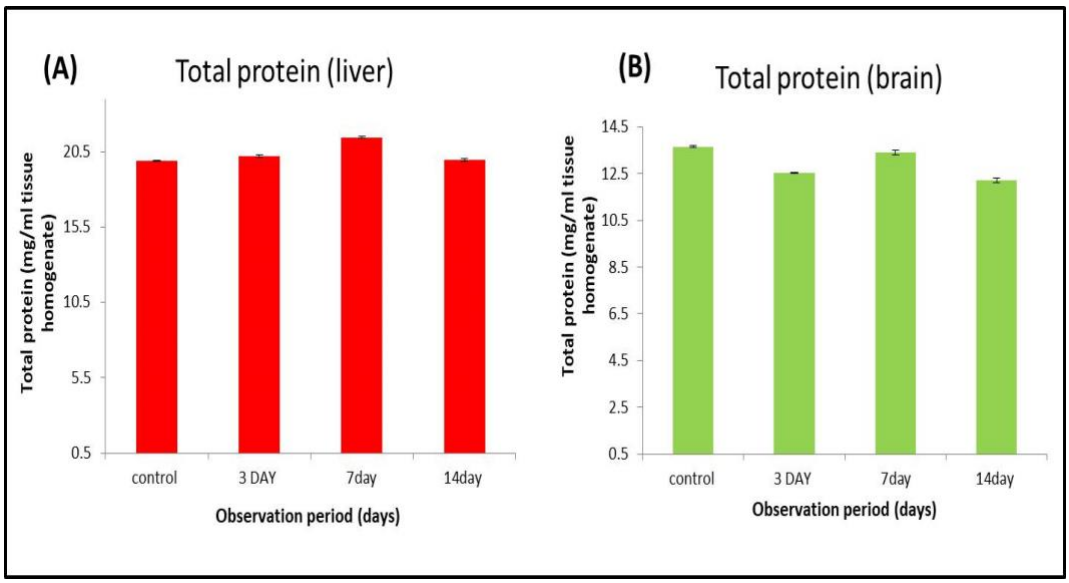

Figure 4.46: Total protein content in liver (A) and brain (B) tissue homogenates of experimental animals. n=3, the data represent mean ± SD

4.6.11.2 Antioxidant assays in liver

Liver was isolated from both control and treatment group animals and subjected to various antioxidant assays such as LPO, GSH, GR, GPx and SOD in 10% liver tissue homogenate **(Figure 4.47**).

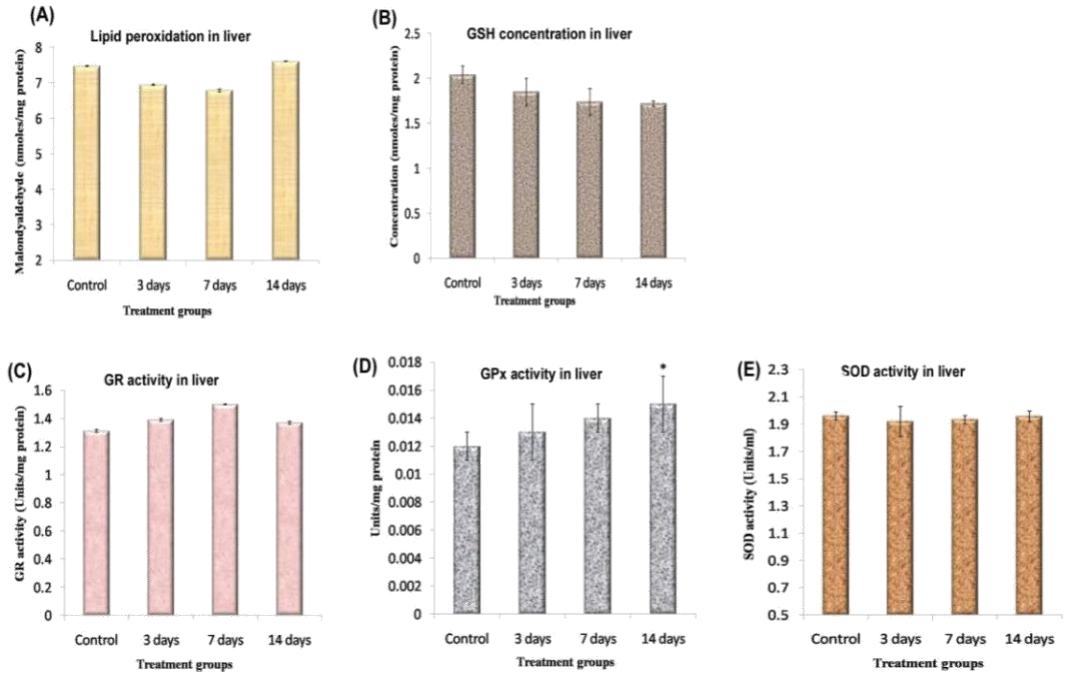

Figure 4.47: Various antioxidant status such as (A) lipid peroxidation, (B) GSH, (C) GR, (D) GPx and (E) SOD activity in 10% liver tissue homogenates of control and treatment groups. n=3, the data represent mean ± SD. Asterisk denotes statistically significant difference with control (*p< 0.05)

4.6.11.2.1 Lipid peroxidation (LPO)

Lipid peroxidation status was analyzed by evaluating the malondialdehyde production in the liver tissue homogenate of both control and treatment group animals. No statistically significant alteration in the level of malondialdehyde production was observed in the treatment groups (3rd day: 6.95±0.004, 7th day: 6.79±0.002 and 14th day: 7.61±0.003) with that of the control untreated group (8.48±0.01).

Even then, a slight increase in LPO status was found in the control group but was not significant. Results were expressed in nmoles/mg protein (**Figure 4.47, A)**.

4.6.11.2.2 Reduced Glutathione (GSH)

Reduced glutathione (GSH) level was analyzed in the liver tissue homogenate of both control and WS_2 QDs administered rats. No statistically significant increase in the level of GSH content was observed in any of the treated groups (3^{rd} day: 1.85±0.15, 7^{th} day: 1.74±0.15 and 14^{th} day: 1.72±0.03) when compared with that of the control group (2.04±0.10). GSH content was observed to be slightly low in all the treated group liver samples when compared to the control group but was not a significant difference (**Figure 4.47, B)**. Results were expressed in nmoles/mg protein.

4.6.11.2.3 Glutathione Reductase (GR)

No statistically significant alteration in GR level was observed in any of the treated group animals (3^{rd} day: 1.39±0.01, 7^{th} day: 1.50±0.01 and 14^{th} day: 1.37±0.002). The values were comparable with that of the control group animals (1.31±0.01). A slight hike in GR activity was observed in the 7^{th} day group but was not statistically significant (**Figure 4.47, C)**. Results were expressed in Units/mg protein.

4.6.11.2.4 Glutathione Peroxidase (GPx)

No statistically significant alteration in GPx activity was observed in any of the treated groups (3^{rd} day: 0.013±0.002, 7^{th} day: 0.014±0.003 and 14^{th} day: 0.017±0.002). The results were highly comparable with that of the control group (0.012±0.001). Results were expressed in Units/mg protein (**Figure 4.47, D)**.

4.6.11.2.5 Superoxide dismutase (SOD)

SOD activity was analyzed in the liver tissue homogenate of both control and treated group animals. No statistically significant alteration was observed in the treated groups (3^{rd} day: 1.92±0.11, 7^{th} day: 1.93±0.03 and 14^{th} day: 1.95±0.04) when compared with that of the control group (1.96±0.03). Results were expressed in Units/ml tissue homogenate (**Figure 4.47, E)**.

4.6.11.3 Antioxidant assays in brain

Brain was isolated from both control and treated group animals and was subjected to various antioxidant assays such as LPO, GSH, GR, GPx and SOD in 10% brain tissue homogenate (**Figure 4.48**).

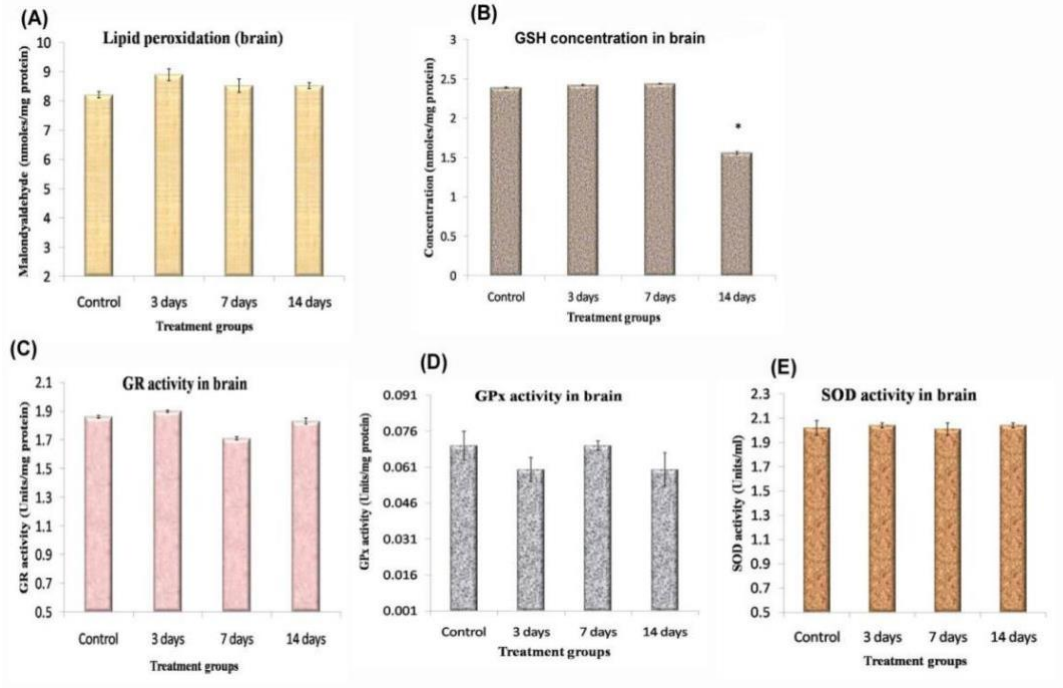

Figure 4.48: Antioxidant status in brain tissue homogenate of rats exposed to WS_2 QDs. (A) Lipid peroxidation, (B) GSH concentration, (C) GR activity, (D) GPx activity and (E) SOD activity in brain. . n=3, the data represent mean ± SD. Asterisk above values denotes statistically significant difference, compared with the control group (*$p<0.05$)

4.6.11.3.1 Lipid peroxidation (LPO)

No statistically significant alteration in malondialdehyde production was found in any of the treatment groups (**Figure 4.48, A)**. LPO status of brain tissue homogenate of both control (8.21±0.001) and treated group animals (3rd day: 8.98±0.002, 7th day: 8.53±0.003 and 14th day: 8.52±0.001) were similar. Results were expressed in nmoles/mg protein.

4.6.11.3.2 Reduced Glutathione (GSH)

GSH level in the brain tissue homogenate of both treated (3rd day: 2.42±0.01, 7th

day: 2.44±0.005 and 14th day: 1.56±0.02) and control groups (2.39±0.01) were analyzed. A slight statistically significant decrease in GSH content was observed in 14th day group (**Figure 4.48, B)**. No statistically significant alteration in the GSH content was observed in any other treated groups. Results were expressed in nmoles/mg protein.

4.6.11.3.3 Glutathione reductase (GR)

No statistically significant changes in the GR activity were observed in the WS_2 QDs administered groups (3rd day: 1.98±0.01, 7th day: 1.71±0.008 and 14th day: 1.83±0.01) with that of the control group (1.86±0.02). A very slight increase in GPx activity was observed in the 3rd day group animals but was not statistically significant (**Figure 4.48, C)**. Results were expressed in Units/mg protein.

4.6.11.3.4 Glutathione peroxidase (GPx)

GPx activity was analyzed in the brain tissue homogenate of both control and treated group animals (**Figure 4.48, D)**. No significant change was observed in the treatment groups (3rd day: 0.053±0.009, 7th day: 0.079±0.02 and 14th day: 0.061±0.009) with that of control group (0.072±0.01). Results were expressed in Units/mg protein.

4.6.11.3.5 Superoxide dismutase (SOD)

SOD activity was analyzed in the brain tissue homogenate of both control and treated groups (**Figure 4.48, E)**. No statistically significant alteration was observed in the treatment groups (3rd day: 2.04±0.02, 7th day: 2.01±0.05 and 14th day: 2.04±0.02) when compared with that of the control group (2.02±.06). Results were expressed in Units/ml tissue homogenate.

4.6.12 Spleenocytes Proliferation Assay

Spleen was collected from the experimental animals, spleenocytes were isolated and cultured. Spleenocyte proliferation was analyzed using tritiated thymidine assay. Results indicate similar proliferative status in all the experimental animals and were comparable with that of the untreated control animals **(Figure 4.49)**.

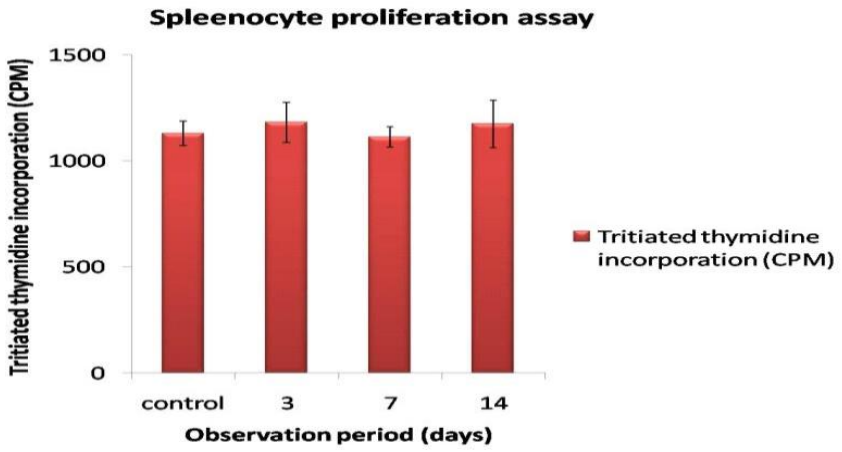

Figure 4.49: Spleenocyte proliferation assay in spleenocytes isolated from Sprague Dawley rats of 3 days, 7 days and 14 days of WS_2 QDs exposure. Control group represent untreated animals. n=3. Data represents mean±SD

4.6.13 Blood Kinetics

Toxicokinetics in blood samples collected at regular intervals was analyzed by ICP-MS to detect the presence of the administered compound in the blood of the experimental animals upto 14 days. Blood was collected at 1h, 3h, 6h, 24h, 3days, 7 days and 14 days and subjected to ICP-MS analysis. **Figure 4.50** showed that the blood collected immediately after 1h of i.p administration showed maximum retention of the compound. Gradually with the increase in time, detection of the compound in blood slows down, which suggested the possibility of further distribution of the administered compound to major organs like liver, kidney *etc*., and further excretion possibility of the compound. After 14 days observation period, much less than 1% of the administered compound was found to be retained in the blood of the experimental animals.

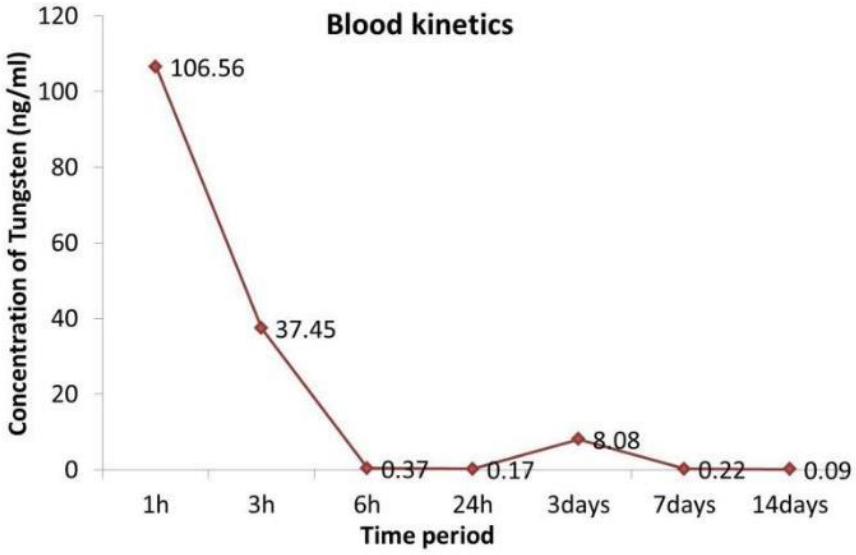

Figure 4.50: ICP-MS analysis to detect the retention possibility of the compound in blood for extended time period upto 14 days

CHAPTER 5: DISCUSSION

5. DISCUSSION

5.1 Synthesis and characterisation of WS_2 QDs

The discovery of graphene and its analogs has become a great sensation that has dominated various scientific disciplines for the search of other 2D layered materials, which possess profound characteristics that can surpass the defective side of graphene. Due to this upcoming surge, various new 2D materials such as transition metal dichalcogenides (TMDCs), transition metal dioxides (TMDOs), clay materials, graphitic carbon nitrile, and ultrathin black phosphorus came into forefront research disciplines. Tungsten disulphide (WS_2) is an attractive candidate that belongs to TMDC family of compounds has got recent scientific attention owing to its appealing intrinsic characteristics. Among the various nano dimensionalities of this material, QD morphology has got appreciable attention due to its profound characteristics such as quantum confinement effect and stable bright fluorescence emission, which can be applied for various biomedical applications.

WS_2 QDs are synthesized easily and efficiently by solvent-assisted exfoliation, mechanical exfoliation, chemical vapor deposition, hot injection, ultrasonic cavitation, lithium intercalation, microwave-assisted methods and so on. In the present study, sonication mediated solvothermal exfoliation using NMP solvent was followed for the synthesis of WS_2 QDs from bulk WS_2 crystals, which yielded highly monodispersed QDs of 3-4nm size and spherical morphology. The synthesized QDs emit strong and stable cyan green fluorescence under UV illumination at 370nm.

The synthesized QDs were subjected to various sophisticated characterization techniques to confirm its physico-chemical characteristics. One important factor that influences nanomaterial toxicity is its various physico-chemical characteristics, therefore it is highly imperative to effectively characterize the material before moving on to biological studies (Li *et al.* 2015).

The synthesized WS_2 QDs were characterized for its size, morphology, surface charge, surface chemistry, chemical composition, exfoliation efficiency, fluorescence emission and stability. The absorbance spectra of the QDs were observed to be peaked at 370nm. Keeping 370nm as the excitation wavelength, the emission wavelength was observed at 450-500nm which corresponds to cyan green fluorescence. This correlates well with the size of the QDs (3-4nm) observed via HR-TEM analysis.

XRD analysis showed that the characteristic broadening of peaks and reduction in peak intensity while thinning down to quantum confinement level was strictly attributed to the QD morphology. When compared to bulk material, most of the characteristic peaks of bulk material got disappeared after exfoliation into WS_2 QDs. Even then, 2 significant peaks at 2θ =19.8 and 28.9 that correspond to the diffraction peaks at (002) and (101) lattice planes of WS_2 were conserved to confirm the material integrity after exfoliation (Yan *et al.* 2020). The XRD report was extremely comparable with that reported by Stengl *et al.*,(2015), in which a solvent mediated exfoliation strategy of WS_2 QDs from bulk WS_2 was exploited. After exfoliation into WS_2 QDs, the XRD pattern showed a broad hump without any diffraction peaks as observed in bulk powder. This strictly confirmed that while thinning down to QD

dimensionality the highly crystalline bulk powder became amorphous QDs. Broadening of diffraction peaks and subsequent disappearance of the respective peaks corresponds to the presence of extreme low dimension nanomaterials like QDs.

The size and morphological features were confirmed using High Resolution Transmission Electron Microscopy (HR-TEM). The size distribution pattern was observed to be in the range of 3-4nm with uniform spherical morphology. A highly monodispersed pattern was observed in the TEM grid where particles were eventually distributed with uniform size and morphology. No agglomeration tendency was observed for the synthesized WS_2 QDs. Under high magnification at 2nm zooming, the distinctive lattice fringes were observed showing d-spaces as 0.24nm, which corresponds to the (101) crystalline face of WS_2. This was in comparison with the HR TEM images of WS_2 QDs reported by Shengjie Zu *et al.*,(2015). Moreover, the SAED pattern confirmed the diffraction data obtained from XRD in which, after exfoliation the highly crystalline bulk powder became amorphous QDs showing characteristic diffused ring SAED pattern. The presence of diffused rings instead of spotlights in the SAED confirmed the amorphous nature of the synthesised QDs (Czigány and Hultman. 2010).

FTIR spectroscopy was carried out to evaluate the changes in the intact chemical composition of WS_2 while thinning down to quantum confinement levels. From the results, it was evident that WS_2 QDs maintained the intact chemical composition similar to that of bulk WS_2 crystals even after vigorous exfoliation and high-

temperature treatments. The characteristic peak at 464cm^{-1} in bulk material is due to W-S vibrations. Peaks at ~887cm^{-1} in bulk material and ~923cm^{-1} in QDs correspond to S-S vibrations and the bands positioned at ~542cm^{-1} in QDs and ~597cm^{-1} in bulk material are related to W-S vibrations (Hazarika SJ and Mohanta.
2017). Characteristic peaks at 1261cm^{-1} (C-N stretching) and 2914cm^{-1} (CH_2 asymmetric stretching) were probably due to the attachment of NMP residues over the WS_2 QDs surface (Xu *et al.* 2019). Peaks at 1403cm^{-1} and 1618cm^{-1} shows stretching deformations of hydroxyl group. A typical peak observed at 2960cm^{-1} confirmed the presence of hydroxyl groups over the WS_2 QDs surface (Vattikuti *et al.* 2016). Moreover, the presence of hydroxyl and carboxyl groups over the QD surface was deemed to be responsible for the high water dispersibility and stability of the synthesized WS_2 QDs. These peaks were not observed in bulk material as the bulk WS_2 is not water dispersible.

XPS spectrum was used to confirm the surface elemental composition and chemical state of WS_2 QDs. It was observed from the XPS data that, the S/W ratio for the WS_2 QDs was 1.75, nearly stoichiometric to the intact atomic ratio of WS_2 QDs (Yin *et al.* 2019). The characteristic bands 31.2eV and 33.2eV that corresponds to $4f_{7/2}$ and $4f_{5/2}$ represents $^{+}4$ oxidation state of tungsten. Similarly, the 160.2eV and 161.8eV bands correspond to $^{-}2$ oxidation state of sulphur. The results were well comparable with the literature reported by Huang *et al.*,(2016).

Thermogravimetric analysis showed that the QDs retained high stability upto 450^{0}C temperature rise. With an increase in temperature upto 700^{0}C, 8-10% material

degradation was evidenced, which corresponds to surface solvent degradation. Another possibility is via disulphide decomposition into sulphur with subsequent oxidation of sulphur followed by sulphur oxide loss. DTA analysis results showed that the net reaction favors an endothermic reaction with an observed melting temperature of 466.65^0C.

Surface charge is a crucial factor that affects the toxicity of any material. Therefore the net surface charge of the synthesized WS_2 QDs was analyzed by zeta potential analysis. Zeta potential value (-25mV) suggested a net negative surface charge for the synthesized QDs. Cationic QDs shows the tendency to form adduct with DNA grooves, whereas anionic QDs will tend to repel from the DNA; thereby avoid DNA adduct formation. The synthesized WS_2 QDs were found to possess an anionic surface charge. Therefore it can be inferred that the QDs will tend to avoid binding to negatively charged biomolecules, prevents platelet aggregation and hemolysis (Bhandavat *et al.*, 2012). The dried WS_2 QDs were subjected to fluorescent microscopic observation and observed bright fluorescence under green emission filter. The synthesized QDs were highly stable upto 100 days under normal room temperature.

5.2 Stability analysis of WS_2 QDs

Stability of the synthesized WS_2 QDs was analyzed by UV/Visible spectroscopy and fluorescence emission spectroscopy by keeping WS_2 QDs dispersed in water for about 100 days at room temperature. Readings were procured at 20 days interval. The results confirmed the extremely high stability of the QDs for 100 days at room temperature.

5.3 Endotoxin detection

Endotoxin content was assessed using Charles River Endosafe PTS Kit and the results showed that the endotoxin level was well below the United States Pharmacopia recommended levels of ≤ 0.5 EU/ml.

Various physico-chemical characterization datas suggested that, the synthesized WS_2 QDs possess excellent monodispersive nature with uniform size distribution pattern and spherical morphology. The QDs possess excellent water dispersibility and stability. The QDs emit strong cyan green fluorescence and was stable upto 100 days retaining its intact chemical composition and surface chemistry. Therefore further *in vitro* cytotoxicity analysis followed by *in vivo* acute toxicity studies were done using the synthesized WS_2 QDs. For the *in vitro* studies, a stock concentration of 2mg/ml and subsequent diluted standards of varying concentrations (10, 20, 40, 80, 160, 320 and 640µg/ml) were used. For the *in vivo* studies, 10mg/kg body weight WS_2 QDs were administered intraperitoneally in Sprague Dawley rats.

5.4 *In vitro cytotoxicity and nano-bio interaction studies*

For the *in vitro* cytotoxicity and bio-nano interaction studies, LN-229 glioblastoma cells were used, which was procured from NCCS Pune. It has a doubling time of 24h and maintained at 5% CO_2 and 37^0 C temperature.

5.4.1 Particle uptake by flow cytometry

Flow cytometry is a reliable, robust and high throughput method to detect and quantify NP uptake in cells. European Research Infrastructure Quality Nano has developed certain standard procedures for this and an easy reliable method is by analysing the SSC/FSC changes (Salvati *et al.* 2018). Cellular uptake of WS_2 QDs was confirmed by flow cytometry. The results confirmed that the synthesised WS_2 QDs were effectively uptaken by LN-229 cells, which attributed a shift in SSC while conserving FSC intact. This shift in SSC indicates increase in cell granularity due to WS_2 QDs uptake by cells. FSC did not show any change which is a suggestive of conserving intact morphology of cells even after QD uptake.

5.4.2 QD uptake and intracellular localisation

WS_2 QDs uptake and intracellular localisation of the QDs was confirmed by fluorescent microscopy by counterstaining actin filaments and nucleus by Rhodamine-phalloidin and DAPI dyes respectively. The synthesised QDs emitted bright cyan green fluorescence that account for the sensitivity of this platform for uptake confirmation. Fluorescent microscopic observation confirmed that the synthesised QDs were localised inside the cytoplasm around the nucleus.

5.4.3 Dose response by MTT assay

MTT assay is a colorimetric assay used for the detection of the overall cellular metabolic activity by assessing the mitochondrial integrity. Here, at a stock

concentration of 2mg/ml, with varying concentrations, a dose dependent increase in cytotoxicity was observed only after 160µg/ml concentration for both 24h and 48h. For 10, 20, 40, 80 and 160µg/ml concentrations, LN-229 cells showed metabolic activity similar to the negative control cells. Various studies have reported the toxicity of different nanodimensions of WS_2. Extremely low cytotoxic response of WS_2 nanotubes in human bronchial epithelial cells was reported by Pardo *et al*., (2014). Similarly, the biocompatibility of WS_2 inorganic nanotubes and fullerene like WS_2 particles was reported by Goldman *et al.,* (2015) in which the rate of proliferation and cell viability was reported to be not affected by the particles at any of the selected concentrations (upto 100µg/ml) in salivary gland cells. The cytotoxic response of WS_2 QDs in HeLa and HepG2 cells was reported by Yong *et al.*, (2015). The reports clearly indicate that at any of the selected concentrations (upto 200µg/ml), the cells showed no significant cytotoxic response. A similar family compound MoS_2 QDs were analyzed to screen the sensitivity towards endothelial cell lines such as HUVEC and HCAEC by MTT assay and the results reported that the cells were able to tolerate MoS_2 QDs upto 100µg/ml (Ke *et al.* 2018). In the present study, a more appreciable trend in cytotoxicity was observed by WS_2 QDs in LN-229 glioblastoma cells upto 160µg/ml concentration from 2mg/ml stock. Certain nanoparticles were reported to interfere with the MTT reagent giving imprecise results (Liang *et al*. 2015). Hence in the present study it was counter checked and concluded that no such responses were evidenced and concluded that WS_2 QDs are not interfering with the MTT reagent at any of the selected concentrations.

5.4.4 QD dissolution and cytotoxicity

Quantum dots being highly potential candidates for biomedical applications often tend to stay back from the main stream due to certain perceptions related to their toxicity. The major among the factors include QD dissociation and related toxicity (Gidwani *et al*. 2021). This hindrance was mainly faced by Cadmium containing QDs such as CdS, CdSe *etc.,*. This is because; the dissociated Cd^{2+} ions are potentially more toxic than the parent compound and may lead to ROS generation (Tsoi *et al.* 2013). Here, WS_2 could probably dissociate into W^{4+} ions; but under normal circumstances this will not happen because WS_2 bond is chemically well strong enough to withstand such dissociation. TGA reports also suggest the highest level of stability of this typical compound. Yet then, the possibility of WS_2 QDs dissociation was analyzed and compared for the cytotoxic response. The results showed no evident QD dissociation related toxic responses when compared to direct QD exposed cells.

5.4.5 Neutral red uptake assay

Lysosomal integrity with the binding of neutral red dye is a sensible indicator of cell viability as a function of lysosomal membrane integrity. Depending on the extend of lysosomal integrity, the cells will take up this supravital dye that contains a weak positive charge (Shah *et al*. 2020). At acidic pH (intact lysosomes) the neutral red dye will emit red color, which was then quantitatively and qualitatively analyzed. Here, more than 80% cells were functionally active and viable upto 160µg/ml

WS_2 QDs exposure. This data was well comparable with the MTT reports suggesting that WS_2 QDs will not alter both mitochondrial and lysosomal activity, which are considered as the vital sub cellular organelles that controls cellular metabolic activities.

5.4.6 LDH Assay

LDH assay is a quantitative assay for the estimation of cell viability. LDH is a stable cytoplasmic enzyme. Once a toxic response occur associated with plasma membrane damage, which is a characteristic mechanism of apoptosis/ necrosis mediated cell death, this LDH enzyme will get released into the medium supernatant. Subsequently lactate and NAD^+ will react to release pyruvate and NADH. This NADH is further quantified by measuring the absorbance spectrophotometrically and is directly proportional to the LDH release and cytotoxicity (Kumar *et al.* 2018). Here, only a slight increase in NADH release was noticed in 24h WS_2 QDs exposed cells. But for 48h exposure, a significant dose dependant NADH release was observed.

5.4.7 Cellular morphology analysis by phase-contrast microscopy

Morphology of LN-229 cells after WS_2 QDs exposure was analysed by phase contrast microscopy. The results showed that, for 24h exposure, at the highest concentration of 640µg/ml, the cells showed cellular phenotypic changes like wrinkled morphology with cell shrinkage. After 48h incubation with WS_2 QDs, these morphological changes started observing from 320µg/ml onwards. More than 60% of the cells were found to be round and dead at 640µg/ml concentration.

5.4.8 Live/ dead assay

Live/ dead cell population was analysed using Calcein AM/ PI FACS analysis (Bratosin *et al.* 2005). Calcein will be selectively uptaken by live cells only; whereas PI will penetrate those cells with highly challenged membrane permeability. The results confirmed that, a concentration dependant increase in dead cell population was observed from 320µg/ml concentration onwards. Rest of the concentrations were similar to that of the untreated negative control cells. Even then, more than 80% of the cells were found to be viable upto 320µg/ml concentration. With a stock concentration of 2mg/ml, it is not surprising that a significant level of toxicity is elicited at 640µg/ml concentration as almost all the NPs elicit a highly toxic response at this particular concentration due to possible mechanical and oxidative stress imposed by the NPs on delicate cells.

5.4.9 ROS generation studies

ROS generation mainly contributes to the cytotoxic potential of NPs. Hydroxyl, peroxyl and reactive nitrogen species are the major contributors of ROS. ROS generation after WS_2 QDs exposure was analysed by DCFH-DA and Griess reagent assays for hydroxyl and RNS radicals respectively. The results indicated that hydroxyl/ peroxyl and RNS mediated ROS responses were evident from 320µg/ml concentration onwards. But rest of the lower concentrations showed a response similar to the untreated negative control cells. This confirmed that, only at the highest intolerable concentrations, cells showed a more ROS response which is comparable with any other NP exposure in live cells. Most of the reported QDs so far elicited a

higher level of ROS generation at concentrations even well below 100µg/ml (Chen *et al*. 2018). To further confirm whether this reduced ROS generation is due to the inherent catalase activity of the glioma cells, the ROS scavenging tendency of LN-229 cells was analysed using catalase inhibitor NaN_3. The results showed that no profound inherent ROS scavenging property was elicited by LN-229 cells and the depth of ROS generation was typically contributed by the WS_2 QDs only. Therefore, the aforementioned hypothesis of catalase mediated ROS scavenging efficacy was counterchecked and confirmed.

5.4.10 CBB staining for morphology analysis

CBB staining was used to analyse the morphological changes and cytoskeletal integrity in cells exposed to WS_2 QDs for both 24h and 48h exposure. The results clearly indicate that no significant morphological anomalies were observed in the cells exposed to selected concentrations of WS_2 QDs for 24h. But at the same time, after 48h WS_2 QDs exposure, significant morphological changes were observed in cells exposed to the highest concentration (320µg/ml). Subsequently a significant reduction in cell number was also observed for the same.

5.4.11 Lysosomal integrity by acridine orange staining

Lysosomal integrity was analysed by acridine orange staining. Both qualitative and quantitative analysis reports suggests that the lysosomes were intact and active in all the treatment group cells and were comparable with that of the untreated negative control. Only a very slight reduction in red fluorescence was observed at the highest

concentration (320µg/ml). In a study to evaluate the photothermal therapeutic efficiency of a related compound; MoS_2 nanoflakes, varying concentrations of (20, 40, 60 and 80 µg/ml) PEGylated MoS_2 nanoflakes was incubated with 4T1 cells (Feng *et al.*2015). The results showed concomitant and reliable trend with that of the present study with no detectable destabilisation of lysosomal membrane integrity at any of the selected concentrations. A similar study using MoS_2 QDs (another TMDC family compound) reported that, upon exposure of MoS_2 QDs to endothelial cell lines such as HUVEC and HCAEC, acidic vesicles such as late endosomes and lysosomes were quantified. The results indicate that the cells maintained excellent lysosomal integrity upto 50µg/ml concentration (Ke *et al.* 2018). A more appreciable trend was observed with WS_2 QDs in the present study, in which LN-229 cells showed excellent lysosomal membrane integrity upto high concentration of 320µg/ml. This clearly suggests that the synthesised WS_2 QDs are highly biocompatible even at very high concentration in which most of the similar compounds shows a tendency of increased cytotoxicity.

5.4.12 Mitochondrial membrane potential by JC-1 probe

Mitochondria often referred to as the powerhouse of the cell, is the organelle that plays critical role in regulating major cellular biochemical events. One major mechanism that is tightly regulated by mitochondria is the apoptosis mediated cell death. Severe loss in mitochondrial membrane potential (MMP) attenuates the possibility of cytotoxic response in cells. The heterogeneity in the MMP of live cells can be understood by using lipophilic cationic JC-1 dye, which specifically stains

highly active mitochondria as red while counterstaining the cytoplasmic region as green (Sivandzade *et al.* 2019). The possible cytotoxic effect of WS_2 QDs was analysed by evaluating the loss of MMP in LN-229 cells using JC-1 staining. A significant reduction in MMP was found at the highest concentration (320µg/ml) exposed cells only, whereas rest of the cells were similar to that of the untreated control cells. A dose dependant reduction in MMP is a suggestive towards mitochondrial pathway mediated apoptosis. Depolarisation of MMP is an early marker of apoptosis, which occurs prior to chromatin condensation and nuclear damage. Such a depolarisation trend was evident only at the highest concentration whereas the rest of the concentrations were observed to be comparable to that of the untreated negative control.

5.4.13 Cytoskeletal integrity by Rhodamine-Phalloidin staining

The eukaryotic cytoskeleton mainly comprised of three major components, microtubules, intermediate filaments and actin filaments which co-ordinately act together to support the cellular cytoskeleton. Cells that follow an apoptosis mediated cell death pattern were reported to maintain intact cell cytoskeleton integrity until late apoptotic stage, whereas necrotic cells will end up with sudden loss of cytoskeletal integrity with the release of cytoplasmic contents (Konopleva *et al.* 1999). Chances are more likely to happen for *in vitro* cell culture systems in which; the apoptosis induction will eventually progress towards a secondary necrosis process which entails with the significant loss of cytoskeletal integrity. Another possibility of cytoskeletal rearrangements following NP exposure is via DNA Damage Response

(DDR) associated with the activation of certain factors such as RhoA and RhoA/ROCK (Rho associated protein kinase) which eventually paves to cytoskeletal rearrangements (Amano *et al.* 2010). In the present study, even at the highest selected concentration also, LN-229 cells exposed to WS_2 QDs maintained intact cytoskeletal integrity. This confirms another finding that the possible cell death followed by WS_2 QDs exposure at the highest selected concentrations was not possibly due to necrotic mechanism. In a study with similar material MoS_2, F-actin stained with Alexa Fluor® 568 conjugated phalloidin in 4T1 cells indicated that the

cells maintained excellent actin filament integrity upto 80µg/ml concentration after 24h exposure. The present study evidenced that even at a high concentration of 320µg/ml of WS_2 QDs exposure, LN-229 glioblastoma cells showed excellent actin filament stability.

5.4.14 Membrane integrity by EtBr: FACS

The structural integrity of eukaryotic organelle membrane is of prime importance while considering the metabolic fate of a cell. While considering the cell membrane integrity followed by NP exposure, both chemical composition of the material as well as the physical stress induced by the material can further prolong to rupture of cell membrane. Membrane integrity loss after QD exposure was analysed by EtBr staining FACS. A dose dependant increase in EtBr uptake was evidenced in all the selected concentrations but was not a noteworthy response because even a minute stress can evoke membrane damage to glioblastoma cells which will eventually lead to more EtBr uptake. Therefore, when compared with untreated negative control,

a much elicited QD exposure related membrane integrity loss was not evidenced at any of the selected concentrations.

5.4.15 Cell cycle analysis

During a cell cycle event there are certain checkpoints that help to regulate the cell cycle by temporarily arresting the cell, thereby allowing time for cellular repair mechanisms to take place. Any uneven events such as cellular damage or DNA fragmentation occurred will be accompanied by increased sub-G0/GI phase. A prominent cell cycle arrest was evidenced in the 'S' phase at this concentration that correlate with the apoptotic induction at this concentration. One recent study reported a more or less similar effect of TiO_2 NPs by arresting S phase in A549 cells promoting the cells to further undergo apoptosis (Kansara *et al.* 2015).

Usually, an arrest in the G0/G1 phase in cell cycle is accomplished by nutrient starvation. Such an arrest was neither visible at any of the selected concentrations. The amount of PI intensity is well correlated with the DNA content inside the cells. Since the amount of DNA doubles from G0/G1 (singlet DNA-n) to G2 (doublet DNA-2n) cell cycle phase transition, the PI fluorescence intensity will be doubled. All the concentrations maintained this diploid (2n) DNA content which indicates that DNA replication machinery was not affected at any of the selected concentrations (Khan *et al.* 2018).

Another study reported the impact of Silica NPs in inducing G2/M checkpoint arrest in HL-7702 liver cells, which is the DNA damage analysis checkpoint. Cells that have a defective G2/M phase will allow the cells to directly enter into mitotic phase before DNA repair and eventually leads to apoptosis (Yang *et al*. 2019). Such an event was not observed in any of the selected concentrations.

5.4.16 Apoptosis by Annexin V/PI FACS

Generally the mechanisms of cell death mediated by NP occur via apoptosis, necrosis or by the combination of both. To specify, silica NPs were reported to induce apoptosis in hepatocytes. Necrosis is typically an unregulated process that accompany with plasma membrane rupture mediated outburst of cellular components. On the other hand, apoptosis is a highly regulated process that involves various molecular signalling cascades operated with the aid of certain family of enzymes known as Caspases and associated factors. Certain changes such as blebbing, chromosome condensation, DNA fragmentation and cell shrinkage associated changes were characteristic to apoptosis mediated cell death. Outward flipping of phosphatidyl serine residues is a typical characteristic feature of apoptosis activation. In contrast to necrotic cells, apoptotic cells maintain intact cell membrane integrity until late apoptotic phase (Konopleva *et al.* 1999). Inorder to ascertain the mechanism of cell death mediated by WS_2 QDs, Annexin V/PI mediated apoptosis analysis was done, in which Annexin V complex shows a strong Ca^{2+} dependant affinity towards this phosphatidyl serine residues when it is in the outside leaflet of

plasma membrane. LN-229 cells were exposed to varying concentrations of WS_2 QDs and evaluated for the possibility of apoptosis pathway activation. Annexin/PI flow cytometry was done to evaluate the possible apoptosis mediated cell death. Cells exposed to higher concentrations of WS_2 QDs (160µg/ml and 320µg/ml concentrations) showed a more apoptosis mediated cell death pattern. A dose dependant increase in Annexin V positive cells was evidenced, which concluded that the cell death mechanism mediated by WS_2 QDs is mainly apoptosis mediated and not necrosis. A more dead cell population evidenced at the highest selected concentration of 320µg/ml is due to the mechanical stress induced by more QD uptake by the cells. But the extend of apoptosis mediated by WS_2 QDs is highly negligible when compared with the apoptotic response of Silver NPs even at a very low concentration of 20µg/ml in HepG2 cells (Zhu *et al.* 2016).

5.4.17 Caspase 3 expression analysis: FACS

Apoptosis is a highly regulated process so that once it started the whole pathway will get activated, which includes the activation of a caspase-dependent proteolytic cascade. Caspase 3 is an executionary caspase that actively participate in the final cell substrate degradation pathways of apoptosis. It is actively involved in both intrinsic and extrinsic pathways of apoptosis. Caspase 3 is an indispensable hallmark protease responsible for apoptosis mediated DNA fragmentation, chromatin condensation and cellular blebbing (Porter and Janicke.1999). Several literatures have reported that Caspase 3 dependant apoptosis is mediated by brain glial cells. Therefore, to confirm apoptosis mediated cell death pathway followed by WS_2 QDs exposure on LN-229 cells, Caspase 3 expression analysis was done by flow cytometry. The results were in agreement with the Annexin V/PI assay results stating

that the cell death pattern followed by WS_2 QDs exposed LN-229 glioblastoma cells is apoptosis mediated. Both the highest concentrations of 160µg/ml and 320µg/ml showed increased expression of Caspase 3 protein when compared with that of untreated control cells. This confirmed that a dose dependant increase in late apoptotic cell population was evidenced. A similar study confirmed the increased expression of Caspase 3 protein in MCF -7 cells (Laha *et al.* 2014).

5.4.18 NF-κB activation assay

NF-κb is a nuclear transcription factor that actively participates in various cellular metabolic machineries such as innate immune response, cell proliferation, apoptosis activation as well as stress response adaptation processes in cells. An increased NF-κb expression was evidenced in cells treated with silver NPs (AgNPs) with an average particle size of 20nm in HepG2 and A549 cells (Stepkowski *et al.* 2014). Likewise, Gold NPs (10nm) were reported to induce the transcriptional activation of the same in B-lymphocytes that accounts for the increased expression of downstream signalling cascade proteins and subsequent pro-inflammatory cytokine production (Sharma *et al.* 2013). Inorder to confirm whether a similar cytokine expression was observed in LN-229 cells after exposure with WS_2 QDs, NF-κb expression by flow cytometry was done. The results confirmed that a negligible level of NF-κb was evidenced in cells treated with 320µg/ml QDs, which can be due to the stress induced by the cells because of cell-cell or cell-QD interactions. Several studies have confirmed that, as the size of NPs decreases; the possibility of activation of nuclear transcription factors responsible for cell cycle regulation, cytokine activation

as well as apoptosis induction will gradually tend to increase. The present study confirmed that the WS_2 QDs at lower concentrations behaved in a similar trend as observed in untreated negative control cells. A marginal level of NF-κB expression is normally observed in cancerous cells; especially in glioblastoma cells; due to high proliferation potential, which accounts for the minimal expression of the same in negative control cells. In general, a significant alteration in NF-κB signalling will always suggests a potential for off-target effects with *in vivo* applications. The present study confirmed that, WS_2 QDs did not evoke any such responses in LN-229 glioblastoma cells at any of the selected concentrations.

5.4.19 Tritiated thymidine incorporation assay

Possible genotoxic effect that subsequently leads to cell proliferation arrest in LN-229 cells exposed to WS_2 QDs was analysed by tritiated thymidine incorporation assay. The results suggest that a significant reduction in cell proliferation status was evidenced at the highest selected concentration of 640µg/ml. The highest selected concentration (640µg/ml) showed a more or less similar response like that of 0.02% phenol treated positive control cells. As this assay measures the radioactivity corresponds to the tritiated thymidine incorporated newly synthesised DNA strands in highly proliferative cells, the assay marks a hallmark category analysis for detecting cell proliferation status followed by QD exposure.

5.4.20 DNA ladder assay

The present study confirmed that, upon exposure to 320 and 640µg/ml concentrations of WS_2 QDs for 24h, prominent DNA breakage bands were evidenced in agarose gel electrophoresis. Upto 160µg/ml, the DNA was intact and highly comparable with that of the negative control. Therefore, it can be inferred that WS_2 QDs exposure resulted in chromosomal DNA degradation into small internucleosomal fragments, a biochemical hallmark of cells undergoing apoptosis (Bannazadeh et al. 2013). This suggested an induction of apoptotic DNA fragmentation in response to QD exposure. The results showed comparable trend with a study reported by Guilbert *et al.*, (2011) in which; it was reported that, 500µg/ml exposure of a tungsten compound WO_4^{2-} induced prominent DNA breakage in developing B-lymphocytes. The results were confirmed using Western blotting experiments using antibodies against γH2AX, which noticed a phosphorylated histone variant that is induced upon DNA breakage.

5.4.21 Hoechst staining for nuclear condensation

Chromosomal condensation, DNA fragmentation and nuclear shrinkage are characteristics of apoptosis. Hoechst staining was done to analyse the possible nuclear condensation and DNA fragmentation followed by WS_2 QDs exposure. A slight nuclear condensation tendency was evidenced at the 320µg/ml concentration while rest of the concentrations were highly comparable with that of untreated negative control cells. The results were in agreement with the Annexin/PI, Caspase 3 apoptosis induction studies and DNA ladder analysis in which such changes in chromosomal and nuclear condensation are characteristic features of apoptosis cell death pathway.

5.5 Acute toxicity studies using Sprague-Dawley rats

In acute toxicity studies, a single dose exposure of the test compound is executed to ascertain the adverse effects in animal models. Based on the concept of humane endpoints, any animal experiment in toxicology should be preceded by 3 R's such as Reduction, Replacement and Refinement, which was outlined according to 'The Principles of Humane Experimental Technique'. Safety assessment and subsequent dose range findings in rodents are highly acceptable, especially in rats which closely resembles human in biochemical, metabolic and physiological aspects (Sharp and Villano. 2012). In the present study, healthy adult Sprague-Dawley rats weighing 300-350g were used for the acute toxicity studies after i.p exposure of WS_2 QDs. The animals were randomly divided into 4 groups of 3 animals each; representing control (untreated groups), 3 days, 7 days and 14 days based on the period of observation and subsequently subjected to various toxicity studies to confirm the acute toxic response of the administered compound in rats.

5.5.1 Clinical/ behavioural signs of toxicity

Clinical and behavioural changes in rats exposed to WS_2 QDs were monitored on a regular basis. No observable changes were noticed which confirmed that the animals were well tolerated with the administered WS_2 QDs. None of the animals showed any signs of morbidity or mortality after intraperitoneal administration of WS_2 QDs.

5.5.2 Body weight and organ weight

Body weight and growth pattern of WS_2 QDs administered rats remained unaltered suggesting the non toxic nature of the material. All the experimental animals were healthy throughout the experimental period. Organ weights of major organs such as liver, kidney, brain and spleen were checked. No significant organ weight changes were observed in any of the treatment groups and were comparable with that of the control groups.

5.5.3 Gross pathology

Gross pathological observations showed no signs of toxicity. No observable lesions or organ damages were found. All the animals after cervical dislocation were observed for gross pathological evaluation to see any visible alterations such as lumps, lesions, or organ damages. All the major organs were intact and highly comparable with respect to structural features with that of untreated control groups.

5.5.4 Hematology

Almost all the hematological parameters were observed to be comparable with that of the untreated control groups. No suggestive anaemia was noticed in any of the experimental animals as the RBC and Hb count was normal, which correlate with the proper health status of the experimental animals. A significant increase in WBC and platelet count in the 3^{rd} day indicates an immediate onset immune response but

came back to normal level in 7 days and 14 days. However, it could be predicted that NPs having extreme low size and spherical morphology can enter into lymphatic system and elicit an immediate inflammatory response at high concentrations. This could be the reason for the increase in WBC count on the 3rd day (Hamrahi *et al.* 2012). A similar category material, MoS_2 NPs, administered intraperitoneally at a dosage of 10mg/kg body weight in Sprague Dawley rats were reported to elicit severe alterations in the major hematological parameters such as RBCs, WBCs, hemoglobin (Hb), hematocrit (HCT), eosinophil, neutrophil, lymphocyte, and monocyte count (Asadi *et al.* 2017). In the present study with WS_2 QDs, no such severe alterations were observed in any of the treatment groups.

5.5.5 Serum biochemistry analysis

Major serum biochemical parameters such as ALT, AST and ALP levels were observed to be increased on the 3rd day of observation but traced back to normal levels in 14 days. A similar observation was found in another study, in which Sprague Dawley rats administered with both 5mg/kg and 10mg/kg body weight MoS_2 NPs (i.p) were observed to elicit a significant difference in serum ALT and ALP levels after one day observation period (Asadi *et al.* 2017). A persistent increase in ALT and ALP levels in serum are suggestive of liver damage and another suggestive for altered ALT levels can be due to altered purine metabolism in liver. But such a persistent alteration was not observed in the present study as the ALT, ALP levels came down to normal level in 14 days time period. Moreover, serum albumin level was highly comparable in all the treatment groups with respect to

control. If any prominent liver damage persists, the albumin level will get reduced considerably. Here no such changes were observed. Acute stress can therefore be a reason for the detection of elevated liver enzymes in blood (Gao *et al*. 2013). Various studies have reported that if the stress response is not strong enough to evoke a permanent liver, kidney damage in the body, the extend of damage to these organs cannot be considered as serious and at the same time highly recoverable in no time (Gao *et al.* 2013). Several studies suggest that with the exposure of stress factors, the hypothalamic-pituitary-adrenal axis will get overexcited releasing more glucocorticoids which will eventually lead to increased glucose level in blood (Dhalla *et al.* 2000). This was noticed in the 3rd day experimental animal in which an increased glucose level was observed in the serum. This can have a direct influence on liver by altering the oxidative parameters in liver leading to ALT, AST and ALP secretion but this is a highly reversible process (Mittler. 2002). Increase in the level of both glucose and liver enzyme can correlate to the acute stress related liver response in the early onset exposed experimental animals. Urine analysis also confirmed that no noticeable levels of bilirubin were detected in urine, which accounts for the lack of permanent liver damage. Hypercreatinaemia is associated with liver damage, but no significant increase in creatinine level was observed in the serum of any of the treatment group animals again confirmed lack of consistent liver or kidney damage (Clayton *et al.* 2004).

5.5.6 Urine analysis

Urine analysis confirmed that all the parameters like ketone bodies, nitrite, urobilinogen, bilirubin and glucose level were highly comparable with that of the control group. No blood cells were detected in urine. Moreover the pH of urine was also comparable with that of the untreated control group. This confirmed lack of a permanent kidney damage in the experimental animals.

5.5.7 Organ damage

Organ damage in Sprague Dawley rats due to WS_2 QDs administration was analysed by histopathological examination of major organs such as liver, kidney, brain and spleen. H&E staining was used to stain tissue sections. The results were compared and correlated with the hematological, serum biochemical and urine analysis results to further came to a conclusion.

5.5.7.1 Liver

Liver is the major organ that involve in the detoxification pathway of major metabolites. Increased ALT (SGOT), AST (SGPT) level is a suggestive marker for liver damage, which is characterised with loss of cellular integrity of hepatocytes. Liver biomarker elevation in blood can also be possible due to acute stress and related biochemical changes in the physiological system. This is characterised with an elevated glucose level due to hyperactivation of the hypothalamic-pituitary-

adrenal axis releasing more glucocorticoids. This will elevate glucose level along with liver biomarkers. In the present study, a significant increase in ALT, AST level was observed along with hyperglycemia which suggests that the possible elevation in liver biomarkers is due to acute stress response in 3rd day group animals. But these changes came back to normal level in 7 and 14 days, which made it evident that no irreparable and irreversible liver damages were evidenced in any of the treatment group animals followed by WS_2 QDs exposure. Serum creatinine level was also evidenced to be normal and comparable with that of the untreated control group. Since hypercreatinemia is associated with direct liver damage, no such changes were observed in any of the treatment groups again confirmed lack of prominent liver damages in Sprague Dawley rats after WS_2 QDs exposure.

5.5.7.2 Kidney

WS_2 QDs being highly water dispersible showed excretion route via urine rather than feces. Therefore, it is not surprising that the kidney histology of immediate exposure group (3rd day group) showed slight changes. Degenerated renal tubules were observed in the 3rd day kidney. At the same time healthy Bowman's capsule was noticed in the tissue sections and the epithelial lining covering the Bowman's capsule seemed intact. Urine analysis report suggests that leukocyte, nitrite, urobilinogen, ketone bodies and glucose content were normal and comparable with that of control groups. pH and specific gravity of urine was found to be comparable with that of the control groups. No detectable level of blood cells was observed in any of the urine

samples of the experimental animals. Serum creatinine level was also found to be highly comparable with that of the untreated control groups. This suggest that the normal kidney functioning was neither altered nor adversely affected by WS_2 QDs administration. A similar study in mice exposed to pristine MoS_2 nanosheets (a similar family compound) showed severe nephrotoxicity concerned with changes in hematological, biochemical and histological parameters after 1.5mg/kg body weight exposure in mice. But with 1mg/kg body weight exposed mice, no such significant alterations were found (Umakant *et al.* 2021). Therefore it can be concluded that an immediate onset exposure dependant nephrotoxicity was evidenced in the present study also but the noticeable changes came back to normal in a few days.

5.5.7.3 Brain

Since extreme nanosized particles like QDs were reported to cross BBB and elicit adverse effects in brain, similar effect associated with WS_2 QDs was also analysed after i.p administration in Sprague Dawley rats. Inorder to analyse the possible brain tissue damage, direct brain histology and antioxidant parameter analysis were done. ICP-MS results showed that 7^{th} day animals showed retention of the compound in brain tissues which shows the possibility of the QDs in crossing the blood brain barrier. After 14 days period, most of the administered compound got excreted out from the system. Histopathology of brain tissue sections from treatment group animals was highly comparable with that of the control group animals. No neuronal swelling, vacuolation or tissue degeneration was observed. Active glial cells and neurons were visible. Brain antioxidant parameters such as GSH, GPx, GR, SOD

and lipid peroxidation status were similar to that of the control group animals. No significant changes were noticed which confirmed lack of brain tissue damage post WS_2 QDs exposure in Sprague Dawley rats.

5.5.7.4 Spleen

Spleen is the major organ responsible for the clearance of abnormal RBCs and particulate antigens from the blood stream. The red pulp region in spleen is responsible for blood filtration, whereas the white pulp region is rich in immune cells (B&T lymphocytes). In the present study, no observable pathological lesions or tissue damages were observed in the spleen of the treatment group animals after intraperitoneal administration of WS_2 QDs. No macrophage infiltrations were observed in the spleen of the treatment group rats. Hematological studies also concluded that the RBC count and Hb level were normal in all the experimental animals. Therefore proper blood filtration has consistently taken place even after WS_2 QDs exposure in rats. This also correlates with the lack of observable level spleen tissue histological changes. The histology reports of spleen after QD administration was well comparable with the study reported by Umakanth *et al.*, (2021).

5.5.8 Antioxidant Assays

5.5.8.1 In liver

Total protein content in liver tissue homogenate was observed to be comparable with

that of untreated control animals. Lipid peroxidation status was evaluated by estimating the MDA release. No statistically significant alteration was observed in any of the treatment groups. Similarly, other antioxidant enzymes such as GSH, GR, and SOD activity was also observed to be normal and highly comparable in all the treatment groups when compared with that of the untreated control. A slight increase in GPx activity was observed in the 14^{th} day group liver.

5.5.8.2 In brain

Total protein content in brain tissue homogenate of all the experimental animals was highly comparable with that of the untreated control groups. Antioxidant parameters such as lipid peroxidation status, GR, GPx and SOD of treatment group animals were highly comparable with that of the untreated control. A slight decrease in GSH level was observed in the 14^{th} day group brain.

5.5.9 Immunotoxicity by spleenocytes proliferation assay

Spleenocyte proliferation usually occurs in response to an immune trigger. NPs are reported to be efficient in evoking an immune response which can trigger major immune response pathways in the physiological system (Zha *et al.* 2019). In the present study, no significant changes were observed in the spleenocyte proliferation status in any of the treated groups when compared with that of the untreated control animals. This indicates that no significant toxic response was elicited by the administered compound *in vivo;* in Sprague Dawley rats. In contrary to the increased WBC count observed in the 3^{rd} day experimental group animals, the spleenocyte

proliferation status was observed to be normal and highly comparable with that of untreated control group animals. This suggests that even though the immediate onset exposure of WS_2 QDs evoked a slight immune response but was not prolonged and sufficient enough to evoke significant lymphocyte proliferation.

5.5.10 ADME and toxicokinetics

Owing to the ultrafine size, NPs like quantum dots can enter into the circulatory and lymphatic system whereby distributed to major vital organs to elicit adverse effects. ADME profiling was done by evaluating the elemental distribution in major organs such as liver, kidney, brain and spleen along with feces and urine. Subsequent organ damage if any; was analysed by histological examination using Hematoxylin and Eosin staining.

Absorption is the process of entering a compound into the blood stream. After intraperitoneal exposure, soluble tungsten compounds such as WS_2 can get easily absorbed and distributed in major organs such as liver, kidney, spleen *etc*.,. Biodistribution was analysed by ICP-MS. The results suggested that, 7^{th} day observed the maximum biodistribution of the compound in all the major organs. Afterwards by day 14, it came back to normal level comparable to that of control. When compared to other organs, kidney was observed to retain the compound to a greater extend. Elemental detection in urine and feces suggested that the excretion of the compound after metabolism could be mediated by renal pathway because urine showed maximum tungsten content than feces.

Metabolism is the process of biotransformation of the parent compound once it is absorbed from the blood stream into major organs such as liver. This will facilitate the removal of the toxic compound from the system. The possible WS_2 metabolism was analysed by comparing hematological, biochemical parameters in blood and by analysing the histopathological lesions in major organs. It is not possible to directly analyse the metabolic byproducts of WS_2 QDs using ICP-MS as it will not discriminate between the subsequent ionic forms of the parent compound. There are possibilities that tungsten compounds once enter into the circulation can convert to tungstate ions. To date, no relevant evidences were known regarding the metabolism of tungstate ions (WO_4^{2-}). But one *in vitro* study has reported that tungstate ion when bind with albumin and other related proteins in serum (molecular weight ≥ 300kDa) forms protein bound tungsten. But these complexes being highly unstable can revert back with the release of bare tungstate ions in no time. Therefore, further adverse effects were not reported (Rodriguez *et al*. 2008). This finding was further confirmed in rats, in which it was confirmed that more than 80% of the tungsten was bound to protein (albumin) in a highly unstable manner. But with reduced glutathione and transferrin, no such complex formation was evidenced. In another study, after systemic distribution, tungsten as tungstate ions get deposited in bone and subsequently improved bone the mineralisation process (Lemus and Venezia. 2015). But the exact reason behind this bone mineralisation; whether it is due to chemical speciation of tungsten or due to cellular processes has not evidenced yet. Here, in the present study, most of the tungsten compound administered is found to be excreted through urine. Urine and feces collected from both the control and treatment group

animals were subjected to ICP-MS analysis to elucidate the excretion route. ICP-MS report suggested that the major excretion route of the compound is via renal excretion as a major amount of the element tungsten was detected in urine than feces. These findings along with the high material detection in kidney and suggestive histopathological lesions as well as tissue degeneration in kidney strengthened the possibility of renal excretion of the compound.

Certain studies confirmed that sparingly soluble tungsten compounds such as metallic tungsten (W, WC, and W_2C) can be easily eliminated via feces. But the as synthesised WS_2 compound; being highly water dispersible; can get easily excreted via urine rather than feces. This is the main causative factor behind possible nephrotoxicity and kidney damages often reported with soluble tungsten compounds after *in vivo* administration (Rajendran *et al*. 2012). The third day exposure caused slight nephrotoxicity but came back to normal level in 7 and 14 days strengthened this possibility. Histopathological changes in 3^{rd} day group kidney histology confirmed this but evident tissue regeneration was observed in the subsequent day groups, which confirmed that the possible nephrotoxicity is repairable by body's own mechanism. As most of the water dispersible metallic compounds are excreted through kidney and gastrointestinal routes, these findings cannot be regarded as highly unexpected (Lemus and Venezia. 2015). No carcinogenic effects were reported till date for tungsten compounds. The present study, which is mainly aimed at evaluating the possible toxic effects of tungsten compound made it clear that at the selected dosage, WS_2 QDs didnot evoke any noticeable level of toxic impact in living system. Hence the ADME profiling seemed to be appreciable enough to validate this material safe intended for biomedical and related applications.

CHAPTER 6: SUMMARY AND CONCLUSION

6. SUMMARY AND CONCLUSION

6.1 Summary

WS_2 QDs are inorganic semiconductor NPs that possess numerous applications in various fields such as electronics, optoelectronics, energy storage and biomedicine. QDs can be synthesized easily and efficiently by various physical and chemical routes such as solvent assisted exfoliation, mechanical exfoliation, chemical vapor deposition, lithium intercalation *etc.*,. In the present study, WS_2 QDs was synthesized using sonication assisted solvothermal exfoliation using NMP solvent, which yielded highly monodispersed QDs of 3-4nm size and spherical morphology. The synthesized QDs emit strong and stable cyan green fluorescence under UV illumination at 370nm. The total yield after complete exfoliation process was approximately 30%. The synthesized WS_2 QDs were subjected to various sophisticated characterization techniques to confirm its chemical composition, elemental state, morphology, thermal stability, size and surface charge.

One important factor that influences nanomaterial toxicity is its various physico-chemical characteristics, therefore it is highly imperative to effectively characterize the material before moving on to biological studies. In this context, an effort was made to analyse the toxicity profiling of this emerging material in both *in vitro* and *in vivo* models. Bio-nano interaction and cytotoxicity studies were done using LN-229 glioblastoma cells. The particles were well characterized before proceeding to cellular studies for its physico-chemical characteristics. Cellular uptake, *in vitro* imaging ability, cytotoxicity analysis, cellular metabolic state, lysosomal integrity,

mitochondrial membrane potential, cytoskeletal rearrangements, pro-inflammatory cytokine expression studies, cell death pathway analysis, nuclear condensation, DNA fragmentation, Caspase 3 expression and cell cycle arrest were analysed in LN-229 cells after QD exposure.

Acute toxicity studies were carried out in Sprague Dawley rats after intraperitoneal administration of 10mg/kg body weight of WS_2 QDs. All the animals were monitored for clinical/ behavioral signs of toxicity, body weight changes and acute stress responses. All the animals were euthanized on 3^{rd}, 7^{th} and 14^{th} days of observation period and major organs such as liver, kidney, brain and spleen were collected for further analysis. Blood, urine and feces were collected before euthanisation. Hematology and blood biochemistry were done to evaluate organ toxicity (liver, kidney). Spleen was subjected to spleenocyte proliferation to evaluate immunotoxicity. Biodistribution and ADME was analysed by ICP-MS in liver, kidney, brain, spleen, blood, urine and feces. Blood withdrawn at regular time intervals was used for toxicokinetics and further retention possibility analysis of the material in the system.

6.2 Methodology adapted for the study

- Synthesis of WS_2 QDs having spherical morphology and strong cyan green fluorescence was done using solvothermal exfoliation using NMP solvent as the exfoliation medium.

- Optical characterization was done using UV/Visible and fluorescence emission spectroscopy.

- Physico-chemical characterization was done using HR-TEM, FTIR, XPS, XRD, TGA and Zeta potential.
- Endotoxin content was analysed using PTS Endosafe kit.
- Nano-bio interactions and *in vitro* cytotoxicity studies were done using LN-229 human glioblastoma cells. LN-229 cells were cultured in DMEM media supplemented with 10% FBS. Flow cytometry and fluorescent microscopy were carried out for cellular uptake of QDs.
- Cell viability, cellular metabolic activity, mitochondrial activity (MTT), lysosomal integrity (NRU), ROS production (DCFHDA, Griess reagent assay), morphological changes (phase contrast microscopy, CBB staning), lysosomal membrane stability (AO staining), mitochondrial membrane potential (JC-1 staining), actin filament integrity (Rhodamine-phalloidin staining) were studied.
- NF Kappa B expression, EtBr FACS, live/ dead analysis (Calcein AM/PI FACS) was studied.
- Cell death pathway elucidation by Annexin V/PI FACS and confirmation of apoptosis mediated cell death mechanism by Caspase 3 expression were done.
- Effect of toxicity evoked by QD dissolution was studied in LN-229 cells.
- Effect of inherent catalase activity in ROS generation was studied by pre-treating the cells with sodium azide catalase inhibitor and compared the effect.
- DNA fragmentation after WS_2 QDs exposure was analysed by agarose gel electrophoresis, Hoechst staining was used for nuclear condensation analysis.

- Cell cycle analysis was done to analyse the possibility of cell cycle arrest in the major cell cycle check points after QD exposure.

- Acute toxicity studies were done in Sprague Dawley rats exposed to 10mg/kg body weight WS_2 QDs via intraperitoneal administration. The animals were kept for 3, 7 and 14 days observation. Untreated animals were kept as control group.

- All the animals were observed for any kind of morbidity or mortality, body weight changes and behavioral toxicity signs during the observation period. At the end of the observation period, before euthanisation, blood, feces and urine were collected. Subsequent hematology, blood biochemistry and urine analysis were done to analyse the systemic toxicity including liver and kidney function.

- Major organs such as liver, kidney, brain and spleen were collected and subjected to ICP-MS for elemental detection and histopathology analysis.

- Blood, urine, feces and organs (liver, kidney, brain, spleen) were subjected to ICP-MS analysis for biodistribution and blood samples collected at regular intervals were analysed for blood kinetics by ICP-MS.

- Lipid peroxidation status and major antioxidant assays (GSH, GR, GPx, SOD) were carried out in liver and brain tissue homogenates of the experimental animals to study the oxidative stress.

- Spleenocytes proliferation assay by tritiated thymidine incorporation was done to study immunotoxicity.

6.3 Major findings of the study

- A facile solvothermal synthesis method achieved by sonication and temperature treatment sufficiently yielded WS_2 QDs of bright cyan green fluorescence under UV illumination.
- The synthesized WS_2 QDs were spherical in morphology with a characteristic size of 3-4nm, evidenced by HRTEM analysis.
- No endotoxin content was evidenced in the synthesized QDs and the endotoxin value obtained was 0.05 EU/ml which was well below the US Pharmacopia approved limit of 0.5 EU/ml.
- Fluorescence emission spectroscopy confirmed the emission wavelength at 450-500nm that corresponds to cyan green fluorescence.
- FTIR and XPS analysis confirmed the chemical composition and elemental state of the QDs. XRD report confirmed the effective exfoliation efficiency from bulk WS_2 powder to extremely small WS_2 QDs. TGA analysis confirmed the excellent thermal stability of the material upto 450^0C. The surface charge of the synthesized QDs was observed to be -25mV. The total yield after complete exfoliation process was approximately 30%.
- Cellular interaction studies using LN-229 human glioblastoma cells showed that upto 160µg/ml concentration, the cells showed excellent mitochondrial activity, lysosomal integrity and well reduced cytotoxicity.
- The observed IC_{50} concentration for the synthesized QDs was 363.90µg/ml.

- A significant ROS generation potential was observed from 320µg/ml concentration onwards.
- No significant mitochondrial hyper polarization or lysosomal membrane integrity loss was observed upto 320µg/ml.
- Actin filaments were observed to be intact even at the highest selected concentration.
- LN-229 cells after WS_2 QDs exposure followed a Caspase dependant apoptosis
- mediated cell death.

  Cell cycle analysis showed that at the highest selected concentration an extended 'S' phase was evident that corresponds to apoptosis induction.
- Highest concentration evidenced prominent DNA fragmentation.
- No significant NF Kappa B expression was evidenced in LN-229 cells after WS_2 QDs exposure.
- Acute toxicity studies showed no clinical or behavioral signs of toxicity. Single
- exposure of 10mg/kg body weight of WS_2 QDs did not evoke any changes in hematological parameters.
- Slight increase in biochemical parameters such as AST, ALT was evidenced in the 3^{rd} day treatment group but came back to normal in 7^{th} and 14^{th} days. This could be due to the acute stress response due to immediate onset particle exposure.
- Brain, liver and spleen histology were normal in all the treatment groups. Only kidney showed prominent degeneration on the 3^{rd} day but significant tissue regeneration was evidenced in the 7^{th} and 14^{th} days.

- Moreover, the serum creatinine content was observed to be normal and highly comparable with that of the untreated control animals again confirmed that the normal kidney functioning was not adversely affected to any extend.
- No significant changes in antioxidant status and lipid peroxidation level were observed in any of the treatment groups.
- Spleenocyte proliferation status was well comparable with that of the untreated control groups suggesting lack of immunotoxic effect.
- Biodistribution analysis by ICP-MS showed that the kidney showed maximum biodistribution of the compound when compared to other organs. 7^{th} day showed the maximum retention of the compound in major organs, especially in kidney.
- Blood kinetics by ICP-MS suggested that after 14 days of observation period, merely low quantity of the material was found to be retained in the blood and on an average; more than 98% of the compound is getting either distributed in several organs or getting excreted out in 14 days period.
- ADME status confirmed that the excretion route of the administered QDs is via renal excretion pathway through urine.

6.4 Conclusion

WS_2 QDs synthesized via sonication assisted solvothermal exfoliation method yielded bright cyan green fluorescent QDs having lateral dimension of 3-4nm. The synthesized QDs was further characterized using Fluorescence emission spectroscopy, HRTEM, XRD, FTIR, XPS, TGA and Zeta potential to determine the

fluorescence emission, structure, morphology, crystallinity, effective exfoliation efficacy, chemical composition, elemental state, thermal stability and surface charge respectively . The synthesized QDs were highly water dispersive in nature. Under longer wavelength UV illumination, the QDs emitted bright stable cyan green fluorescence. WS_2 QDs exhibited spherical morphology with a size of 3-4nm without any aggregation tendency. QDs were observed to be highly monodispersive and possess excellent stability upto 100 days under room temperature. WS_2 QDs exhibited high thermal stability upto 450^0C temperature, which was evidenced in TGA analysis. To determine the effect of WS_2 QDs in *in vitro* cellular environment, bio-nano interaction and cytotoxicity studies were conducted using LN-229 glioblastoma cells. MTT, NRU and LDH assays showed that upto 160µg/ml concentration, WS_2 QDs did not evoke any cytotoxic response and further a dose dependant cytotoxic response was evident. No observable sub cellular organelle integrity loss was evidenced at any of the selected concentrations.

Upto 10mg/kg bodyweight administration, these QDs was confirmed to be safe in *in vivo* conditions also. Single exposure of 10mg/kg body weight of WS_2 QDs did not evoke any major pathological lesions in major organs and did not alter the hematological and biochemical parameters towards an irreversible toxic effect. Even though slight tissue degeneration was observed in the 3^{rd} day group kidney, prominent tissue regeneration was evidenced in the subsequent days. Serum creatinine content was observed to be normal and highly comparable with that of untreated control animals again confirmed that the normal kidney functioning was not adversely affected to any extend. Lack of oxidative stress after WS_2 QDs

exposure was evidenced in the antioxidant status analysis in brain and liver tissue homogenates of treatment group animals. This again confirmed the non toxic nature of the synthesised QDs. ICP-MS based biodistribution analysis concluded that none of the major organs retained the material apart from kidney (for 3^{rd} day treatment group) after 10mg/kg body weight administration of the compound. Kidney showed prominent elemental detection when compared to other organs such as liver, brain and spleen due to the possible renal excretion and reabsorption tendency of the compound as it is highly water dispersible. ADME profiling confirmed that the major route of excretion followed by the material was renal excretion as urine rather than feces. This could be because of the excellent water dispersive nature of WS_2 QDs. Blood kinetics data suggested that, after 14 days of observation, only less than 1% of the administered compound was found to be retained in blood.

Before validating any nanomaterial safe to be applicable for biomedical applications, intact toxicological evaluation is a mandatory criterion. To the best of our knowledge, an indepth toxicological evaluation of this emerging material was demonstrated for the first time in this study, which opens new windows for promoting the application scope of this excellent candidate material. The present study concluded that WS_2 QDs did not evoke any toxic effects or inflammatory responses in both *in vitro* and *in vivo* systems. Hence the study confirmed that, WS_2 QDs materials are potentially applicable for various biomedical applications such as extended dynamic imaging guided therapies like PET, SPECT, PAT, PTT, PDT, drug delivery, biosensing, target analyte detection *etc*.,.

REFERENCES

Aeschbacher M, Reinhardt CA and Zbinden G (1986) A rapid cell membrane permeability test using flourescent dyes and flow cytometry. *Cell biology and toxicology*2(2): 247-255.

Akhtar MJ, Ahamed M and Alhadlaq H (2020) Gadolinium Oxide Nanoparticles Induce Toxicity in Human Endothelial HUVECs via Lipid Peroxidation, Mitochondrial Dysfunction and Autophagy Modulation. *Nanomaterials*, 10(9):1675.

Alexis F, Pridgen E, Molnar LK and Farokhzad OC (2008) Factors affecting the clearance and biodistribution of polymeric nanoparticles. *Molecular pharmaceutics*5(4): 505-515.

Alsaedi II, Taqi ZJ, Hussien AMA, Sulaiman GM and Jabir MS (2019) Graphene nanoparticles induces apoptosis in MCF-7 cells through mitochondrial damage and NF-KB pathway. *Materials research express*, 6(9): 095413.

Amano M, Nakayama M and Kaibuchi K (2010) Rho-kinase/ROCK: a key regulator of the cytoskeleton and cell polarity. *Cytoskeleton*67(9): 545-554.

Anju S and Mohanan PV (2020) Biomedical applications of transition metal dichalcogenides (TMDCs). *Synthetic Metals* 116610.

Ariga K, Nishikawa M, Mori T, Takeya J, Shrestha LK and Hill JP (2019) Self-assembly as a key player for materials nanoarchitectonics. *Science and technology of advanced materials*20(1): 51-95.

Asadi F, Mohseni M, Noshahr KD, Soleymani FH, Jalilvand A and Heidari A (2017) Effect of molybdenum nanoparticles on blood cells, liver enzymes, and sexual hormones in male rats. *Biological trace element research*175(1): 50-56.

Aschner M, Allen JW, Kimelberg HK, LoPachin RM and Streit WJ (1999) Glial cells in neurotoxicity development. *Annual review of pharmacology and toxicology*, 39(1): 151-173.

Auffan M, Rose J, Wiesner MR and Bottero JY (2009) Chemical stability of metallic nanoparticles: a parameter controlling their potential cellular toxicity in vitro. *Environmental Pollution*157(4): 1127-1133.

Bai X, Wang J, Mu X, Yang J, Liu H, Xu F, Jing Y, Liu L, Xue X, Dai H and Liu Q, (2017) Ultrasmall WS_2 quantum dots with visible fluorescence for protection of cells and animal models from radiation-induced damages. *ACS Biomaterials Science & Engineering*3(3): 460-470.

Bailes J (2020) Photostability of Semiconductor Quantum Dots in Response to UV Exposure. In: *Nanoparticles in Biology and Medicine*, Humana, New York, pp. 343-349.

Bannazadeh Amirkhiz M, Rashtchizadeh N, Nazemiyeh H, Abdolalizadeh J, Mohammadnejad L and Baradaran B (2013). Investigating apoptotic effects of methanolic extract of Dorema glabrum seed on WEHI-164 Cells. *International Scholarly Research Notices, 2013*.

Barabadi H, Najafi M, Samadian H, Azarnezhad A, Vahidi H, Mahjoub MA, Koohiyan M and Ahmadi A (2019) A systematic review of the genotoxicity and antigenotoxicity of biologically synthesized metallic nanomaterials: are green nanoparticles safe enough for clinical marketing. *Medicina*, 55(8): 439.

Beauchemin D (2017) Inductively coupled plasma mass spectrometry methods 236-245.

Bera D, Qian L, Tseng TK and Holloway PH (2010) Quantum dots and their multimodal applications: a review. *Materials*3(4): 2260-2345.

Bhandavat R, David L and Singh G (2012) Synthesis of surface-functionalized WS2 nanosheets and performance as Li-ion battery anodes. *The journal of physical chemistry letters*, *3*(11): 1523-1530.

Bianco S, Grigolini P and Paradisi P (2005) Fluorescence intermittency in blinking quantum dots: Renewal or slow modulation.*The Journal of chemical physics*, 123(17): 174704.

Blanco JLJ, Benito JM, Mellet CO and Fernández JMG (2017) Molecular nanoparticle-based gene delivery systems.*Journal of Drug Delivery Science and Technology*42: 18-37.

Blott EJ and Griffiths GM (2002) Secretory lysosomes.*Nature reviews Molecular cell biology*3(2): 122-131.

Borenfreund E and Puerner JA (1985) Toxicity determined in vitro by morphological alterations and neutral red absorption. *Toxicology letters*24(2-3): 119-124.

Borzelleca JF (2000) Paracelsus: herald of modern toxicology. *Toxicological Sciences* 53(1): 2-4.

Bratosin D, Mitrofan L, Palii C, Estaquier J and Montreuil J (2005) Novel fluorescence assay using calcein-AM for the determination of human erythrocyte viability and aging. *Cytometry Part A: the journal of the International Society for Analytical Cytology*66(1): 78-84.

Brus LE (1983) A simple model for the ionization potential, electron affinity, and aqueous redox potentials of small semiconductor crystallites.*The Journal of chemical physics*, 79(11): 5566-5571.

Buseck P, Cowley J and Eyring L (1989) *High-Resolution Transmission Electron Microscopy: And Associated Techniques*, Oxford University Press.

Buzea C, Pacheco II and Robbie K (2007) Nanomaterials and nanoparticles: sources and toxicity. *Biointerphases*2(4): 17-71.

Caigas SP, Cheng MC, Lin TN, Santiago SRMS, Yuan CT, Yang CC, Chou WC and Shen JL (2018) P-type doping of WS_2 quantum dots via pulsed laser ablation. *ACS Photonics*, 5(12): 4828-4837.

Caigas SP, Santiago SRM, Lin TN, Lin CAJ, Yuan CT, Shen JL and Lin TY (2018) Origins of excitation-wavelength-dependent photoluminescence in WS_2 quantum dots.*Applied Physics Letters*112(9): 092106.

Champion JA and Mitragotri S (2006) Role of target geometry in phagocytosis.*Proceedings of the National Academy of Sciences*, 103(13): 4930-4934.

Chen J, Li X, Liu X, Yan H, Xie Z, Sheng Z, Gong X, Wang L, Liu X, Zhang P and Zheng H (2018) Hybrid $MoSe_2$-indocyanine green nanosheets as a highly efficient phototheranostic agent for photoacoustic imaging guided photothermal cancer therapy. *Biomaterials science*6(6): 1503-1516.

Chen JB, Yousefi H, Nemr CR, Gomis S, Atwal R, Labib M, Sargent E and Kelley SO (2019) Nanostructured Architectures for Biomolecular Detection inside and outside the Cell. *Advanced Functional Materials* 1907701.

Chen N, He Y, Su Y, Li X, Huang Q, Wang H, Zhang X, Tai R and Fan C (2012) The cytotoxicity of cadmium-based quantum dots. *Biomaterials*33(5): 1238-1244.

Chen T, Li L, Xu G, Wang X, Wang J, Chen Y, Jiang W, Yang Z and Lin G (2018) Cytotoxicity of InP/ZnS quantum dots with different surface functional groups toward two lung-derived cell lines.*Frontiers in pharmacology*9: 763.

Cheng ZL, Ma L and Liu Z (2020) Hydrothermal-assisted grinding route for WS_2 quantum dots (QDs) from nanosheets with preferable tribological performance. *Chinese Chemical Letters* 32(1): 583-586.

Cherian RS, Anju S, Paul W, Sabareeswaran A and Mohanan PV (2019) Organ distribution and biological compatibility of surface-functionalized reduced graphene oxide.*Nanotechnology* 31(7):1-27.

Chia YY and Tay MG (2014) An insight into fluorescent transition metal complexes. *Dalton Transactions*, 43(35): 13159-13168.

Christen V, Camenzind M and Fent K (2014) Silica nanoparticles induce endoplasmic reticulum stress response, oxidative stress and activate the mitogen-activated protein kinase (MAPK) signaling pathway. *Toxicology reports*1: 1143-1151.

Clayton TA, Lindon JC, Everett JR, Charuel C, Hanton G, Le Net JL, Provost JP and Nicholson JK (2004) Hepatotoxin-induced hypercreatinaemia and hypercreatinuria: their relationship to one another, to liver damage and to weakened nutritional status. *Archives of toxicology*78(2): 86-96.

Coro J, Suarez M, Silva LS, Eguiluz KI and Salazar-Banda GR (2016) Fullerene applications in fuel cells: A review. *International Journal of Hydrogen Energy*41(40): 17944-17959.

Czigány Z and Hultman L (2010) Interpretation of electron diffraction patterns from amorphous and fullerene-like carbon allotropes. *Ultramicroscopy*110(7): 815-819.

de Araujo RE and Dominguez CT (2020) Absolute and Relative Methods for Fluorescence Quantum Yield Evaluation of Quantum Dots. In: *Quantum Dots*, Humana, New York, pp. 37-51.

Delwatta SL, Gunatilake M, Baumans V, Seneviratne MD, Dissanayaka ML, Batagoda SS, Udagedara AH and Walpola PB (2018). Reference values for selected hematological, biochemical and physiological parameters of Sprague-Dawley rats at the Animal House, Faculty of Medicine, University of Colombo, Sri Lanka. *Animal models and experimental medicine*, 1(4): 250-254.

Dhalla NS, Temsah RM and Netticadan T (2000) Role of oxidative stress in cardiovascular diseases.*Journal of hypertension*18(6): 655-673.

Dresselhaus MS, Lin YM, Rabin O, Jorio A, Souza Filho AG, Pimenta MA, Saito R, Samsonidze G and Dresselhaus G (2003) Nanowires and nanotubes. Materials Science and Engineering: C 23(1-2): 129-140.

Dresselhaus MS (2013) Intercalation in layered materials, *MRS Bulletin* 12: 24-28.

Dukhin SS and Labib ME (2013) Convective diffusion of nanoparticles from the epithelial barrier toward regional lymph nodes.*Advances in colloid and interface science*199: 23-43.

Eaton DL and Gilbert SG (2008) Principles of toxicology. *Casarett & Doull's toxicology: The basic science of poisons* 11-43.

Ekimov AI and Onushchenko AA (1981) Quantum size effect in three-dimensional microscopic semiconductor crystals. *Jetp Letters*34(6): 345-349.

Ellenbecker MJ and Tsai CSJ (2015) Routes of exposure for engineered nanoparticles. *Exposure Assessment and Safety Considerations for Working with Engineered Nanoparticles* 39-50.

El-Seedi HR, El-Shabasy RM, Khalifa SA, Saeed A, Shah A, Shah R, Iftikhar FJ, Abdel-Daim MM, Omri A, Hajrahand NH and Sabir JS (2019) Metal nanoparticles fabricated by green chemistry using natural extracts: biosynthesis, mechanisms, and applications. *RSC advances*9(42): 24539-24559.

Feng W, Chen L, Qin M, Zhou X, Zhang Q, Miao Y, Qiu K, Zhang Y and He C (2015) Flower-like PEGylated MoS_2 nanoflakes for near-infrared photothermal cancer therapy. *Scientific reports*5(1): 1-13.

Fischer AH, Jacobson KA, Rose J and Zeller R (2008) Hematoxylin and eosin staining of tissue and cell sections. *Cold spring harbor protocols*, pp. (5) 4986.

Frantsuzov P, Kuno M, Janko B and Marcus RA (2008) Universal emission intermittency in quantum dots, nanorods and nanowires. *Nature Physics*4(7): 519-522.

Fu SC, Liu JM, Lee KI, Tang FC, Fang KM, Yang CY, Su CC, Chen HH, Hsu RJ and Chen YW (2020) Cr (VI) induces ROS-mediated mitochondrial-dependent apoptosis in neuronal cells via the activation of Akt/ERK/AMPK signaling pathway. *Toxicology in Vitro*65: 104795.

Fukui KI, Namai Y and Iwasawa Y (2002) Imaging of surface oxygen atoms and their defect structures on CeO_2 (1 1 1) by noncontact atomic force microscopy.*Applied surface science*188(3-4): 252-256.

Gao X, Zeng Y, Liu S and Wang S (2013) Acute stress show great influences on liver function and the expression of hepatic genes associated with lipid metabolism in rats. *Lipids in Health and disease*12(1): 1-6.

Garcia-Pinel B, Porras-Alcala C, Ortega-Rodriguez A, Sarabia F, Prados J, Melguizo C and Lopez-Romero JM (2019) Lipid-based nanoparticles: application and recent advances in cancer treatment. *Nanomaterials*9(4): 638.

Garg M, Vishwakarma N, Sharma AL, Mizaikoff B and Singh S (2020) Lysine-Functionalized Tungsten Disulfide Quantum Dots as Artificial Enzyme Mimics for Oxidative Stress Biomarker Sensing. *ACS omega*5(4): 1927-1937.

Geiger PJ and Bessman SP (1972) Protein determination by Lowry's method in the presence of sulfhydryl reagents.*Analytical biochemistry*49(2): 467-473.

Gidwani B, Sahu V, Shukla SS, Pandey R, Joshi V, Jain VK and Vyas A (2021) Quantum dots: Prospectives, toxicity, advances and applications. *Journal of Drug Delivery Science and Technology* 61: 102308.

Goldman EB, Zak A, Tenne R, Kartvelishvily E, Levin-Zaidman S, Neumann Y, Stiubea-Cohen R, Palmon A, Hovav AH and Aframian DJ (2015) Biocompatibility of tungsten disulfide inorganic nanotubes and fullerene-like nanoparticles with salivary gland cells. *Tissue Engineering Part A* 21(5-6): 1013-1023.

Goodell V, dela Rosa C, Slota M, MacLeod B and Disis ML (2007) Sensitivity and specificity of tritiated thymidine incorporation and ELISPOT assays in identifying antigen specific T cell immune responses. *BMC immunology8*(1): 1-8.

Graham UM, Jacobs G, Yokel RA, Davis BH, Dozier AK, Birch ME, Tseng MT, Oberdorster G, Elder A and DeLouise L (2017) From dose to response: in vivo nanoparticle processing and potential toxicity. In *Modelling the Toxicity of Nanoparticles, Springer Cham*, pp. 71-100.

Guilbert C, Kelly ADR, Petruccelli LA, Lemaire M and Mann KK (2011) Exposure to tungsten induces DNA damage and apoptosis in developing B lymphocytes. *Leukemia*25(12): 1900-1904.

Gupta R, Valappil MO, Sakthivel A, Mathur A, Pundir CS, Murugavel K, Narang J and Alwarappan S (2020) Tungsten disulfide Quantum Dots Based Disposable Paper Based Lab on GenoChip for Specific Meningitis DNA Detection. *Journal of The Electrochemical Society*167(10): 107501.

Habib MR, Chen W, Yin WY, Su H and Xu M (2019) Simulation of Transition Metal Dichalcogenides. In: *Two Dimensional Transition Metal Dichalcogenides*, Springer, Singapore, pp. 135-172.

Poh TY, Ali NATBM, Mac Aogáin M, Kathawala MH, Setyawati MI, Ng KW and Chotirmall SH (2018) Inhaled nanomaterials and the respiratory microbiome: clinical, immunological and toxicological perspectives. *Particle and fibre toxicology 15*(1): 1-16.

Halim MA (2013) Harnessing sun’s energy with quantum dots based next generation solar cell.*Nanomaterials*3(1): 22-47.

Halliwell B and Whiteman M (2004) Measuring reactive species and oxidative damage in vivo and in cell culture: how should you do it and what do the results mean*? British Journal of Pharmacology* 142 (2): 231–255.

Hamrahi-Michak M, Sadeghi SA, Haghighi H, Ghanbari-Kakavandi Y, Razavi-Sheshdeh SA, Noughabi MT and Negahdary M (2012) The toxicity effect of cerium oxide nanoparticles on blood cells of male Rat. *Annals of Biological Research*3(6): 2859-2866.

Han N and Ho JC (2014) One-dimensional nanomaterials for energy applications. In: *Nanocrystalline Materials*, Elsevier Academic Press, pp. 75-120.

Hang DR, Sun DY, Chen CH, Wu HF, Chou MM, Islam SE and Sharma KH (2019) Facile Bottom-up Preparation of WS_2-Based Water-Soluble Quantum Dots as Luminescent Probes for Hydrogen Peroxide and Glucose. *Nanoscale research letters*14(1): 1-15.

Harhaji L, Isakovic A, Raicevic N, Markovic Z, Todorovic-Markovic B, Nikolic N, Vranjes-Djuric S, Markovic I and Trajkovic V (2007) Multiple mechanisms underlying the anticancer action of nanocrystalline fullerene. *European journal of pharmacology*568(1-3): 89-98.

Hazarika SJ and Mohanta D (2017) Inorganic fullerene-type WS_2 nanoparticles: processing, characterization and its photocatalytic performance on malachite green. *Applied Physics A* 123(5): 381.

Horlick G (1968) Introduction to Fourier transform spectroscopy. *Applied spectroscopy*22(6): 617-626.

Hou J, Wang L, Wang C, Zhang S, Liu H, Li S and Wang X (2019) Toxicity and mechanisms of action of titanium dioxide nanoparticles in living organisms. *Journal of environmental sciences75*: 40-53.

Hou Y, Ye J, Gui Z and Zhang G (2008) Temperature-modulated photoluminescence of quantum dots. *Langmuir*24(17): 9682-9685.

Hu L, Zhang C, Zeng G, Chen G, Wan J, Guo Z, Wu H, Yu Z, Zhou Y and Liu J (2016) Metal-based quantum dots: synthesis, surface modification, transport and fate in aquatic environments and toxicity to microorganisms. *RSC advances*6(82): 78595-78610.

Huang J, Wang X, Li J, Cao L, Xu Z and Wei H (2016) WS_2-Super P nanocomposites anode material with enhanced cycling stability for lithium ion batteries. *Journal of Alloys and Compounds* 673: 60-66.

Hulla JE, Sahu SC and Hayes AW (2015) Nanotechnology: History and future. *Human & experimental toxicology*34(12): 1318-1321.

Hussain S, Akbar K, Vikraman D, Liu H, Chun SH and Jung J (2018) $WS_2/CoSe_2$ heterostructure: A designed structure as catalysts for enhanced hydrogen evolution performance. *Journal of industrial and engineering chemistry*65: 167-174.

Iwasawa Y, Oyama N and Kunieda H (2000) Proceedings of the international conference on colloid and surface science (Tokyo, 5-8 November 2000). *Studies in surface science and catalysis* 289-208.

Jacak L, Hawrylak P and Wojs A (2013) Quantum dots.*Springer Science & Business Media* 1-18.

Jayakumar A, Surendranath A and Mohanan PV (2018) 2D materials for next generation healthcare applications.*International journal of pharmaceutics*551(1-2): 309-321.

Jiang Y and Tian B (2018) Inorganic semiconductor biointerfaces.*Nature Reviews Materials*3(12): 473-490.

Kansara K, Patel P, Shah D, Shukla RK, Singh S, Kumar A and Dhawan A (2015) TiO_2 nanoparticles induce DNA double strand breaks and cell cycle arrest in human alveolar cells. *Environmental and molecular mutagenesis*56(2): 204-217.

Kargozar S, Hoseini SJ, Milan PB, Hooshmand S, Kim HW and Mozafari M (2020) Quantum Dots: A Review from Concept to Clinic.*Biotechnology Journal* 15(12): 2000117.

Ke S, Lai Y, Li L, Tu L, Wang Y, Ren L, Ye S and Yang P (2018) Molybdenum Disulfide Quantum Dots Attenuates Endothelial-to-Mesenchymal Transition by Activating TFEB-Mediated Lysosomal Biogenesis. *ACS Biomaterials Science & Engineering*5(2): 1057-1070.

Kermanizadeh A, Chauche C, Brown DM, Loft S and Moller P (2015) The role of intracellular redox imbalance in nanomaterial induced cellular damage and genotoxicity: a review. *Environmental and Molecular Mutagenesis*56(2): 111-124.
Khan I, Saeed K and Khan I (2019) Nanoparticles: Properties, applications and toxicities.*Arabian Journal of Chemistry*12(7): 908-931.

Khan MI, Sobocinska AA, Brodaczewska KK, Zielniok K, Gajewska M, Kieda C, Czarnecka AM and Szczylik C (2018) Involvement of the CB 2 cannabinoid receptor in cell growth inhibition and G0/G1 cell cycle arrest via the cannabinoid agonist WIN 55,212–2 in renal cell carcinoma. *BMC cancer*18(1): 1-17.

Klaassen, CD (2013) *Casarett and Doull's toxicology: the basic science of poisons*, New York: McGraw-Hill (1236): 189-190.

Klaessig F, Marrapese M and Abe S (2011) Current perspectives in nanotechnology terminology and nomenclature. In: *Nanotechnology standards*, Springer, New York, NY, pp. 21-52.

Knudsen KB, Northeved H, Ek PK, Permin A, Gjetting T, Andresen TL, Larsen S, Wegener KM, Lykkesfeldt J, Jantzen K and Loft S (2015) In vivo toxicity of cationic micelles and liposomes. *Nanomedicine: Nanotechnology, Biology and Medicine*11(2): 467-477.

Kohli R (2012) Methods for monitoring and measuring cleanliness of surfaces. In: *Developments in Surface Contamination and Cleaning*, William Andrew Publishing, pp. 107-178.

Konopleva M, Zhao S, Xie Z, Segall H, Younes A, Claxton DF, Estrov Z, Kornblau SM and Andreeff M (1999) Apoptosis. *Drug Resistance in Leukemia and Lymphoma III* 217-236.

Kumar P, Nagarajan A and Uchil PD (2018) Analysis of cell viability by the lactate dehydrogenase assay. *Cold Spring Harbor Protocols* (6): 095497.

Kurapati Rajendra, Kostas Kostarelos, Maurizio Prato, AlbertoBianco (2016) Biomedical uses for 2D materials beyond graphene: current advances and challenges ahead. *Advanced Materials* 28 (29) 6052–6074.

Laha D, Pramanik A, Maity J, Mukherjee A, Pramanik P, Laskar A and Karmakar P (2014) Interplay between autophagy and apoptosis mediated by copper oxide nanoparticles in human breast cancer cells MCF7. *Biochimica et Biophysica Acta (BBA)-General Subjects*1840(1): 1-9.

Lawrence T (2009) The nuclear factor NF-κB pathway in inflammation. *Cold Spring Harbor perspectives in biology*1(6): 001651.

Lazarovits J, Chen YY, Sykes EA and Chan WC (2015) Nanoparticle–blood interactions: the implications on solid tumour targeting. *Chemical Communications*51(14): 2756-2767.

Lee YK, Choi EJ, Webster TJ, Kim SH and Khang D (2015) Effect of the protein corona on nanoparticles for modulating cytotoxicity and immunotoxicity.*International journal of nanomedicine*10: 97-113.

Lemus R and Venezia CF (2015) An update to the toxicological profile for water-soluble and sparingly soluble tungsten substances. *Critical reviews in toxicology*45(5): 388-411.

Li BL, Chen LX, Zou HL, Lei JL, Luo HQ and Li NB (2014) Electrochemically induced Fenton reaction of few-layer MoS_2 nanosheets: preparation of luminescent quantum dots via a transition of nanoporous morphology. *Nanoscale*6(16): 9831-9838.

Li X, Liu W, Sun L, Aifantis KE, Yu B, Fan Y, Feng Q, Cui F and Watari F (2015) Effects of physicochemical properties of nanomaterials on their toxicity. *Journal of biomedical materials research Part A* 103(7): 2499-2507.

Li X, Lovell JF, Yoon J and Chen X (2020) Clinical development and potential of photothermal and photodynamic therapies for cancer. *Nature Reviews Clinical Oncology*17(11): 657-674.

Liang L, Cui M, Zhang M, Zheng P, Deng Z, Gao S, Wang X, Zhang X, Wang C, Liu Y and Xie L (2015) Nanoparticles' interference in the evaluation of in vitro toxicity of silver nanoparticles. *RSC Advances* 5(82): 67327-67334.

Liao W, Zhang L, Zhong Y, Shen Y, Li C and An N (2018) Fabrication of ultrasmall WS_2 quantum dots-coated periodic mesoporous organosilica nanoparticles for intracellular drug delivery and synergistic chemo-photothermal therapy. *OncoTargets and therapy*11: 1949.

Liu L, Zhang X, Yang L, Ren L, Wang D and Ye J (2017) Metal nanoparticles induced photocatalysis. *National Science Review* 4 (5): 761-780.

Liu N and Tang M (2020) Toxicity of different types of quantum dots to mammalian cells in vitro: An update review. *Journal of Hazardous Materials* 399: 122606.

Liu X, Yan B, Li Y, Ma X, Jiao W, Shi K, Zhang T, Chen S, He Y, Liang XJ and Fan H (2020) Graphene Oxide-Grafted Magnetic Nanorings Mediated Magnetothermodynamic

Therapy Favoring Reactive Oxygen Species-Related Immune Response for Enhanced Antitumor Efficacy. *ACS nano*14(2): 1936-1950.

Liu Y, Li W, Lao F, Liu Y, Wang L, Bai R, Zhao Y and Chen C (2011) Intracellular dynamics of cationic and anionic polystyrene nanoparticles without direct interaction with mitotic spindle and chromosomes. *Biomaterials*32(32): 8291-8303.

Lovisolo D, Dionisi M, Ruffinatti FA and Distasi C (2018) Nanoparticles and potential neurotoxicity: Focus on molecular mechanisms. *AIMS Molecular Science*5: 1-13.

Lu J, Tang M and Zhang T (2019) Review of toxicological effect of quantum dots on the liver.*Journal of Applied Toxicology*39(1): 72-86.

Luby BM, Walsh CD and Zheng G (2019) Advanced photosensitizer activation strategies for smarter photodynamic therapy beacons.*Angewandte Chemie International Edition*58(9): 2558-2569.

Marklund S and Marklund G (1974) Involvement of the superoxide anion radical in the autoxidation of pyrogallol and a convenient assay for superoxide dismutase.*The FEBS Journal* 47: 469-474.

Matula K, Richter L, Adamkiewicz W, Akerstrom B, Paczesny J and Holyst R (2016) Influence of nanomechanical stress induced by ZnO nanoparticles of different shapes on the viability of cells. *Soft Matter*12(18): 4162-4169.

Meckbach L, Stroucken T and Koch SW (2018) Giant excitation induced bandgap renormalization in TMDC monolayers. *Applied Physics Letters*112(6): 061104.

Mishra V, Gurnany E and Mansoori MH (2017) Quantum Dots in Targeted Delivery of Bioactives and Imaging. In: *Nanotechnology-Based Approaches for Targeting and Delivery of Drugs and Genes*, Elsevier Academic Press, pp. 427-450.

Mittler R (2002) Oxidative stress, antioxidants and stress tolerance. *Trends in plant science*7(9): 405-410.

Mize CE and Langdon RG (1962) Hepatic glutathione reductase I. Purification and general kinetic properties.*Journal of Biological Chemistry* 237: 1589-1595.

Mohid SA, Ghorai A, Ilyas H, Mroue KH, Narayanan G, Sarkar A, Ray SK, Biswas K, Bera AK, Malmsten M and Midya A (2019) Application of tungsten disulfide quantum dot-conjugated antimicrobial peptides in bio-imaging and antimicrobial therapy. *Colloids and Surfaces B: Biointerfaces*176: 360-370.

Molaei MJ (2020) Principles, mechanisms, and application of carbon quantum dots in sensors: a review. *Analytical Methods*12(10): 1266-1287.

Mordorski B, Landriscina A and Friedman A (2016) An Overview of Nanomaterials in Dermatology. In: *Nanoscience in Dermatology*, Elsevier Academic Press, pp. 31-46.

Morgan DM (1998) Tetrazolium (MTT) assay for cellular viability and activity. In: *Polyamine protocols*, Humana Press, pp. 179-184.

Moron MS, Depierre JW and Mannervik B (1979) Levels of glutathione, glutathione reductase and glutathione S-transferase activities in rat lung and liver. *Biochimica et Biophysica Acta (BBA)-General Subjects* 582: 67-78.

Mutavdžić D, Xu J, Thakur G, Triulzi R, Kasas S, Jeremic M, Leblanc R and Radotić K (2011) Determination of the size of quantum dots by fluorescence spectroscopy. *Analyst*136(11): 2391-2396.

Nasrollahzadeh M, Sajadi SM, Sajjadi M and Issaabadi Z (2019) An Introduction to Nanotechnology. In: *Interface science and technology*, Elsevier Academic Press, 28, pp. 1-27.

Nimesh S, Chandra R and Gupta N (2017) *Advances in nanomedicine for the delivery of therapeutic nucleic acids*, Woodhead Publishing, UK.

Okado-Matsumoto A, Fridovich I (2001) Subcellular distribution of superoxide dismutases (SOD) in rat liver: Cu,Zn-SOD in mitochondria. *Journal of Biological Chemistry* 276**:** 38388-93.

Ostergaard G, Hansen H, Ottesen JL, Hau J and Schapiro SJ (2010) Handbook of laboratory animal science, Volume I: Essential Principles and Practices: 680-700

Paparazzo E (1988) XPS analysis of oxides.*Surface and Interface Analysis*12(2): 115-118.

Pardo M, Shuster-Meiseles T, Levin-Zaidman S, Rudich A and Rudich Y (2014) Low cytotoxicity of inorganic nanotubes and fullerene-like nanostructures in human bronchial epithelial cells: relation to inflammatory gene induction and antioxidant response. Environmental science & technology 48(6): 3457-3466.

Patel JP and Parsania PH (2017) biodegradable composites.*Biodegradable and Biocompatible Polymer Composites: Processing, Properties and Applications* 55.

Pawar RS, Upadhaya PG and Patravale VB (2018) Quantum Dots: Novel Realm in Biomedical and Pharmaceutical Industry. In: *Handbook of Nanomaterials for Industrial Applications,* Elsevier Academic Press, pp. 621-637.

Peynshaert K, Soenen SJ, Manshian BB, Doak SH, Braeckmans K, De Smedt SC and Remaut K (2017) Coating of Quantum Dots strongly defines their effect on lysosomal health and autophagy. *Acta biomaterialia*48: 195-205.

Pietryga JM, Schaller RD, Werder D, Stewart MH, Klimov VI and Hollingsworth JA, (2004) Pushing the band gap envelope: mid-infrared emitting colloidal PbSe quantum dots. *Journal of the American Chemical Society*126(38): 11752-11753.

Mordorski Pisanic Ii TR, Zhang Y and Wang TH (2014) Quantum dots in diagnostics and detection: principles and paradigms. *Analyst*139(12): 2968-2981.
Porter AG and Janicke RU (1999) Emerging roles of caspase-3 in apoptosis. *Cell death & differentiation*6(2): 99-104.

R Rama A, Jimenez-Lopez J, Cabeza L, Jimenez-Luna C, C Leiva M, Perazzoli G, Hernandez R, Zafra I, Ortiz R, Melguizo C and Prados J (2016) Last advances in

nanocarriers-based drug delivery systems for colorectal cancer. *Current Drug Delivery*13(6): 830-838.

Radisavljevic B, Radenovic A, Brivio J, Giacometti V and Kis A (2011) Single-layer MoS_2 transistors.*Nature nanotechnology*6(3): 147.

Radu GL, Truica GI, Penu R, Moroeanu V and Litescu SC (2012) Use of the Fourier transform infrared spectroscopy in characterization of specific samples. *UPB Scientific Bulletin B: Chemical and Materials Science*74(4): 137-148.

Rajendrakumar SK, Uthaman S, Cho CS and Park IK (2018) Nanoparticle-based phototriggered cancer immunotherapy and its domino effect in the tumor microenvironment. *Biomacromolecules* 19(6): 1869-1887.

Rajendran N, Hu SC, Sullivan D, Muzzio M, Detrisac CJ and Venezia C, (2012) Toxicologic evaluation of tungsten: 28-day inhalation study of tungsten blue oxide in rats. *Inhalation toxicology*24(14): 985-994.

Reimann SM and Manninen M (2002) Electronic structure of quantum dots.*Reviews of modern physics*74(4): 1283-1298.

Rodriguez-Farinas N, Gomez-Gomez MM and Camara-Rica C (2008) Study of tungstate–protein interaction in human serum by LC–ICP-MS and MALDI-TOF. *Analytical and bioanalytical chemistry*390(1): 29-35.

Rotruck J, Pope A, Ganther H, Swanson A, Hafeman DG and Hoekstra W (1973) Selenium: biochemical role as a component of glutathione peroxidase.*science*179: 588-590.

Saadat YR, Saeidi N, Vahed SZ, Barzegari A and Barar J (2015) An update to DNA ladder assay for apoptosis detection. *BioImpacts: BI*, 5(1): 25-28.

Sadeghi S, Kumar BG, Melikov R, Aria MM, Jalali HB and Nizamoglu S, (2018) Quantum dot white LEDs with high luminous efficiency. *Optica*5(7): 793-802.

Sadik OA (2013) Anthropogenic nanoparticles in the environment. *Environmental Science: Processes & Impacts*15(1): 19-20.

Salvati A, Nelissen I, Haase A, Aberg C, Moya S, Jacobs A, Alnasser F, Bewersdorff T, Deville S, Luch A and Dawson KA (2018) Quantitative measurement of nanoparticle uptake by flow cytometry illustrated by an interlaboratory comparison of the uptake of labelled polystyrene nanoparticles. *NanoImpact*9: 42-50.

Samadi-Maybodi A and Farzinia H (2018) Application of CdS QDs incorporated in magnetized powder activated carbon for degradation of some dyes: photodegradation process and comprehensive catalytic and spectroscopic studies. *Journal of Photochemistry and Photobiology A: Chemistry*357: 103-117.

Sargent EH (2012) Colloidal quantum dot solar cells.*Nature photonics*6(3): 133-135.

Shafagh M, Rahmani F and Delirezh N (2015) CuO nanoparticles induce cytotoxicity and apoptosis in human K562 cancer cell line via mitochondrial pathway, through reactive oxygen species and P53. *Iranian journal of basic medical sciences*, 18(10): 993-1000.

Shah J, Bhagat S and Singh S (2020) Standard biological assays to estimate nanoparticle toxicity and biodistribution. In: *Nanotoxicity*, Elsevier Academic Press, pp. 71-104.

Sharma M, Salisbury RL, Maurer EI, Hussain SM and Sulentic CE (2013) Gold nanoparticles induce transcriptional activity of NF-κB in a B-lymphocyte cell line. *Nanoscale*5(9): 3747-3756.

Sharp P and Villano JS (2012) *The laboratory rat*. CRC press, United States.

Sheng Y, Wang X, Fujisawa K, Ying S, Elias AL, Lin Z, Xu W, Zhou Y, Korsunsky AM, Bhaskaran H and Terrones M (2017) Photoluminescence segmentation within individual hexagonal monolayer tungsten disulfide domains grown by chemical vapor deposition. *ACS applied materials & interfaces*9(17): 15005-15014.

Shengjie Xu, Li D and Wu P (2015) One-pot, facile, and versatile synthesis of monolayer MoS_2/WS_2 quantum dots as bioimaging probes and efficient electrocatalysts for hydrogen evolution reaction. *Advanced Functional Materials*, 25(7):1127-1136.

Shin SK, Yoon HJ, Jung YJ and Park JW (2006) Nanoscale controlled self-assembled monolayers and quantum dots. *Current opinion in chemical biology*10(5): 423-429.

Shukla S, Jadaun A, Arora V, Sinha RK, Biyani N, Jain VK (2015) In vitro toxicity assessment of chitosan oligosaccharide coated iron oxide nanoparticles. *Toxicology Reports* 2, 27–39.

Sivandzade F, Bhalerao A and Cucullo L (2019) Analysis of the mitochondrial membrane potential using the cationic JC-1 dye as a sensitive fluorescent probe. *Bio-protocol*, *9*(1): e3128.

Sohaebuddin SK, Thevenot PT, Baker D, Eaton JW, Tang L (2010) Nanomaterial cytotoxicity is composition, size, and cell type dependent. Particle FibreToxicology 7.

Song WJ, Jeong MS, Choi DM, Kim KN and Wie MB (2019) Zinc oxide nanoparticles induce autophagy and apoptosis via oxidative injury and pro-inflammatory cytokines in primary astrocyte cultures. *Nanomaterials*9(7): 1043.

Splendiani A, Sun L, Zhang Y, Li T, Kim J, Chim CY, Galli G and Wang F (2010) Emerging photoluminescence in monolayer MoS_2. *Nano letters*10(4): 1271-1275.

Srikanth K (2020) Routes of Exposures and Toxicity of Nanoparticles. In: *Model Organisms to Study Biological Activities and Toxicity of Nanoparticles*, Springer, Singapore, pp. 267-276.

Stepkowski TM, Brzoska K and Kruszewski M (2014) Silver nanoparticles induced changes in the expression of NF-κB related genes are cell type specific and related to the basal activity of NF-κB. *Toxicology in Vitro*28(4): 473-478.

Stern ST, Adiseshaiah PP and Crist RM (2012) Autophagy and lysosomal dysfunction as emerging mechanisms of nanomaterial toxicity. *Particle and fibre toxicology*9(1): 9-20.

Stetefeld J, McKenna SA and Patel TR (2016) Dynamic light scattering: a practical guide and applications in biomedical sciences. *Biophysical reviews*8(4): 409-427.

Sun L, Cai J, Sun Y and Zhang D (2019) Three-dimensional assembly of silver nanoparticles spatially confined by cellular structure of Spirulina, from nanospheres to nanosheets. *Nanotechnology*30(49): 495704.

Swaminathan J, Subbiah R and Singaram V (2016) Defect-Rich Metallic Titania (TiO1. 23) An Efficient Hydrogen Evolution Catalyst for Electrochemical Water Splitting.*ACS Catalysis*6(4): 2222-2229.

Swart HC and Kroon RE (2019) Ultraviolet and visible luminescence from bismuth doped materials. *Optical Materials: X*, *2*: 100025.

Toh RJ, Sofer Z, Luxa J, Sedmidubsky D and Pumer M (2017) 3R phase of MoS_2 and WS_2 outperforms the corresponding 2H phase for hydrogen evolution. *Chemical Communications*53(21): 3054-3057.

Tsoi KM, Dai QIN, Alma BA and Chan WC (2013) Are quantum dots toxic?Exploring the discrepancy between cell culture and animal studies. *Accounts of chemical research* 46(3): 662-671.

Umakant Yadav, Singh V, Mishra H, Saxena PS and Srivastava A (2021) Evaluation of in vitro and in vivo toxicity of pristine molybdenum disulphide nanosheets in Swiss albino mice. *bioRxiv*.

Van De Ven AL, Mack A, DunnerJr K, Ferrari M and Serda RE (2012) Preparation, characterization, and cellular associations of silicon logic-embedded vectors. In *Methods in enzymology*, Elsevier Academic Press 508, pp. 1-16.

Vance ME, Kuiken T, Vejerano EP, McGinnis SP, Hochella Jr MF, Rejeski D and Hull MS (2015) Nanotechnology in the real world: Redeveloping the nanomaterial consumer products inventory. *Beilstein journal of nanotechnology* 6(1): 1769-1780.

Vandebriel RJ and De Jong WH (2012) A review of mammalian toxicity of ZnO nanoparticles. *Nanotechnology, science and applications*5: 61.

Vasudevan D, Gaddam RR, Trinchi A and Cole I (2015) Core–shell quantum dots: Properties and applications.*Journal of Alloys and Compounds*636: 395-404.

Vattikuti SP, Byon C and Chitturi V (2016) Selective hydrothermally synthesis of hexagonal WS_2 platelets and their photocatalytic performance under visible light irradiation. *Superlattices and Microstructures* 94: 39-50.

Vinluan RD and Zheng J (2015) Serum protein adsorption and excretion pathways of metal nanoparticles.*Nanomedicine*10(17): 2781-2794.

Walters C, Pool E and Somerset V (2016) Nanotoxicology: a review. *Toxicology-new aspects to this scientific conundrum. InTech*, 45-63.

Worsfold P, Townshend A, Poole CF and Miro M (2019) *Encyclopedia of analytical science*, Elsevier.

Wypij M, Jędrzejewski T, Ostrowski M, Trzcinska J, Rai M and Golinska P (2020) Biogenic silver nanoparticles: assessment of their cytotoxicity, genotoxicity and study of capping proteins. *Molecules*25(13): 3022.

Xing Y and Rao J (2008) Quantum dot bioconjugates for in vitro diagnostics & in vivo imaging. *Cancer Biomarkers*4(6): 307-319.

Xu S, Li D and Wu P (2015) One-pot, facile, and versatile synthesis of monolayer MoS_2/WS_2 quantum dots as bioimaging probes and efficient electrocatalysts for hydrogen evolution reaction. *Advanced Functional Materials*25(7): 1127-1136.

Xu Y, Yan L, Li X and Xu H (2019) Fabrication of transition metal dichalcogenides quantum dots based on femtosecond laser ablation. *Scientific reports*9(1): 1-9.

Xu Z, Lv Y, Li J, Huang F, Nie P, Zhang S, Zhao S, Zhao S and Wei G (2019) CVD controlled growth of large-scale WS_2 monolayers. *RSC advance*9(51): 29628-29635.

Yan F, Sun Z, Xu J, Li H and Zhang Y (2020) WS_2 quantum dots-MnO_2 nanosheet system for use in ratiometricfluorometric/scattered light detection of glutathione. *Microchimica Acta*187: 1-9.

Yan Y, Zhang C, Gu W, Ding C, Li X and Xian Y (2016) Facile synthesis of water-soluble WS_2 quantum dots for turn-on fluorescent measurement of lipoic acid. *The Journal of Physical Chemistry C*120(22): 12170-12177.

Yang C, Feng G, Wang S, Dai J, Zhan Y and Zhou S (2017) Wavelength-tunable photoluminescence of ZnSe quantum dot micelles synthesized by femtosecond laser ablation in microfluidics. *Chemical Physics Letters*684: 409-413.

Yang W, Kawai H, Bosman M, Tang B, Chai J, Le Tay W, Yang J, Seng HL, Zhu H, Gong H and Liu H (2018) Interlayer interactions in 2D WS_2/MoS_2 heterostructures monolithically grown by in situ physical vapor deposition. *Nanoscale*10(48): 22927-22936.

Yao J, Li P, Li L and Yang M (2018) Biochemistry and biomedicine of quantum dots: from biodetection to bioimaging, drug discovery, diagnostics, and therapy. *Actabiomaterialia*74: 36-55.

Yin W, He D, Bai X and William WY (2019) Synthesis of tungsten disulfide quantum dots for high-performance supercapacitor electrodes. *Journal of Alloys and Compounds* 786:764-769.

Yin W, Liu X, Zhang X, Gao X, Colvin VL, Zhang Y and Yu WW (2020) Synthesis of Tungsten Disulfide and Molybdenum Disulfide Quantum Dots and their Applications. *Chemistry of Materials* 32(11):4409-4424.

Yong Y, Cheng X, Bao T, Zu M, Yan L, Yin W, Ge C, Wang D, Gu Z and Zhao Y (2015) Tungsten sulfide quantum dots as multifunctional nanotheranostics for in vivo

dual-modal image-guided photothermal/radiotherapy synergistic therapy. *ACS nano*9(12): 12451-12463.

Zha S, Rong J, Guan X, Tang Y, Han Y and Liu G (2019) Immunotoxicity of four nanoparticles to a marine bivalve species, Tegillarca granosa. *Journal of hazardous materials*377: 237-248.

Zhang C, Yong Y, Song L, Dong X, Zhang X, Liu X, Gu Z, Zhao Y and Hu Z (2016) Multifunctional WS_2 @ Poly (ethylene imine) Nanoplatforms for Imaging Guided Gene-Photothermal Synergistic Therapy of Cancer. *Advanced healthcare materials*5(21): 2776-2787.

Zhang M, Bishop BP, Thompson NL, Hildahl K, Dang B, Mironchuk O, Chen N, Aoki R, Holmberg VC and Nance E (2019) Quantum dot cellular uptake and toxicity in the developing brain: implications for use as imaging probes. *Nanoscale advances*1(9): 3424-3442.

Zhang S, Jia X and Wang E (2016) Facile synthesis of optical pH-sensitive molybdenum disulfide quantum dots. *Nanoscale*8(33): 15152-15157.

Zhang TG, Zhang YL, Zhou QQ, Wang XH and Zhan LS (2020). Impairment of mitochondrial dynamics involved in iron oxide nanoparticle-induced dysfunction of dendritic cells was alleviated by autophagy inhibitor 3-methyladenine. *Journal of Applied Toxicology*40(5): 631-642.

Zhao X, Ma X, Sun J, Li D and Yang X (2016) Enhanced catalytic activities of surfactant-assisted exfoliated WS_2 nanodots for hydrogen evolution. *ACS nano*10(2): 2159-2166.

Zhu B, Li Y, Lin Z, Zhao M, Xu T, Wang C and Deng N (2016) Silver nanoparticles induce HePG-2 cells apoptosis through ROS-mediated signaling pathways. *Nanoscale research letters*11(1): 1-8.

Zhu C, Huang Y, Xu F, Gao P, Ge B, Chen J, Zeng H, Sutter E, Sutter P and Sun L (2017) Defect-Laden $MoSe_2$ Quantum Dots Made by Turbulent Shear Mixing as Enhanced Electrocatalysts. *Small*13(27): 1700565.

Zielinska A, Carreiro F, Oliveira AM, Neves A, Pires,B, Venkatesh DN, Durazzo A, Lucarini M, Eder P, Silva AM and Santini A (2020) Polymeric nanoparticles: production, characterization, toxicology and ecotoxicology. *Molecules*25(16): 3731.

Zyuzin MV, Yan Y, Hartmann R, Gause KT, Nazarenus M, Cui J, Caruso F and Parak WJ (2017) Role of the protein corona derived from human plasma in cellular interactions between nanoporous human serum albumin particles and endothelial cells. *Bioconjugate chemistry*28(8): 2062-2068.

Kumar G, Degheidy H, Casey BJ and Goering PL (2015) Flow cytometry evaluation of in vitro cellular necrosis and apoptosis induced by silver nanoparticles. *Food and Chemical Toxicology* 85: 45-51.

Stengl V, Tolasz J and Popelková, D (2015) Ultrasonic preparation of tungsten disulfide single-layers and quantum dots.*RSC advances*5(109): 89612-89620.

Yang Y, Du X, Wang Q, Liu J, Zhang E, Sai L, Peng C, Lavin MF, Yeo AJ, Yang X and Shao H (2019) Mechanism of cell death induced by silica nanoparticles in hepatocyte cells is by apoptosis. *International journal of molecular medicine*, 44(3): 903-912.

ANNEXURE

List of publications

1. **Anju Surendranath[1]** Mohanan PV (2022) Solvothermal exfoliation assisted synthesis of transition metal dichalcogenide based tungsten disulphide quantum dots (WS_2 QDs) and cellular QD-bio interaction in LN-229 human glioblastoma cells, Material Science and Engineering B, 115907 (**Corresponding author and first author)**

2. **Anju S** and Mohanan PV (2020) Biomedical applications of transition metal dichalcogenides (TMDCs). *Synthetic Metals*, 116610.

3. **Anju S**, Mohanan PV (2020) Nanomedicine: future perspectives and Challenges. Chapter 22 In Book: Functional Bionanomaterials: From Biomolecules to Nanoparticles. *Springer Nature*. Edition 1, Series: ISSN 2523-8027. Pages: 451-476.

4. **Anju Surendranath**, Ashtami Jayakumar, Mohanan P.V (2019) Black phosphorus, A prospective graphene substitute for biomedical applications, Material Science and Engineering C, 9: 978-993. Elsevier.

5. Ashtami J, *__Anju S__, Mohanan PV (2019) Conformity of dextran-coated fullerene C70 with L929 fibroblast cells, Colloids and Surfaces B: Biointerfaces, 184: 110530. Elsevier.

6. RS Cherian RS, *__S.Anju__, Willi Paul, Sabareeswaran A, Mohanan P.V (2019**),** Organ distribution and biological compatibility of surface functionalized reduced graphene oxide, Nanotechnology, 31: 7 *31*(7):_075303. .IOP Publishing.

7. **Anju S**, Prajitha N, Sukanya VS, Mohanan PV (2019) Complicity of degradable polymers in healthcare applications, Materials today chemistry 16: 100236. Elsevier.

8. **Anju S**, Ashtami J, Mohanan P.V (2019) Effect of Surface Modified Fullerene C70 on the ROS Production and Cellular Integrity Using Chinese Hamster Ovarian Cells, General Chemistry.

8. **Anju S**, Prajitha N, Reshma VG, Mohanan PV (2019) Black phosphorous quantum dots. In book: Black Phosphorous: Synthesis, Properties and Applications. *Springer Nature.*

9. Ashtami Jayakumar, *__Anju Surendranath__, Mohanan PV (2018) 2D materials for next generation health care applications, International Journal of Pharmaceutics, 551(1-2), 309-321. Elsevier.

Conferences

1. **Anju Surendranath,** Mohanan PV (2021) Tungsten disulphide Quantum Dots mediated cellular responses in glioblastoma cell lines, presented at the 40th annual Conference of Society of Toxicology, India and International Webinar on 'Pharmacology and Toxicology' jointly organized by PGIMER Chandigarh and SCTIMST Trivandrum, 29-30 January 2021.

2. **Anju Surendranath,** Mohanan PV (2021) ROS generation and related cytotoxicity evaluation of fullerenes in *in vitro* system, presented at the 40th annual Conference of Society of Toxicology, India and International Webinar on 'Pharmacology and Toxicology' jointly organized by PGIMER Chandigarh and SCTIMST Trivandrum, 29-30 January 2021.

3. **Anju Surendranath,** Megha KB, Mohanan PV (2021) Development of Vaccine for Covid-19: a sleepless effort of scientific community, presented at the 40th annual Conference of Society of Toxicology, India and International Webinar on 'Pharmacology and Toxicology' jointly organized by PGIMER Chandigarh and SCTIMST Trivandrum, 29-30 January 2021.

4. **Anju Surendranath,** Mohanan P.V (2019) Nano-bio interactions of tungsten disulphide quantum dots (WS_2 QDs) in LN-229 glioblastoma cell lines. Presented at International Conference on Emerging Advancement in Science and Technology (ICEAST) & 10th Indo-Japan Science and Technology Conclave, Manekshaw Centre NewDelhi, 5-6 September 2019.

5. **Anju Surendranath**, Ashtami Jayakumar, Mohanan PV (2018) Cytocompatibility of C70 fullerene nanocomposite using CHO cells. Presented at the 'International Conference on the Role of Toxicology in Public Health & 38th Annual Conference of Society of Toxicology, India, Sri Balaji Vidyapeeth, Puducherry, India, 12-14 December 2018.

6. Ashtami Jayakumar, **Anju Surendranath**, Mohanan PV (2018) Fullerene 70; A promising nanoparticle for biomedical applications. Presented at the 'International Conference on the Role of Toxicology in Public Health & 38th Annual Conference of Society of Toxicology, India, Sri Balaji Vidyapeeth, Puducherry, India, 12-14 December 2018.

7. **Anju Surendranath**, Ashtami Jayakumar, Mohanan PV (2018). Characterisation and cytocompatibility of surface modified C70 fullerene nanoparticles using CHO cell lines. Presented at 28th Swedeshi Science Congress, National Institute for Interdisciplinary Sciences and Technology, Thiruvananthapuram, Kerala, India, 7-9 November 2018.

8. Ashtami Jayakumar, **Anju Surendranath**, Mohanan PV (2018) Interaction of surface functionalized fullerene C70 with L929 cells. Presented at 28th Swedeshi Science Congress, National Institute for Interdisciplinary Sciences and Technology, Thiruvananthapuram, Kerala, India, 7-9 November 2018.

Awards and Achievements

1. **Best Oral Presentation award** for the research paper entitled 'Tungsten disulphide Quantum Dots mediated cellular responses in glioblastoma cell lines' (Anju Surendranath, Mohanan PV) at the 40th Annual Conference of Society of Toxicology, India and International Webinar on 'Pharmacology and Toxicology', jointly organized by PGIMER Chandigarh and SCTIMST Trivandrum, 29-30 January 2021.

2. **UGC (JRF-2016-17) Junior Research Fellowship (Rank 47):** Junior Research Fellowship from University Grants Commission (Govt. of India), New Delhi.

3. **National Eligibility Test (NET-2016-17),** University Grants Commission, Govt. of India, New Delhi.

4. **INSPIRE-Scholarship for Higher Education (2011-2016):** Department of Science and Technology (DST), Govt of India for being top 1% students All India topped in higher secondary level examination.